

EVALUATION OF RECYCLED PLASTIC PINS AS SHEAR KEYS IN MSE WALL BASE

by

PRABESH BHANDARI

Presented to the Faculty of the Graduate School of  
The University of Texas at Arlington in Partial Fulfillment  
of the Requirements  
for the Degree of

DOCTOR OF PHILOSOPHY IN CIVIL ENGINEERING

THE UNIVERSITY OF TEXAS AT ARLINGTON

May 2021

Copyright © by Prabesh Bhandari 2021

All Rights Reserved



## ACKNOWLEDGEMENTS

I would like to express my sincere gratitude to my supervising professor, Dr. MD. Sahadat Hossain, for his continuous support, motivation, guidance, and valuable suggestions throughout my graduate studies. He made sure that I succeeded in my endeavors by providing me the platform, sharing his experiences, and creating a learning environment. I am deeply grateful for the opportunity to work under him as a part of his research team.

I would like to acknowledge Dr. Xinbao Yu, Dr. Seyed Mohsen Shahandashti, and Dr. Muhammad N. Huda for providing their constructive comments and valuable time to serve on my dissertation committee. I would also like to thank the Texas Department of Transportation (TxDOT) for funding this research. A special thanks goes to the Hunter Ferrell Landfill in Irving for their immense help with the field activities.

I would like to specially thank all the SWIS members for their support during my studies. The fieldworks would not have been possible without the invaluable help of Md. Azijul Islam and Faria Fahim Badhon. I am very thankful to the unwavering support and assistance of Pratibha Pandey, Sachini Madanayake, Muhasina Manjur Dola, Cory Rauss, Dr. Anuja Sapkota, Dr. Nur Basit Zaman, Dr. Asif Ahmed, and Dr. Jobair Bin Alam. It has truly been a life-changing experience to be a part of this team.

Finally, and most importantly, I would not have been able to get here without the endless love, trust, encouragement, and belief of my parents and brother. No words can describe my gratitude towards them. I am grateful towards all my friends here in Arlington who made this journey worthwhile. I thank God for giving me the strength, patience, and hope to complete my degree.

March 25, 2021

## ABSTRACT

### EVALUATION OF RECYCLED PLASTIC PINS AS SHEAR KEYS IN MSE WALL BASE

Prabesh Bhandari, Ph.D.

The University of Texas at Arlington, 2021

Supervising Professor: MD. Sahadat Hossain

Mechanically Stabilized Earth (MSE) walls have been widely used as retaining structures due to their flexible nature, a better tolerance against differential settlement, and many other factors. However, external stability problems of MSE walls have been an issue in North Texas over decades. Lateral displacement of the wall occurs, giving rise to sliding failure, when there is insufficient shear strength at the wall base to produce adequate frictional resistance. Such failures can cause significant maintenance, repair, and cost implications for the state department of transportation. Furthermore, MSE walls also undergo global failure due to weak soil conditions along with high lateral pressures. Typical recommended solutions consist of either increasing the weight of the wall, increasing the length of the heel slab, or using wall anchors and helical tiebacks, which are all expensive. On the other hand, incorporating a shear key at the wall base has proven to completely restrict the lateral sliding of walls. However, for MSE retaining structures, incorporating a concrete shear key is challenging due to its expensive cost and rigid nature, which undermines the most important feature of an MSE wall which is the flexible nature of its base. A possible solution could be using recycled plastic pins (RPP) as shear keys. The success of RPPs in providing sufficient lateral support to sliding soil mass in slopes could be imitated in an MSE wall to deliver the required lateral resistance against sliding. As the RPPs are made from recycled plastics,



they are highly cost-saving when compared to concrete. They are comparatively flexible in nature and require almost no maintenance.

The main objective of the study is to investigate the effectiveness of RPPs in increasing the lateral stability of MSE wall system. Four test sections were constructed, out of which three were reinforced with 10 ft. long RPPs at the wall base. One test section was left unreinforced as a control section. The three test sections were reinforced with 4x4 inches RPP at 3 ft. c/c, 4x4 inches RPP at 2 ft. c/c, and 6x6 inches RPP at 3 ft. c/c. The RPPs inside the wall were extended 2 ft. above the foundation into the reinforced zone. Two rows of RPPs were installed fully flushed to the ground surface in front of the test wall. Vertical and horizontal inclinometer casings along with earth pressure plates were used to monitor the performance of the test sections over a period of almost two years.

The field results showed that the lateral resistance of the RPP reinforced sections increased by 75% to 89% in comparison to the control section. The control section failed about 8 months after construction, while the RPP reinforced sections were stable. The vertical settlement of the RPP reinforced sections decreased by 48% to 68% in comparison to the control section, while the maximum lateral earth pressure reduced by 66% to 76% in the RPP reinforced sections. Finite element studies in PLAXIS 2D showed that larger cross-section and closer spacing of RPPs provided better lateral resistance. Lateral displacement and lateral stress reduction prediction models were developed using the modeling results. Based on the performance monitoring results and further analyses, it can be concluded that the RPPs can be effectively used as shear keys in MSE walls. They can be incorporated at the wall base during design for improving the lateral resistance of MSE walls.

## Table of Contents

ACKNOWLEDGEMENTS .....	iii
ABSTRACT .....	iv
List of Figures.....	xii
List of Tables.....	xx
Chapter 1 INTRODUCTION.....	1
1.1 Background .....	1
1.2 Problem Statement .....	4
1.3 Research Objectives .....	6
1.4 Dissertation Organization.....	7
Chapter 2 LITERATURE REVIEW.....	10
2.1 Introduction.....	10
2.2 Benefits of MSE Wall .....	11
2.3 Elements of MSE Wall .....	13
2.4 Construction of MSE Wall .....	15
2.4.1 MSE Wall with Precast Panel Facings .....	15
2.4.2 MSE Wall with Flexible Facings .....	18
2.5 Design Overview of MSE Wall in the United States .....	20
2.6 Design Criteria of MSE Wall.....	21
2.7 External Stability of MSE Wall.....	23
2.7.1 Sliding and Overturning.....	25

2.7.2	Bearing Capacity .....	26
2.7.3	Global Stability .....	28
2.8	Factors Affecting Performance of MSE Walls .....	30
2.8.1	Effect of Reinforcement Type.....	31
2.8.2	Effect of Reinforcement Stiffness.....	31
2.8.3	Effect of Facing Stiffness .....	33
2.8.4	Effect of Backfill Soil.....	34
2.8.5	Effect of Foundation Soil .....	34
2.8.6	Effect of Compaction.....	35
2.9	Previous Experimental Findings on Lateral Resistance of MSE Wall.....	36
2.10	Previous Findings on Vertical Settlement and Deep-Seated Failure of MSE Wall.....	49
2.11	Analytical Solutions .....	52
2.12	Lateral Resistance of MSE Wall Using Shear Key .....	62
2.13	Lateral Resistance of Piles.....	69
2.14	Improvement of Bearing Capacity Using Piles.....	72
2.15	Recycled Plastic Pins.....	74
2.15.1	Manufacturing Process of RPP.....	75
2.15.2	Engineering Properties of RPP .....	76
2.15.3	Field Scale Studies Using RPP .....	80
2.16	Numerical Study Using Finite Element Modeling.....	84

2.17	Statistical Modeling .....	92
2.18	Limitations of Previous Studies .....	94
Chapter 3 METHODOLOGY .....		95
3.1	Project Background .....	95
3.2	Site Selection .....	95
3.3	Site Investigation .....	97
3.3.1	Geotechnical Drilling .....	97
3.3.2	Geophysical Testing.....	101
3.4	Laboratory Testing .....	103
3.4.1	Gravimetric Moisture Content Test .....	103
3.4.2	Grain Size Distribution Test .....	104
3.4.3	Atterberg's Limit Test .....	107
3.4.4	Strength Test.....	108
3.5	Reinforcement Mechanism Using Recycled Plastic Pin .....	109
3.6	Design of Field Test Sections .....	111
3.7	Field Installation and Instrumentation .....	117
3.7.1	Installation of Recycled Plastic Pins .....	117
3.7.2	Instrumentation.....	120
3.7.3	Construction of Test Sections .....	125
3.8	Performance Monitoring Plan .....	128
Chapter 4 RESULTS AND DISCUSSION .....		129

4.1	Background .....	129
4.2	Lateral Displacement of Wall Base .....	129
4.2.1	Vertical Inclinator Results.....	129
4.2.2	Comparison with Previous Studies .....	136
4.3	Settlement of Wall Base .....	140
4.3.1	Horizontal Inclinator Results .....	140
4.3.2	Comparison with Previous Studies .....	144
4.4	Earth Pressure Plate Results .....	146
4.5	Correlation Between Earth Pressure and Lateral Displacement .....	148
4.6	Effectiveness of the RPP Reinforcement Approach .....	149
Chapter 5 NUMERICAL STUDY .....		155
5.1	Background .....	155
5.2	Finite Element Based Numerical Model .....	155
5.2.1	Model Calibration Using the Control Section .....	158
5.2.2	Numerical Modeling of the Reinforced Sections .....	161
5.3	Parametric Study.....	162
5.3.1	Effect of Foundation Soil Strength .....	164
5.3.2	Effect of RPP Parameters .....	166
5.3.3	Effect of MSE Wall Height.....	170
5.4	Passive Pressure Due to RPPs .....	171
5.5	Reduction in Active Lateral Pressure Due to RPPs .....	177

5.6	Global Stability .....	181
Chapter 6 DEVELOPMENT OF DESIGN METHODOLOGY .....		186
6.1	Background .....	186
6.2	Statistical Analysis .....	187
6.3	Statistical Analysis of Lateral Displacement .....	188
6.3.1	Selection of Parameters .....	188
6.3.2	Correlation Analysis .....	189
6.3.3	Development of Preliminary Model .....	191
6.3.4	Verification of Preliminary Model.....	193
6.3.5	Transformation of Variables .....	196
6.3.6	Verification of Final Model.....	198
6.3.7	Selection of Final Model.....	200
6.3.8	Validation of the Final Prediction Model.....	201
6.4	Statistical Analysis of Lateral Pressure Reduction .....	202
6.4.1	Selection of Parameters .....	202
6.4.2	Correlation Analysis .....	203
6.4.3	Development of Preliminary Model .....	205
6.4.4	Verification of Preliminary Model.....	206
6.4.5	Transformation of Variables .....	209
6.4.6	Verification of Final Model.....	211
6.4.7	Selection of Final Model.....	214

6.4.8	Validation of the Final Prediction Model.....	216
6.5	Probabilistic Analysis .....	217
6.5.1	Probabilistic Analysis for Lateral Displacement .....	219
6.5.2	Probabilistic Analysis for Lateral Pressure Reduction .....	223
6.6	Modified Factor of Safety Against Sliding .....	226
6.7	Design Steps for Calculation of Modified Factor of Safety Against Sliding ....	229
6.7.1	Calculation Example .....	231
6.8	Limitations of the Prediction Models .....	239
Chapter 7	SUMMARY AND CONCLUSIONS.....	241
7.1	Background .....	241
7.1.1	Site Investigation.....	242
7.1.2	Lateral Displacement of Wall Base .....	242
7.1.3	Settlement of Wall Base.....	243
7.1.4	Earth Pressure Plates .....	243
7.1.5	Numerical Study .....	244
7.1.6	Design Methodology .....	246
7.2	Recommendations for Future Studies .....	247
REFERENCES.....		249
APPENDIX A.....		268
APPENDIX B.....		273
BIOGRAPHY.....		288

## List of Figures

Figure 1-1 A Typical MSE Wall with RPPs as Shear Keys.....	6
Figure 2-1 Typical Section of MSE Wall .....	14
Figure 2-2 Construction Sequence of MSE Wall with Precast Panel Facing (a). Leveling Pad (Passe, 2000) (b). Erection of Precast Panel (c). Spreading of Fill Material (d). Placement and Connection of Reinforcement (e). Compaction of Reinforced Fill Material (Berg et al., 2009) .....	18
Figure 2-3 Lift Construction Sequence of MSE Wall with Flexible (Geosynthetic) Facing	20
Figure 2-4 Requirement of MSE Wall Embedment Depth (a). Level Toe Condition (b). Benched Slope Toe Condition .....	23
Figure 2-5 Potential External Failure Mechanisms of a MSE Wall (Elias et al., 2001) .....	24
Figure 2-6 Ultimate Bearing Capacity of Rigid Footing.....	27
Figure 2-7 A Typical Section of MSE Wall for Global Stability Analysis (Keystone, 2003).....	29
Figure 2-8 Effect of Geogrid Stiffness on Wall Facing Displacement (Pierson et al., 2011).....	33
Figure 2-9 Lateral Displacements Experienced on Phase I Construction (a). During Stage I Construction (b). Due to Placement of the Bridge Superstructure (Abu-Hejleh et al., 2000) .....	38
Figure 2-10 Measured Lateral Wall Movement of Each Segmental Panel at the End of Construction (Horpibulsuk et al., 2011).....	40
Figure 2-11 Measured Lateral Movement After the Completion of Construction (Horpibulsuk et al., 2011).....	40
Figure 2-12 Locations of Pressure Transducers Behind the Wall (Fang and Ishibashi, 1986) .....	41



Figure 2-13 Lateral Displacement of the Face of MSE Wall (Stuedlein et al., 2007) .....	44
Figure 2-14 Deflections of the Drilled Shaft Retaining Wall Under Study (Brown et al., 2015) .....	47
Figure 2-15 Lateral Wall Deflection (Ahmadi and Bezuijen, 2018) .....	48
Figure 2-16 Cumulative Lateral Displacement Profiles with Depth (Stark et al., 2019)....	50
Figure 2-17 Incremental Lateral Displacement Profiles with Depth (Stark et al., 2019) ...	51
Figure 2-18 (a). Openings Between the Panels of the MSE Wall (b). Outward Rotation of the Wing Wall (c). Separation of Wing Wall from Abutment (Samtani et al., 2005).....	52
Figure 2-19 Idealized Soil Pressure Distribution Along the Length of Pile (Prasad and Chari, 1999) .....	56
Figure 2-20 Calculation of Ultimate Lateral Capacity of Pile (Prasad and Chari, 1999) ...	57
Figure 2-21 Experimental Setup for Pile Load Capacity Test (Sastry and Meyerhof, 1994) .....	58
Figure 2-22 Flexible and Equivalent Rigid Pile Concept (Sastry and Meyerhof, 1994)....	59
Figure 2-23 Schematic Distribution of Lateral Soil Pressure on Pile Shaft (Sastry and Meyerhof, 1989) .....	60
Figure 2-24 Schematic of a Conventional Retaining Wall with Shear Key (Jamal, 2017)	63
Figure 2-25 Schematic and Baseline Model of MSE Wall for Numerical Analysis (a). Detail of MSE Wall (b). Detail of Concrete Key (Kim and Bilgin, 2007) .....	65
Figure 2-26 Effect of Concrete Key on the Lateral Deformation of MSE Wall (Kim and Bilgin, 2007) .....	66
Figure 2-27 Horizontal Deformation in Relation to Precipitation with Time (a). Precipitation (b). Elevation 3 (c). Elevation 2 (d). Elevation 1 (Benjamin et al., 2007) .....	69
Figure 2-28 Pile Lateral Capacity from the Model (Sawwaf, 2006) .....	70

Figure 2-29 Load vs. Deflection Curves for the Single and Group Piles (Rollins et al., 2010) .....	71
Figure 2-30 Effect of (a). Embankment Height and (b). Pile Elastic Modulus on Maximum Settlement of Pile Supported Embankment on Soft Soil (Han and Gabr, 2002) .....	73
Figure 2-31 Deformation and Tension Force on Geogrid (Han et al., 2011) .....	73
Figure 2-32 Layout of RPP at US-287 Slope (Khan, 2014) .....	81
Figure 2-33 Variation of Horizontal Displacement in (a). Reinforced Section 1 (b). Reinforced Section 2 (Khan, 2014) .....	82
Figure 2-34 Comparison of Incremental Settlement Between US-287, I-35 and SH-183 Reinforced Sections (Rauss, 2019) .....	83
Figure 2-35 Soil Profile and Selected Instrumentation for MSE Wall on I-15 (Budge et al., 2006) .....	85
Figure 2-36 Comparison of Vertical Extensometer Data with PLAXIS Model Data (Budge et al., 2006) .....	86
Figure 2-37 Comparison of Horizontal Inclinator Data with PLAXIS Model Data (Budge et al., 2006) .....	87
Figure 2-38 Lateral Pressure Acting on the Wall Stem (Rouili et al., 2005) .....	89
Figure 2-39 Layout of Retaining Wall and Sensors Under Study (Damians et al., 2015)	89
Figure 2-40 Model Predicted Displacements (a). Total Displacement (291 mm) (b). Vertical Displacement (179 mm) (Hossain et al., 2012) .....	91
Figure 3-1 Site Location Map .....	96
Figure 3-2 Suitable Slope and Area for Construction of Test Sections .....	97
Figure 3-3 Location of the Soil Borings .....	98
Figure 3-4 (a). Drilling Setup (b). TCP Test (c). Undisturbed Shelby Tube Samples .....	100
Figure 3-5 Resistivity Imaging Survey Lines .....	102

Figure 3-6 Resistivity Imaging Result Along the Slope (Line 1) .....	102
Figure 3-7 Resistivity Imaging Result Across the Toe (Line 2).....	102
Figure 3-8 Variation of Moisture Content with Depth at the Toe of the Slope .....	104
Figure 3-9 Hydrometer Samples .....	105
Figure 3-10 Grain Size Distribution Curves of the Foundation Soil .....	106
Figure 3-11 Grain Size Distrubution Curve of the Backfill Sand .....	107
Figure 3-12 Plasticity Chart for the Foundation Soil .....	108
Figure 3-13 Unconfined Compressive Strength.....	109
Figure 3-14 Schematic of RPP Reinforced MSE Wall (Not to Scale) .....	110
Figure 3-15 Layout of Control Section SC_Control (a) Plan (b) Section .....	113
Figure 3-16 Layout of Reinforced Section SR_4x3 (a) Plan (b) Section .....	114
Figure 3-17 Layout of Reinforced Section SR_4x2 (a) Plan (b) Section .....	115
Figure 3-18 Layout of Reinforced Section SR_6x3 (a) Plan (b) Section .....	116
Figure 3-19 Boundary of the Test Sections .....	117
Figure 3-20 Installation Sequence of Recycled Plastic Pins.....	119
Figure 3-21 Installation Sequence of Horizontal Inclinator Casings .....	122
Figure 3-22 Installation Sequence of Vertical Inclinator Casings .....	124
Figure 3-23 Model 4810 Earth Pressure Cell .....	124
Figure 3-24 Construction of Test Sections.....	125
Figure 3-25 Backfilling of the Test Sections.....	127
Figure 4-1 Lateral Displacement with Depth of Section SR_4x3.....	130
Figure 4-2 Lateral Displacement with Depth of Section SR_4x2.....	131
Figure 4-3 Lateral Displacement with Depth of Section SR_6x3.....	132
Figure 4-4 Lateral Displacement with Depth of Section SC_Control .....	133
Figure 4-5 Failure of the Control Section (SC_Control).....	133

Figure 4-6 Comparison of Lateral Displacement of Wall Base .....	135
Figure 4-7 Comparison of Lateral Displacement of Ground Level with Rainfall .....	136
Figure 4-8 Cumulative Lateral Displacement Profiles with Depth (Reprinted from Stark et al., 2019, © ASCE).....	137
Figure 4-9 Incremental Lateral Displacement Profiles with Depth of the Test Sections .	138
Figure 4-10 Vertical Displacement of Wall Base in SR_4x3.....	141
Figure 4-11 Vertical Displacement of Wall Base in SR_4x2.....	142
Figure 4-12 Vertical Displacement of Wall Base in SR_6x3.....	142
Figure 4-13 Vertical Displacement of Wall Base in SC_Control .....	143
Figure 4-14 Comparison of Vertical Displacement of Wall Base .....	144
Figure 4-15 Change of Lateral Pressure with Rainfall.....	147
Figure 4-16 Change in Normalized Lateral Pressure with Lateral Wall Displacement (a). Reprinted from Fang and Ishibashi (1986), © ASCE (b). Current Study .....	149
Figure 4-17 Comparison of Lateral Displacement of Ground Level .....	150
Figure 4-18 Comparison of Maximum Vertical Displacement of Wall Base .....	151
Figure 4-19 Decrease in Maximum Lateral Pressure with RPP Reinforcement.....	152
Figure 4-20 Comparison of the Coefficient of Lateral Earth Pressure in the Current Study and Jiang et al. (2016) .....	153
Figure 5-1 Geometry of the Wall in the FE Model .....	157
Figure 5-2 Mesh Connectivity in the FE Model.....	158
Figure 5-3 Comparison of Field and Model Horizontal Displacements of SC_Control...	160
Figure 5-4 Failure Pattern of (a) FE Model and (b) Field Control Section .....	161
Figure 5-5 Comparison of Field and Model Horizontal Displacements of the Reinforced Test Sections .....	162
Figure 5-6 Parametric Study Matrix .....	164

Figure 5-7 Effect of Foundation Soil Strength ( $c-\phi$ ) on Lateral Displacement of MSE Wall Base (a). RPP Size 4x4 inches (b). RPP Size 6x6 inches.....	165
Figure 5-8 Effect of Foundation Soil Friction Angle ( $\phi$ ) on Lateral Displacement of MSE Wall Base (a). RPP Size 4x4 inches (b). RPP Size 6x6 inches.....	166
Figure 5-9 Effect of RPP Size on Lateral Displacement of MSE Wall Base (a). Variable RPP Spacing (b). Variable Wall Height.....	167
Figure 5-10 Effect of RPP Spacing on Lateral Displacement of MSE Wall Base (a). RPP Size 4x4 inches (b). RPP Size 6x6 inches.....	168
Figure 5-11 Effect of RPP Extension on Lateral Displacement of MSE Wall Base (a). Variable Wall Height (b). Variable RPP Spacing .....	170
Figure 5-12 Effect of Wall Height on Lateral Displacement of MSE Wall Base (a). RPP Size 4x4 inches (b). RPP Size 6x6 inches.....	171
Figure 5-13 Strain Wedge in Uniform Soil (Adapted from Ashour et al., 1998).....	172
Figure 5-14 Schematics of (a). Laterally Loaded Pile (b). Soil Pressure Around Circumference of Pile (c). Variation of Earth Pressure with Displacement (Adapted from Mei et al., 2009 and Ni et al., 2018).....	173
Figure 5-15 Variation of Earth Pressure with Displacement for the First Row of RPP in SR_4x3.....	175
Figure 5-16 Distribution of Lateral Pressure on the First Row of RPP in SR_4x3 .....	176
Figure 5-17 Comparison of Field and Model Lateral Pressure at the Base of the Test Sections (a). First Phase Loading (b). Second Phase Loading .....	178
Figure 5-18 Effect of RPP Spacing on Lateral Pressure Reduction at MSE Wall Base (a). Variable Wall Height (b). Variable RPP Size (c). Variable Foundation Soil Strength ( $c-\phi$ ) .....	180
Figure 5-19 Factor of Safety Versus Lambda ( $\lambda$ ) Plot (Geo Studio, 2020).....	182

Figure 5-20 SLOPE/W Outputs of the Global Factor of Safety.....	185
Figure 6-1 Statistical Analysis Flow for the Model Development.....	188
Figure 6-2 Residuals vs. Fitted Values Plot for the Preliminary Model.....	193
Figure 6-3 Normal Probability Plot for the Preliminary Model.....	194
Figure 6-4 Box-Cox Plot for Transformation of Response Variable ( $\lambda = 0.384$ ).....	196
Figure 6-5 Residuals vs. Fitted Values Plot for the Final Model.....	198
Figure 6-6 Normal Probability Plot for the Final Model.....	199
Figure 6-7 Validation of Final Prediction Model.....	202
Figure 6-8 Residuals vs. Fitted Values Plot for the Preliminary Model.....	207
Figure 6-9 Normal Probability Plot for the Preliminary Model.....	208
Figure 6-10 Residuals vs. Wall Height Plot for the Preliminary Model.....	210
Figure 6-11 Residuals vs. Fitted Values Plot for the Final Model.....	212
Figure 6-12 Residuals vs. Wall Height Plot for the Final Model.....	213
Figure 6-13 Normal Probability Plot for the Final Model.....	213
Figure 6-14 Validation of Final Prediction Model.....	217
Figure 6-15 Flow for the Probabilistic Analysis.....	219
Figure 6-16 Probability Density Function for Lateral Displacement.....	222
Figure 6-17 Cumulative Distribution Function for Lateral Displacement.....	222
Figure 6-18 Probability Density Function for Lateral Pressure Reduction.....	225
Figure 6-19 Cumulative Distribution Function for Lateral Pressure Reduction.....	225
Figure 6-20 Typical Cross-Section of an MSE Wall (Das, 2015).....	227
Figure 6-21 (a). Lateral Displacement and (b). Lateral Pressure Reduction Charts.....	230
Figure 6-22 Flowchart for Calculation of Modified Factor of Safety Against Sliding.....	231
Figure 6-23 MSE Wall Configuration for Calculation Example.....	232
Figure 6-24 Lateral Displacement for the Calculation Example.....	234

Figure 6-25 Lateral Pressure Reduction for the Calculation Example.....	235
Figure 6-26 RPP Reinforcement for Calculation Example.....	236
Figure 6-27 Probabilistic Analysis Charts for Calculation Example (a) Lateral Displacement (b) Lateral Pressure Reduction .....	237
Figure 6-28 Probability Density of Modified Factor of Safety for Calculation Example ..	238

## List of Tables

Table 2-1 Typical Minimum Length of Reinforcement .....	22
Table 2-2 Minimum MSEW Embedment Depths .....	22
Table 2-3 Factor of Safeties Used for MSE Wall Design (Aubeny et al., 2014) .....	26
Table 2-4 Required Gradation for Reinforced Soil (Allan Block, 2016) .....	30
Table 2-5 Unknown Parameters and Equations (Ahmadabadi and Ghanbari, 2009) .....	54
Table 2-6 Results of Uniaxial Compression Tests (Bowders et al., 2003) .....	76
Table 2-7 Results of Four-Point Bending Test (Bowders et al., 2003) .....	77
Table 2-8 Comparison of Flexural Properties of Typical RPP Material with and without Hygrothermal Cycling (Krishnaswamy and Francini, 2000) .....	78
Table 2-9 Cost Per Square Foot of Reinforcement for US-287, I-35 and SH-183 (Rauss, 2019) .....	84
Table 3-1 Geotechnical Drilling Details .....	98
Table 3-2 Particle-Size Distribution .....	106
Table 3-3 USCS Classification of Foundation Soil .....	107
Table 3-4 Layout of RPPs in the Reinforced Test Sections .....	112
Table 3-5 Average RPP Driving Time .....	120
Table 3-6 Performance Monitoring Schedule .....	128
Table 4-1 Settlement Improvement Factor of the Test Sections .....	146
Table 5-1 Properties of the Structural Elements in the FE Model .....	157
Table 5-2 Properties of the Geogrid in the FE Model .....	157
Table 5-3 Properties of the Soil in the FE Model .....	160
Table 5-4 Global Factor of Safety of the Test Sections .....	183
Table 6-1 Correlation Between the Predictor Variables .....	190
Table 6-2 Correlation Between the Lateral Displacement and Predictor Variables .....	191



Table 6-3 Parameter Estimates of the Preliminary Model .....	192
Table 6-4 ANOVA Summary of the Preliminary Model .....	192
Table 6-5 Parameter Estimates of the Final Model .....	197
Table 6-6 ANOVA Summary of the Final Model .....	197
Table 6-7 Summary of Best Subset Selection Method .....	200
Table 6-8 Correlation Between the Predictor Variables.....	204
Table 6-9 Correlation Between the Lateral Pressure Reduction and Predictor Variables.....	205
Table 6-10 Parameter Estimates of the Preliminary Model .....	206
Table 6-11 ANOVA Summary of the Preliminary Model.....	206
Table 6-12 Parameter Estimates of the Final Model .....	211
Table 6-13 ANOVA Summary of the Final Model .....	211
Table 6-14 Summary of Best Subset Selection Method .....	215
Table 6-15 Parameters for Sample Probabilistic Analysis of Lateral Displacement.....	221
Table 6-16 Parameters for Sample Probabilistic Analysis of Lateral Pressure Reduction.....	224
Table 6-17 Range of Input Parameters for the Models.....	239

## Chapter 1

### INTRODUCTION

#### 1.1 Background

Retaining walls are designed to hold soils between two different elevations and support the soil mass laterally. Atkinson (2007) defined retaining walls as structural members that act as a beam with loads acting on either side and are mostly used to stabilize vertical cuts and slopes. Steep cuts are restrained laterally by retaining walls so that more space is saved with the steepness of the slope. The types of retaining wall differ by their load supporting principles and the functions they perform. The materials used in the retaining structure vary from concrete and stone used in gravity type walls to steel and wood used in sheet piling.

Reinforced soil or Mechanically Stabilized Earth (MSE) walls are also widely used to hold steep slopes due to many advantages over the traditional concrete retaining wall. Alzamora and Anderson (2009) defined MSE walls as earth retaining structures that are composite in nature and act integrally to resist lateral pressures. One major benefit of MSE walls is that they can tolerate differential settlements much better than rigid concrete walls due to their flexible nature (Berg et al., 2009). MSE walls were conceived in the 1960s, while the first such wall in the United States was constructed in 1972 (Berg et al., 2009). Due to their increased reliability and economic benefits, MSE walls experienced a considerable rise since the 1970s (Dantal, 2013). Koerner and Koerner (2013) estimated that almost 150,000 MSE walls have been constructed worldwide. Several federal, state, and private projects have used MSE walls over the last three decades due to their dependability, constructability, and cost effectiveness (Mahmood, 2009). 72% of all retaining walls constructed by the Texas Department of Transportation

(TxDOT) from August 2010 to September 2011 were MSE walls (Delphia, 2011), making TxDOT one of the leading transportation agencies in the United States in the application of MSE walls.

As with conventional retaining walls, MSE walls also may experience failure resulting from external or internal stability. Sliding, bearing capacity, overturning, and overall/global stability failures of the MSE wall, which are external stability problems, have been an issue in North Texas over decades (Aubeny et al., 2014). Lateral displacement of the wall occurs, giving rise to sliding failure, when there is insufficient shear strength at the wall base to produce adequate frictional resistance (Das, 2015). A low-budget MSE wall without regard for adequate base shear resistance is certain to slide outwards due to lateral earth pressures (Zaman, 2019). As a consequence, it might affect structures near the base and top of the wall (Schmidt and Harpstead, 2011; Aubeny et al., 2014; Babu et al., 2016). Lateral movement of the wall could cause washout/loss of drainage soil due to wall panel openings, leading to failure of the wall (Alzamora and Anderson, 2009). A case study by Aubeny et al. (2014) investigated the possible causes of failure of two MSE walls along IH 10 in Beaumont, Texas. Forensic analysis, along with field evidence, suggested lateral sliding as the possible cause of wall distress. There have been numerous studies conducted to evaluate the lateral resistance of MSE walls in different conditions (Bell et al., 1983; Jiang et al., 2015; Jiang et al., 2016; Zaman, 2019). However, research on improving the shear resistance of MSE walls have not been conducted on a large scale.

Generally, the resistance against lateral sliding is mainly dependent on the friction between the foundation soil and the wall base (Das, 2015). This friction directly depends on the combined weight of the wall and the backfill soil on the heel of the base, which

provide the normal vertical force (Das, 2015). However, due to lateral pressures higher than the design pressure, along with weak foundation soil, this frictional resistance is not always adequate to resist the sliding of the wall. Few approaches can be considered to improve the sliding resistance such as to increase the weight of the wall or to increase the length of the heel slab (Das, 2015), which is an effective but expensive solution because of the greater amount of concrete required. Some studies have investigated the effect of footing shape, specifically sloped-bottom footing, on increasing the shearing resistance of retaining walls (Horvath, 1991). Another approach is the use of a shear key at the base slab of the wall (Kim and Bilgin, 2007). Shear key provides additional resistance against sliding, due to the passive pressure generated from the soil in front of the key (Das, 2015). This passive earth resistance is directly proportional to the depth of the shear key (Sarath et al., 2011). The use of a shear key can improve the factor of safety against sliding by considerably increasing the sliding resistance of a retaining wall as shown by Sarath et al. (2011). Using a shear key is much more cost-effective compared to the former approaches as well. A shear key is generally incorporated at the base (toe, below stem, heel) of any gravity or cantilever retaining wall to increase the frictional resistance against sliding, which has not been predefined in case of MSE walls. As such, designing a shear key at the base of the MSE wall can considerably improve the resistance against sliding.

Recycled Plastic Pins (RPP) are lightweight materials fabricated predominantly from recycled plastics and other waste materials such as polymers, fly ash, and saw-dust (Chen et al., 2007). RPP is a sustainable material that requires almost no maintenance and is resistant to moisture, corrosion, insects, and rotting (Krishnaswamy and Francini, 2000). Typically, more than 50% of the feedstock used for plastic lumber is composed of polyolefin in the form of high-density polyethylene (HDPE), low-density polyethylene

(LDPE), and polypropylene (PP) (Chen et al., 2007; Khan, 2014). The polyolefin used in the combination acts as an adhesive that helps to combine high melt plastics and additives such as fiberglass and wood fibers within a rigid structure. RPPs have been used successfully in recent years as a shallow slope stabilization technique. The RPPs intercept potential sliding surfaces, thereby providing additional resistance to maintain long term stability of the slope (Khan, 2014). Previous literature (Khan, 2014; Tamrakar, 2015; Sapkota, 2019; Bhandari et al., 2020) have shown the innovative application of RPPs in stabilizing shallow slope failures across North Texas. RPPs have also been recently investigated on their ability to strengthen foundation soil of embankments (Islam et al., 2021a; Islam et al., 2021c) and MSE walls (Badhon et al., 2021).

## 1.2 Problem Statement

A major mode of external failure for MSE retaining walls is the lateral displacement of the wall. When the lateral earth pressure exerted by the retained soil exceeds the frictional resistance between the foundation soil and the wall base, the MSE wall tends to slide outwards. This sliding failure bears a huge maintenance cost for state departments throughout the United States (Aubeny et al., 2014). The outward lateral movement of the wall damages structures both near the base and on the top of the wall. Babu et al. (2016) demonstrated a forensic analysis of a road approach embankment retaining wall and showed that due to the lateral movement of the wall - the road approach embankment separated from the wall, which led to significant distresses on the flexible pavement. Generally suggested solutions to improve the lateral resistance of a retaining structure consists of either increasing the weight of the wall, increasing the length of the heel slab, or using wall anchors and helical tiebacks, which are all expensive. On the other hand, incorporating a shear key at the wall base helps in improving the sliding resistance of the wall which significantly increases the factor of safety against sliding (Sarath et al., 2011).

However, for MSE retaining structures, incorporating a shear key is challenging due to the following limitations.

- Since a shear key is constructed from concrete, using it for an MSE wall will become very expensive.
- With a concrete shear key, the problem of corrosion due to moisture is inherent.
- The rigid nature of concrete undermines the most important feature of an MSE wall which is the flexible nature of its base.

This poses a limitation in the current state of knowledge and practice regarding sliding resistance of MSE walls.

Therefore, an innovative and cost-effective method of controlling the sliding failure of an MSE retaining structure is needed. A possible solution could be using recycled plastic pins as shear keys. The success of RPPs in providing sufficient lateral support to sliding soil mass in slopes could be imitated in an MSE wall to deliver the required lateral resistance against sliding force from the retained backfill. The concept of the research, as shown in Figure 1-1, is to utilize RPPs to provide additional passive force to resist the active lateral pressure from the backfill. The pins are thus expected to improve the shear resistance of the MSE wall base. Khan (2014) demonstrated the successful use of RPPs in reducing the lateral movement of a concrete retaining wall when driven into the ground in front of the wall. Furthermore, a preliminary study was conducted by Zaman (2019) to experiment the use of RPPs in controlling the sliding failure in MSE walls. The author reported that the method could produce approximately 84% reduction in the lateral displacement of MSE wall base. As the RPPs are made from recycled plastics, they are highly cost-saving when compared to concrete (Chen et al., 2007). They are comparatively flexible in nature and require almost no maintenance. RPPs are

lightweight, less susceptible to chemical and biological degradation, and resistant to moisture (Krishnaswamy and Francini, 2000). Apart from the structural benefits, the use of RPP reduces the waste volume entering the landfill and provides additional market for recycled plastic (Loehr et al., 2000).

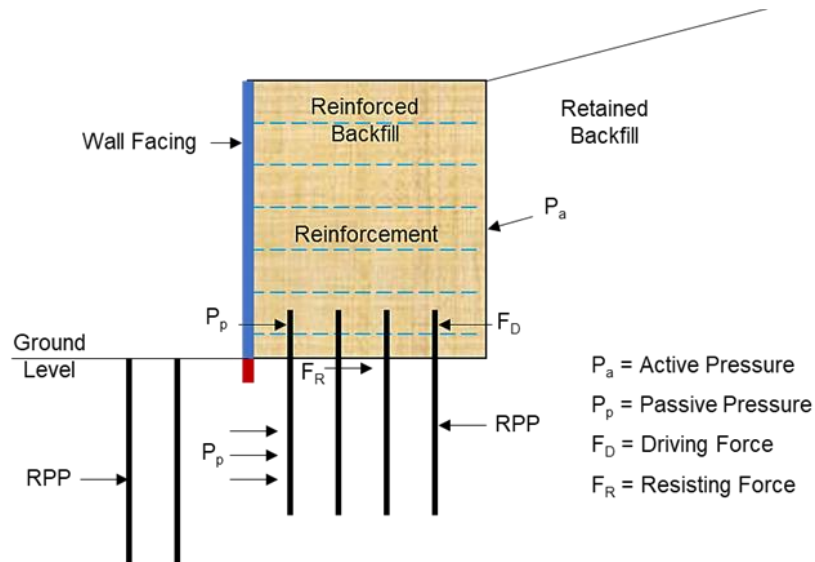


Figure 1-1 A Typical MSE Wall with RPPs as Shear Keys

### 1.3 Research Objectives

The main objective of the study is to investigate the effectiveness of recycled plastic pins in increasing the lateral stability of MSE wall system. Additionally, the effect of different sizes and spacings of RPP will be evaluated in order to determine the optimum design for improving the shear capacity of an MSE retaining structure. The specific tasks to achieve the objective of the study include:

1. Reconnaissance of a specific site for the field scale study.
2. Site investigation of the selected site.
3. Preparation of layout for the field test sections.

4. Field installation of RPPs and construction of test sections.
5. Instrumentation of the constructed test sections for performance evaluation.
6. Regular performance monitoring of the RPP reinforced MSE wall system.
7. Analysis of the field data for evaluating the effectiveness of using RPPs.
8. Finite element numerical modeling of the field test sections to conduct parametric studies.
9. Development of a design methodology for constructing MSE walls with RPPs as shear keys.

#### 1.4 Dissertation Organization

The dissertation is organized into seven chapters. The summary of each chapter is presented as follows:

Chapter 1 presents the background, problem statement, and research objectives of the current study. The contents of each chapters are also summarized.

Chapter 2 summarizes the literature on past studies conducted in the field of MSE retaining walls. The chapter starts with general information about MSE walls, including their benefits, construction process, and design criteria. Then, the factors affecting the performance of such walls are discussed. Previous studies conducted on the lateral resistance, vertical settlement, and global stability of MSE walls are explained. A brief overview on the improvement of lateral resistance using other conventional techniques is presented. The properties and past studies on the effective use of RPPs are also discussed. Finally, the limitations of previous studies are outlined establishing the importance of the current study.



Chapter 3 focuses on the field activities carried out under this study. A brief description of the project site is given followed by the site investigations performed. The laboratory tests conducted on the soil samples are discussed. The reinforcement mechanism of using RPPs as shear keys at the wall base is explained. Then, layout and design of the field test sections are presented. Later, the RPP installation along with construction of field test sections are shown. Subsequently, the process of instrumentation for the performance monitoring is elucidated. Finally, the regular performance monitoring plan is tabulated.

Chapter 4 presents the field monitoring results of the test sections. Vertical inclinometer, horizontal inclinometer, and pressure plate data are presented for all the four test sections. The results of the RPP reinforced sections are compared with the results of the control section. Subsequently, the effectiveness of the RPP reinforcement mechanism is also estimated quantitatively. Relevant comparisons with previously published literature have also been presented for each instrumentation monitoring.

Chapter 5 describes the finite element modeling conducted for the study. This chapter presents the steps involved in the model calibration and validation. Parametric studies were conducted on the effects of varying foundation soil strength, RPP parameters, and MSE wall height. The reduction in lateral pressure due to RPPs have been estimated numerically using the calibrated model. Lastly, the global stability of the field test sections was evaluated using limit equilibrium methods. The aim was to quantify the improvement in global factor of safety due to RPPs.

Chapter 6 depicts the statistical analysis conducted on the results of the numerical study. Multiple linear regression analyses were conducted to develop prediction models for lateral displacement and lateral pressure reduction factor for RPP reinforced MSE walls.

Probabilistic analyses on the uncertainty of foundation soil strength were studied and presented in this chapter. A modified factor of safety against sliding was formulated for the RPP reinforced walls. Finally, the steps for incorporating RPPs at the wall base are outlined with a design/calculation example.

Chapter 7 summarizes the major conclusions from the field monitoring results, numerical study, statistical analysis, and design methodology. Finally, recommendations for further studies are presented.

## Chapter 2

### LITERATURE REVIEW

#### 2.1 Introduction

Highways, power grids, communication networks, and water pipe systems are all crucial infrastructure systems for modern cities and societies. In spite of their importance, the condition of these infrastructure networks in the United States is inadequate. The infrastructure system of the United States received a C- score from the American Society of Civil Engineers which corroborates this statement (ASCE, 2021). Therefore, research into infrastructure repair and restoration is extremely important. There is an expanding body of literature on the restoration of electrical grids (Shahidehpour et al., 2016), communication networks (Sterbenz et al., 2010), and water pipe networks (Pudasaini et al., 2017; Pudasaini and Shahandashti, 2018; Shahandashti and Pudasaini, 2019; Pudasaini and Shahandashti, 2020) that demonstrates the significance of such studies. Highway system rehabilitation has received a major consideration from researchers because of its importance. A major component of an efficient highway system is a retaining structure which plays a crucial factor in highway designs.

Retaining walls can be defined as structural members that act as a beam with loads acting on either side and are mostly used to stabilize vertical cuts and slopes (Atkinson, 2007). Steep cuts are restrained laterally by retaining walls so that more space is saved with the steepness of the slope. They are used to bound soils between two different elevations. The types of retaining wall differ by their load supporting principles and the functions they perform. The materials used in the retaining structure vary from concrete and stone used in gravity type walls to steel and wood used in sheet piling. Steel-reinforced concrete is used mostly for cantilevered walls. Reinforced soil or Mechanically

Stabilized Earth (MSE) walls are also widely used to hold steep slopes due to the many advantages over traditional concrete retaining wall, which will be discussed in detail in following sections. One major benefit of MSE walls is that they can tolerate differential settlements much better than rigid concrete walls, due to their flexible nature (Berg et al., 2009). MSE wall was introduced in the 1960s, while the first such wall in the United States was constructed in 1972. Since then, the use of MSE walls has been widely adopted by different state agencies.

## 2.2 Benefits of MSE Wall

Alzamora and Anderson (2009) defined MSE walls as earth retaining structures which are composite in nature and act integrally to resist lateral pressures. Conventional retaining walls have seen a gradual replacement over the years by the more flexible MSE walls. One of the most important advantage of MSE walls over traditional reinforced concrete and concrete gravity walls is the potential to withstand differential settlements due to poor subgrade condition. Berg et al. (2009) estimated a cost saving of more than 50 percent for MSE walls with poor subgrade condition, as the cost for improvement of poor foundation is eliminated. Due to the control in differential settlements, the common problem of cracks in surface and facing panels is also reduced by a large factor. Also, MSE walls have proven to be much more stable in seismically active zones than the conventional rigid concrete retaining structures. Other benefits of MSE walls are described as follows:

### Design

1. As the MSE walls are flexible enough to withstand differential settlements, they do not require rigid and unyielding foundation.
2. They can hold steep to vertical slopes, thereby, removing the need for any right-of-way acquisition which bears a considerable cost.

3. They are technically feasible to heights over 100 ft. (30 m). The increasing limitations in right-of-way and space have given rise to design and construction of MSE walls over 20 m (Sankey and Soliman, 2004).

#### Construction

4. The construction process is relatively simple, fast and cost-effective.
5. Use of heavy equipment and skilled craftsmen is not required, thus, reducing the overall project cost.
6. Site preparation prior to construction is comparatively less. Also, the space required for construction is rather less compared to traditional concrete retaining walls.

#### Aesthetics

7. The aesthetics of the wall can be improved with various options for the wall facing. Precast concrete panels with assorted shapes, sizes, colors and textures are readily available, with options for custom-design as well. Also, geogrid-wrapped and wire-mesh facings can be planted with vegetation, which will blend with the surrounding site environment.

As pointed above, MSE walls have shown their advantages both during the design and construction phases. It can be stated that these benefits substantially reduce the cost and time schedule throughout the project timeline. Apart from the above-mentioned conveniences of MSE walls, they have been reported to be effectively used as structural elements in excavation stabilization as well (Christopher et al., 1990).

One potential disadvantage that could be associated with reinforced soil walls are that they require a certain type of granular fill, which may be uneconomical in some projects due to huge transportation costs. Also, the excavation required behind the wall face to

install reinforcements may be relatively large. An important conception related to MSW walls is that the design responsibility is distributed between the material suppliers and owners (Berg et al., 2009). The reinforced zone cannot be used for installing or repairing utilities, as it should not be dug due to potential damage to reinforcements.

### 2.3 Elements of MSE Wall

The MSE wall is a unit comprising of various components/elements with specific functions. Figure 2-1 shows the different elements of an MSE wall. The four major components are:

- i. Wall Facing
- ii. Reinforcement Material
- iii. Reinforced Backfill Soil
- iv. Retained Backfill Soil

Each component has a particular role to play in the overall stability of the wall. The wall facing is constructed in front of the reinforced backfill soil. The major role of wall facing is to hold the backfill soil in place and to prevent it from getting out between reinforcements. They generally do not have structural function and are merely used as a boundary for the structure which control the aesthetics of the wall (Berg et al., 2009). Wall facing can be made of precast concrete panels, which is the most commonly used material in MSE walls on public roads (Alzamora and Anderson, 2009). Other widely used facing materials are dry cast modular blocks, shotcrete, gabions, welded wire mesh, metal sheets and plates, wrapped sheets of geosynthetics, and wood lagging and panels. Reinforcements are placed horizontally behind the wall facing at pre-specified heights in accordance with the lift height of reinforced backfill soil. The major function of reinforcement material is to strengthen the backfill soil, so it can be regarded as a critical component in determining the stability and effectiveness of MSE wall. Reinforcement materials are both metallic,

such as mild steel, and non-metallic (polyester or polyethylene comprising polymeric materials).

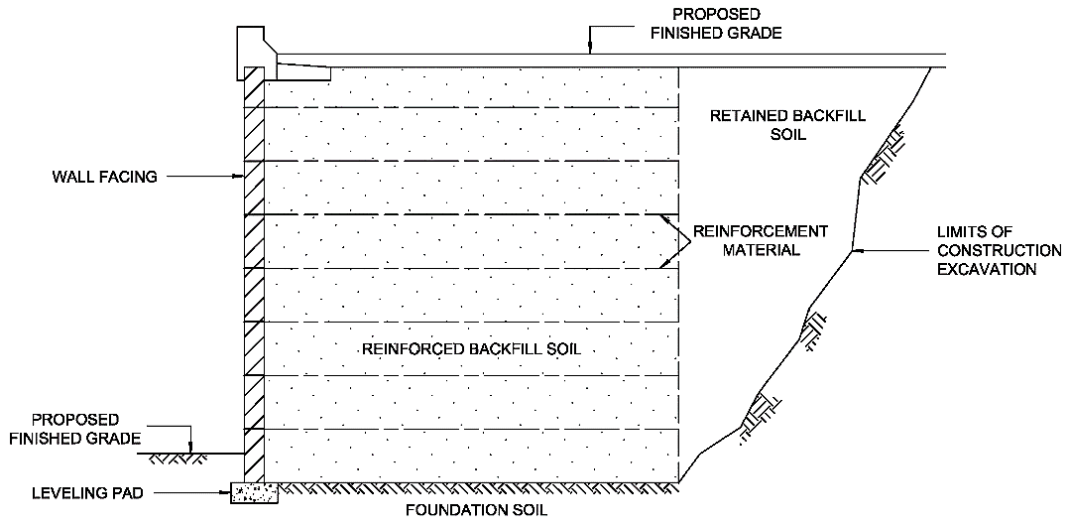


Figure 2-1 Typical Section of MSE Wall

The backfill material immediately after the facing panels is known as reinforced backfill soil. The reinforced backfill is compacted to required density in pre-specified lift thickness. The construction of MSE wall is carried out in lifts with the block facing being placed with each layer of reinforced backfill. Various agencies have different specifications for the reinforced backfill as its quality plays a significant role in the durability and constructability of the wall. High quality, well graded granular materials are required to ensure proper drainage of water from the backfill (Berg et al., 2009). The retaining property of most of the MSE walls depend on friction between reinforcement materials and the corresponding fill soil. Thus, granular materials with high friction characteristics are needed in such cases. Better durability conditions for the metallic reinforcements also give way for the use of less reinforcements. The retained backfill is the soil placed between the mechanically stabilized backfill zone and the existing ground soil.

## 2.4 Construction of MSE Wall

The incorporation of materials to reinforce existing soil has been followed since primitive times. Throughout human history, straws, sticks, branches, wooden pegs and bamboo to name a few, were used to stabilize soil. The reinforcement techniques gradually evolved with time. French architect and engineer Henri Vidal, in 1966, studied about reinforced earth using a system of long closely-spaced 100 mm wide steel strips which were attached to a metallic facing and extending back into the soil delivering frictional resistance (Vidal, 1966, 1969b, 1970). Following his research, modern reinforced earth system, or MSE wall, was developed. Berg et al. (2009) reported that the first MSE wall built in the United States was on California State Highway 39, northeast of Los Angeles in 1972. Due to the increased reliability and economic benefits, MSE walls experienced a considerable rise since the 1970's. Koerner and Koerner (2013) estimate that almost 150,000 MSE walls have been constructed worldwide.

The construction sequence of MSE walls can be differentiated according to the type of panel facing, i.e., precast panel facing or flexible facing.

### 2.4.1 *MSE Wall with Precast Panel Facings*

#### Preparation of subgrade

The ground where the wall is to be erected, is cleared of all vegetation, organic matter, slide debris and other uneven materials. The ground is then compacted to make it level, with ground improvement necessary for unstable foundation conditions. Foundation soil with high swell potential could be stabilized using chemical treatments (Gautam et al., 2020).



#### Placement of leveling pad

A generally unreinforced concrete pad is constructed as a guide for erecting facing panels. The leveling pad does not act as a structural foundation support. The sizes might differ according to the type of facing panel, with wider concrete pads recommended for modular block units.

#### Construction of the first row of facing panels

The first row of facing panels is erected on the leveling pad simultaneously with the placement of soil backfill. The first row of panels might be full, or half-height, depending upon the type of facing. The first level is generally braced for maintaining stability and alignment, while other successive rows are just wedged and clamped to adjacent panels.

#### Placement and compaction of reinforced wall fill to the level of reinforcement

The backfill soil in the reinforced zone is placed in uniform loose lift of thickness not exceeding 12 in. (300 mm). The fill is then compacted to the specified density, generally 95 to 100 percent of AASHTO T-99 maximum density. The compaction moisture contents are suggested to be on the dry side of optimum condition. The fill should be dumped into or parallel to the rear and middle of the reinforcement and bladed toward the front face. The placement and compaction of retained backfill soil should be carried out simultaneously with the reinforced zone.

#### Placement of the first layer of reinforcement materials

The reinforcing elements are placed over the compacted fill and connected, generally perpendicular, to the facing panels.

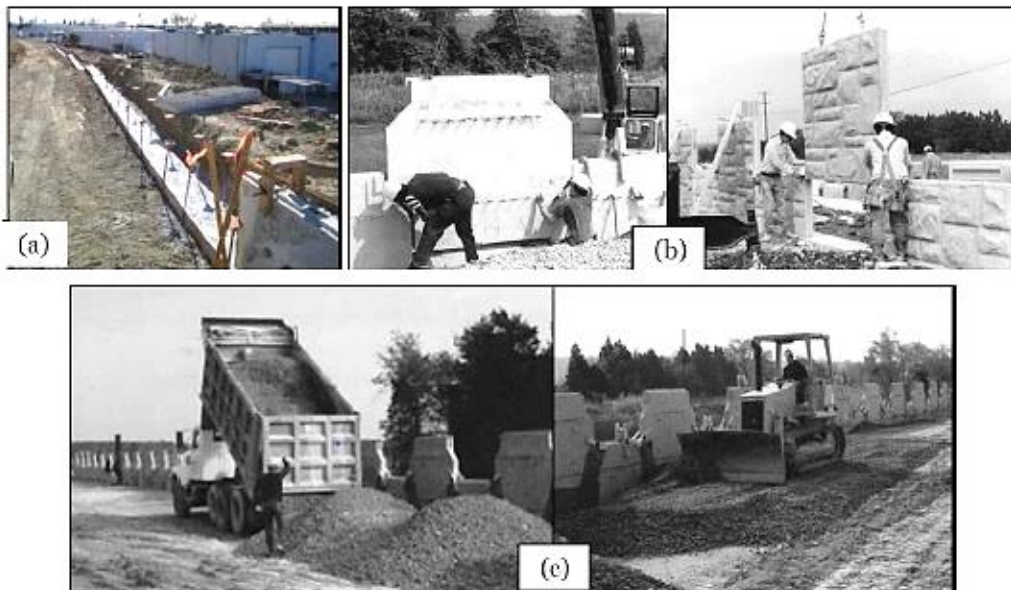
Continuation of backfill placement and compaction along with placement of reinforcements

The steps outlined above are repeated until the wall reaches its designed height.

Construction of traffic barriers and copings

After the erection of the final row of facing panels along with completion of fill to the final grade, traffic barriers and other appurtenances are constructed.

Figure 2-2 shows the construction sequence of MSE walls with precast panel facings.



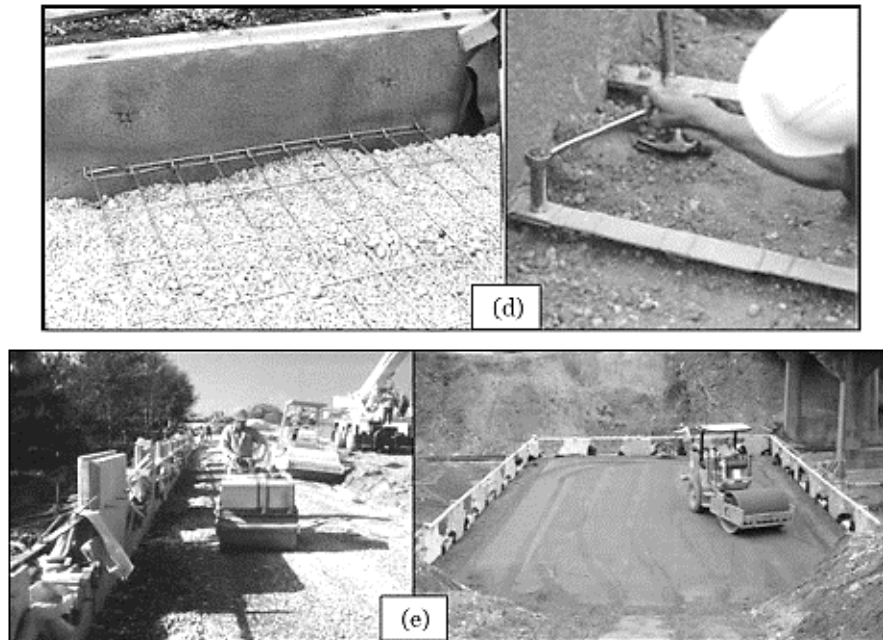


Figure 2-2 Construction Sequence of MSE Wall with Precast Panel Facing (a). Leveling Pad (Passe, 2000) (b). Erection of Precast Panel (c). Spreading of Fill Material (d). Placement and Connection of Reinforcement (e). Compaction of Reinforced Fill Material (Berg et al., 2009)

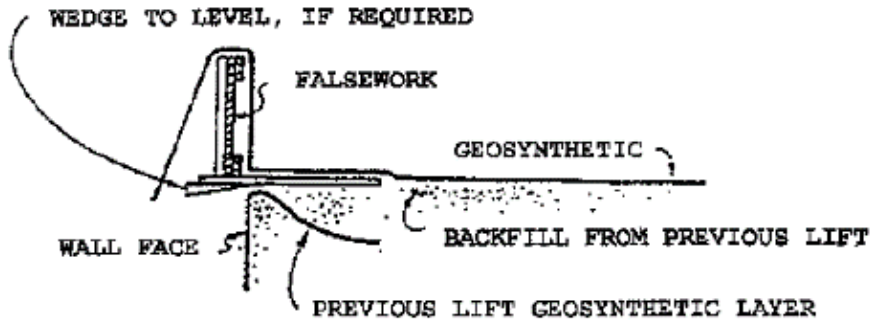
#### 2.4.2 MSE Wall with Flexible Facings

These types of walls have the reinforcement material itself extended as the facing element. The construction sequence is similar to that of walls with precast panel facings, however, only a level grade is required for erecting the first level of facing element. The flexible facing types include welded wire mesh, geotextiles, geogrids or gabions.

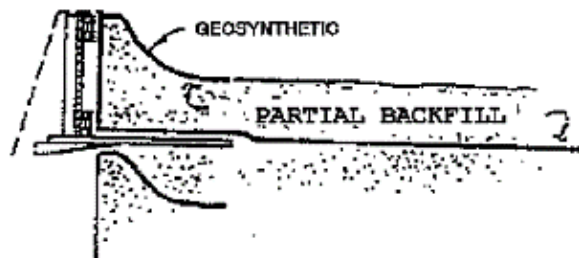
An exception to the construction schedule is the way the first reinforcing layer is placed. Reinforcement with anisotropic strength properties (i.e., many geosynthetics) have to be positioned such that the principal strength direction is perpendicular to the face of the wall. Pins should be used to secure reinforcement to prevent movement while laying the

fill. The adjacent sheets should be overlapped a minimum of 6 in. (150 mm) along the edges perpendicular to the face. The edges of geogrid or wire mesh reinforcement can be tied or butted and clipped together.

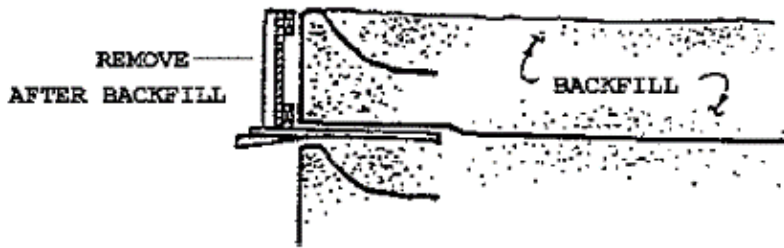
Face forms should be used to place the geosynthetic layers, with form holders placed at the base of each layer (at approximately 4 ft. horizontal intervals) acting as temporary support of face forms. Figure 2-3 illustrates this placement technique. The supports ensure attainment of good compaction. In the case of geogrids and wire mesh, a geotextile or hardware cloth may be required to hold the wall fill material at the face. A hand-operated vibratory compactor is suggested to compact wall fill within 3 ft. (~ 1 m) of the wall face. In some cases, shotcrete is also applied over the flexible facing.



(1) PLACE FALSEWORK AND GEOSYNTHETIC ON PREVIOUS LIFT



(2) PLACE/COMPACT PARTIAL BACKFILL AND OVERLAP GEOSYNTH



(3) PLACE/COMPACT REMAINDER OF BACKFILL LIFT

Figure 2-3 Lift Construction Sequence of MSE Wall with Flexible (Geosynthetic) Facing

### 2.5 Design Overview of MSE Wall in the United States

MSE walls are generally designed as a soil mass with discrete soil reinforcement modeled as tension inclusions. The fundamental methodology used for design is known as the Simplified Method, which was first established as an allowable strength design (ASD) method. This method was then updated later to the current load and resistance factor design methodology. The Simplified Method is widely used for transportation walls that are generally near vertical in batter, have uniform soil reinforcement lengths, and use a select granular reinforced soil fill. This design procedure does not consider the wall facing element as a contributor to the internal stability of the reinforced mass. However, AASHTO (2014) and GEC 11 (2009) provide guidance for factoring deep facing elements into external stability analysis, significantly battered walls, and non-uniform reinforcement length into design.

In terms of reinforcement material type, the Simplified Method can be applied to steel strip, steel mat, geogrid, and geotextile soil reinforcements. As of now, neither AASHTO (2014) nor GEC 11 (2009) provide design guidelines for the use of geosynthetic strap reinforcements.

On the other hand, FHWA has developed an approach for designing closely spaced geosynthetic reinforced soil walls based upon composite action (FHWA, 2011a). It considers the reinforced soil and reinforcements as a composite mass. Lately, this method has been used for design of abutments supporting bridges and has also been integrated into design of generally single span bridges.

## 2.6 Design Criteria of MSE Wall

Design practice or codes such as contained in Article 11.10 of 2007 AASHTO LRFD Specifications for Highway Bridges govern the performance criteria for MSE walls with respect to design requirements. These requirements consider load and resistance factors with respect to various failure modes and materials, and for various limit states. Performance criteria are both site and structure-dependent. Structure-dependent criteria consist of safety factors or a consistent set of load and resistance factors as well as tolerable movement criteria of the specific MSE structure selected. The following site-specific project criteria need to be established during the start of design:

- Design limits and wall height: The type of structure and external loading configurations can be determined only after establishing the length and height of the wall required to meet project geometric requirements.
- Alignment limits: As alignments vary with batter of wall system, the horizontal (perpendicular to wall face) limits of bottom and top of wall alignment must be fixed. The alignment constraints may limit the type and maximum batter of the wall facing, particularly with Modular Block Wall (MBW) units.
- Length of reinforcement: A minimum reinforcement length of  $0.7H$ , 'H' being height of the wall, is recommended for MSE walls. Structures subjected to surcharge loads, or where foundation conditions affect lateral sliding and/or global/compound slope

stability, require longer lengths of reinforcement. Table 2-1 shows the minimum length of reinforcement required for different cases.

Table 2-1 Typical Minimum Length of Reinforcement

Case	Typical Minimum L/H Ratio
Static loading with or without traffic surcharge	0.7
Sloping backfill surcharge	0.8
Seismic loading	0.8 to 1.1

Source: GEC 11

- External loads: Soil surcharges required by the geometry, adjoining footing loads, traffic loads, and impact load from traffic are all considered as external loads. As outlined in Article 3.11.6.4 (AASHTO, 2007), the magnitude of the minimum traffic loads is a uniform load equivalent to 2 ft. (0.6 m) of soil over the traffic lanes.
- Wall embedment: The minimum depth of the top of the leveling pad from the finished grade should be dependent on bearing capacity, settlement, and global stability considerations. Table 2-2 shows the recommended minimum embedment depths according to current practice based on local bearing considerations.

Table 2-2 Minimum MSEW Embedment Depths

Slope in Front of Wall	Minimum Embedment Depth to Top of Leveling Pad*
All Geometries	2 ft. minimum
Horizontal (walls)	H/20
Horizontal (abutments)	H/10
3H:1V	H/10
2H:1V	H/7
1.5H:1V	H/5

Slope in Front of Wall	Minimum Embedment Depth to Top of Leveling Pad*
* Minimum depth is the greater of applicable values listed, frost depth, or scour depth.	

Source: GEC 11

Higher values of embedment may be required on foundation soils susceptible to considerable shrinkage and swelling, seismic activity, and/or scour. Also, required embedment depth may increase based on bearing capacity, settlement, and/or global stability calculations. A minimum horizontal bench 4 ft. (1.2 m) wide as measured from the face should be provided in front of walls founded on slopes. The bench may be formed, or the slope continued above that level (AASHTO, 2007) (Figure 2-4). The function of the horizontal bench is to provide resistance against general bearing failure and, to provide access for maintenance inspections (AASHTO, 2007).

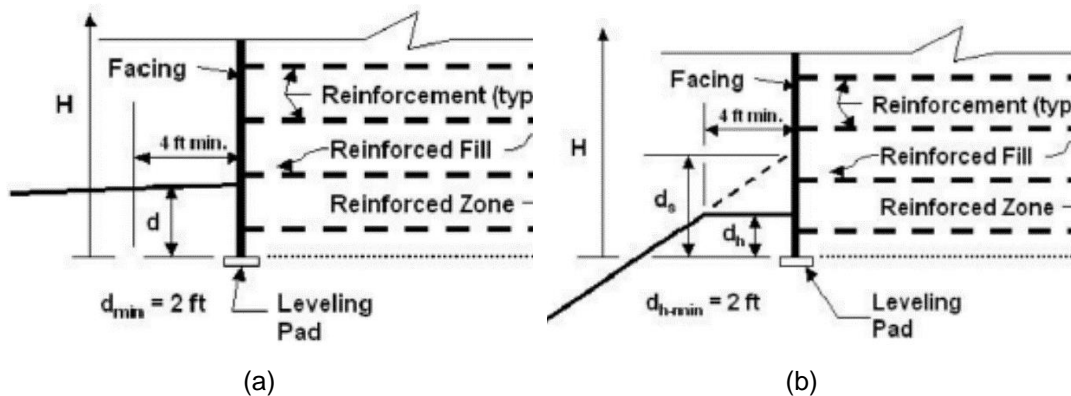


Figure 2-4 Requirement of MSE Wall Embedment Depth

(a). Level Toe Condition (b). Benched Slope Toe Condition

## 2.7 External Stability of MSE Wall

Consideration should be given to the different possible external failures while designing MSE walls. Proper geometries should be determined to prevent the possible external



failures. As done with traditional retaining structures, four types of potential external failure mechanisms are usually taken into consideration (Figure 2-5) as follows:

- ❖ Base Sliding
- ❖ Overturning
- ❖ Bearing Capacity Failure
- ❖ Overall/Global Stability (Deep Seated Stability Failure)

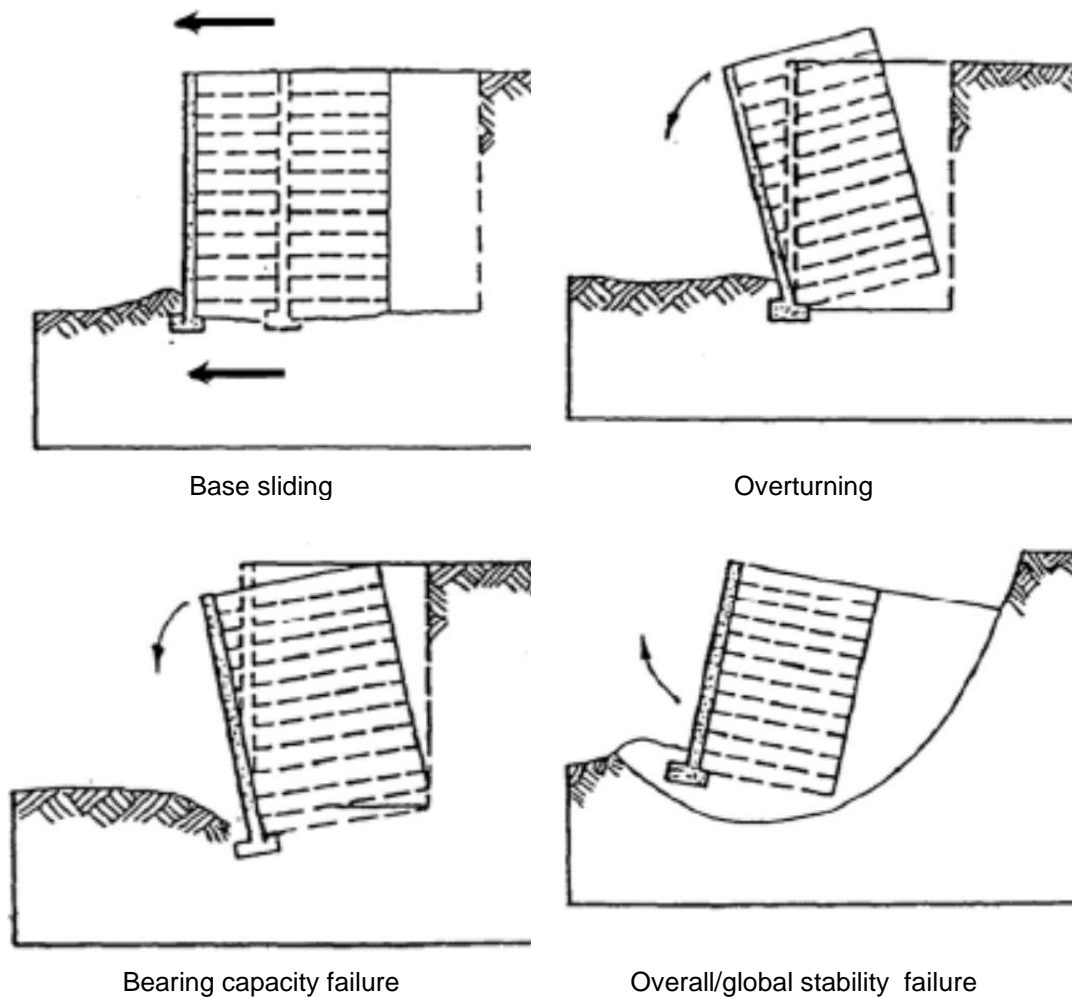


Figure 2-5 Potential External Failure Mechanisms of a MSE Wall (Elias et al., 2001)

According to FHWA, the same external stability guidelines that are followed for conventional rigid retaining walls (gravity and cantilever walls) can be adopted for MSE walls as well. Elias et al. (2001) reported that it is “justified” to follow these external stability guidelines for MSE walls.

### 2.7.1 Sliding and Overturning

Limit equilibrium method has been reported as an appropriate method for the sliding analysis which completely satisfies the equilibrium assumption (Leshchinsky and Han, 2004). Although the methods of checking sliding and overturning have been widely accepted, there are disagreements or concerns on the reliability of factor of safety calculated for sliding and overturning. Since soil is heterogenous, an uncertainty or risk is involved in the FS calculations due to the variable soil properties. Chalermyanont and Benson (2005) published a study showing the influence of highly variable properties of backfill soil on the calculated factor of safeties. Table 2-3 presents the FOSs used by TxDOT and other agencies. The following equation can be used to calculate the factor of safety against sliding for a retaining wall:

$$F.S. = \frac{\gamma_r HL \tan(k\phi')}{qHK_{of} + 0.5\gamma_f H^2 K_{of}}$$

Where,

$\gamma_r$  = Unit weight of the reinforced soil

H = Height of the wall

L = Width of the foundation

$\phi'$  = Friction angle of the reinforced soil

q = Surcharge

$\gamma_f$  = Unit weight of the fill soil

Table 2-3 Factor of Safeties Used for MSE Wall Design (Aubeny et al., 2014)

Failure Mode	TxDOT	WisDOT (WisDOT, 2006)	CalTrans (CalTrans, 2004)
Sliding	FOS $\geq$ 1.5	1.5 for spread footing on soil or rock and 1.0 for pile footings	1.5
Overturning	FOS $\geq$ 2.0	1.3 (Global)	1.5
Bearing Capacity	FOS $\geq$ 1.3 (Global)	1.5 for footings on pile or rock 2.0 for footings on soil	3.0
Eccentricity, e	$e < L/6$ (middle third)	N/A	$e < L/6$ (on soil) $e < L/4$ (on rock)
Pullout	FOS $\geq$ 1.5	1.5	1.5

### 2.7.2 Bearing Capacity

The theory of bearing capacity was formulated by Terzaghi in 1943. Berg et al. (2009) represented the mechanism of bearing capacity as shown in Figure 2-6. When a rigid footing is used, punching failure may occur due to compression of the soil under the footing. This is accompanied by development of vertical shear at the edge of the footing. Heaving may occur at a certain distance from the footing edge; however, it may not be seen at the footing edge. A reasonably large settlement indicates the ultimate bearing capacity failure. As proposed by Terzaghi, the following equation can be used to calculate the ultimate bearing capacity:

$$q_u = cN_c + \gamma D_f N_q + \frac{1}{2} \gamma B N_\gamma$$

Where,

$q_u$  = Ultimate bearing capacity

$c$  = Cohesion of foundation soil

$N_c, N_q, N_\gamma$  = Bearing capacity factors

$\gamma$  = Unit weight of foundation soil

$D_f$  = Embedment factor for foundation

$B$  = Width of footing

The above-mentioned equation by Terzaghi was formulated based on Prandtl's theory for plastic failure of metal under rigid punching. However, the base of an MSE wall is relatively flexible, therefore, precise predictions of bearing capacity for MSE walls cannot be expected using Terzaghi's equation. The equation would produce a rather conservative result. Many studies have been performed to unify the global stability and bearing capacity analyses to overcome this limitation; however, no breakthrough has been accomplished till date (Aubeny et. al., 2014).

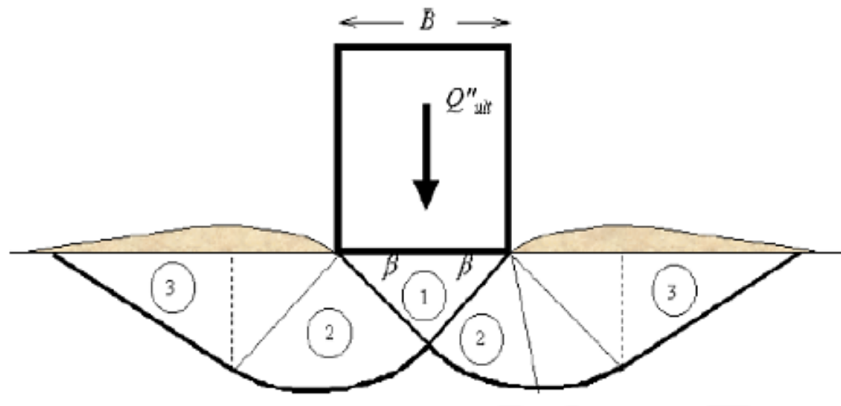


Figure 2-6 Ultimate Bearing Capacity of Rigid Footing

The conventional approach to construct an MSE wall involves the use of a concrete leveling pad at the base of the facing. However, the surcharge is placed on the other side

by backfill soil. The current equation by Terzaghi does not consider the effect of surcharge and associated potential failure patterns. One approach to improve the bearing capacity of the MSE wall foundation could be to increase the width of the wall base/foundation. This can be done by increasing the length of the reinforcement at the wall base, thereby, increasing the width of the reinforced zone. It has been shown by previous studies that an MSE wall undergoing bearing capacity failure will exhibit rotation about the toe. This increases the chances of the reinforced zone separating from the retained zone. Aubeny et al. (2014) reported that the bearing capacity failure of an MSE wall will not lead to punching failure; instead, the wall movement will be dominated by rotation due to the constant lateral force.

### *2.7.3 Global Stability*

An overall or global stability analysis is needed for MSE walls to investigate the rotational or compound failure mechanisms which are relatively different than simple sliding and overturning analysis. It is even more required for complex MSE walls constructed on steep slopes, weak soils, and/or tiered wall sections. It helps to distinguish probable failure planes through the wall system in cases when the reinforcement specifications are insufficient.

Commercially available software following limit equilibrium and finite element methods such as Geostudio SLOPE/W, GSTABL, and PLAXIS can be used to model MSE walls and perform global stability analysis. A minimum global factor of safety of 1.3 may be adequate for simple MSE walls. However, this factor may be increased to a minimum of 1.5 for critical walls such as those retaining bridge abutments as stated by AASHTO.

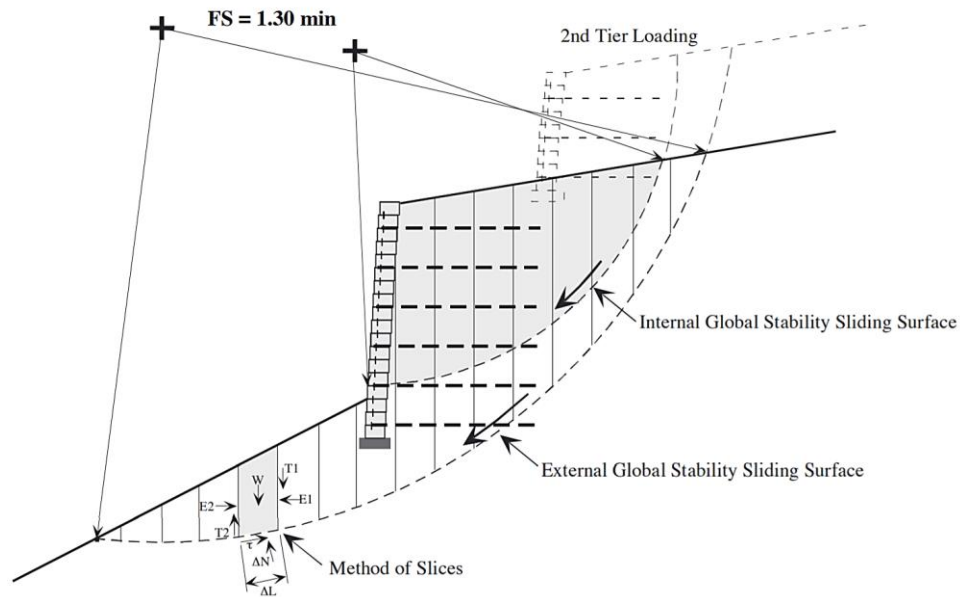


Figure 2-7 A Typical Section of MSE Wall for Global Stability Analysis (Keystone, 2003)

As per previous studies, global stability analysis should be more focused for some critical conditions such as:

- i. Walls with slopes below or above.
- ii. Walls built in sites with clays, silts, poorly graded sands, expansive clays and/or soils with a PI greater than 20 and or a LL greater than 40.

For walls with global stability concerns, it is common practice to increase the stability by (Allan Block, 2016):

- i. Increasing the length of the reinforcement layers to force the minimum slip arcs deeper into the hillside, where they will encounter stronger soils.
- ii. Increasing the depth of buried block to force the minimum slip arcs deeper into the hillside.

- iii. Using reinforcement layers with high strength and mechanical properties to force the minimum slip arcs deeper into the hillside.
- iv. Increasing the friction angle of the reinforced soil will increase the soil's shear resistance which will increase overall stability.
- v. The reinforced soil must meet or exceed the designed friction angle. It must be free of debris and consist of one of the following inorganic USCS soil types: GP, GW, SW, SP, GP-GM or SP-SM meeting the following gradation (Table 2-4) as determined in accordance with ASTM D6913.

Table 2-4 Required Gradation for Reinforced Soil (Allan Block, 2016)

Sieve Size	Percent Passing
1 in. (24 mm)	100-75
No. 4 (4.75 mm)	100-20
No. 40 (0.425 mm)	0-60
No. 200 (0.075 mm)	0-35

- v. Foundation soil improvements may be done when weak foundation soil can be the main cause of global instabilities.
- vi. Steep slopes in the vicinity of MSE walls can be stabilized through other sustainable methods such as with the use of RPPs (Bhandari et al., 2020) or vegetation (Islam and Badhon, 2020; Islam et al., 2021b).

## 2.8 Factors Affecting Performance of MSE Walls

There are many factors that affect the performance or design of MSE walls. All the elements in an MSE wall play an important role in determining the end performance and stability of the wall. Mirmoradi and Ehrlich (2016) evaluated the effect of different wall parameters on the distribution of reinforcement load in reinforced walls, using both

laboratory-scale model and FE analysis. The main finding was that the combined effect of the considered parameters (facing and reinforcement stiffness, toe resistance and height) on the distribution of the maximum reinforcement load with depth may be limited to approx. 4 m (~13 ft.) above the base of the wall. For high walls, the wall height has a stronger effect than facing stiffness on the distribution of reinforcement load. Some other factors affecting the wall performance are explained in this section as follows:

#### *2.8.1 Effect of Reinforcement Type*

Bilgin and Mansour (2014) studied the effects of different reinforcement types on the design reinforcement length of MSE walls. The types of reinforcement in the study were geogrids, geotextiles, metal strips, and metal bar mats. A major finding was that the conventional rule of  $0.7H$  as the minimum length of reinforcement required ('H' being the height of wall), could be reduced to as much as  $0.5H$ . The bearing capacity of foundation soil does not generally govern the reinforcement length unless the soil is relatively weaker. Metal strips usually require the longest lengths, while metal bar mats need the shortest lengths. It was found that the reinforcement type has more significance when the wall height is low.

#### *2.8.2 Effect of Reinforcement Stiffness*

A study was undertaken by Pierson et al. (2011) to study the effect of geogrid stiffness on lateral resistance of cast-in-place shafts and MSE wall facing deflections. A field-scale MSE wall, 6.1m tall and 45m long, was constructed with eight 0.9m diameter cast-in-place shafts within the reinforced fill. The shafts were spaced various distances from the wall facing. The wall facing consisted of dry cast modular blocks. The geogrid was cut for the shaft to go through it. A hydraulic cylinder was used for loading and the shafts were loaded up to a desired displacement. Photogrammetry was used to monitor the wall



facing displacement. Finite difference method, using FLAC3D, was used for conducting a parametric study on the effects of geogrid properties to the lateral resistance of shafts. Mohr-Coulomb was used as the soil constitutive model. Although a continuous material was used for the wall facing initially, parametric studies later signified the importance of wall facing to the wall performance. Thus, the final model used discrete modular blocks for the facing. The study revealed that care should be given while selecting the soil-geogrid interaction coefficients. The following relation was used to estimate the geogrid to soil interface friction angle ( $\delta$ ):

$$C_i = \frac{\tan(\delta)}{\tan(\theta)}$$

Where, coefficient of geogrid interaction ( $C_i$ ) is an estimated value between 1.0 to 0.68. The study found that a reduced coefficient of geogrid interaction reduces the lateral load at the shaft for the same displacement. The wall facing also showed less movement for a given shaft displacement with a higher geogrid coefficient of interaction. The typical geogrid stiffness reduction for the weak direction (plane parallel to the wall facing) is 1/10<sup>th</sup> of the stiffness in the strong direction. Biaxial or triaxial geogrid was recommended instead of uniaxial geogrid. This is due to the reduction of shaft load by about 19% on average with a reduction in the geogrid stiffness in the weak direction. Furthermore, there was an increase in wall facing movement as well. The increase in overall stiffness of the geogrid significantly reduced the shaft and wall facing movement. An increase in overall geogrid stiffness from 1X to 12X (X being the original stiffness), showed a gradual reduction in the wall facing displacement.

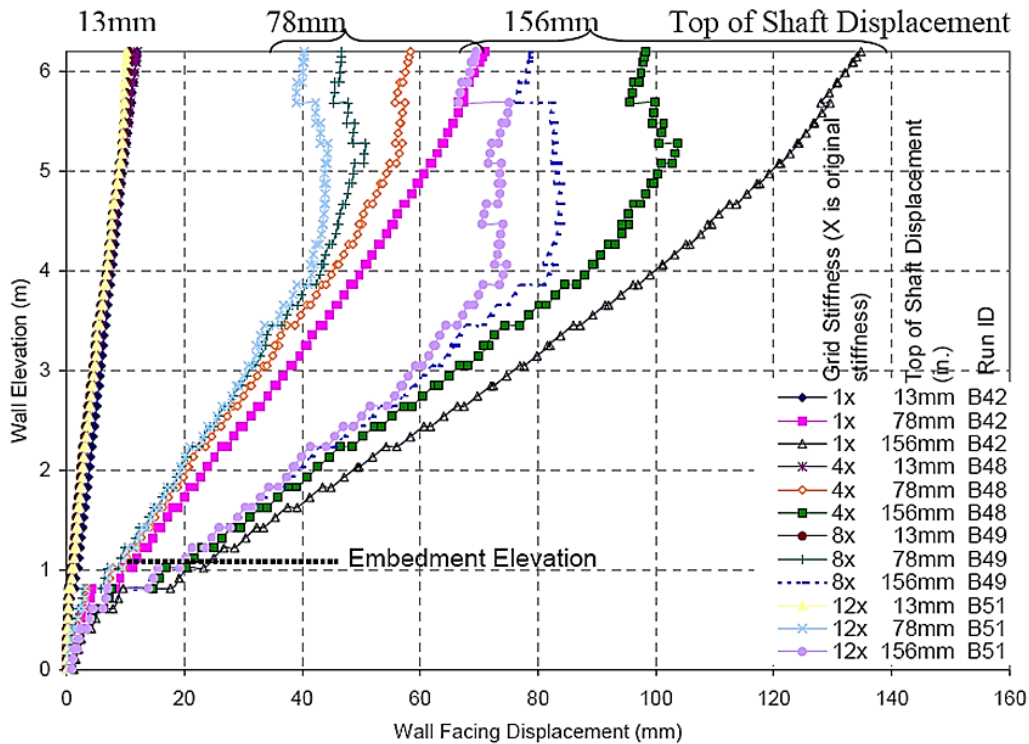


Figure 2-8 Effect of Geogrid Stiffness on Wall Facing Displacement (Pierson et al., 2011)

### 2.8.3 Effect of Facing Stiffness

Bathrust et al. (2006) conducted a study to experimentally verify that the facing stiffness of a geosynthetic reinforced soil retaining wall plays a major role in determining the design requirement of the geosynthetic reinforcement. It was found that the resistance provided by stiff facing is much more than flexible-wrapped facing – which in turn helps in resisting deformation of retaining walls. The study also focused on the strains produced in the reinforcements. The reinforcement strains were found to be as much as five times more in the case of retaining walls with flexible-wrapped facing than in walls with stiff facing. The authors suggested that disregard of facing stiffness leads to overestimation of geosynthetic reinforcement requirements.

#### *2.8.4 Effect of Backfill Soil*

A case study was undertaken by Hossain et al. (2012) to investigate the possible reasons of excessive lateral movements observed in a retaining wall in Lancaster, TX. The main reason for the excessive movement was attributed to the presence of large percentage of fines (28% to 38%) in the backfill soil. The large proportion of fines consequently decreased the drainage rate in the backfill soil, thereby, increasing the pore water pressure. Resistivity imaging survey was also performed which showed two perched water zones which increased in size after few months, and eventually caused bulging of the wall facings. Typically, sand is regarded as a suitable material for backfilling due to its drainage property and better shear strength. The shear strength is dependent on other soil properties, some of which are quantified by previous studies (Badhon and Islam, 2017; Chowdhury et al., 2018). Reclaimed asphalt pavement (RAP) and recycled crushed concrete aggregate (RCCA) have also been looked upon as suitable granular fills, mostly for temporary walls, due to their sustainability and low life cycle cost. Their promising use in pavement base and subbase along with documentation of properties (Faysal, 2017; Timsina et al., 2019; Imtiaz et al., 2020) open as an alternative to traditionally used natural aggregates and sands.

#### *2.8.5 Effect of Foundation Soil*

Alzamora and Anderson (2009) reviewed the performance issues of some MSE walls throughout the US. The authors reported that weak foundation soil or the erosion of foundation soil was one of the major factors affecting wall performance. Global stability failure, bearing capacity failure, or sliding failure of MSE walls have been attributed to weak foundation soil (Koerner and Soong, 2001; Alzamora and Anderson, 2009; Koerner and Koerner, 2013; Aubeny et al., 2014). Salman et al. (2017) presented the detailed design approach and analysis of an MSE wall foundation improvement. The paper

presented a design and build approach of using cast-in-place drilled shaft and a combination of aggregate and geogrid for the improvement of soft soil foundation in Grapevine, Texas. The MSE wall sustained a 100-year design flood elevation after the area received approx. 62 inches of rainfall in 2015. Differential settlement of the wall facing, and reinforced soil zone can produce significant lateral displacement and settlement at the top of the wall, along with an increase of lateral earth pressure and geogrid strain (Sadat et al., 2018). Rammed Aggregate Piers® have also been showed to significantly reduce the settlement of weak foundation soils and increase the bearing capacity and global stability factor of safeties of MSE walls (Michhimer et al., 2009).

#### *2.8.6 Effect of Compaction*

The construction of retaining walls involves compaction of backfill material with certain compaction effort. This compaction will also lead to an increase in the lateral pressure, which is not generally taken into account during design. Duncan et al. (1991) conducted a study to investigate the change in lateral earth pressure due to compaction efforts in retaining wall backfill. The major finding of the study was that compaction-induced earth pressures do not change substantially with time for sand backfills. However, in clay backfills, the high compaction-induced horizontal pressures tend to reduce over time to normal at-rest values. The study developed various charts and adjustment factors from parametric studies to estimate the changes in lateral pressure due to compaction of backfill material.

Ehrlich et al. (2012) evaluated the effect of compaction effort on the performance of geosynthetic reinforced soil walls. Two laboratory-scale MSE walls were constructed with the same specifications, except the compaction effort. The backfill soil was compacted using 73 kPa (1.52 kips) in one wall, whereas the other wall was compacted using just 8

kPa (0.17 kips). The major finding of the study was that heavy compaction effort produced an over-consolidated system with a stiffer behavior after construction. This made the structure less sensitive to surcharge application after construction, thereby resulting in smaller lateral deformations during the life of MSE wall. The heavy compaction pre-stressed the reinforcement at the end of construction, although after surcharge, the maximum mobilized tensions along the reinforcements in both the light and heavily compacted soils were almost same.

## 2.9 Previous Experimental Findings on Lateral Resistance of MSE Wall

Deformation of an MSE wall may cause minor to disastrous failure of the structures supported by the wall, for example failure of embankment slope or bridge abutment, deformation/distresses of highway roads and bridges, among others. Lateral displacement of the wall could cause washout/loss of drainage soil due to wall panel openings, leading to failure of the wall. There have been numerous studies conducted to evaluate the lateral resistance of MSE walls in different conditions. Babu et al. (2016) demonstrated a forensic analysis of a road approach embankment retaining wall and showed that due to the lateral movement of the wall - the road approach embankment separated from the wall, which led to significant distresses on the flexible pavement. The authors demonstrated back analysis of the failure mechanism and concluded that the failure was due to a combined action of sliding and overturning.

An MSE wall exhibits outwards lateral displacement when the shear resistance at the wall base is insufficient or less than the sliding force. The shear resistance at the wall base is dependent on the properties of the foundation and the reinforced soil. The weight of the wall along with length of reinforcement are other important factors to be considered for increasing the base shear resistance. A low-budget MSE wall without regard for

adequate base shear resistance is certain to slide outwards due to lateral earth pressures (Zaman, 2019). As a consequence, structures near the base and top of the wall might get affected (Schmidt and Harpstead, 2011).

Abu-Hejleh et al. (2000) conducted a study on a geosynthetic-reinforced segmental retaining wall in Colorado. The Founders/Meadows Bridge was completed by the Colorado Department of Transportation in July 1999. The MSE wall system supported the bridge and the approaching roadway structures. In order to control differential settlement between the bridge and the approaching roadway, the reinforcements in the reinforced zone were extended beneath the bridge foundation and the roadway structure. Considering the structure as an experimental study, a comprehensive material/soil testing, instrumentation, and monitoring program was planned into the construction operations. Two phases of instrumentation program were incorporated with the second phase being more comprehensive than the first. Three sections were instrumented to monitor the external displacements of the wall, internal soil stresses, reinforcement strains, and moisture contents. The monitoring started during the construction phases and continued even after the structure was opened to traffic. It was found that the maximum outward displacement experienced in one of the sections during the first stage of construction was approximately 9 mm (0.35 inches). The other stages of construction, including the placement of the bridge superstructure, brought about approximately 7 mm to 9 mm of maximum outward movements. Figure 2-9 shows the observed lateral displacements.

Based on the preliminary monitoring results, it was reported that the horizontal pressures at the wall facing and the maximum tensile strains on the reinforcements were

considerably below the design specified values. These results indicated that the CDOT and AASHTO design guidelines used at that time were conservative.

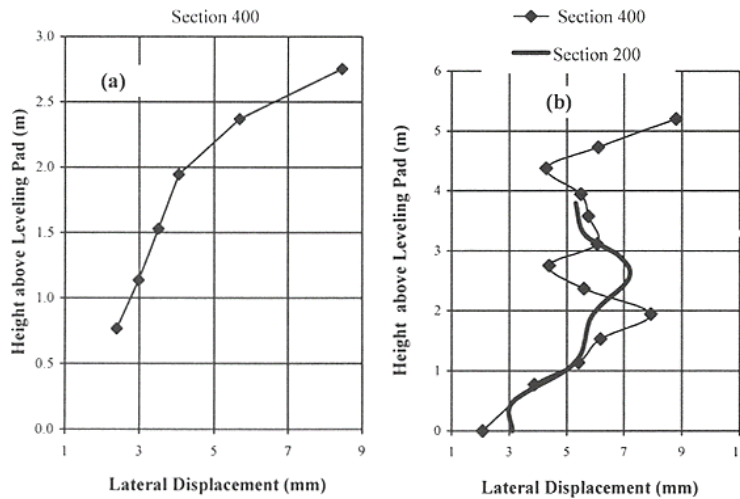


Figure 2-9 Lateral Displacements Experienced on Phase I Construction (a). During Stage I Construction (b). Due to Placement of the Bridge Superstructure  
(Abu-Hejleh et al., 2000)

A test study on the performance of an MSE wall reinforced with inextensible earth reinforcements made of both longitudinal and transverse members was published by Horpibulsuk et al. (2011). The test MSE wall was fully instrumented to monitor the lateral displacement of the test section. The foundation of the section was composed of hard soil layer. The wall height was 19.69 ft. (6 m). The wall was 29.53 ft. (9 m) long and 19.69 ft. (6 m wide) at the top, while it was 39.37 ft. (12 m) long and 68.9 ft. (21 m) wide at the base. The facing of the wall was composed of 4.92 x 4.92 x 0.46 ft (1.5 x 1.5 x 0.14 m) dimension segmental concrete blocks. The full construction was completed in approximately 20 days.

The lateral displacement of each segmental panel was measured at the completion of construction using a theodolite, the results of which are plotted in Figure 2-10 (a). The plot showed that the highest lateral movement occurred at the top of the wall. However, the authors mentioned that such a plot could be misrepresentative. The lateral movements in the graph are cumulative values since all the panels are connected to each other. This suggests that the maximum lateral movement cannot be at the top. A relative lateral movement was then calculated and plotted for each panel. The relative movement here is the difference in the cumulative lateral movements of continuous panels. Figure 2-10 (b) shows that the maximum lateral movement was in fact observed at the base rather than at the top. The isolated relative movements indicated that the lateral movement of the panel increased with increasing depth of the wall. The authors stated that this was due to the increase in backfill earth pressure with depth. The highest lateral earth pressure was at the base of the wall, which subsequently produced the maximum displacement at the wall base. A vertical inclinometer casing was also driven near the wall facing to measure the lateral displacement of the facing with time. Figure 2-11 shows the cumulative displacement plots of the inclinometer casing at different time after construction. A maximum movement of 9 mm was measured after 47 days from construction. The authors also stated that settlement induced lateral displacement was almost negligible in this case, since the foundation soil was hard.



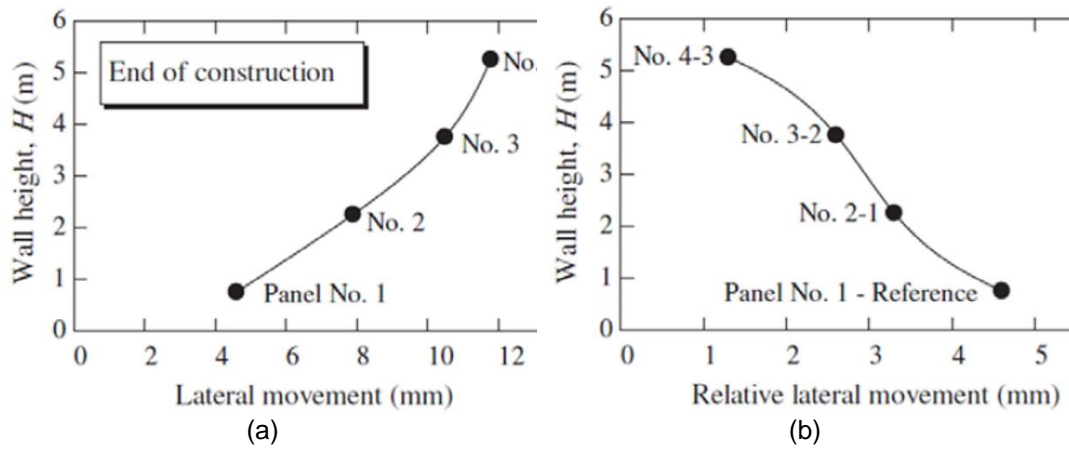


Figure 2-10 Measured Lateral Wall Movement of Each Segmental Panel at the End of Construction (Horpibulsuk et al., 2011)

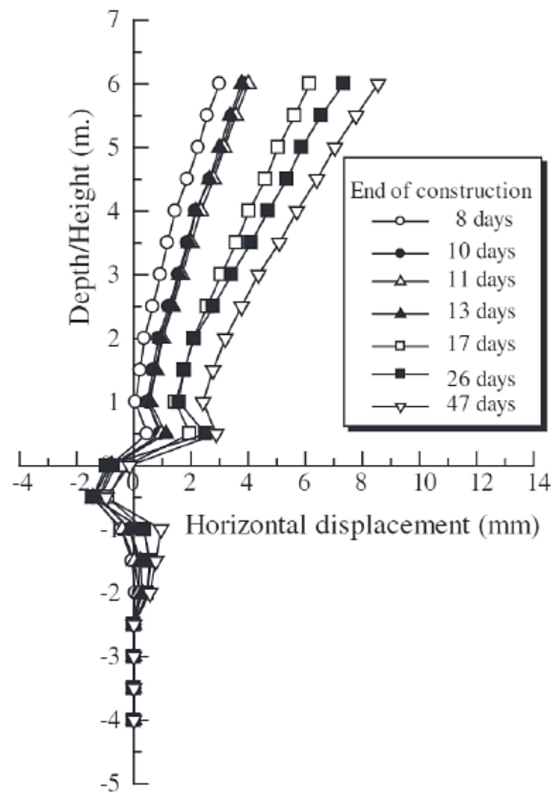


Figure 2-11 Measured Lateral Movement After the Completion of Construction (Horpibulsuk et al., 2011)

Fang and Ishibashi (1986) conducted a study to evaluate the relationship between lateral earth pressures and wall displacement brought about by rotational movement. The authors conducted the investigation in the University of Washington's shaking table and retaining wall assembly. The wall assembly was instrumented with four load cells used to estimate the lateral thrust, the point of application of the thrust, and the wall frictional angle. Six soil pressure transducers, monitoring the distribution of soil pressure, were also used to measure the lateral earth pressures. Air-dried Ottawa silica sand was used as the backfill material. The density of the backfill was controlled using vibration of the soil container. The setup of the retaining wall is shown in Figure 2-12.

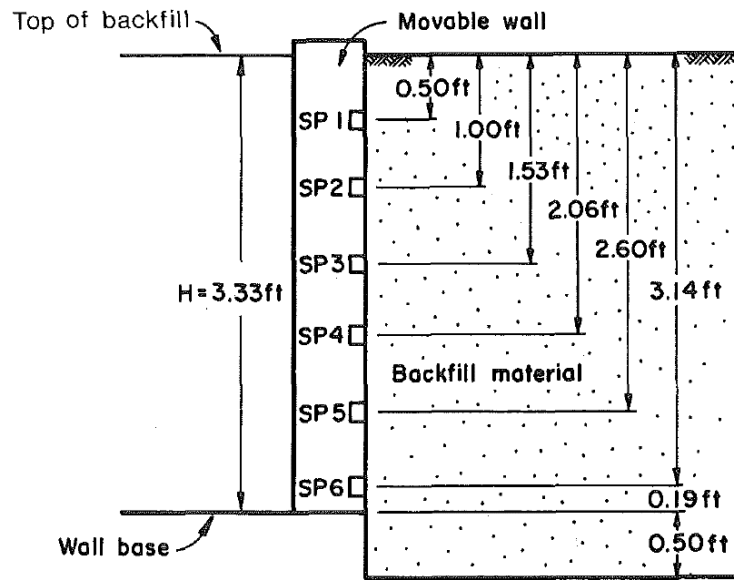


Figure 2-12 Locations of Pressure Transducers Behind the Wall

(Fang and Ishibashi, 1986)

The earth pressures were measured for the wall rotation about the top. The lower earth pressure transducers (SP3, SP4, SP5 and SP6) initially recorded an abrupt decrease in stresses with wall rotation, which attained almost constant values afterwards. The upper

earth pressure transducers (SP1 and SP2) initially recorded an increase in pressure with increasing wall rotation, which then decreased with further wall rotation. The authors reasoned that the initial increase in the pressure at the upper transducers was due to arching effect of the backfill soil at the upper region.

The lateral earth pressure decreased rapidly and stayed steady thereafter in all the pressure transducers in case of translational movement and rotation about the base of the wall. It was also noted that the point of application of the resultant force above the base of the wall increases with increasing soil density, and the point of application of active thrust, in the case of wall rotation about its base, is located about  $0.275H$  above the base of the wall. The research concluded that the general idea of linear pressure distribution behind a retaining wall does not validate for a wall rotating about the top – the distribution of active stresses is nonlinear due to soil arching.

Stuedlein et al. (2007) demonstrated a case study of an MSE wall which was to be constructed to support the third runway at Seattle-Tacoma International Airport located in Seattle, Washington. The design showed that the north side MSE wall needed to be about 1150 ft. (350 m) long and 85 ft. (26 m) high constructed in two tiers. The exposed wall height was to be 77.5 ft. (23.6 m). The subsurface investigation showed that the foundation soil was composed of 10 to 16.5 feet (3 to 5 m) of loose to medium dense slightly gravel, silty sand (including existing fill), 10 to 16.5 feet (3 to 5 m) of soft to medium stiff clayey silt and stiff to very stiff sandy silt over glacially overridden dense to very dense, slightly silty to silty, slightly gravelly to gravelly sand. The geotechnical report also indicated that 10 ft. (3 m) thick deposits of very soft, silty, sandy peat were present beneath some sections of the wall footprint. The construction specifications recommended the use of materials and reinforcements which met or exceeded the

minimum criteria set by AASHTO Standard Specifications for Highway Bridges. The wall construction started on February 2005, and it lasted nearly 88 days until the completion of the first tier of the wall. The construction of the second tier began after 140 days from the start of the initial wall construction. It lasted about 31 days until the completion of the second tier. Instrumentations were carried out for monitoring the wall performance. Wall displacements, reinforcement tensile strains, and piezometric levels were periodically measured. The lateral displacement of the MSE wall was monitored using readings taken from three inclinometer casings.

The monitoring results showed that the lateral movements were mostly limited to less than 0.2 inches (5 mm), with a maximum of 0.28 inches (7 mm) within the glacially overridden and subgrade improved fill soils. A maximum displacement of 1.2 inches (30 mm) was measured at the top of the wall. However, the authors reasoned that this displacement was due to a sharp change in the geometry of the wall facing, along with concentration of shear stresses at the interface of improved subgrade and native foundation soil. The lateral displacement plots from the inclinometer demonstrated that the wall displacements increased with increasing wall height. The maximum lateral movements were found to be 0.35, 0.79 and 1.22 inches (9, 20 and 31 mm), at the end of tier 1 construction, near the end of tier 2 construction, and the final inclinometer reading, respectively. Figure 2-13 shows the lateral displacements obtained from the displacement monitoring points (DMP) at the tallest portion of the wall face. Three displacement profiles corresponding to the end of tier 1 construction, end of tier 2 construction, and the final reading are plotted. The maximum displacement of the wall face was found to be approx. 0.4 inches (10 mm), which can be explained by the time delay in readings between the baseline survey and face panel construction.

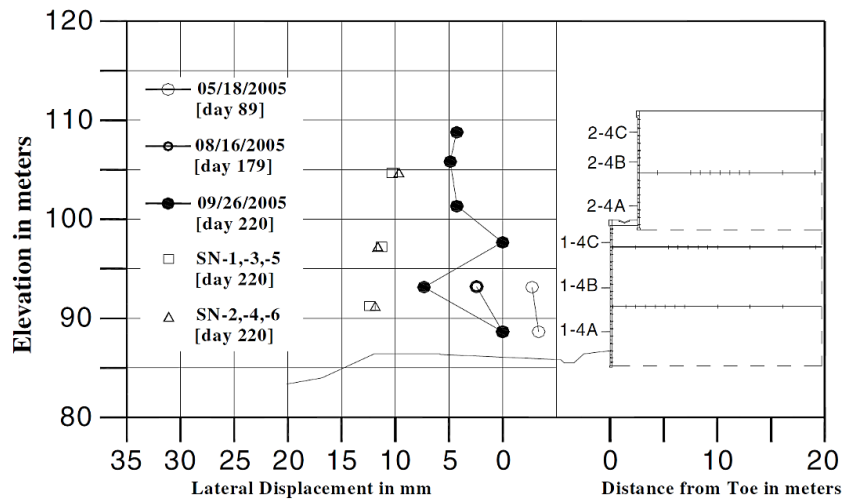


Figure 2-13 Lateral Displacement of the Face of MSE Wall (Stuedlein et al., 2007)

Another study was conducted and presented by Stuedlein et al. (2010) describing a different section of the same MSE wall constructed for the third runway at the Seattle-Tacoma International Airport. The wall was four-tiered, with a length of 1430 ft. (436 m) and height of 150 ft. (46 m). The exposed height of the MSE wall was about 138 ft. (42 m) with a face area of about 130,200 ft<sup>2</sup> (12,100 m<sup>2</sup>). The authors reported that it was the tallest MSE wall in the western hemisphere at that time based on the literature. As mentioned earlier, the subsurface investigation revealed that the top 10-12 ft. of foundation soil was soft peat, interlayered with loose to medium dense silty sand and sandy peat, over glacially overridden dense to very dense, slightly gravelly, silty to very silty sand. The weak soil was excavated up to 12 ft. (4 m) depth until the dense to very dense glacially overridden soil, which was then replaced with densely compacted granular backfill to provide a high strength foundation for the MSE wall. The construction guidelines specified the materials and reinforcements of high grade based on AASHTO Standard Specifications for Highway Bridges (AASHTO 1996 and Interim Updates).

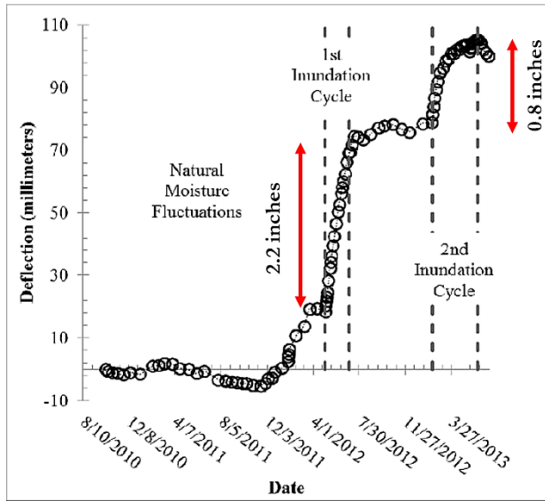
The construction of the MSE wall section started on January 2005. The first tier was 48 ft. (15 m) high which took 58 days to complete. Construction of the second tier, which was 38.4 ft. (11.7 m) high, started on day 72, which took 41 days to complete. The third and fourth tiers were 37.7 and 26 ft. (11.5 and 7.9 m) high, the construction of which began on days 131 and 205, and took 44 and 42 days to complete, respectively. The final grading at the design elevation of the wall was conducted between days 406 and 420. The performance monitoring of the wall section was conducted using vertical inclinometer which measured the lateral displacement of the wall. The inclinometer results indicated that the largest lateral wall displacement occurred at the base of the wall just above the toe. The maximum lateral displacement was recorded to be 0.3 inches (8 mm) at the end of the second-tier construction. The lateral displacements increased with increasing wall height and reached a displacement of 1.8 inches (45 mm) at the end of the fourth-tier construction.

An experimental study was undertaken by Fang et al. (1994) to evaluate the changes in magnitude and point of application of passive earth pressures with different types of wall movements. The results showed that for a wall under translational movement, the passive pressure distribution is hydrostatic in nature. However, for a wall under rotation about the top or rotation about the bottom, the distribution of lateral pressure is not linear. For rotation about the top, the point of application is  $0.18H$  above the wall base; whereas, it is  $0.55H$  above the wall base for rotation about the bottom.

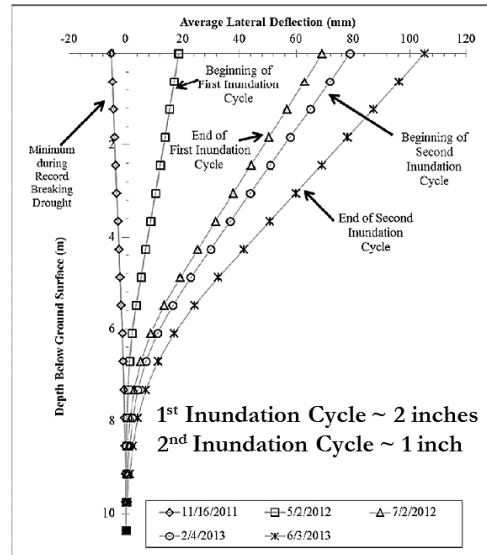
Bathrust et al. (2000) performed a full-scale testing of geosynthetic reinforced walls to identify important performance features of such soil structures. The sensor readings indicated that the largest load at the end of construction in a reinforcement used with modular block facing is at the connection joint. A hard facing column was found to reduce

reinforcement strains; thus, proper consideration should be given to hard facing column as a structural member. The study concluded that apart from the self-weight of blocks, the total vertical normal load at the toe of the facing column also depends on the soil down drag forces acting at the back of the facing column.

Brown et al. (2015) monitored a full-scale drilled shaft retaining wall in expansive clay subjected to moisture fluctuations. The wall was constructed on a site underlain by approx. 15 meters (49 ft.) of overconsolidated, stiff to hard, highly plastic clay. The groundwater table was approx. 2.4 meters (7.9 ft.) below the ground surface. The test wall consisted of 25 drilled shafts, each with a diameter of 0.61 meters (2 ft.) and c-c spacing of 0.76 meters (2.5 ft.). The performance monitoring was done with various instrumentations which included fiber optic strain gauges, inclinometer casings, thermocouples, and linear displacement potentiometer. The performance monitoring was continued for 4 years in order to capture the effects of extreme moisture fluctuations. The results showed that there was a record dry period during spring and summer of 2011, which decreased the top-of-wall deflection to -5.1 mm (0.2 inches). Controlled inundation was carried out behind the wall to create an upper-bound loading condition in 2012 and 2013. The top-of-wall deflection and average deflection of inclinometer casing behind the wall are shown in Figure 2-14.



(a). Top-of-Wall Deflections



(b). Average Deflection of Inclinometer Behind the Wall

Figure 2-14 Deflections of the Drilled Shaft Retaining Wall Under Study (Brown et al., 2015)

A field scale investigation was carried out by Onodera et al. (2004) with the objective of evaluating the performance of geogrid reinforced soil walls after 7-12 years of construction. The wall facing deformation followed a linear pattern with the largest displacement at the top layer in case of flexible wall facing. In the case of relatively stiff wall facing, the deformation followed an arc shaped pattern with its peak close to the middle of the wall height. The increase in horizontal displacement of all the walls under study were found to be most during and just after construction. The incremental displacement gradually decreased with time. The vertical settlement of foundation soil was uniform at the wall base in case of flexible wall facing. However, in the stiff wall facing, the vertical settlement was highly localized at the bottom of the wall facing.



Ahmadi and Bezuijen (2018) compared the performance of two full-scale MSE walls under strip footing load with a rigid and flexible wall facing. The walls were 4 m high, 4 m wide and 3 m long. Plywood face and concrete face were used for the flexible and rigid facing, respectively. Eight layers of polyester geogrid (PET) at 0.5 m vertical spacing were used. Strain gauges, pressure gauges and LVDTs were used as instrumentations. The results showed non-linear distribution of vertical earth pressures with depth, which was more than the theoretical value in the wall with flexible facing. Furthermore, the maximum lateral pressure in the model with the flexible facing was higher than that in the model with the rigid facing. The depth of maximum pressure decreased with the distance from the wall in both the models. Reinforcement strains were lower for the rigid face than for the flexible face. In the flexible facing wall, the strains decreased with increasing distance from the facing panel, due to more pronounced effect of compaction load near the wall face. The displacements as shown by inclinometer readings were generally higher in the flexible wall model. For the flexible face, the maximum lateral wall deflection occurred in  $z/H = 0.81$ .

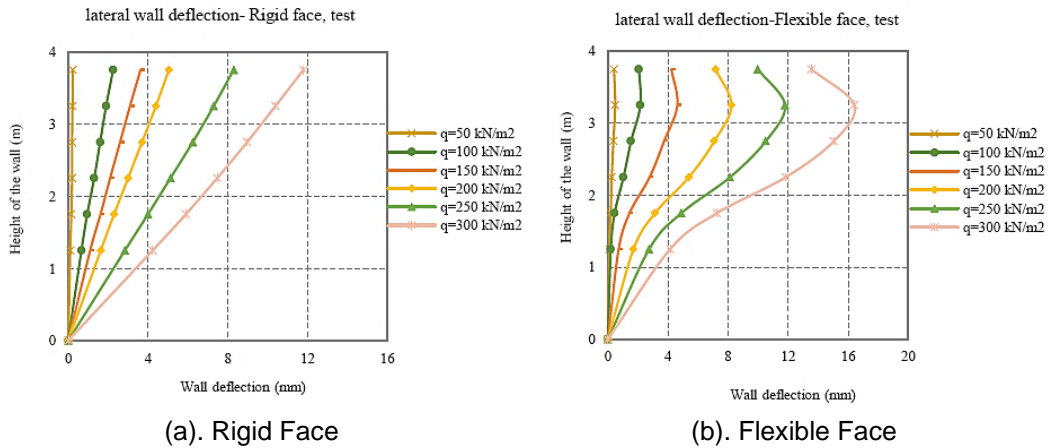


Figure 2-15 Lateral Wall Deflection (Ahmadi and Bezuijen, 2018)

2.10 Previous Findings on Vertical Settlement and Deep-Seated Failure of MSE Wall  
Suzuki (1988) conducted a study on 11 embankment sites by measuring the underground horizontal displacement, horizontal displacement on the ground surface, and embankment settlement. Vertical inclinometer casings were used to monitor the variation in underground lateral displacement. The author established various relationships between the lateral displacement of ground and embankment settlement. The lateral displacement was estimated to be 5-20% of the vertical settlement.

Another study was conducted by Sadat et al. (2018) to examine the effects of MSE wall base differential settlement on the performance of the wall. A field scale MSE wall was constructed too close to the edge of a slope, and the material underlying the facing was much more compressible than the material underlying the reinforced zone. This caused the wall facing to settle more than the reinforced zone. The differential settlement caused significant bulging at the MSE wall with the maximum lateral displacement occurring at about 1 m (3.28 ft.) from the base of the wall. Similarly, the maximum increase in lateral earth pressure also occurred at about 3.28 ft. from the wall base.

Stark et al. (2019) published a case study about a 32 ft. high MSE wall supporting a highway bridge abutment. Metal strips were used as reinforcements in the MSE wall. Steel H-piles were driven through the reinforced zone of the MSE wall via corrugated metal pipes (CMPs) to support the bridge abutments. Rammed Aggregate Piers were installed in the foundation soil prior to the construction of MSE wall to improve the bearing capacity of the soil. However, the wall did not perform very well as it exhibited significant movements. Later, the wall was rejected by the local Department of Transportation due to its unacceptable performance as the wall moved a lateral distance of about 18 inches (measured through surveying since the initial location was surveyed at

the beginning of construction). Settlement plates and vertical slope inclinometers were installed to monitor the vertical settlement and lateral movement of the wall, respectively. The authors analyzed a number of possible failure mechanisms and concluded that deep seated shear failure was the reason for such high movements. Two slope inclinometers (SI-1 and SI-2) were installed in front of the wall facing, while SI-3 was installed in the approach embankment soil backfill. The cumulative lateral displacement profiles of all the three inclinometers are presented in Figure 2-16. It is to be noted that the sensors were installed after most of the settlement and lateral movement had already taken place. This explains the small displacements recorded and presented in Figure 2-16 even though the final lateral movement was about 18 inches.

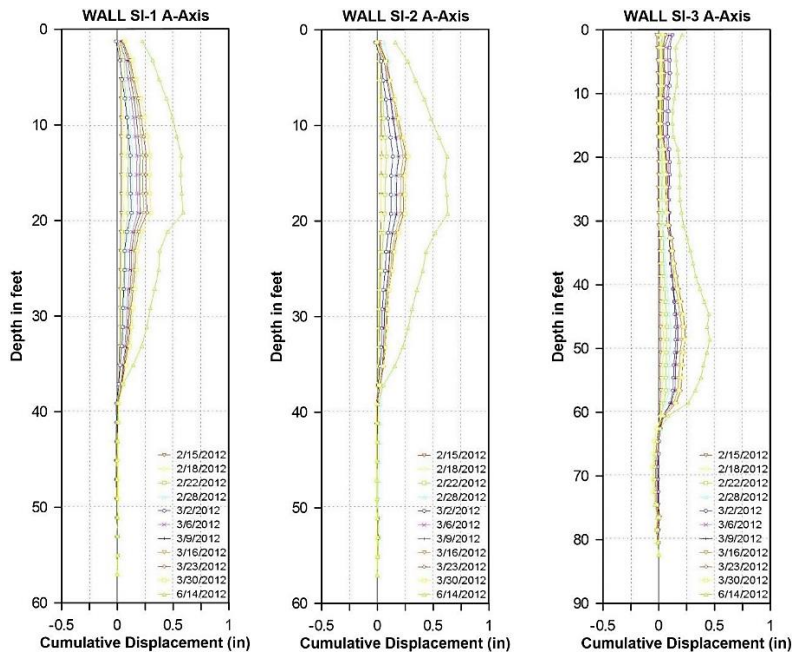


Figure 2-16 Cumulative Lateral Displacement Profiles with Depth (Stark et al., 2019)

The plot shows higher movements around 20 ft. depth than at the top for SI-1 and SI-2, which opts out the possibility of lateral spreading linked with vertical settlement (Suzuki,

1988). SI-3 which is located far behind the wall face (55 ft.) is in an area not susceptible to lateral spreading. Most of the movements were seen at a depth of 59 ft. in SI-3. The study also provided incremental displacement profiles (Figure 2-17), which show the maximum displacement around the similar deeper depths as mentioned above. A spike in the incremental displacement profiles indicates the location of lateral movement, which is the failure or shear surface. This evidence of deep failure was verified by presence of tension cracks on the surface of the approach embankment.

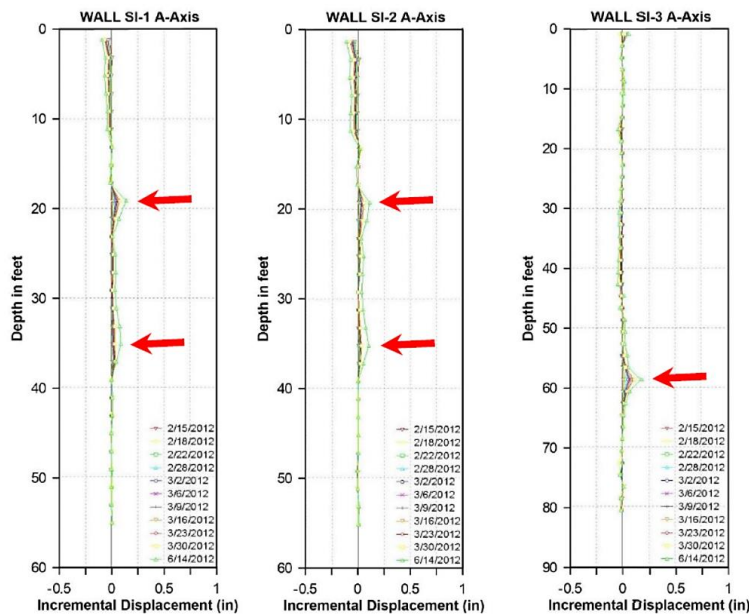


Figure 2-17 Incremental Lateral Displacement Profiles with Depth (Stark et al., 2019)

A case study on the failure analysis of a 45 ft. (14 m) high MSE wall in Arizona was presented by Samtani et al. (2005). Site investigations showed that the facing panels had separated from each other by as much as 5 inches (125 mm) within a distance of 30 to 70 ft. (9 to 21 m) from the wall corner (Figure 2-18 a). At the same time, the wing wall at the end of the bridge abutment had separated from the abutment (Figure 2-18 c) due to the wall's outward rotation (Figure 2-18 b). Based on the analysis and distress patterns,

the authors concluded that the failure mechanism of the wall consisted of global instability along with bearing capacity failure.

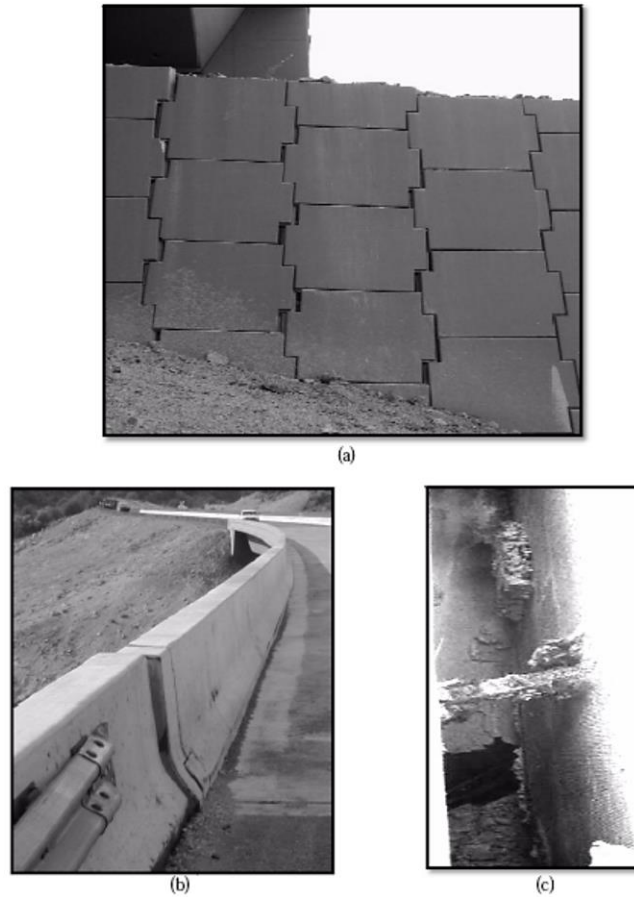


Figure 2-18 (a). Openings Between the Panels of the MSE Wall (b). Outward Rotation of the Wing Wall (c). Separation of Wing Wall from Abutment (Samtani et al., 2005)

### 2.11 Analytical Solutions

The mechanistic approach of equation development or an analytical solution to a problem is more reliable as it gives an exact solution. A numerical approach, on the other hand, tends to give an approximate solution within a range of values. There have been abundant studies in the solutions through analytical approach of lateral earth pressures

and retaining wall problems. One such study was conducted by Bang (1985) to determine the magnitude and distribution of active earth pressure behind retaining walls. The study developed analytical equations to calculate degree of lateral earth pressure at various amounts of outward wall tilt about the base. A basis for the study was that the friction angle was assumed to be fully mobilized just at the surface of the wall at initial active state, i.e., when there is no wall rotation. As the wall rotates, and when the full active condition exists along the entire depth of wall, friction angle becomes fully mobilized at the base as well. The outcomes of the method were compared to results from finite element modeling, which exhibited very good agreement between the predicted and the measured lateral earth pressures.

A study by Chang (1997) developed a modified Coulomb's solution of active pressure for evaluating the deformation pattern and the associated mobilization of shearing resistance in a rotating retaining wall. The author used Coulomb's active earth pressure theory incorporating the initial stress condition. Simplified distributions of the mobilized angle of internal friction and locally mobilized angle of wall friction were suggested for the development of solution. The results compared fairly well with FE modeling, with the rotation about base model showing better conformity than the case with rotation about top. A reason for this could be due to not including the effect of arching in the developed analysis.

Fang et al. (2002) experimentally investigated the reliability of Coulomb and Terzaghi theories to estimate passive earth pressure. It was found that passive earth pressures calculated using Coulomb and Terzaghi solutions with peak internal friction angle overestimated the ultimate passive thrust (for dense sand backfill). For loose sand backfill, the same solutions underestimated the ultimate passive thrust. However, use of

residual internal friction angle proved to be in good agreement with the experimental results. A similar study by Fang et al. (1997) compared the agreement of Coulomb and Rankine earth pressures with experimental data for sloping backfill. For retaining wall with sloping backfill, Coulomb's theory proved to be more reliable than Rankine's theory. For a wall moving away from the backfill, Rankine's theory tends to overestimate the active thrust. On the other hand, for a wall moving towards the backfill, Rankine's theory tends to underestimate the passive thrust.

Ahmadabadi and Ghanbari (2009) developed an analytical solution to calculate active earth pressure behind retaining walls with a cohesive-frictional backfill soil. The authors followed the horizontal slices method (HSM) by dividing the failure wedge into a number of horizontal slices. An assumption which was not done by previous studies is considering the value of shear force between horizontal slices to be unequal. For the unreinforced cohesive-frictional backfill,  $4n$  formulation was followed with four unknown parameters and four equations to solve the unknowns (Table 2-5 a). For the reinforced backfill,  $5n$  formulation was followed with an addition of tensile force of the reinforcements as the fifth unknown parameters (Table 2-5 b). Finally, the active earth pressures calculated from the proposed method were compared to results from previous published methods.

Table 2-5 Unknown Parameters and Equations (Ahmadabadi and Ghanbari, 2009)

(a). Unreinforced Backfill

Unknowns	Number	Equations	Number
$H_i$	$n$	$\sum F_x = 0$	$n$
Inter-slice shear force		For each slice	
$N_i$	$n$	$\sum F_y = 0$	$n$
Normal force at base of each slice		For each slice	
$S_i$	$n$	$\sum M_o = 0$	$n$
Shear force at base of each slice		For each slice	
$P_i$	$n$	$S_i = N_i(\tan \phi) + C$	$n$
Net force on wall		For each slice	

(b). Reinforced Backfill

Unknowns	Number	Equations	Number
$H_i$	$n$	$\sum F_x = 0$	$n$
Inter-slice shear force		For each slice	
$N_i$	$n$	$\sum F_y = 0$	$n$
Normal force at base of each slice		For each slice	
$S_i$	$n$	$\sum M_o = 0$	$n$
Shear force at base of each slice		For each slice	
$T_i$	$n$	$S_i = N_i(\tan \phi) + c$	$n$
		For each slice	
$P_i$	$n$	$\tau_m = \lambda (\tau_f)$	$n$
Net pressure on wall		For each slice	

The angle of failure wedge and lateral pressure on wall calculated from the proposed method were in excellent agreement with the values determined using Rankine, Coulomb, and Cheng (2003). However, when comparing with Das and Puri (1996), the failure wedge angle was in good agreement with a maximum difference of about 3.5% for higher cohesion strength values, whereas the lateral pressure at higher cohesion strength values were noticeably different. The proposed method was compared with Shekarian et al. (2008) and MSEW software (AASHTO method) for reinforced backfills. The failure angle wedge, tensile force of reinforcements and pressure on the wall were in good agreement. The active earth pressure on the wall decreased with increasing cohesion strength of the backfill soil, and an increase in the number of reinforcements.

A modified method to predict soil pressure distribution and ultimate lateral capacity for rigid piles in cohesionless soils was formulated by Prasad and Chari (1999). An experimental setup with a smooth steel model pile in well graded angular dry sand was used for the study. Pressure transducers and load cell were used to measure the soil pressure on pile and load on pile, respectively. A total of 15 tests were conducted at different embedment ratios (embedded length of pile/diameter of pile) of 3, 4, 5 and 6. The load was applied in increments, with each load lasting until the rate of deflection was less than 0.025 mm/min. The results indicated that the lateral capacity of the piles increased with increasing soil density. The authors idealized the soil pressure distribution along the length of piles based on the experimental results, as shown in Figure 2-19. The pressure on the front side of pile (passive side), reaches the maximum at  $0.6x$ , 'x' being the distance from surface to the point of pile rotation. After 'x', the pressure increases in the opposite direction on the other side. It then reaches a maximum at the pile tip, the magnitude of which is 1.7 times the soil pressure at  $0.6x$  depth. The pressure distribution across the width (diameter) of the pile was also measured. It was found that the



maximum pressure is reached at a plane perpendicular to the load and is zero at a plane parallel to the load. The authors thus recommended to use 80% of the peak pressure as the average uniform pressure across the pile width for design purposes.

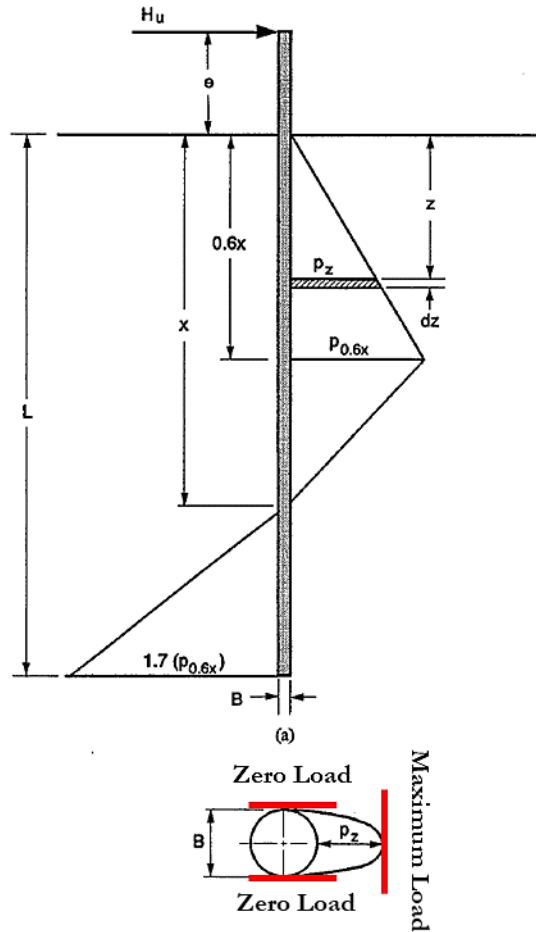


Figure 2-19 Idealized Soil Pressure Distribution Along the Length of Pile (Prasad and Chari, 1999)

Based on the experimental results and the idealized soil pressure distribution, the authors proposed an analytical method to calculate the ultimate lateral capacity of pile, which is shown as a flowchart in Figure 2-20.

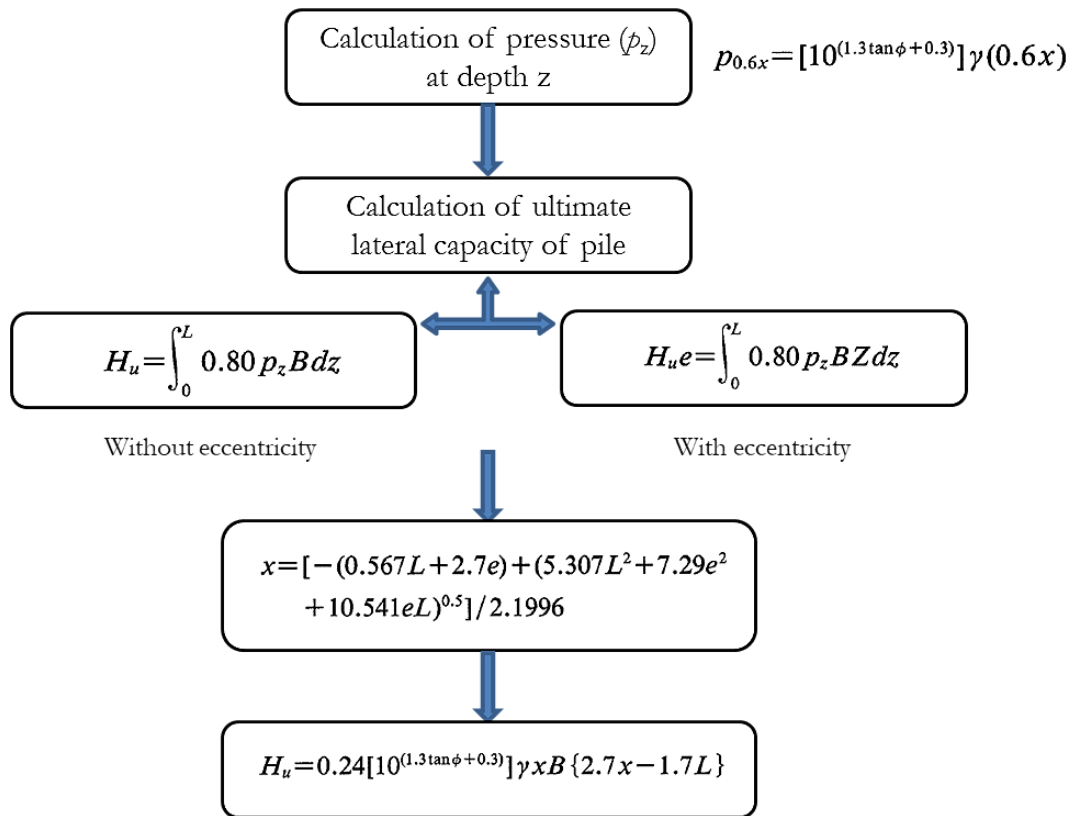


Figure 2-20 Calculation of Ultimate Lateral Capacity of Pile (Prasad and Chari, 1999)

Sastry and Meyerhof (1994) conducted a series of lab-scale experimental studies to analyze the lateral behavior of flexible piles. The authors studied the lateral behavior of flexible piles in layered sands consisting of loose sand overlying compact sand under vertical eccentric and central inclined loads. The experimental setup used for the test is shown in Figure 2-21. Dry, angular, coarse to medium silica sand was used. A vertical, smooth, hollow PVC pipe (length = 1250 mm, outside diameter = 73 mm, wall thickness = 7.4 mm) was used as the pile. Diaphragm-type pressure transducers, electric wire resistance strain gauges, load cell, and proving ring were used to measure lateral soil pressures on the pile, bending moments along the pile depth, load at the pile toe, and

total load applied to the pile head, respectively. The required inclination of load was achieved by an appropriate combination of horizontal and vertical loads, while the vertical eccentric load was applied to a pile arm rigidly connected to the pile head.

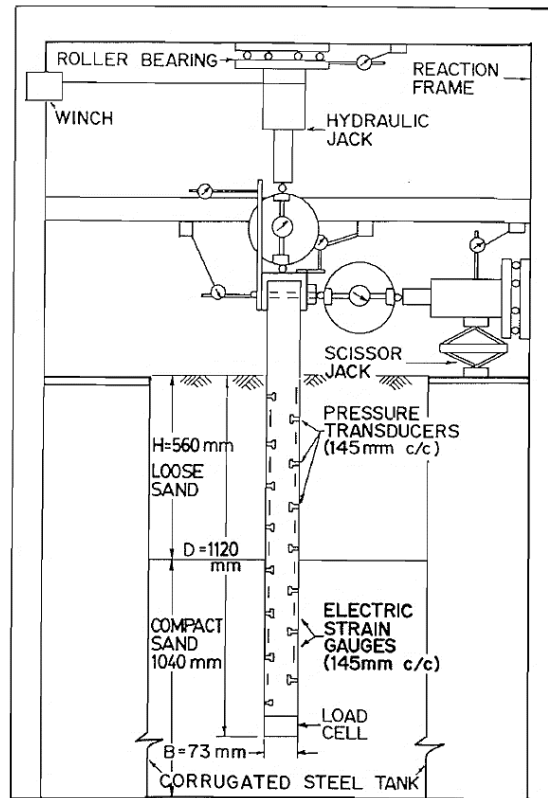


Figure 2-21 Experimental Setup for Pile Load Capacity Test (Sastry and Meyerhof, 1994)

The lateral capacity was evaluated based on an equivalent rigid pile concept (Figure 2-22). The ultimate effective depth ( $D_{eu}$ ) of an equivalent rigid pile was formulated as follows:

$$\frac{D_{eu}}{D} = m K_r^{0.12} \leq 1$$

The ratio was obtained as 0.64 for the study. In general, the theoretical lateral soil pressure was higher and deeper than the observed experimental value. An interesting

observation was that the strength of the soil surrounding the lower half of the pile did not seem to influence the maximum lateral pressure. There was a reasonable agreement between the observed and calculated bending moments. The theoretical bending moments were computed using data based on the triangular lateral pressure distribution on an equivalent rigid pile of depth  $D_{eu}$ .

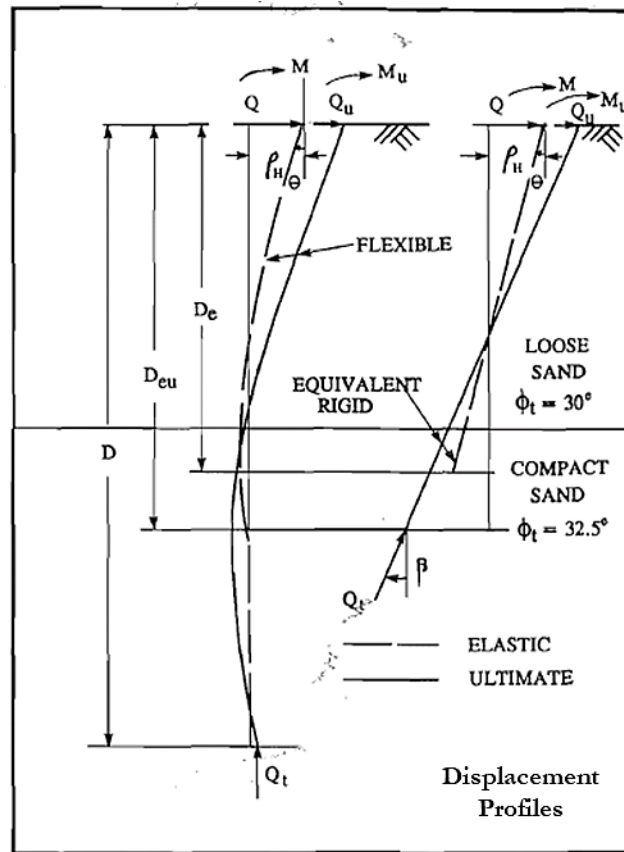


Figure 2-22 Flexible and Equivalent Rigid Pile Concept (Sastry and Meyerhof, 1994)

Another such research, Sastry and Meyerhof (1989), studied the lateral behavior of flexible piles in homogenous loose sand and soft clay under central inclined loads. The experimental setup was same as that in the previous test. Three tests were conducted using loose, dry, medium to coarse silica sand, while three tests were performed using

soft saturated clay of medium plasticity. The pile and the instrumentation were also same as that of the previous test. The theoretical empirical relations were in close agreement, although somewhat conservative, with the experimental results of bearing capacity in both sand and clay. In general, the theoretical lateral soil pressure was higher and deeper than the observed value. In clay, the theoretical lateral pressure increased at the ground level and had a maximum value of about  $2c_u$ . Beyond this, the pressure distribution was similar to that of sand. The schematic distribution of lateral soil pressure on pile shaft (Figure 2-23) shows that the pressure is different only near the ground surface, after which the distribution follows the same trend for both sand and clay. The groundline lateral displacement of a fully embedded pile can be expressed as (Meyerhof et al., 1988):

$$y_0 = I_{yr} Q / (E_{se} D_e F_{yf})$$

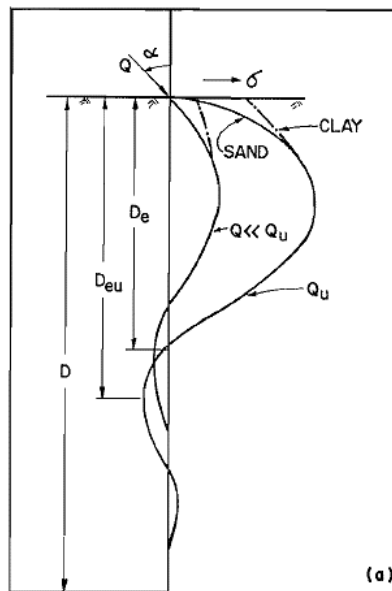


Figure 2-23 Schematic Distribution of Lateral Soil Pressure on Pile Shaft (Sastry and Meyerhof, 1989)

The ultimate and elastic effective depth ratios ( $D_{eu}/D$ ) and ( $D_e/D$ ) decrease with inclination. The ratios are unity at vertical load ( $\alpha = 0^\circ$ ) and decrease to minimum values for a horizontal load ( $\alpha = 90^\circ$ ). The authors also proposed relations to estimate effective embedment depth ratios which are as follows:

Pile in Sand (Meyerhof et al., 1988 for elastic; Meyerhof and Sastry, 1985 for ultimate)

$$D_e/D = \sqrt{(y_{0r}F_{yr})/(y_{0f}F_{yf})} \leq 1 \quad D_{eu}/D = \sqrt{Q_{uf}/Q_{ur}} \leq 1$$

Pile in Clay (Meyerhof et al., 1988 for elastic; Meyerhof and Sastry, 1985 for ultimate)

$$D_e/D = (y_{0r}F_{yr})/(y_{0f}F_{yf}) \leq 1 \quad D_{eu}/D = Q_{uf}/Q_{ur} \leq 1$$

Sastry and Meyerhof (1989)

$$(D_{eu}/D)_\alpha = 1 - \frac{\alpha}{45^\circ} \left\{ 1 - \left( \frac{D_{eu}}{D} \right)_{90} \right\} \\ 0 \leq \alpha \leq 45^\circ$$

$$(D_{eu}/D)_\alpha = \left( \frac{D_{eu}}{D} \right)_{90} \\ 45^\circ \leq \alpha \leq 90^\circ$$

Meyerhof et al. (1988) also performed a study to estimate the ultimate lateral resistance and the groundline lateral deflections of single and group flexible piles subjected to horizontal load. Dry sand with medium to coarse angular silica grains was used for some tests, while, saturated clay of medium plasticity was used for some. Steel, timber and nylon piles (diameter = 12.5 mm) with various embedded lengths up to 610 mm was used. For the group effect, 2 x 2 piles with c-c spacing of 38 mm (3 pile diameters) connected by a steel or timber cap at the top were used. The piles were loaded to failure at a horizontal displacement rate of about 0.1 mm/min by a horizontal load. Pile displacements and rotations were measured at the top of the piles. The results were

similar to that of rigid piles. The ultimate load generally occurred at a pile head displacement of about 2-4% of the effective pile length and a rotation of about 1-2°. The ultimate load decreased rapidly with decreasing relative pile stiffness for both the cases with single pile and group piles. The horizontal groundline deflections increased rapidly with decreasing relative pile stiffness and also with smaller  $D/B$  ratios.

#### 2.12 Lateral Resistance of MSE Wall Using Shear Key

The resistance against lateral sliding in a conventional retaining wall is largely due to the frictional resistance at the wall base. The shear resistance generated at the interface of the wall base and the foundation soil helps in resisting the lateral driving force. This frictional resistance is directly proportional to the normal force or the weight of the backfill acting on the wall base. A longer length of the base slab also provides a better resistance. However, due to many reasons, such as improper construction, use of low-grade backfill, weak foundation soil, and actual lateral pressure being more than design, the frictional resistance at the wall base is not always adequate to hold the retaining wall in place. Generally, a higher resistance can be achieved by either increasing the weight of the wall or the length of the heel slab. Nevertheless, these can be expensive solutions. Another approach is to use a shear key at the wall base as shown in Figure 2-24. A shear key provides additional passive pressure from the soil in front of the shear key and therefore, resists the lateral driving force. Since even a small depth of shear key has shown to increase the lateral resistance considerably, this method can be regarded more cost-effective than the former approaches. Sarath et al. (2011) demonstrated that a shear key can improve the sliding factor of safety considerably by resisting the lateral driving force in a retaining wall. The study recommended that the highest resistance was achieved when the shear key was located at the heel of the base slab. In terms of location of shear key, the study compared three different scenarios with the shear key

located at the heel, below the stem, and toe. It was found that the earth pressure was relatively lesser in the case of heel, which in turn resulted in greater factor of safety against sliding.

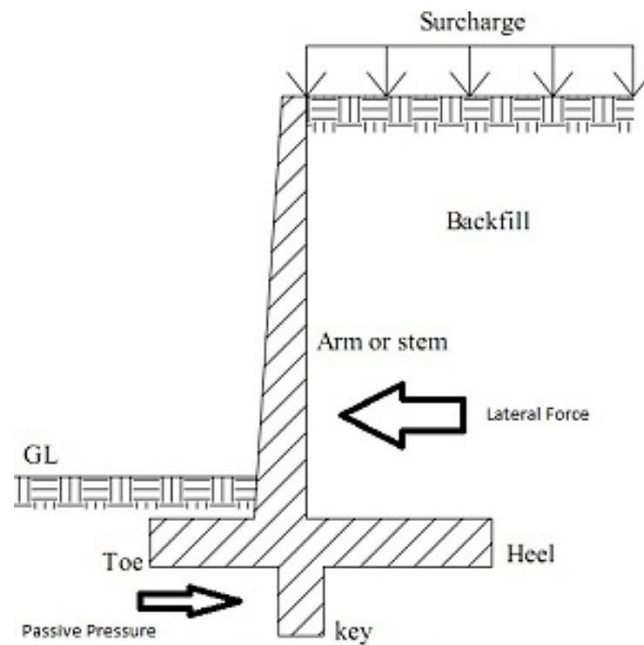


Figure 2-24 Schematic of a Conventional Retaining Wall with Shear Key (Jamal, 2017)

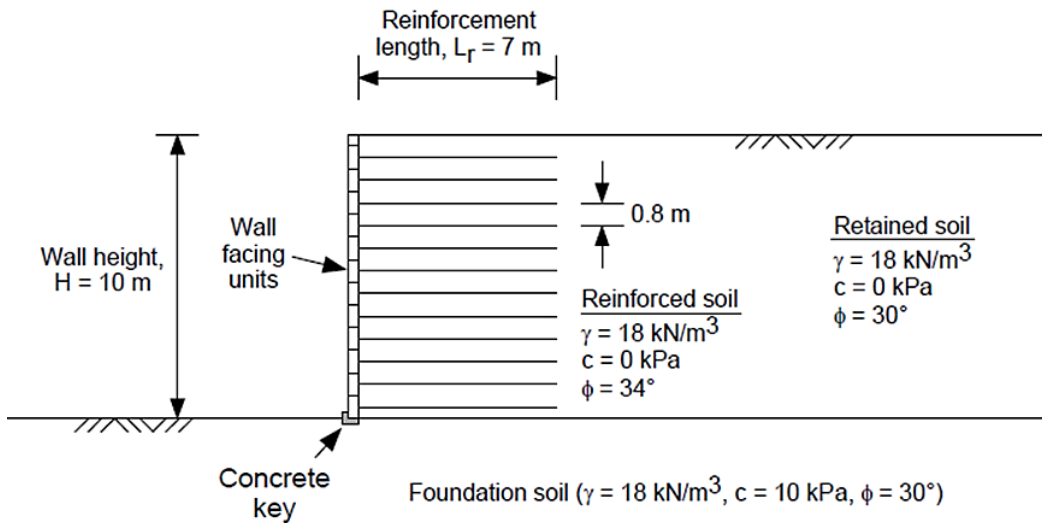
In the same way, a shear key could be incorporated at the base of an MSE wall to increase the lateral stability. The additional passive pressure thus generated can improve the sliding factor of safety.

Bhuiyan et al. (2012) investigated the effect of plastic shear pins on the interface shear behavior of modular retaining wall block units. A series of direct shear tests were conducted under varied normal loading conditions on two layers of "I" blocks connected with plastic shear pins. The blocks were tested in both infilled (with granular aggregates) and empty conditions. The results indicated that the shear pins further increased the



shear force due to its restraints at connection points. It was found that plastic pins along with granular infill provide better results in terms of shear resistance. The strength (apparent cohesion) exhibited by the pins were found to be comparatively independent of the normal force.

Kim and Bilgin (2007) numerically studied the effectiveness of using a concrete shear key at the base of an MSE wall to increase the resistance against lateral sliding. The authors reported significant reductions in the wall lateral displacement. The study showed the effect of different key sizes for varying reinforcement lengths and foundation soil friction angles. PLAXIS 2D was used to conduct the numerical analysis where a 10 m high MSE wall was modeled. The detailed geometry of the wall model is presented in Figure 2-25. Plane-strain condition was assumed for the analysis with the use of triangular elements of 15-nodes. No surcharge was considered with the load being applied only through the soil layers. The wall was modeled with soil layers (load) being applied in a number of lifts, each being 2.62 ft. (0.8 m) in thickness. The subsurface soil was modeled as one uniform layer.



(a)

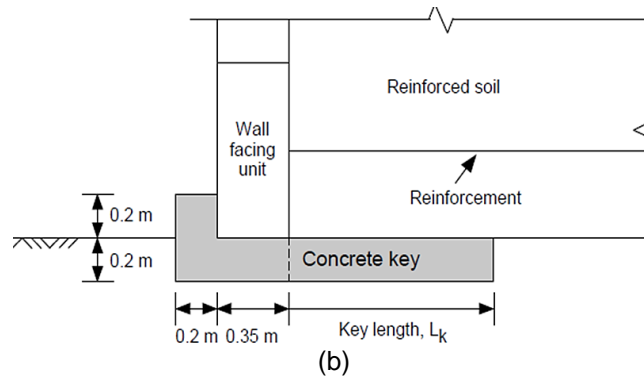


Figure 2-25 Schematics of MSE Wall Model for Numerical Study

(a). Detail of MSE Wall (b). Detail of Concrete Key (Kim and Bilgin, 2007)

A parametric study was conducted which illustrated that irrespective of the reinforcement length or the foundation soil friction angle, the lateral deformation decreases with an increasing length of concrete shear key. Figure 2-26 shows the results from the study, where each curve signifies the final deformed shape of the wall face for varying key length ( $L_k$ ), reinforcement length ( $L_r$ ), and foundation soil friction angle ( $\phi_{sub}$ ) values.

Even though a concrete shear key can be effective, its rigid nature can be a limitation for its application in an MSE wall. MSE wall base is flexible in nature which helps in resisting differential settlements. The rigid nature of concrete can thus undermine one of the most important aspects of an MSE wall. Furthermore, it is relatively expensive to construct a continuous shear key at the wall base. Since the cost-effectiveness of an MSE wall is a deciding factor for its use, a relatively cost-intensive concrete shear key might pose a limitation, particularly for low-budget projects.

Using longer piles at the wall base can also be effective since they not only improve the lateral sliding resistance but provide additional resistance against global or deep-seated failure as well. However, concrete piles will be expensive and other low-cost options such

as timber piles might result in lower design life due to faster degradation. A possible solution could be recycled plastic pins due to their low-cost, and resistance against chemical and biological degradation.

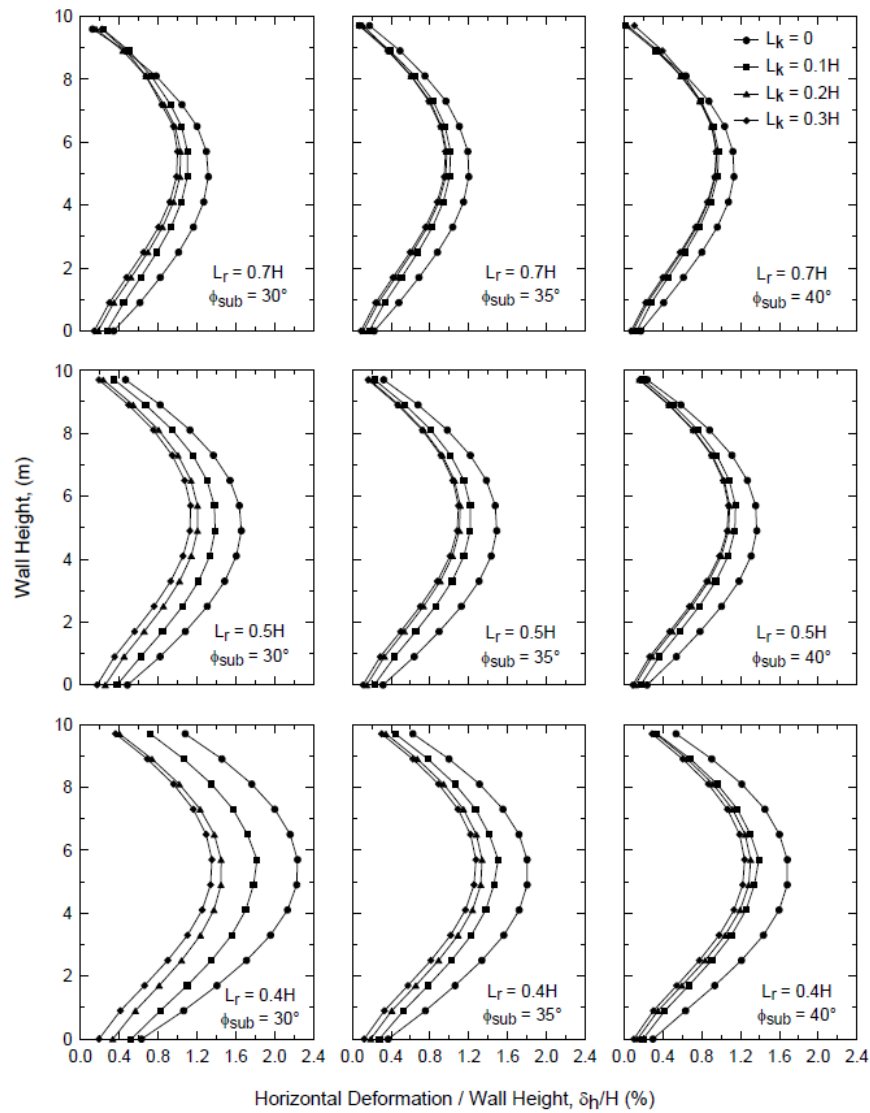


Figure 2-26 Effect of Concrete Key on the Lateral Deformation of MSE Wall  
(Kim and Bilgin, 2007)

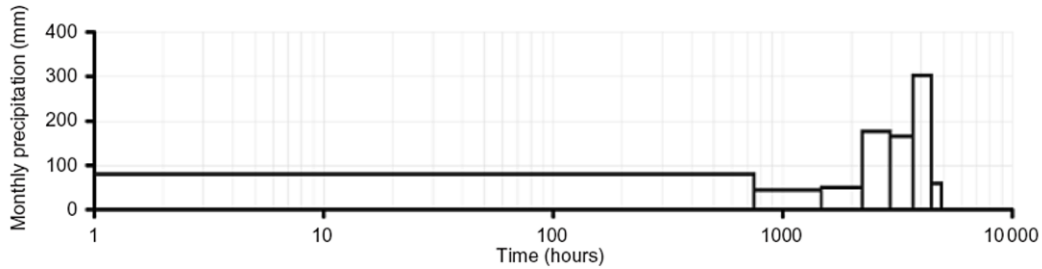
Zaman (2019) conducted a study to evaluate the effectiveness of recycled plastic pins (RPP) in improving the shear resistance of MSE wall base. The author constructed two identical MSE wall test sections of 24 ft. length and loaded with a backfill soil height of 4 ft. The foundation of one section was reinforced with 10 ft. long 4 in. x 4 in. RPP spaced center to center at 3 ft., while the other section served as a control section without any RPPs. The RPPs were installed in such a way that 8 ft. was driven inside the ground while 2 ft. was left above to act as a composite section with the geosynthetic reinforcement and carry the lateral load. The sections were instrumented with vertical inclinometer casings in front of the wall, and pressure plates inside the wall facing. The performance monitoring results showed significant lateral movement in the control section (3.8 inches), while almost no movement was observed in the reinforced section. Further evaluation was done with an increased backfill height of 5 ft (Bhandari et al., 2021). The control section in this case displaced by 1.76 inches, while the lateral displacement was reduced by about 84% (0.29 inches) in the reinforced section.

Finite element modeling was also conducted by the author to carry out a parametric study on the effects of various RPP parameters on the lateral movement of the wall base. The deformation analysis indicated that only 17% of the load carrying capacity of the RPPs had been mobilized. The author concluded that less spacing and larger size of RPPs improve the lateral sliding resistance of MSE wall base significantly. However, the effect of longer lengths of RPP is not so considerable for reducing the lateral sliding of MSE wall base.

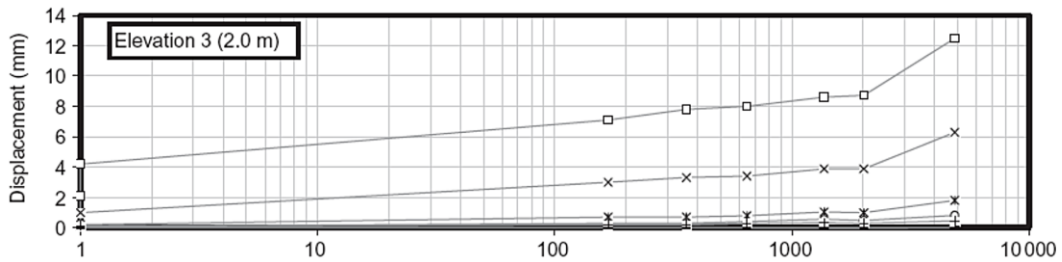
The study also showed that with every major precipitation event, an increase in lateral movement was observed. The sudden change in lateral displacement was speculated to be due to the increased lateral pressure from the backfill which was composed of clay,

which underwent swelling after major precipitation events. During the dry periods, due to shrinkage behavior of the soil, the lateral displacements did not increase significantly.

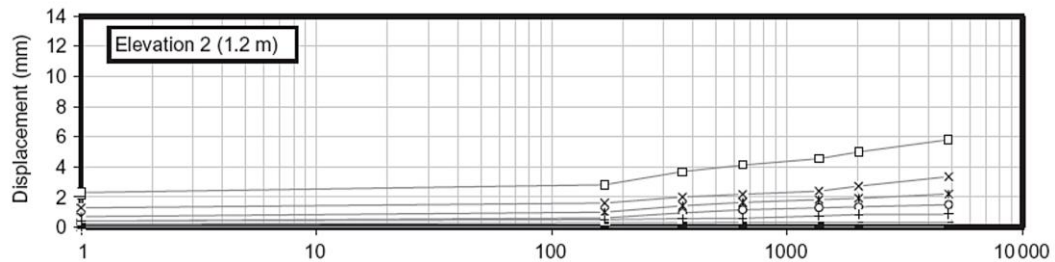
Benjamin et al. (2007) undertook a field study to investigate the performance of geotextile-reinforced soil-retaining walls. The authors assessed the field behavior of eight model geotextile-reinforced soil structures for a broad study. The major finding of the study was that the lateral displacement increased with time and was primarily associated with precipitations events (Figure 2-27). An increase in precipitation brought about an increase in the horizontal displacement of the wall.



(a)



(b)



(c)

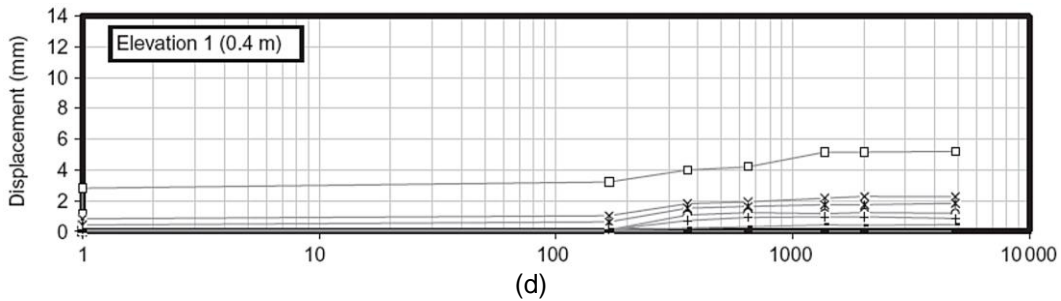


Figure 2-27 Horizontal Displacement in Relation to Precipitation and Time (a).

Precipitation (b). Elevation 3 (c). Elevation 2 (d). Elevation 1 (Benjamin et al., 2007)

### 2.13 Lateral Resistance of Piles

Rollins et al. (2011) conducted a study to assess the effect on lateral resistance of piles near vertical MSE abutment walls. An outcome from the study was that the lateral pile resistances were independent of the distance from the MSE wall facing. The lateral resistance of such piles can be improved by providing longer reinforcement ratios, preferably towards the top surface of wall. This will increase the pull-out resistance, thereby, constraining the wall movement and increasing the pile resistance. A study by Sawwaf (2006) established the effect of geogrid reinforcement in slopes to the lateral response of a pile near the slope crest. A lab scale model was setup with model piles fabricated from steel tubes, and the load was transferred to the piles by a pulley system. The test pile was designed to act as a short rigid pile. Medium to coarse sand was used as backfill. The sand was compacted in layers to achieve 3 cases representing loose, medium-dense, and dense conditions. Geogrid with peak tensile strength of 45 kN/m was used as reinforcement. A total of 36 model tests were carried out by varying different parameters such as length of embedment of pile, diameter of pile, distance of pile from slope crest, number, and length of geogrid reinforcements, etc. The results showed that an increase in the geogrid number improved the lateral load carrying capacity of the

model pile for the same displacement ratio (Figure 2-28). The geogrid created an interlocking action with the sand particles, thus resisting the horizontal shear stress. Also, the pile lateral resistance decreased with the increase in depth of the reinforcement layer.

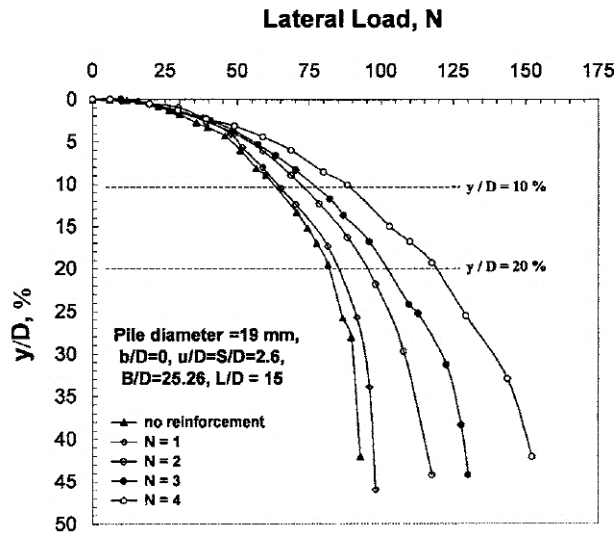


Figure 2-28 Pile Lateral Capacity from the Model (Sawwaf, 2006)

The lateral resistance of the pile improved considerably at a higher number of geogrid layers. Comparing to an unreinforced slope, the gain in lateral resistance was 50% of the lateral load in a reinforced slope with 4 layers of geogrid. It was stated that the geogrid layer transfers the horizontal shear stresses from the front of pile to a larger mass of soil behind the pile creating a larger failure wedge. The effect of geogrid spacing was found to be more pronounced at shallow depths since the soil stiffness is smaller at shallow depths. The effect of geogrid reinforcement was more pronounced in medium-dense to dense sand. The angle of friction increases with the relative density of sand, which increases the adhesion and interlocking between geogrid and soil particles. This ultimately leads to higher pile lateral resistance. The more the embedded length of pile, the more was the increase in stiffness of the surrounding soil. This in turn, increased the

soil resistance against lateral pile displacement. Hence, there was an increase in the lateral load capacity of the pile.

Another study by Rollins et al. (2010) studied the improvement in lateral resistance of pile group in soft clay by replacing the top 5 to 10 pile diameters with compacted granular material. The authors performed four sets of tests – group piles (15 piles) in soft clay, single pile in soft clay, group piles (15 piles) with top 2.4 m replaced with clean compacted sand, and single pile with top 2.4 m replaced with clean compacted sand. The tests were carried out with various target pile displacement increments, with 10 cycles of load applied for each increment. It was found that the peak cycle loads were 66% to 78% higher in sand than in clay for single piles. This indicated that cycling produces greater load reductions in clay than in sand (25% in clay and 20% in sand). For group piles, the improvement in peak loads in sand was only about 30% more than in clay. This is due to greater group interaction effects in the sand relative to that in the clay. It was also found that the failure plane for sand would be flatter and wider due to higher friction angle. Thus, more overlapping of shear zones. Figure 2-29 summarizes the study results.

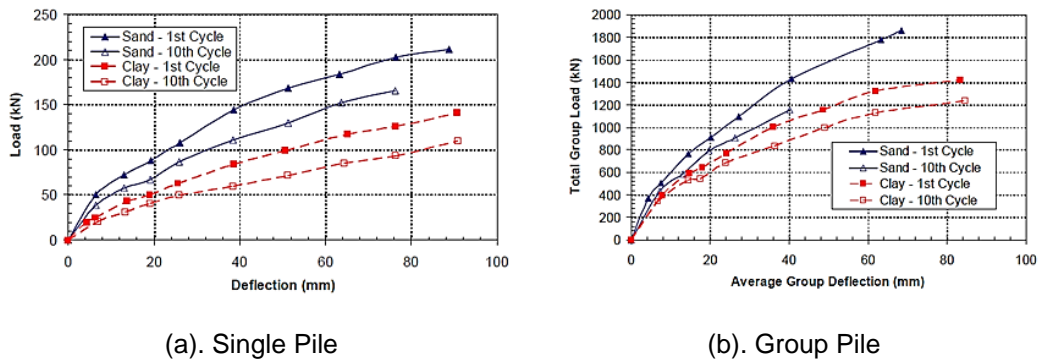


Figure 2-29 Load vs. Deflection Curves for the Single and Group Piles (Rollins et al., 2010)



#### 2.14 Improvement of Bearing Capacity Using Piles

Ariema and Butler (1990) stated that pile supported embankment improves the structural stability and reduces the structural deformation of foundation soil. The findings from Hewlett and Randolph (1988) indicated that piles covering around 10% of the area below an embankment can support more than 60% of the embankment load owing to the arching action in the embankment. Piles are used with geosynthetics as well to act as a composite system to improve the bearing capacity of soil. Geosynthetics when used with piles assist in efficient load transfer to the pile supports. A single layer of geosynthetic reinforcement will perform in tension, while a multilayer system will perform as a relatively more rigid or stiffened platform, like a plate, which is achieved by interlocking of soil particles with the geosynthetics (Han and Gabr, 2002).

A numerical analysis was conducted by Han and Gabr (2002) to study the changes in settlement of pile supported embankment on soft soil due to variation in fill height and pile elastic modulus. Impact of fill height is shown in Figure 2-30 (a) and effect of pile elastic modulus is shown in Figure 2-30 (b). The study showed that at all times, the settlement in the reinforced embankment was always lower than that in the unreinforced embankment. Also, the tension acting on the geogrid reinforcement decreases if there is support for the reinforcement from the foundation soil. However, the tension in the geogrid reinforcement remains constant between pile caps if there is no support and the geogrid reinforcement does not rest on the foundation soil (Figure 2-31, Han et al, 2011).

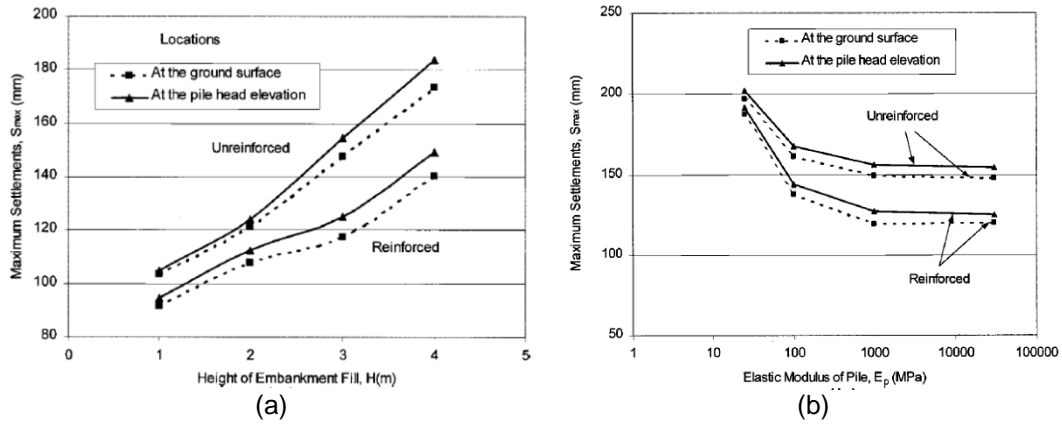


Figure 2-30 Effect of (a). Embankment Height and (b). Pile Elastic Modulus on Maximum Settlement of Pile Supported Embankment on Soft Soil (Han and Gabr, 2002)

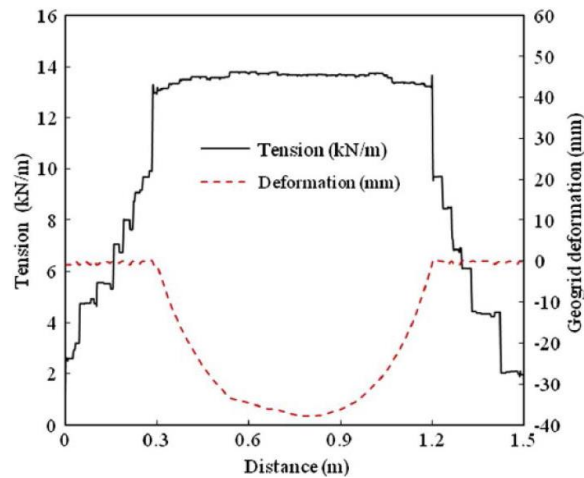


Figure 2-31 Tension and Deformation on Geogrid (Han et al., 2011)

Zaman (2019) conducted a study to improve the bearing capacity of foundation soil under embankment load utilizing recycled plastic pins. A field scale study was conducted with test sections each 15 ft. x 15 ft. in area. The construction and monitoring of the sections were carried out in two phases. For the first phase, two reinforced sections were constructed. The foundation soil of the test sections were reinforced with 4 in. x 4 in. and 6 in. x 6 in. cross-section RPP spaced at 3 ft. c-c. The second phase of study had a test

section, the foundation soil of which was stabilized using 4 in. x 4 in RPP spaced at 3 ft. c-c. The RPPs used in all sections were 10 ft. long and were installed in a staggered pattern. Both the phases constituted of a control section without any RPP. Horizontal inclinometer casing installed at the base of the embankment was used for monitoring the vertical displacement of the foundation soil.

The monitoring results showed that the control section in the first phase settled by almost 2.01 inches. The reinforced sections, however, showed very less settlement. The reduction in foundation settlement was about 60% when it was reinforced with 4 in. x 4 in. RPPs, while it was around 70% when 6 in. x 6 in. RPPs were used. The performance monitoring results of the second phase showed a reduction of about 56% in settlement in the reinforced section when compared to the control section. The author developed a numerical model using PLAXIS 2D to further analyze the test sections with varying RPP parameters. The numerical modeling results showed the support mechanism provided by the RPPs. When the embankment fill settles into the foundation soil, the foundation deforms laterally to accommodate the embankment soil. However, the RPPs when used to reinforce the foundation can restrict the lateral deformation and increase the load carrying capacity of the foundation. The FEM model concluded that increase in RPP size and decrease in RPP spacing significantly improved the bearing capacity of foundation soil. The study deduced that RPPs could be used to increase the load carrying capacity of weak foundation soil and significantly reduce the total and differential settlements of the foundation.

#### 2.15 Recycled Plastic Pins

Recycled plastic pin (RPP) is manufactured primarily from recycled waste plastics with the addition of other waste materials such as fly ash and saw dust (Chen et al., 2007).

They are commercially marketed as plastic lumber. Generally, more than half of the raw materials used for RPP comprises of polyolefin in the form of high-density polyethylene (HDPE), low density polyethylene (LDPE), and polypropylene (PP) (Khan, 2014). The polyolefin, due to its adhesive action, helps in combining high melt plastics with additives like fiberglass and wood fibers to form a rigid structure. RPPs have been successfully used as structural elements for marine and waterfront applications due to their environmental benefits and promising life cycle costs (Khan, 2014). Their use promotes sustainability since practically no maintenance is required for RPPs, especially for underground application, as they are resilient to moisture, corrosion, rotting and insects (Krishnaswamy and Francini, 2000).

#### *2.15.1 Manufacturing Process of RPP*

The first phase in manufacturing RPP involves the collection, cleaning, and pulverization of the raw materials. Roughly 500 soda bottles are used to make one 10 ft. long 4 in. x 4 in. RPP (Hossain et al., 2017). The pulverized raw materials are then melted in an extrusion machine. Malcolm (1995) reported that there are generally two methods to manufacture RPP – continuous extrusion process and injection molding process. In the continuous extrusion process, the molten plastic/raw mix is continuously extruded from a series of dies which can be used to produce RPPs for varying shapes and lengths. Different shapes can be formed during cooling of the extruded plastics. This method needs less labor and is appropriate for mass production due to the fast production time. However, it is difficult to control the cooling process for a uniform cooling which might result in warpage and caving of the pins. Furthermore, significant capital cost or investment is required for this method. The injection molding process, on the other hand, is relatively simpler and economical, albeit, with a limitation in the volume produced due to slower production rate (Malcolm, 1995). The molten plastic/raw material is injected into

a mold that shapes the pin with a fixed length. Uniform cooling can be achieved with this method.

Compression molding process is another method followed by manufacturers (Lampo and Nosker, 1997). In this method, other additive and raw materials are melted and mixed with batches consisting of 50-70% thermoplastics. Then, an automated scraper removes the melted mixture from the plasticator which is pressed through a heated extruder die into premeasured roll-shaped loaves. After this, a press-charging device is used to fill a sequence of compression molds. The final products are then cooled to a temperature of 40 °C inside the mold itself and ejected into a conveyor to be transferred for storage.

#### 2.15.2 Engineering Properties of RPP

The design and field performance of RPPs greatly depend on their engineering properties. The RPPs must have adequate compressive, tensile, and flexural strengths to perform as designed. Bowders et al. (2003) experimentally estimated the relevant engineering properties of RPPs when utilized for slope stabilization. The authors conducted uniaxial compression and four-point flexural tests on different RPP samples from three manufacturers to estimate the variance in properties. The experimental results of the tests are provided in Table 2-6 and Table 2-7 below.

Table 2-6 Results of Uniaxial Compression Tests (Bowders et al., 2003)

Specimen Batch	No. of Specimens Tested	Nom. Strain Rate (%/min)	Uniaxial Compressive Strength (MPa)		Young's Modulus, E <sub>1%</sub> (MPa)		Young's Modulus, E <sub>5%</sub> (MPa)	
			Avg.	Std. Dev.	Avg.	Std. Dev.	Avg.	Std. Dev.
A1	10	-	19	0.9	922	53	390	27
A2	7	0.005	20	0.8	1285	69	378	15

Specimen Batch	No. of Specimens Tested	Nom. Strain Rate (%/min)	Uniaxial Compressive Strength (MPa)		Young's Modulus, E <sub>1%</sub> (MPa)		Young's Modulus, E <sub>5%</sub> (MPa)	
			Avg.	Std. Dev.	Avg.	Std. Dev.	Avg.	Std. Dev.
A3	6	0.006	20	0.9	1220	108	363	27
A4	3	0.004	20	0.9	1377	165	363	25
A5	4	0.006	12	1.0	645	159	225	17
A6	4	0.006	13	0.9	786	106	238	34
B7	2	0.007	14	0.5	541	36	268	3
B8	2	0.006	16	0.4	643	1	308	0.5
C9	3	0.0085	17	1.1	533	84	387	40

Table 2-7 Results of Four-Point Bending Test (Bowders et al., 2003)

Specimen Batch	No. of Specimens Tested	Nom. Def. Rate (mm/min)	Flexural Strength (MPa)	Secant Flexural Modulus, E <sub>1%</sub> (MPa)	Secant Flexural Modulus, E <sub>5%</sub> (MPa)
A1	13	-	11	779	662
A4	3	4.27	18	1388	-
A5	3	5.74	11	711	504
A6	4	3.62	10	634	443
B7	1	4.05	9	544	425
B8	1	5.67	-	816	-
C9	2	3.21	12	691	553

Ahmed (2012) compared the engineering properties of RPP, wood, and bamboo piles when used as structural members. The study exhibited that wood had the highest compressive and flexural strength among the three different types of structural piles. Nonetheless, RPP was successful in facilitating the highest percentage (up to 19%) of soil movement. The main outcome of the study was the chemical and environmental resistance shown by the RPP which was considerably better than the other alternatives. The study indicated that for all the different environmental conditions considered, the maximum reduction in RPP strength was only 8%, while it was approx. 50% and 65% for the wood and bamboo piles, respectively. The high durability and adequate engineering properties of RPPs makes them a promising economically viable alternative over other materials.

Long Term Engineering Properties of RPP

A study on the long-term engineering properties of RPP was conducted where the impacts of outdoor weathering and environmental effects were investigated (Krishnaswamy and Francini, 2000). The authors assessed the effects of UV radiation, thermal expansion, and combined effects of moisture and temperature on the mechanical properties of RPP. The study concluded that there were no noteworthy changes in the flexural modulus and strength of the RPPs (Table 2-8) before and after the hygrothermal cycling as per ASTM D6109.

Table 2-8 Variation in Flexural Properties of Typical RPP Before and After Hygrothermal Cycling (Krishnaswamy and Francini, 2000)

	<b>Secant Modulus (MPa)</b>	<b>Stress at 3% Strain (MPa)</b>
Before cycling	674 ± 44	13 ± 0.83
After cycling	783 ± 99	16 ± 2.76

Breslin et al. (1998) carried out a study to examine the changes in engineering properties of RPPs used for outdoor decks. The authors initially tested the engineering properties of RPPs that were fabricated through the continuous extrusion process. Then, RPP samples used in decks were removed at 2-year intervals and tested for the same properties. The study revealed that there were no evident changes in the properties and the RPPs also did not undergo much warping, cracking, and discoloration.

#### Creep of RPP

RPP is vulnerable to creep and deflection under sustained static load due to its viscoelastic nature. According to Lampo and Nosker (1997), the creep factor of RPP should be highly considered if it is being used for load bearing applications. Due to the inherent viscoelasticity of plastics, a RPP will deform under sustained static loads which is more prominent at higher temperatures. Load-duration factors for use in design specifications have been formulated by previous studies. Any design guidelines for RPP needs to factor in the creep effect.

The heterogenous nature of the raw materials used for manufacturing RPPs lead to variations in the engineering properties of RPPs (Chen et al., 2007). The polymeric constituents of the raw mix undergo higher creep than other materials like timber, concrete, or steel, whilst simultaneously being resistant to chemical and biological degradation. Van Ness et al. (1998) conducted a study on commercially available RPP for long term creep response. Four groups of RPP with different compositions from four different companies were used for the study; some contained mixes of polyolefin, one contained glass fibers; however, all the samples were predominantly made of recycled polyethylene. From the study, it was concluded that the RPP comprising oriented glass fibers had higher creep resistance.



### *2.15.3 Field Scale Studies Using RPP*

Recycled Plastic Pins (RPP) have been successfully employed as an efficient and cost-effective alternative to traditional methods for shallow slope stabilization (Loehr and Bowders, 2007; Khan, 2014). Their exemplary resistance to chemical and environmental degradation has made them a promising substitute for geotechnical and structural applications. Previous studies have demonstrated the effectiveness of RPPs to stabilize shallow slope failures, where the pins provide resistance along the critical slip surface of a slope and improve the factor of safety. Apart from their use in slope stabilization, RPPs have also been demonstrated to perform effectively as shear keys at the base of MSE retaining walls to provide considerable resistance against the lateral driving forces (Zaman, 2019).

Khan (2014) conducted a study utilizing RPPs for shallow slope stabilization. The author described the field performance and subsequent numerical study of the innovative slope stabilization method. The study area was situated over Highway US 287, near the St. Paul overpass in Midlothian, Texas. The slope was 30-35 ft. high with a grade of 3H:1V and was constructed during 2003-2004. During September 2010, due to deformation of the slope, more focused near the crest, cracks started to develop near the pavement shoulder supported by the slope. This led to the requirement of slope stabilization to prevent further deformation.

The slope was reinforced with 4 in. x 4 in. size RPPs at various spacings and lengths. Three alternating sections were reinforced and designated as Reinforcement Section 1, 2, and 3, while two alternating sections were left unreinforced as controls sections and designated as Control Section 1 and 2. Each section was 50 ft. in width. Three inclinometers were installed to monitor the lateral deformation of the sections.

Inclinometers 1 and 3 were installed in Reinforced Section 1 and 2, respectively, while Inclinometer 2 was installed in Control Section 1. Topographical surveying was also conducted to estimate the ground settlement of the sections. It is to be noted that the existing cracks near the pavement shoulder were not sealed, so rainwater intrusion was allowed through the cracks. The field performance of the reinforced sections was compared to that of the control sections. The layout of the field sections is illustrated in Figure 2-32.

The topographical surveying results of the field sections showed that the control sections underwent considerable settlement at the crest (as much as 15 inches). Furthermore, maximum 3 inches incremental settlement took place in about one year. However, the reinforced sections performed very well with almost no incremental settlement. The total settlements estimated in the reinforced sections were within 2-4 inches.

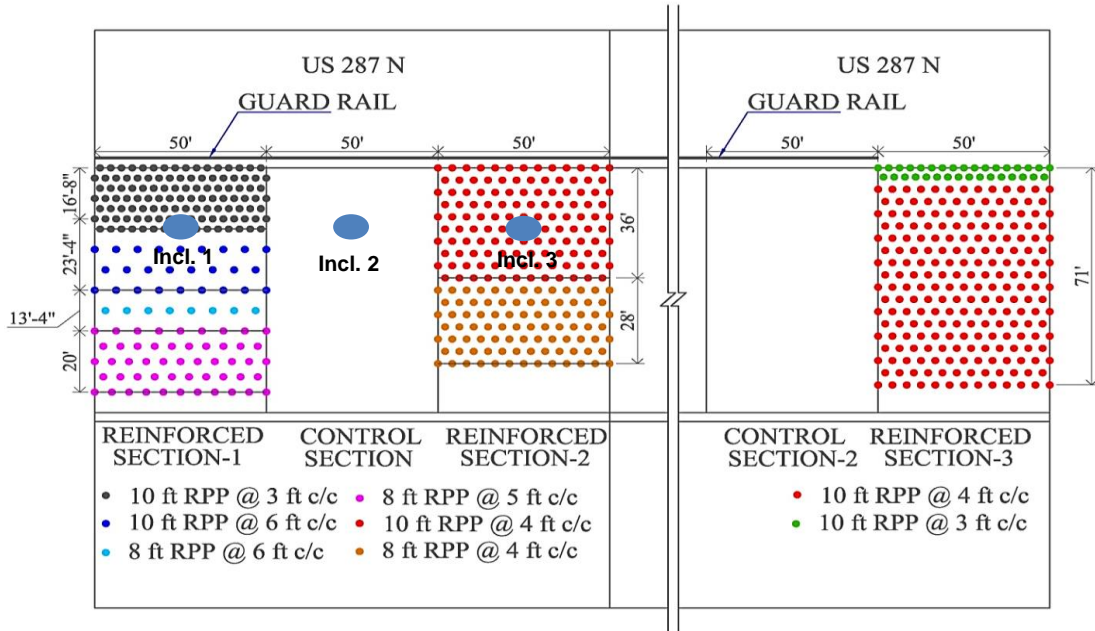


Figure 2-32 Layout of RPP at US-287 Slope (Khan, 2014)

The lateral displacements from Inclinometers 1 and 3 are plotted in Figure 2-33. It can be seen that after the initial load mobilization period, which was slightly more than a year, the incremental displacements had become almost constant. The incremental displacements were less than 0.1 inch in the reinforced sections after the load mobilization. The maximum lateral displacements were 1.3 and 1.8 inches in Inclinometers 1 and 3, respectively.

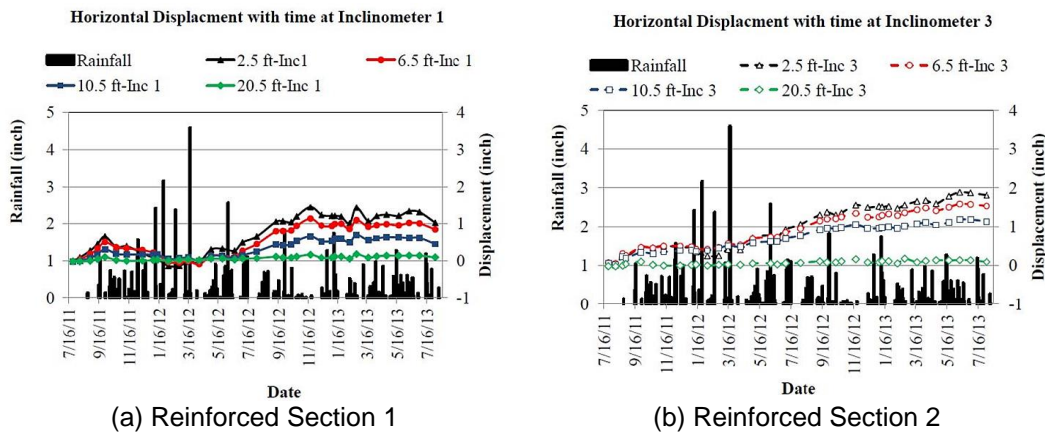


Figure 2-33 Variation of Horizontal Displacement with Time and Rainfall in (a). Reinforced Section 1 (b). Reinforced Section 2 (Khan, 2014)

Rauss (2019) investigated the long-term performance of shallow slopes stabilized with RPP. The author conducted a study on three slopes – US-287 (mentioned above), I-35 overpass at Mockingbird Lane, and SH-183 near the DFW airport in Texas. Both the I-35 and SH-183 slopes were stabilized with closely spaced RPPs at the crest compared to the other parts of the slope. Figure 2-34 presents a comparison of incremental settlement throughout the monitoring period in all the three slope sites.

It was observed that in general the yearly incremental settlements in all the three slopes decreased gradually with time. The readings from 2017-2018 show incremental

settlements as low as 0.15 inch. An unusual increase was seen in 2014-2015 and 2015-2016 in some slopes. The author mentioned that the above-mentioned timelines experienced rather more precipitation than other years. This in turn weakened the plastic clayey soils bringing about more settlement.

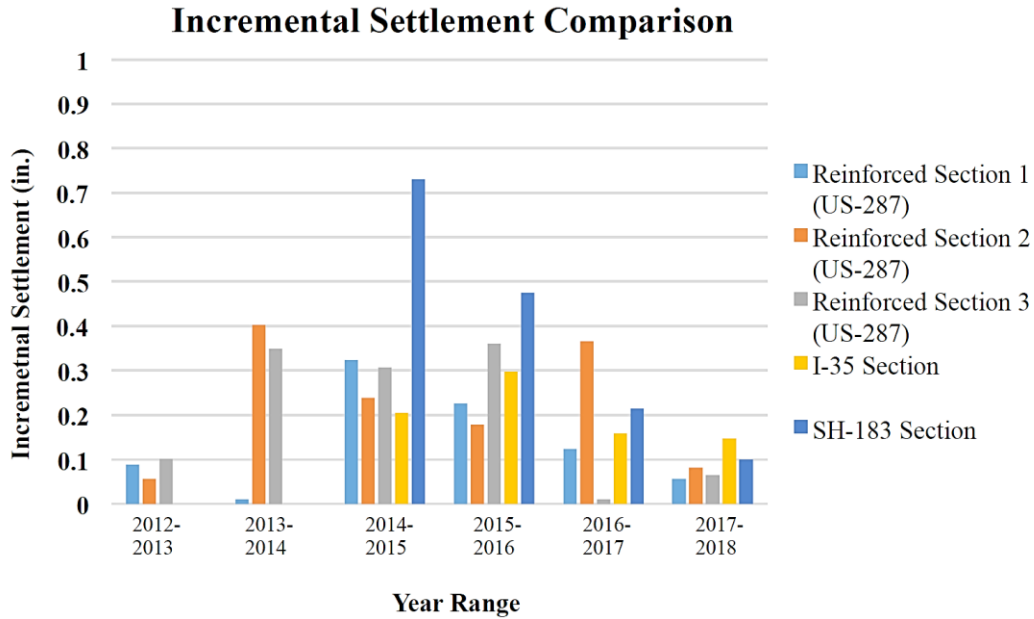


Figure 2-34 Comparison of Incremental Settlement Between US-287, I-35 and SH-183 Reinforced Sections (Rauss, 2019)

The study also compared the cost for the slope stabilization using RPP in all the three sites. Table 2-9 summarizes the cost per square foot of reinforcement for the investigated slopes. It can be stated that the overall cost for stabilizing slopes with RPP is a very cost-effective approach.

Table 2-9 Cost Per Square Foot of Reinforcement for US-287, I-35 and SH-183

(Rauss, 2019)

	<b>US-287</b>	<b>I-35</b>	<b>SH-183</b>
Total Cost (\$)	90,350	49,825	31,875
Area Covered	150 ft. x 73 ft.	50 ft. x 85 ft.	60 ft. x 90 ft.
Cost/Sq. Ft. (\$)	8.25	11.73	5.90

### 2.16 Numerical Study Using Finite Element Modeling

Numerical study using Finite Element Modeling (FEM) has been utilized by researchers to evaluate the field behavior of several geotechnical structures. It provides a basis for evaluating the performance of structures based on rigorous and complicated numerical calculations. Generally, the first step during such studies is calibration of the model to match the field behavior in terms of deformation. Then, further analysis and parametric studies are carried out to evaluate the field performance in a broader aspect. PLAXIS 2D is a two-dimensional finite element method (FEM) program widely utilized in the geotechnical engineering field for numerically analyzing deformation, stability, and groundwater flow (PLAXIS 2D Reference Manual, 2017).

Budge et al. (2006) demonstrated the methodology needed to calibrate a PLAXIS model using field deformations of an MSE wall during construction. The authors used the field data of an MSE wall at Salt Lake City, Utah. The foundation of the wall was composed of soft clayey soil. Extensive instrumentation was done to monitor the behavior of foundation soil and the MSE wall during and after construction. Both vertical and horizontal deformations of the foundation soil and MSE wall were measured during the construction. Vertical stresses developed within the wall and stresses developed in the

reinforcements were also measured. The strength properties of the soil were experimentally determined in the laboratory using constant rate of strain (CRS) consolidation and triaxial tests. A finite element model (Figure 2-35) was developed in PLAXIS 2D following the same wall geometry and soil properties as in the field. The model also shows the layout of horizontal inclinometers and vertical extensometer casings.

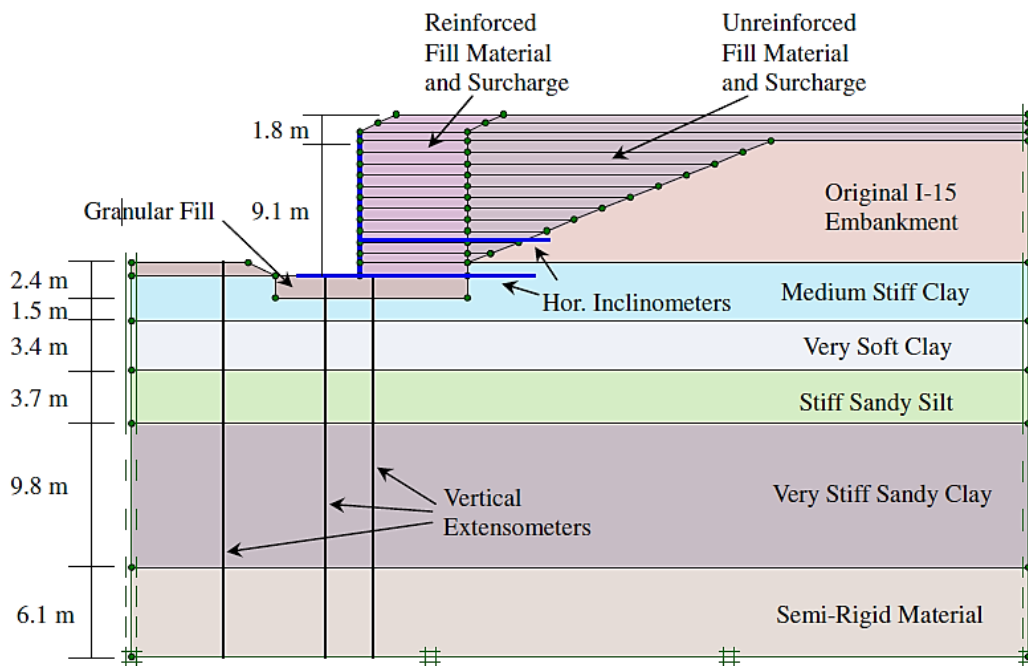


Figure 2-35 PLAXIS 2D Model of MSE Wall on I-15

(Budge et al., 2006)

After the MSE wall was modeled in PLAXIS 2D, the deformations from the FE model were compared to the field deformations. The vertical extensometers gave the settlements in the foundation soil, while the horizontal inclinometers measured the vertical deformations within the wall. Figure 2-36 compares the foundation settlement

obtained from the vertical extensometers and numerical modeling, which were plotted against a reference datum elevation. The numerical model could very well simulate the settlements as measured in the field as both the plot lines were close to each other. Moreover, the numerical model obtained settlements could replicate the significant settlements seen in the soft clay layer between the reference elevations 96 m and 92 m. Figure 2-37 compares the lower horizontal inclinometer data from the field and numerical modeling data at the end of primary consolidation. A satisfactory calibration fit was shown by this graph as well. These plots validate the successful calibration of the FE model with the field behavior.

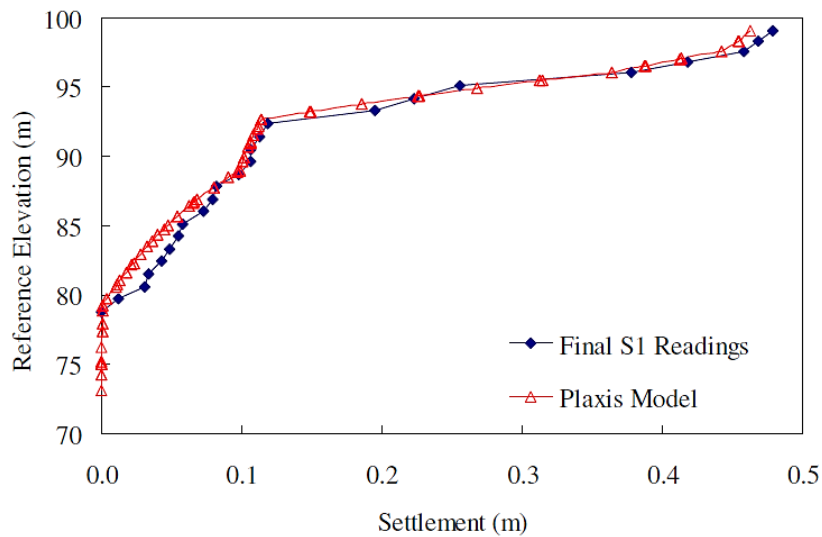


Figure 2-36 Comparison of Vertical Extensometer Data with PLAXIS Model Data  
(Budge et al., 2006)

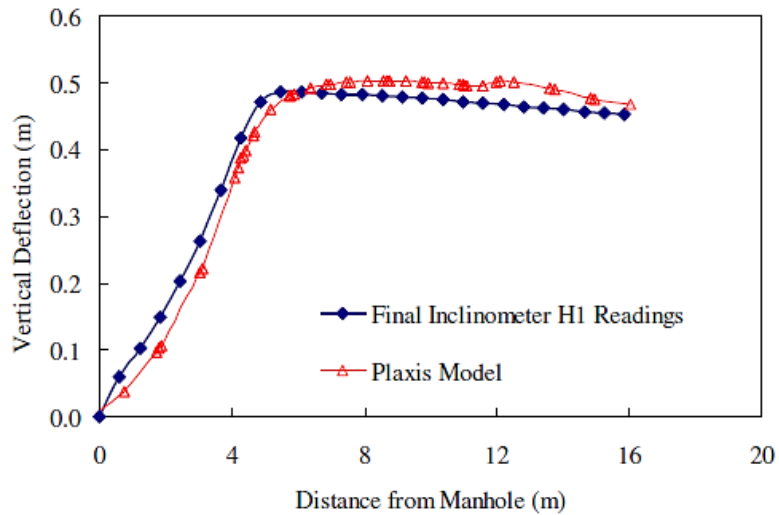


Figure 2-37 Comparison of Horizontal Inclinerometer Data with PLAXIS Model Data  
(Budge et al., 2006)

Singh and Babu (2010) used 2D finite element modeling to numerically simulate the behavior of soil nail walls. The main objective of the study was to compare Hardening Soil (HS) Model and Hardening Soil with Small-Strain Stiffness (HS small) Model with conventional Mohr-Coulomb (MC) Model in numerically simulating a soil nail wall. The outcomes of the study showed that there were minimal changes in the overall wall stability and structural forces such as axial forces, bending moments, and shear forces in the soil nails when advanced soil models were used instead of the MC model. The authors recommended the use of advanced soil models in only such cases where even a slight change in lateral displacement of soil nail wall is expected to affect the wall stability or deformation conditions. Also, when the wall is constructed on soft soils, the advanced models provide a better estimate of the base heave of the excavation.

Huang et al. (2013) used a refined numerical modeling technique to develop an understanding of design methods for laterally-loaded drilled shafts in MSE walls. A major



finding of the study is that a non-linear soil model which can consider stress-dependent, strain hardening/softening behavior will prove to be more effective than the conventional Mohr-Coulomb model. For the wall facing, an assembly of discrete blocks with appropriate interfaces can be modeled rather than a continuous surface which has been followed conventionally. The compaction-induced lateral pressure can be accommodated in the model by simply increasing the permanent lateral pressure during initialization.

Liu (2012) presented a finite element analysis to investigate the lateral facing displacement after years of creep for geosynthetic-reinforced soil segmental retaining walls. The deformation of reinforced soil zone was mainly dependent on the reinforcement spacing and stiffness, rather than the reinforcement length. Only when the reinforcement stiffness was less, along with larger spacing – soil strength played the deciding factor. However, the reinforcement length played the major role while deciding the lateral displacement at the back of the reinforced zone.

Rouili et al. (2005) presented a numerical model of an L-shaped very stiff concrete retaining wall and validated the results using experimental data. The authors conducted a reduced scale (1/60) prototype centrifuge model to collect the experimental data. For the finite element model, PLAXIS 2D with plane strain model was used. The wall was modeled using one-dimensional linear beam element, while hardening soil model in drained conditions was used. Both the numerical model and centrifuge test indicated a combination of rotational and translational movement of the wall. Also, both the test and model exhibited non-linear distribution of lateral earth pressure as shown in Figure 2-38

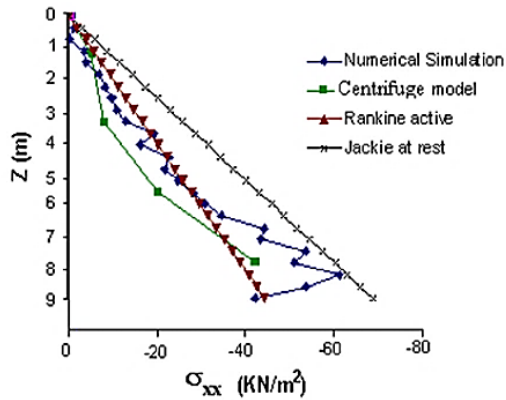


Figure 2-38 Lateral Pressure Acting on the Wall Stem (Rouili et al., 2005)

An extensive study was conducted by Damians et al. (2015) to develop an FEM model to simulate quantitative performance features of a field-scale steel-strip reinforced soil wall.

Figure 2-39 shows the layout of the wall and instrumented sensors.

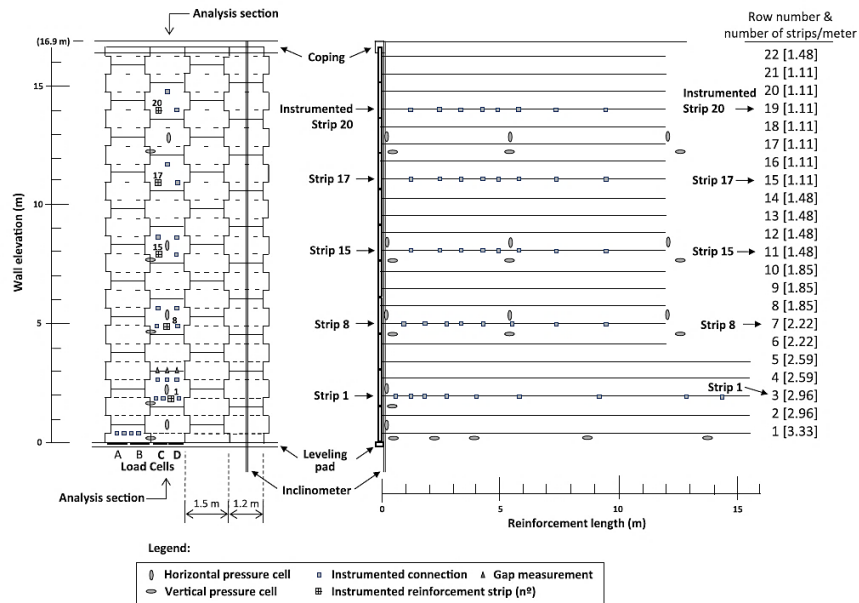


Figure 2-39 Layout of Retaining Wall and Sensors Under Study (Damians et al., 2015)

The wall height was 16.9 m (~55 ft.). The facing was made of precast concrete panels, while ribbed steel strips were used as reinforcement. For the numerical modeling, the

wall facing was modeled using discrete panels, and the steel strips were modeled as continuous sheet elements. Reinforced and retained soil were modeled first using the Mohr Coulomb Model, and second using the nonlinear Hardening Soil Model. The stiffness was reduced by 50% for the soil zone located within 1 m of the back of the facing due to reduced compaction in that region. The interface value (R) was used between 0.2-0.4 for soil-concrete facing panel interface, while it was 0.3 for soil-reinforcement interaction. The vertical toe load was used to calibrate the FE model. The results showed that the vertical toe load increased non-linearly with wall height. The measured and predicted results showed that some down drag force existed such that the toe load is greater than the facing self-weight. The HS model was in good agreement with the field results for the wall embedment case at the bottom of the wall, whereas, between 5-10 m, the MC model performed better. Numerical predictions indicated that the top panels rotated inward as a result of net outward wall deformations that occurred at lower elevations. It was also established that the vertical loads acting through the height of the wall are always greater than the self-weight of the panels. This is due to the panel-soil interface friction and connection down drag forces.

Previous studies mentioned above (Kim and Bilgin, 2007; Sarath et al., 2011; Khan, 2014; Zaman, 2019) utilized PLAXIS 2D to numerically simulate the field conditions of their respective studies. The authors then conducted parametric studies changing various soil and material parameters and evaluating the effect of such changes in the deformation and factor of safety. Hossain et al. (2012) conducted a study with an objective to determine the possible causes of excessive movement in an MSE wall located at State Highway 342 (SH 342) in Lancaster, Texas. Granular soil was used as the backfill material with steel wire meshes as the reinforcement. About 150-mm wide cracks were observed in the pavement due to significant movement of the MSE wall. A

geotechnical site investigation was performed by conducting soil drilling and electrical resistivity imaging (ERI) survey of the subsurface. The soil samples collected during drilling were later tested in the laboratory. Numerical modeling was also conducted using PLAXIS 2D incorporating the elastic perfectly plastic Mohr-Coulomb model. Figure 2-40 presents the model output predicting the total displacement and vertical displacement. The model predicted about 291 mm displacement at the top of the MSE wall, whereas the field observed value for the same location was 300-450 mm. The results of the study demonstrate that numerical modeling using FEM can be regarded as a reliable method to simulate field conditions.

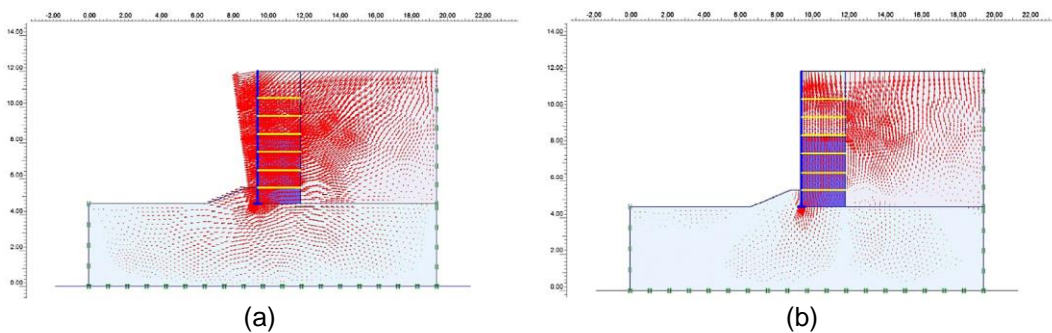


Figure 2-40 Model Predicted Displacements (a). Total Displacement (291 mm) (b). Vertical Displacement (179 mm) (Hossain et al., 2012)

Mahmood (2009) investigated a case history of a failed Segmental Retaining Wall (SRW) located in Rockville, Maryland. The author conducted parametric studies to determine the effect of varying reinforcement and site conditions on MSE wall failure. Stability analyses of the SRW were carried out numerically using PLAXIS 2D. The model values were in close conformity to the field obtained data. This justified the use of numerical modeling to predict field behavior. The study concluded that the wall failure and subsequent collapse were caused by a combination of various factors such as – improper installation of

geogrid due to which adequate tensioning of geogrid was not achieved, insufficient length of geogrid at the upper level of the wall and use of low permeability backfill soil causing inadequate internal drainage which produced large hydrostatic pressure at the wall face.

Parametric studies were carried out to assess the effect of geogrid length, geogrid strength, friction angle and cohesion of backfill soil, and elevation of water level in the reinforced section behind the MSE wall facing. It was found that for conditions with no water table in the wall level, geogrid length should be at least 15 ft. for a 13 ft. high MSE wall. When there is water at mid-level of wall, geogrid length should be 20 ft. An interesting finding of the study was that use of sandy soil with cohesion showed less wall movements than use of cohesionless soil. Furthermore, it was observed that higher geogrid strength tends to produce smaller displacements.

#### 2.17 Statistical Modeling

Field testing, experimental testing, centrifuge modeling, and numerical analysis are effective methods of investigation. However, certain times due to schedule and budget constraints, they are not feasible. In such cases, statistical prediction models have proven beneficial to study or comprehend the behavior of geotechnical structures. Statistical approaches pave way for simpler and cost-friendly assessment of such structures. Such approaches have been widely used to assess the performance of MSE walls (Chalermyanont and Benson, 2004, 2005; Kibria et al., 2014; Bathrust and Yu, 2018; Allen et al., 2019). Studies have shown the use of a calibrated numerical model to extract comprehensive synthetic data and evaluate the behavior of MSE walls (Yu and Bathrust, 2017). Statistical prediction models have been widely accepted for other geotechnical engineering practices as well (Faysal, 2017; Bhandari et al., 2019).

Lin et al. (2016) conducted a study to calculate probabilistic and deterministic values of maximum lateral deformation of MSE wall facing. The authors first used the finite difference method in FLAC to calibrate a model according to physical tests conducted in a controlled laboratory. Sensitivity analyses were performed on various parameters to finalize the most influential factors affecting the lateral displacement. Six factors were chosen as the most significant factors influencing the response. Thereafter, Response Surface Method (RSM) was used to formulate a deterministic quadratic expression to estimate normalized lateral displacement of MSE wall. The authors then conducted large numbers of Monte Carlo simulations using random values of the six selected factors. Finally, as part of a reliability performance-based design framework, the probability of reaching prescribed deformation conditions were predicted. Sayed et al. (2010) performed a similar study where the authors used FEM to numerically model an MSE wall at first. Then, they used the response surface method to determine the reliability of the retaining structure. The probabilistic approach was fruitful in determining the risk of wall failure due to uncertainties in soil properties, and soil-reinforcement interaction parameters. The paper also demonstrates a case study of a failed segmental retaining wall by performing back-analysis using the above-mentioned methods.

Kibria et al. (2014) conducted a study on a steel wire mesh reinforced MSE wall using FEM and multiple linear regression. The paper presents the use of field instrumented data to calibrate an FE model in PLAXIS 2D. Sensitivity analysis was then conducted to investigate the effects of MSE wall height, reinforcement  $L/H$  ratio, reinforced fill friction angle, retained fill friction angle, and reinforcement stiffness on the horizontal displacement of the top of wall facing. Stepwise regression and a coupled interaction surface showed that reinforcement stiffness and length were prominent among other parameters on impacting the horizontal displacement of a wall. However, this was at a

specific wall height, and that the horizontal movement of an MSE wall was highly sensitive to the wall height. Ahmed et al. (2020) conducted a parametric study on RPP stabilized shallow slopes. The authors then used the parametric results to develop a prediction model using a statistical method and a machine learning method. The effect of RPP length and spacing on the factor of safety of slope failure was investigated. It was reported that a higher resistance and subsequently higher factor of safety was achieved with a lower spacing of RPPs.

#### 2.18 Limitations of Previous Studies

Numerous studies have been conducted on the performance of MSE walls, with horizontal displacement of walls taking its fair share. Consequently, methods to improve the lateral displacement of wall facings have been proposed, experimented, and validated. However, there is a gap in the current state of knowledge on the lateral displacement of MSE wall base or the foundation soil. Very limited studies have been carried out regarding the stabilization of MSE walls against lateral sliding. The idea of incorporating concrete shear keys has its own limitations (high cost, rigid nature, susceptible to corrosion), which opens a door for the need of novel stabilization schemes. On the other hand, researchers have documented the successful use of RPPs in stabilizing shallow slope failures. More recently, the benefits, construction methods, and design methodologies of utilizing RPPs have been investigated in North Texas. These studies have shown that the lateral capacity of RPPs is high enough to stabilize the sliding of soil mass in slopes. Having considered all the factors, this study evaluates the performance of RPPs in increasing the shearing resistance of MSE wall base. The following chapters explain the site investigation, construction of field test sections, performance monitoring, and discussion and analysis of results.

## Chapter 3

### METHODOLOGY

#### 3.1 Project Background

The increasing use of MSE walls for retaining slopes and highway embankments necessitates intensive research on the stability of such walls. Lateral sliding, among the external failure mechanisms, has been an ever-increasing issue in North Texas. TxDOT and private contractors likewise have incurred substantial loss because of the MSE walls sliding outwards. Therefore, a novel solution to stabilize MSE walls against lateral sliding is needed. In this regard, the objective of the current study is to develop an innovative and sustainable method to improve the lateral stability of MSE walls using recycled plastic pins. The main idea behind the study is the use of RPP as a shear key at the base of MSE wall to create a composite system. This might increase the shear resistance of the base of wall and control the lateral displacement. Also, the inclusion of RPP to some depth in front of the wall base might restrict the failure plane to progress, thereby, making the wall safe against global failure as well. To achieve this objective, four test sections were required to be constructed for the field scale study: three reinforced sections with varying size and spacing of RPPs and one control section without any RPPs. The test sections had to be instrumented accordingly to monitor the lateral and vertical movement of the base of the wall. This chapter demonstrates the research methodology focusing on the field activities undertaken.

#### 3.2 Site Selection

The first step was to find a suitable site for construction of the field test sections. A location inside Hunter Ferrell Landfill in the City of Irving, Texas was selected for the study. As shown in Figure 3-1, the site is situated inside the landfill at a far distance from



the active working face of the landfill. The study area can be reached by taking the hauling roads inside the landfill, or a road over the levee from the eastern side of the landfill. A new cell construction was undergoing in the landfill. The excavated pile of soil from the new cell construction was used as a sloping ground required for providing the backfill load for the wall. The topography of the site location was advantageous as there was enough sloping ground and space for the wall construction (Figure 3-2). A topographic survey was carried out on February 16, 2019 to estimate the height and inclination of the existing slope at site. The inclined length of the slope was 175 ft. while the height was 50.5 ft. Thus, the inclination of the slope was estimated to be 3.3H : 1V. The geological characterization of the site provided by USGS mentions presence of flood-plain deposits, gravel, sand, silt, silty clay, and organic matter. The sub-surface is characterized by Eagle Ford Shale formation.



Figure 3-1 Site Location Map

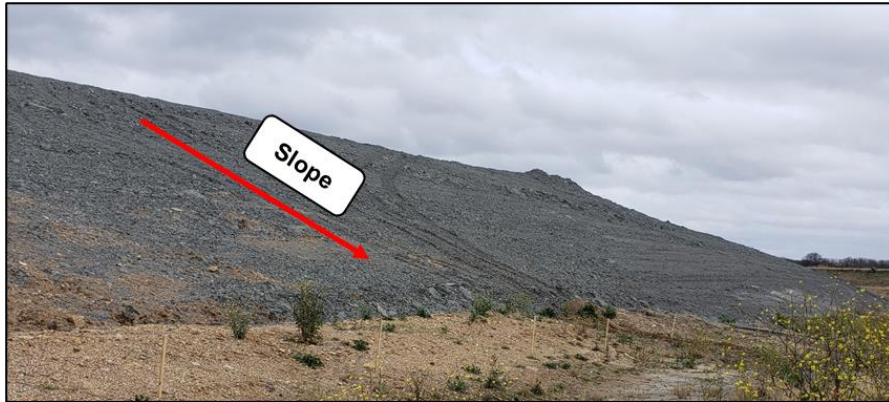


Figure 3-2 Suitable Slope and Area for Construction of Test Sections

### 3.3 Site Investigation

The field work for the site investigation was conducted according to the recommendation of TxDOT Geotechnical Manual, Section 1 – “Soil Survey”. The main objective of the soil investigation was to assess the sub soil condition at the site to determine the suitability of the area for the construction of the test sections.

#### 3.3.1 *Geotechnical Drilling*

Four boreholes were drilled for sub-surface sample collection as shown in Figure 3-3. Each borehole was 20 ft. in depth. The boreholes were located at the toe of the slope where the test sections would be constructed. Hollow-stem augers were used for drilling which were attached to a truck mounted drilling rig. Each auger was 5 ft. in length so subsequent auger sections were attached as the drilling progressed. Both undisturbed and disturbed samples were collected at certain intervals. Some specific information regarding the geotechnical drilling is tabulated in Table 3-1.



Figure 3-3 Location of the Soil Borings

Table 3-1 Geotechnical Drilling Details

Location	Hunter Ferrell Landfill, Irving, Texas
Client	Texas Department of Transportation
Number of bore holes	4 nos.
Drilling depth	20 ft.
Texas Cone Penetrometer (TCP) locations	15 nos.
Undisturbed sample locations	12 nos.
Disturbed sample locations	15 nos.

Undisturbed samples were retrieved from each borehole at 3 depths with approximate 4-5 ft. interval. The sample was collected using a thin-walled Shelby tube sampler with outer diameter of 3 inch. First, the depth to the bottom of the hole was measured to confirm the depth of sample collection. Then, the Shelby tube was jacked to the required

depth, and then carefully taken out to the surface. An extruder was used to extrude the sample from the sampling tube. The extruded sample was then wrapped in a moisture bag and stored in a storage box to be taken to the laboratory for testing.

Disturbed samples were retrieved from each borehole at 4 depths with approximate 4-5 ft. interval. Texas Cone Penetrometer (TCP) was used to measure the soil resistance in order to classify the soil's compactness. TCP was conducted at 4 depths for each borehole. The TCP test was done in accordance with Tex-132-E. The test setup consists of a 170 lb. hammer with a  $24 \pm 0.5$  in. drop, drill stem, an anvil threaded to fit the drill stem and slotted to accept the hammer, and a TCP Cone – 3 in. in diameter with a 2.5 in. long point. The test started with dropping the hammer to drive the penetrometer cone attached to the stem. The cone was driven for 6 inches or 12 blows, whichever came first and seated in the soil. The test then continued with a reference at that point. N-values (number of blows) were noted for the first and second 6 inches for a total of 12 inches for relatively soft materials, while the penetration depth in inches was noted for the first and second 50 blows for a total of 100 blows in hard materials. Figure 3-4 shows the drilling setup and sample collection. Vertical inclinometer was later installed in the same boreholes, which will be explained in the following sections.

The average TCP blow count of the foundation soil was found to be 11 (equivalent SPT=8) and 15 (equivalent SPT=10) at a depth of 5 ft. and 10 ft., respectively. The results indicated that the soil till a depth of 10 ft. from the ground surface was soft to medium clayey sand. Stiff shale formation was encountered after 10 ft. Perched water table was encountered at 10 ft., 12 ft., 9 ft., and 8.5 ft. from the ground surface in BH-1, BH-2, BH-3 and BH-4, respectively. The bore-logs of the four drillings are presented in Appendix A.



(a)



(b)



(c)

Figure 3-4 (a). Drilling Setup (b). TCP Test (c). Undisturbed Shelby Tube Samples



### 3.3.2 *Geophysical Testing*

Geophysical methods of soil investigation can be regarded as an economical and efficient technique to understand the subsurface conditions of soil. They give a general idea about the continuous qualitative change in soil properties, mostly moisture contents and presence of larger voids, of the subsurface. It is an efficient method to visualize the variation in moisture and stratigraphy of subsoil at different times and locations (Kibria, 2014). It can be used in conjunction with geotechnical boring, which only gives detailed information at points rather than the continuous image. One of the prominent methods for geophysical investigation is the Resistivity Imaging (RI).

Resistivity imaging is utilized for visualizing the horizontal and vertical variations in subsurface moisture, environmental anomalies, and near surface geology. Figure 3-5 shows the position of the test sections at the base of slope. Resistivity imaging survey was performed along two lines as shown in Figure 3-5. The survey was performed using 8-channel unit. The system consisted of 28 electrodes placed at 3 ft. spacing along the slope. The total length of the survey line was 81 ft. For RI across the toe, the spacing of electrodes was 6 ft., making the total length 162 ft. Figure 3-6 and Figure 3-7 show the results of the resistivity imaging survey. Higher resistivity indicates relatively dry soil, while lower resistivity indicates higher moisture content.

It can be seen from Figure 3-6 that the resistivity near the surface of the slope is relatively less indicating presence of higher moisture. This indicates seepage of moisture along the slope. Also, the resistivity is higher below the near surface of slope due to presence of voids, as the backfill has not been compacted. Figure 3-7 presents the resistivity across the toe of slope. The overall resistivity is low throughout the section, indicating presence of moisture. The geotechnical drilling results showed presence of perched water table at

approximately 10 ft. from the surface. This was verified from the geophysical testing which showed spatial variation of moisture.

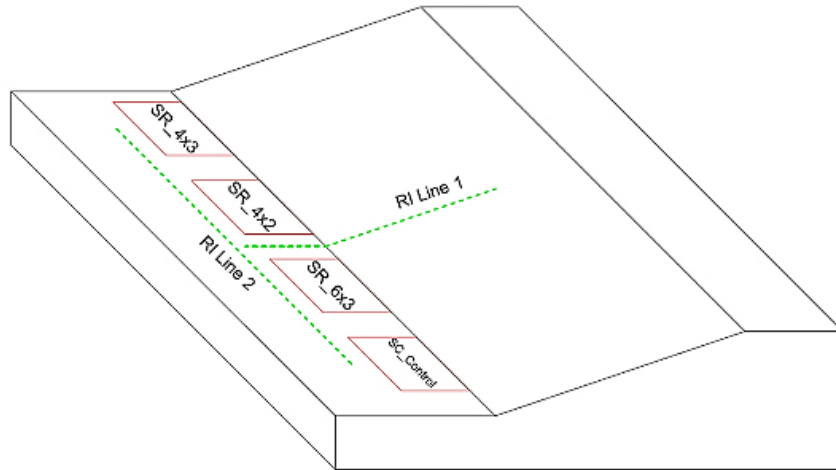


Figure 3-5 Resistivity Imaging Survey Lines

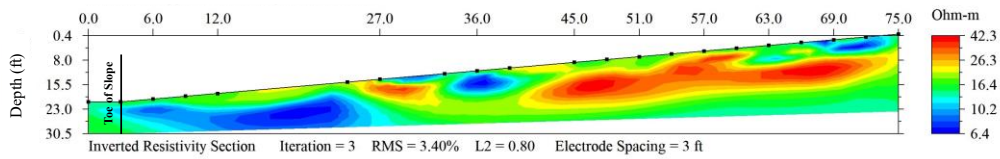


Figure 3-6 Resistivity Imaging Result Along the Slope (Line 1)

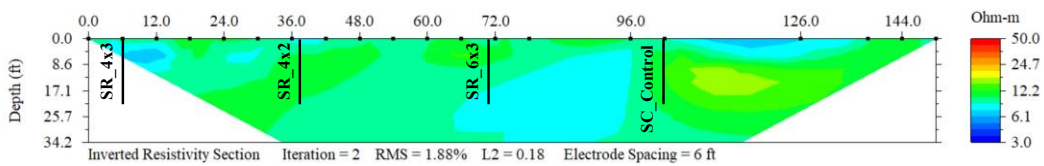


Figure 3-7 Resistivity Imaging Result Across the Toe (Line 2)

### 3.4 Laboratory Testing

The undisturbed samples were used for strength testing, while the disturbed samples were used for determining the physical and mechanical properties of the soil. Disturbed soil samples were also collected from the existing slope and fundamental soil properties were tested in laboratory. Samples of the sand, which was later used in the reinforced zone of the test sections, were also tested for basic soil properties.

#### 3.4.1 *Gravimetric Moisture Content Test*

Disturbed samples were collected from both the toe and the existing slope at the site. Soil samples were collected from the existing slope till a depth of 3 ft. from the surface. Moisture content of the collected samples were determined according to the standard test method ASTM D4643-08.

The moisture content in the existing slope increased with depth and the range of moisture content was within 11.5% - 19%. Figure 3-8 shows the changes in moisture content with depth for the four boreholes at the toe of the slope. It is to be noted that the water content ranges between 10% - 24% in all the boreholes. Even though the perched water table was found at around 10 ft. depth, the moisture content of the soil at deeper depths did not increase significantly. This might be due to the fact that shale with low permeability was found after around 10 ft. depth. This can be an indication that the shale layer is not fully saturated, and the water might just be in perched water pockets present in cracks.



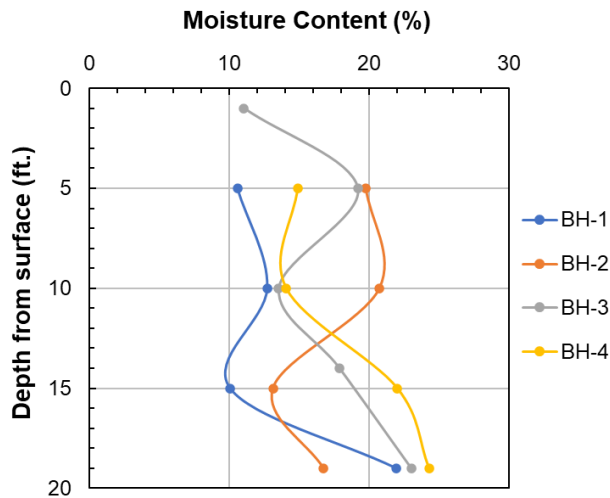


Figure 3-8 Variation of Moisture Content with Depth at the Toe of the Slope

### 3.4.2 Grain Size Distribution Test

The particle-size analysis of soils at different depths was conducted using hydrometer test and mechanical sieve analysis. ASTM Standard D6913 “Standard Test Methods for Particle-Size Distribution (Gradation) of Soils Using Sieve Analysis” was followed for the test. Four samples from 5 ft., 10 ft., 15 ft., and 19 ft. depth were selected from one of the boreholes. At first, 600 gm. of sample from each depth was oven-dried and passed through No. 10 (2.00-mm) sieve. Then, 50 gm. of No. 10 sieve passing sample was used for the hydrometer test. A solution of 40 gm. sodium hexametaphosphate in 1000 ml of distilled water was used as a dispersing agent. All the No. 10 sieve passing soil were soaked in the dispersing agent solution for 16 hrs. Then, the soaked soil-water slurry was transferred to a dispersion cup and stirred with a mechanical stirring apparatus for 1 min. The dispersed solution was then transferred to a glass sedimentation cylinder with a 1000 ml mark. The cylinder was filled with distilled water up to 1000 ml. It was also agitated for 1 min. such that no sediment remained at the bottom of the cylinder. Finally,

hydrometer readings were taken at specified time intervals for 24 hrs. A control solution with the dispersing agent in the same volume as used for the soil dispersion was also made to determine the correction factor. Figure 3-9 shows the four hydrometer samples prepared for the test. The figure acts as a visual representation of the layers of soil at the foundation of the wall. The soil is mostly sandy at the first 5 ft. depth from the surface. Gradually, the clay fraction increases with depth, with dominant presence of shale at the bottom 15-20 ft. depth. The soil retained on No. 10 sieve along with the soil from the hydrometer test which retained on No. 200 sieve was subjected to wet-sieving. Then, using a mechanical sieve machine, all the soil was sieved to obtain the particle-size distribution of the soil. The results of the particle-size distribution have been tabulated in Table 3-2.

Figure 3-9 shows the particle-size distribution graphs of samples from 5 ft., 10 ft., 15 ft., and 19 ft. depth.

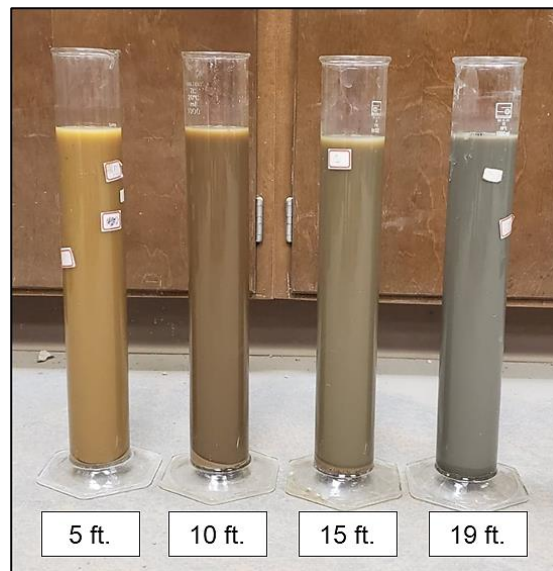


Figure 3-9 Hydrometer Samples

Table 3-2 Particle-Size Distribution

Depth (ft.)	Gravel (%)	Course to Medium Sand (%)	Fine Sand (%)	Silt (%)	Clay (%)	$C_U$	$C_z$
5	39.46	29.95	9.56	8.03	13.00	3661.54	10.10
10	7.75	12.41	58.31	11.53	10.00	100.00	16.35
15	4.11	7.25	9.65	35.49	43.50	10.83	0.09
19	1.44	3.70	9.76	39.60	45.50	5.00	0.20

Note:  $C_U$  = Uniformity Coefficient;  $C_z$  = Coefficient of Gradation

Figure 3-10 shows the particle-size distribution graphs of samples from 5 ft., 10 ft., 15 ft. and 19 ft. depth.

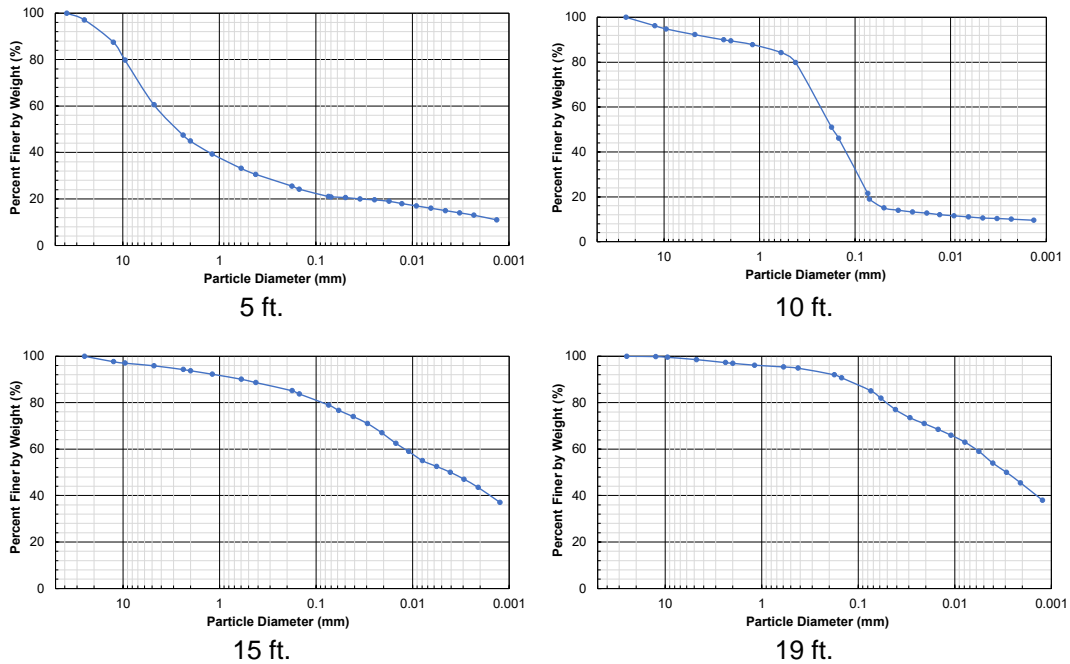


Figure 3-10 Grain Size Distribution Curves of the Foundation Soil

Unified Soil Classification System (USCS) was followed to classify the soil based on the particle-size analysis results, which have been presented in Table 3-3.

Table 3-3 USCS Classification of Foundation Soil

S.N.	Depth (ft.)	Group Symbol	Group Name
1	5	SC	Clayey Sand with Gravel
2	10	SC	Clayey Sand
3	15	CL	Lean Clay with Sand
4	19	CL	Lean Clay

The grain size distribution analysis of the backfill sand was also performed following the similar procedure as outlined above. The size distribution graph and USCS classification are presented in Figure 3-11.

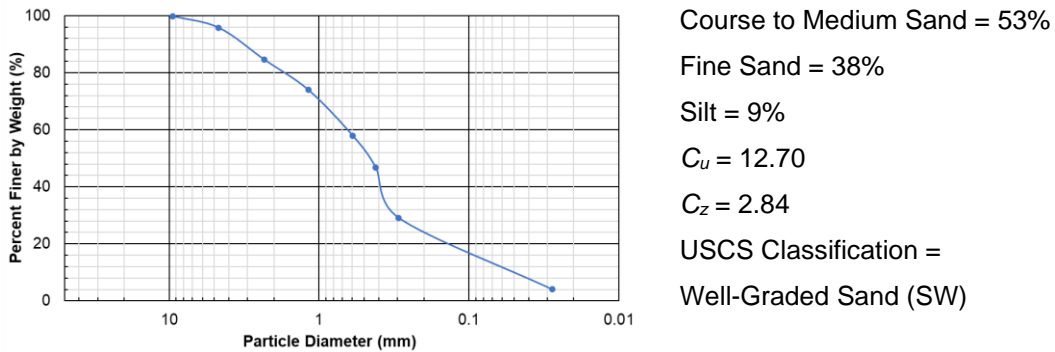


Figure 3-11 Grain Size Distrubution Curve of the Backfill Sand

### 3.4.3 Atterberg's Limit Test

The liquid limit (LL) and plastic limit (PL) of the soil samples collected from the existing slope and toe of the slope were determined as per ASTM standard D4318. The liquid limit was found to be between 42.74 and 46.52 for the existing slope, while it was in the range of 21.36 to 47.58 for the toe of the slope (test sections foundation). Plastic limit

was found to be 24.20 for the retained slope, while it was between 13.45 to 29.02 for the foundation soil.

Finally, plasticity index (PI) of the soil was calculated by using the equation,  $PI = LL - PL$ . The value of plasticity index was calculated to be in the range of 18.54 to 22.32 for the retained soil. The PI ranged from 9.8 to 30.56 for the foundation soil. The PI and LL were plotted on the plasticity chart, which classified the soil as low plastic clay (CL) as shown in Figure 3-12.

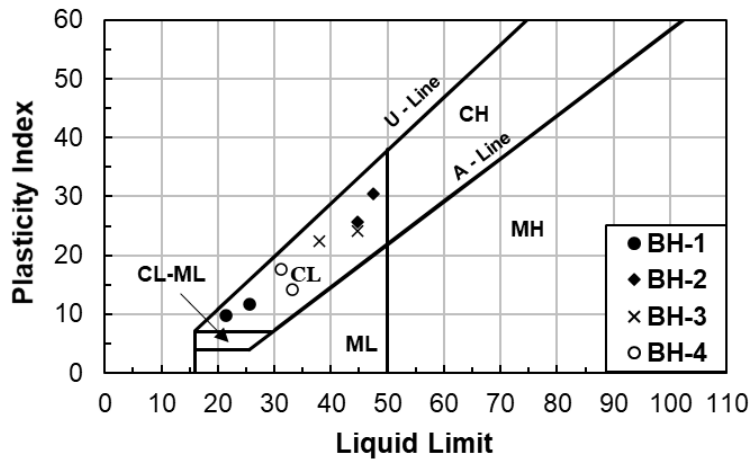


Figure 3-12 Plasticity Chart for the Foundation Soil

#### 3.4.4 Strength Test

Strength characterization of the foundation soil was carried out through Unconfined Compressive Strength (UCS) and Direct Shear (DS) tests. ASTM D2166 was followed for the UCS test on the undisturbed soil samples retrieved at site. ASTM D6528 and ASTM D3080 was followed for the DS tests. The UCS ranged between 3592 - 6600 psf for the soil between 15 – 20 ft. depth (Figure 3-13). The cohesion intercept was found to be in the range of 313 – 418 psf for the soil till a depth of 10 ft. However, the soil after 10 ft. had cohesion in the range of 1796 – 3300 psf. The effective friction angle of the

foundation soil was 25° – 27° till a depth of 10 ft. After which, it was about 15° for the soil at 15 ft. depth.

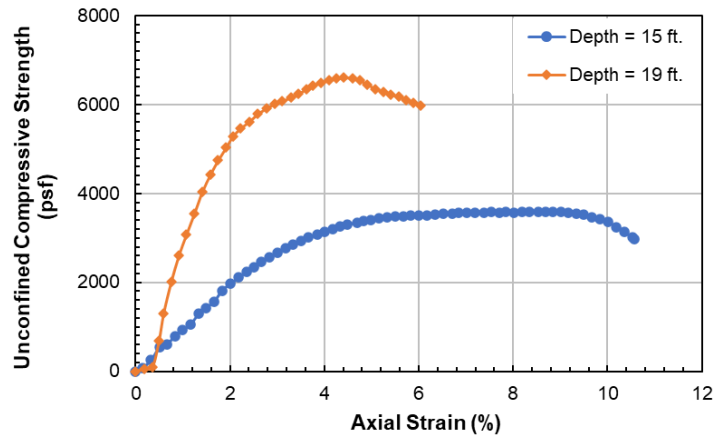


Figure 3-13 Unconfined Compressive Strength

### 3.5 Reinforcement Mechanism Using Recycled Plastic Pin

Khan (2014) indicated that RPPs provided additional resistance along the slip surface to restrict the sliding of soil mass in a slope, thus, increasing the factor of safety. A similar approach was taken while designing the reinforcement layout in the field test sections for this study. The RPPs were proposed to be driven into the foundation soil of an MSE wall by keeping a certain length above the ground. The retaining wall would then be constructed with the extended portion of the RPP as a structural component. This extended portion of the RPP is expected to act as a cantilever beam which will resist the lateral earth pressure. The backfill lateral pressure is anticipated to be intercepted by the RPPs, thereby reducing the net effective pressure acting on the back of the wall face. This will ensure a composite action of the RPPs and wall reinforcement to provide the required resistance against the driving force. The portion of RPP driven into the foundation soil will provide an additional passive force which will increase the factor of

safety against sliding. Furthermore, two layers of RPPs in front of the wall will restrict the global failure planes, in turn improving the global stability of the wall. A schematic of the reinforcement mechanism is shown in Figure 3-14.

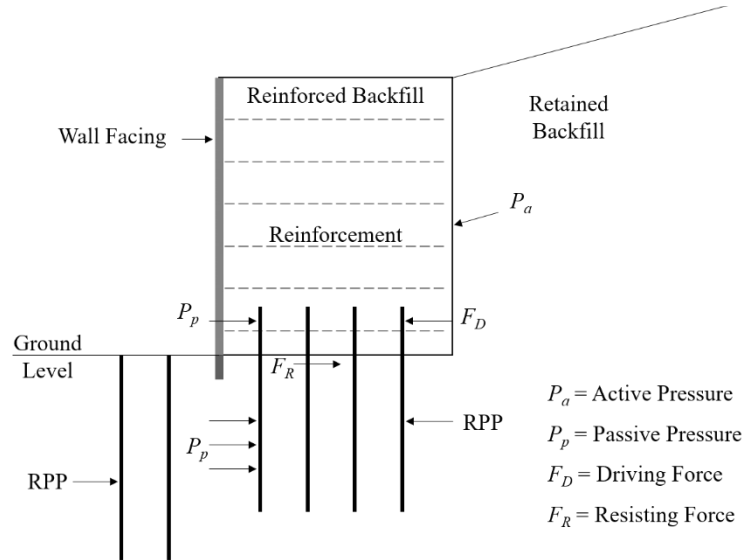


Figure 3-14 Schematic of RPP Reinforced MSE Wall (Not to Scale)

Commercially, RPPs are available in various sizes and lengths. Their mechanical properties vary slightly depending on the constituent recycled plastics obtained from different sources. Previous studies (Breslin et al., 1998; Van Ness et al., 1998) have shown that RPPs reinforced with glass or wood fibers demonstrate improved elastic modulus and creep resistance. Thus, based on the available options, 4 in. x 4 in. (10 cm x 10 cm), and 6 in. x 6 in. (15.24 cm x 15.24 cm) fiber reinforced RPPs were selected for the current study. Khan et al. (2016) conducted 3-point bending tests on nine RPP samples at various loading rates to estimate the flexural strength. The study reported that the elastic modulus and flexural strength of RPPs were between 190 – 200 ksi (1,310 – 1,380 MPa) and 3.1 – 4.7 ksi (21.4 – 32.4 MPa), respectively. Bowders et al. (2003) performed a series of tests on RPPs to study their various engineering properties. The

authors carried out tests on 41 specimens and reported that their uniaxial compressive strength ranged between 1.7 ksi – 2.9 ksi (12 MPa – 20 MPa).

### 3.6 Design of Field Test Sections

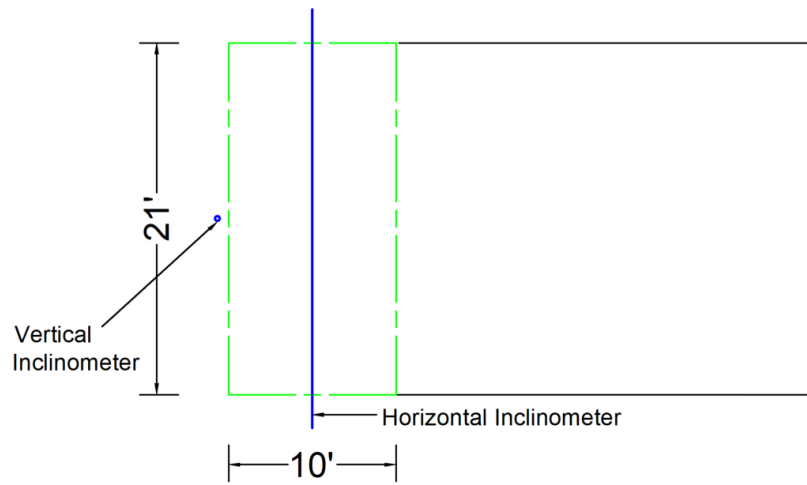
The main objective of the study is to assess the effectiveness of RPPs in increasing the lateral stability along with improving the global/overall stability of MSE wall system. In order to achieve this objective, four test sections were constructed at the designated site location in the City of Irving Landfill. Out of the four test sections, three sections were reinforced with combinations of different RPP sizes and spacings in a staggered pattern, while one section was left un-reinforced and regarded as the control section (SC\_Control). The instrumentation readings of the reinforced sections are compared with each other and the control section to assess the effectiveness of RPP reinforcement. Finite element modeling was conducted using PLAXIS 2D to simulate the field conditions based on the site investigation results. A plane strain model with 15-node triangular elements was chosen for this study. The soil was modeled to follow the Mohr-Coulomb failure criteria. Reinforcement (geogrids) were modeled as linear elastic sheet elements, while the wall facing and RPPs were modeled as plate elements. The backfill soil was considered to exhibit undrained behavior, while the sand was modeled to have drained behavior with no generation of excess pore water pressure. Zaman (2019) estimated the percentage of moment transfer, i.e., the ratio of bending moment on the RPP to the maximum moment capacity of that RPP when the pins are subjected to a similar lateral force. The author reported that only 18% of the moment capacity of the RPP is used when subjected to similar levels of lateral force as expected to be applied to the test sections in this study. Chen et al. (2007) stated that a 100-year design life of RPPs could be anticipated for a moment transfer up to 35%.



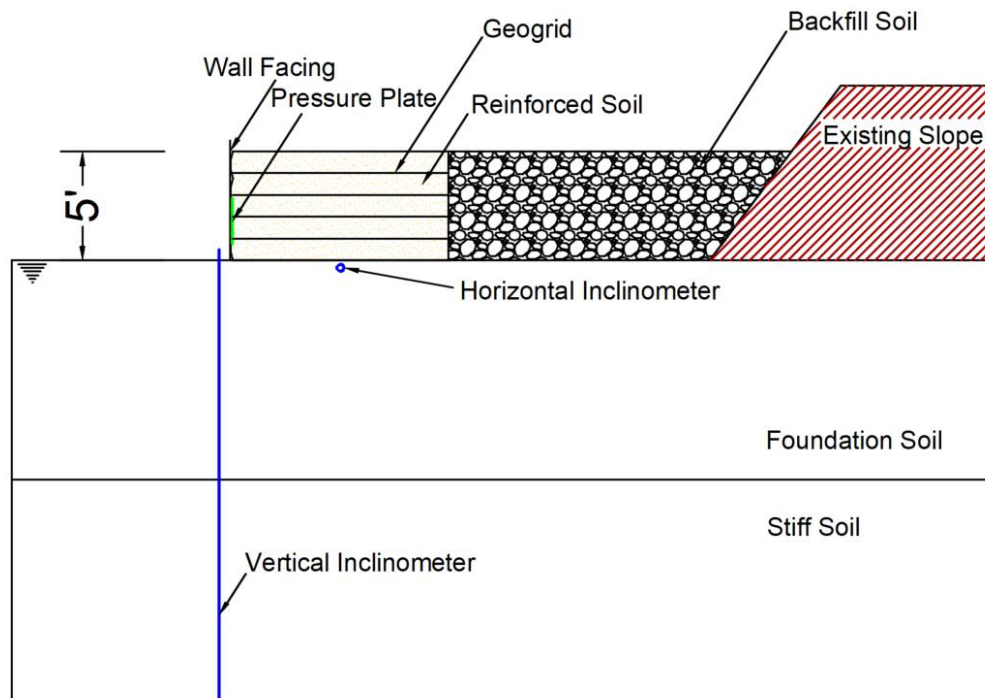
Different RPP layouts were modeled and evaluated before finalizing three combinations to be tested in the field. Each test section is 21 ft. in length and 10 ft. in width. RPPs were installed near the toe of the existing slope, which is shown in the next section. The layout of the pins has been summarized in Table 3-4. The pins inside the test sections were driven only 8 ft. into the ground, while the remaining 2 ft. was extended above the ground. This ensured that the RPP would be attached to the base of the wall acting as a composite section in resisting the lateral forces. Two rows of pins were flushed into the ground at the front of the wall. Figure 3-15 to Figure 3-18 show the proposed layout and section details of the control section, 4 in. x 4 in. spaced at 3 ft. c/c RPP reinforced section, 4 in. x 4 in. spaced at 2 ft. c/c RPP reinforced section, and 6 in. x 6 in. spaced at 3 ft. c/c RPP reinforced section, respectively.

Table 3-4 Layout of RPPs in the Reinforced Test Sections

Section	RPP Specifications		Number of RPP		
	Size	Spacing	Base of Wall	Front of Wall	Total
SR_4x3	4 in. x 4 in.	3 ft. c/c	26	15	41
SR_4x2	4 in. x 4 in.	2 ft. c/c	50	22	72
SR_6x3	6 in. x 6 in.	3 ft. c/c	26	15	41

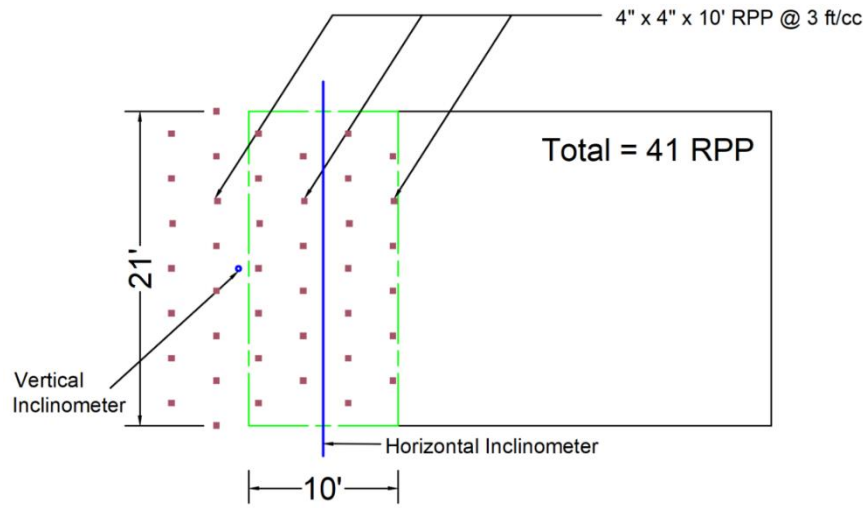


(a)

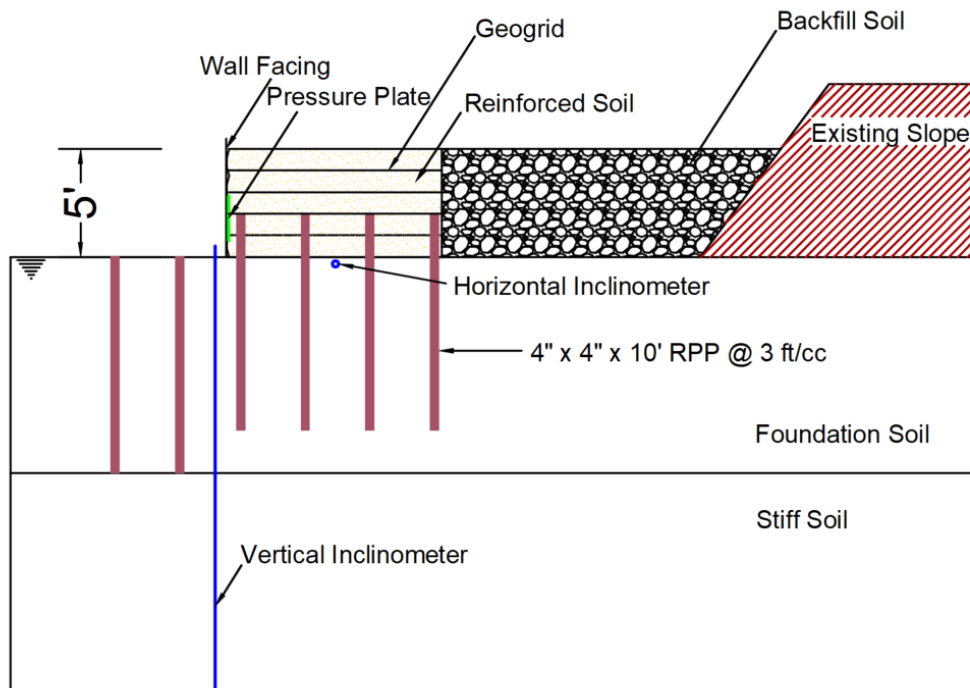


(b)

Figure 3-15 Layout of Control Section SC\_Control (a) Plan (b) Section

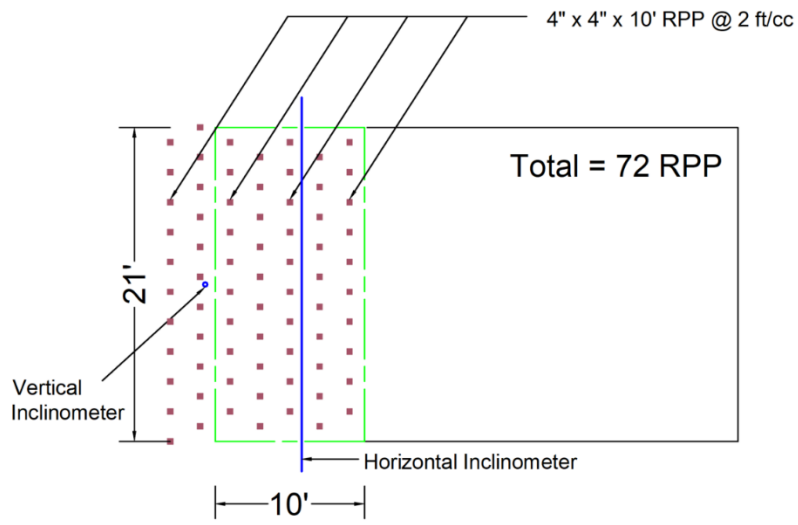


(a)

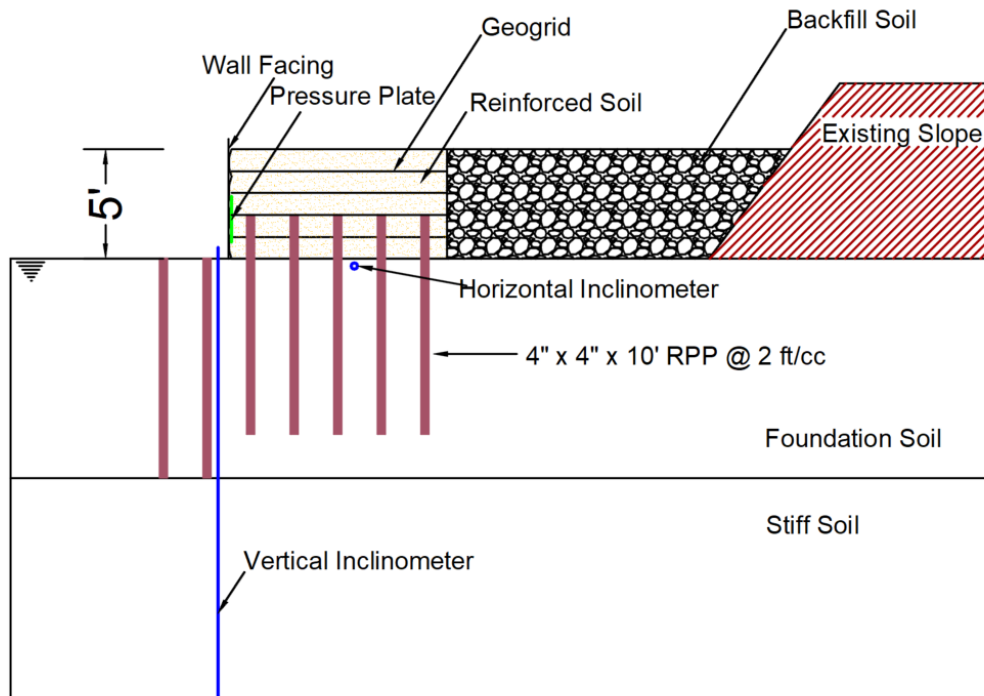


(b)

Figure 3-16 Layout of Reinforced Section SR\_4x3 (a) Plan (b) Section

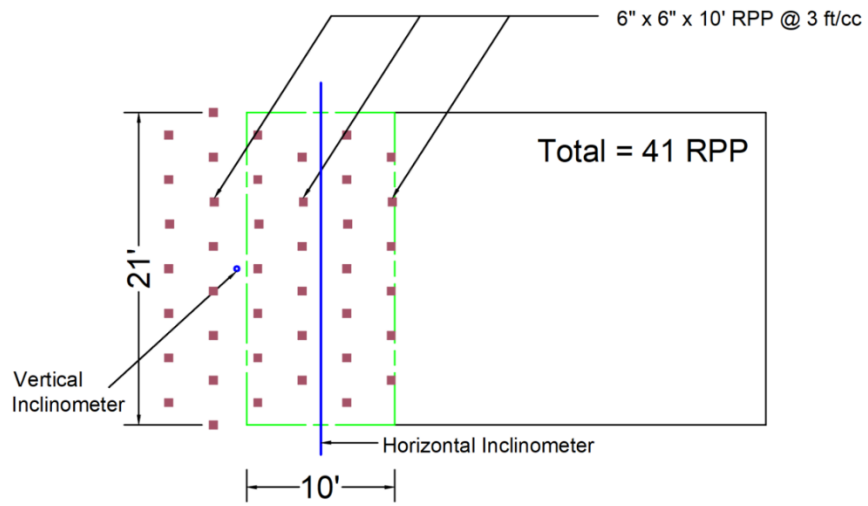


(a)

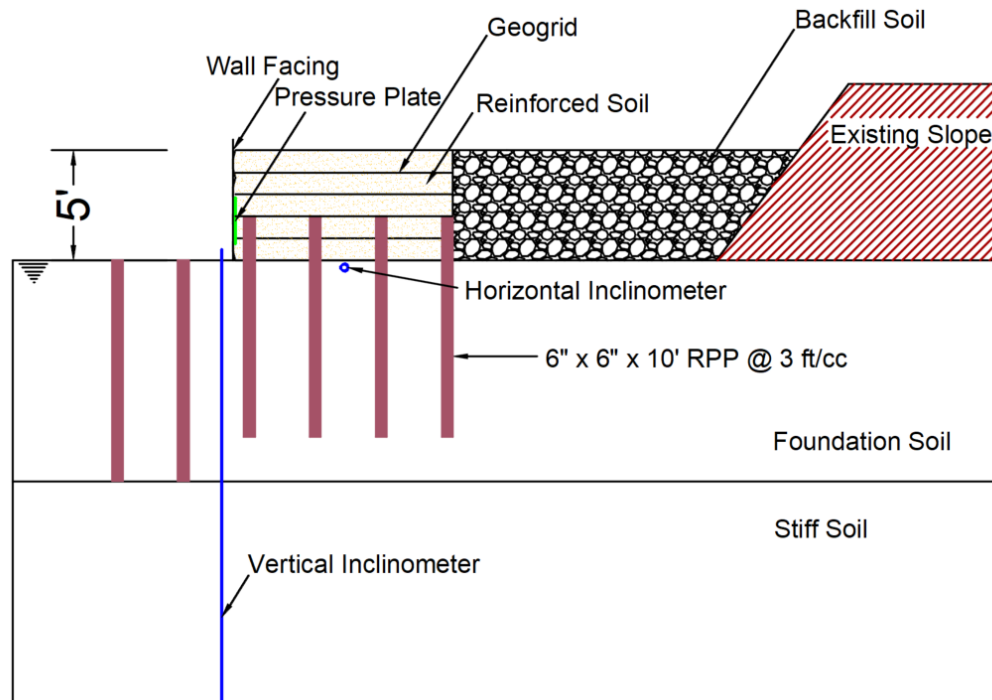


(b)

Figure 3-17 Layout of Reinforced Section SR\_4x2 (a) Plan (b) Section



(a)

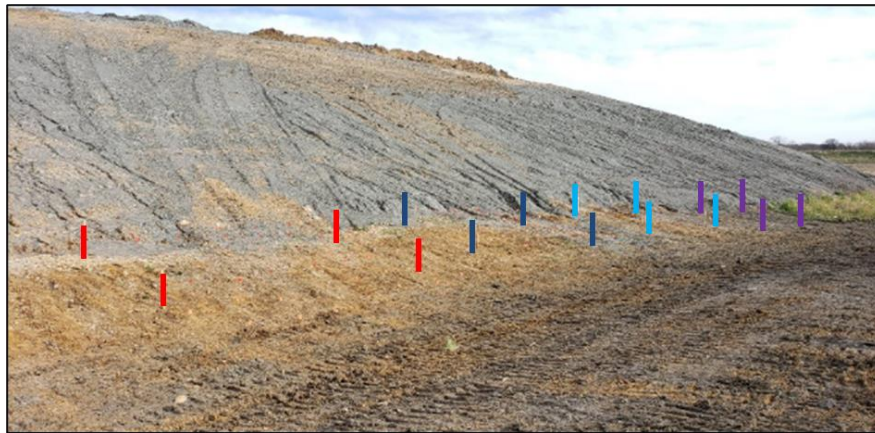


(b)

Figure 3-18 Layout of Reinforced Section SR\_6x3 (a) Plan (b) Section

The test walls were built with triaxial geogrid reinforcement. The height of the wall is 5 ft. and was built in 5 lifts each of 1 ft. thickness. The detail of the wall construction followed by backfilling has been explained in the following sections.

Figure 3-19 shows the boundary of the test sections with flagging for RPP installation. It can be seen that the sections are located just at the toe of the existing slope. The test sections were evenly spaced from each other with a gap of 12 ft. in between.







Legend	
	4 in. x 4 in. section @ 3 ft. c/c
	4 in. x 4 in. section @ 2 ft. c/c
	6 in. x 6 in. section @ 3 ft. c/c
	Control Section (No pins)

Figure 3-19 Boundary of the Test Sections

### 3.7 Field Installation and Instrumentation

#### 3.7.1 Installation of Recycled Plastic Pins

The installation of RPPs took place in February 2019. At first, the area near the toe of the slope was cleared of vegetation and levelled as part of site preparation. For the installation, Link-Belt 350x4 model excavator with NPK GH-15 model hydraulic hammer

was utilized based on previous successful installations. The foundation soil at the site was relatively soft. Thus, the RPPs were driven with comparatively less energy. As shown in Figure 3-20, the pins were first positioned as per the markings (flags) on the ground. Then, the hydraulic hammer attached to the excavator was used for driving the pins into the ground in a staggered pattern. However, due to the soft nature of the soil, some of the pins were driven by just pushing through and not hammering, although, few pins among them had to be hammered for the last 4-5 ft. of length. The RPPs inside the test sections were driven to a depth of 8 ft. The remaining 2 ft. was extended from the foundation to form a composite structure with the reinforced zone of the retaining wall which would act as a shear key at the base of the wall. The 4 in. x 4 in. pins, due to their higher slenderness ratio, are relatively more susceptible to buckling effect when compared to the 6 in. x 6 in. pins. Due to this reason, the 4 in. x 4 in. pins tend to buckle if the soil is stiff. Thus, an iron pin of 3.95 in. x 3.95 in. cross-section and 8 ft. length was used to make a hole up to a desired depth. The RPPs were then installed into those holes by hammering. However, this was not required for the 6 in. x 6 in. pins, as they did not buckle with hammering.



Marking of pins at 8 ft. from the bottom end / 2 ft. from the top end





Positioning the pin at marked location



Placing the hammer system over the pin



Driving the pin upto 8 ft. length



Completed sections

Figure 3-20 Installation Sequence of Recycled Plastic Pins

One important factor that needs to be quantified to assess the effectiveness of utilizing RPPs is the total time required for installing the RPPs. The total RPP driving times were noted down during the installation at the site. Khan (2014) stated that the total time required to install per RPP is the summation of the time required to drive the RPP and



maneuver the drilling rig to the location of the next RPP. Table 3-5 summarizes the average installation time and the driving rate for the different sizes of pins. Although both the sections SR\_4x3 and SR\_4x2 have the same size of pin (4 in.), the pin installation was relatively faster in SR\_4x2. This is because at SR\_4x3, the soil was comparatively stiffer at the last 2 ft. depth of pins. Also, it can be seen that the average time required for the pins which were flushed to the ground were slightly less than the pins which were extended 2 ft. above the ground (for SR\_4x3 and SR\_4x2). The reason for this is that the soil was relatively softer towards the front end of the wall. Moreover, since the pins were stacked nearer to the front end, it was quicker for the operators to maneuver the pins to the desired location.

Table 3-5 Average RPP Driving Time

<b>Test Section</b>	<b>Driving Depth of RPP (ft.)</b>	<b>Average RPP Driving Time (min.)</b>	<b>Average RPP Driving Rate (ft./min)</b>
SR_4x3	8	2.90	2.76
	10	2.73	3.66
SR_4x2	8	2.00	4.00
	10	1.71	5.85
SR_6x3	8	3.95	2.03
	10	4.78	2.09

### 3.7.2 Instrumentation

In order to evaluate and compare the performances of the test sections, several instrumentations were used. All the test sections were instrumented with horizontal inclinometer, vertical inclinometer, and earth pressure plates. The instrumentations have been discussed in the following sections.

### Installation of Horizontal Incliner

Horizontal inclinometer casings were installed in the reinforced and control sections to monitor the vertical movement of the wall base. The horizontal inclinometer readings will determine the settlement of the base of the test sections and help in assessing the effectiveness of RPPs in increasing the bearing capacity of foundation soil. The casings were installed in February 2019. The sequential tasks for the installation of horizontal inclinometer casings were as follows:

1. The alignments of the casings were measured and marked along the sections. A total of 40 ft. trench was marked.
2. The trench was excavated to an approximate width and depth of 6 inches. The base of the trench was compacted and levelled (Figure 3-21 a).
3. Three inclinometer casings, each 10 ft. (total 30 ft.), were connected and taped at the joint. A galvanized steel wire of 1/8 inch diameter was inserted through the casings for pulling the inclinometer while taking measurements.
4. The casings were then placed in the trench (Figure 3-21 b). The base of the trench was checked for uniformness. The casings were taken out and a thin layer of sand was poured to make the base of the trench levelled and to provide a cushion for the inclinometer casing.
5. A 2 ft. hole was dug using hand auger at one end of the trench (Figure 3-21 c-d).
6. The inclinometer casings were again placed in the trench and fast setting concrete was poured into the hole in order to set one end of the casings as fixed to the ground. This ensured a cantilever behavior of the casings (Figure 3-21 e).
7. The trench, along with the inclinometer casings, was then backfilled with soil (Figure 3-21 f).



(a)



(b)



(c)



(d)



(e)



(f)

Figure 3-21 Installation Sequence of Horizontal Incliner Casings

### Installation of Vertical Incliner

The lateral base movement of the test sections were to be monitored using vertical inclinometer. Vertical inclinometer casings (20 ft. depth) were installed close to the outside face of each test section. The casings were installed in the same boreholes drilled for collecting the sub-surface soil samples. After the placement of the inclinometer casing, the inclination of the casing was continuously checked with hand level, while bentonite slurry was poured to backfill the hole. Figure 3-22 shows the sequence of vertical inclinometer casing installation.







Figure 3-22 Installation Sequence of Vertical Inclinometer Casings

Installation of Earth Pressure Plates

Earth pressure plates were attached to the inside of wall facing to monitor lateral soil pressures acting on the wall facing. For the current study, Model 4810 Earth Pressure Cell was selected. The pressure cell was attached to the facing at 1.5 ft. from the bottom of wall base (Figure 3-23).

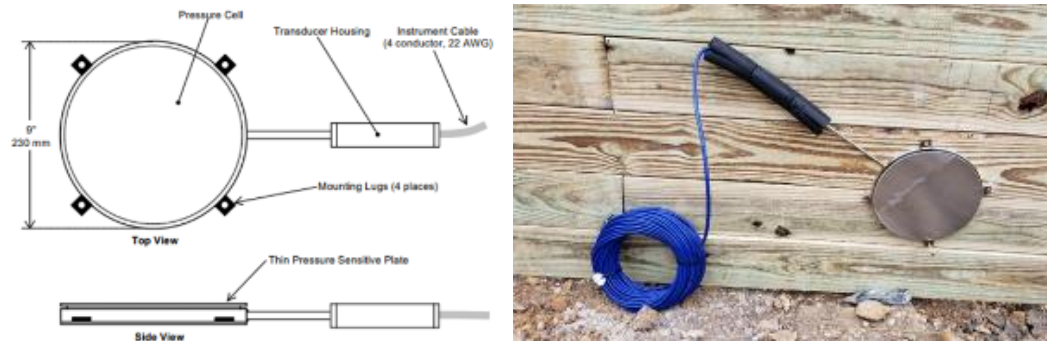


Figure 3-23 Model 4810 Earth Pressure Cell

### 3.7.3 Construction of Test Sections

The test sections were constructed following the installation of RPPs and completion of instrumentation. The first phase of construction included building of wooden fencing, while the second phase was the construction of geogrid reinforced soil wall. The walls are horseshoe shaped with 21 ft. in length and 16 ft. in width. The height of the wall is 5 ft. Raw pressure treated 2" x 6" wooden planks were used which were attached to 3/8" galvanized schedule 40 steel posts spaced 50 inches apart as support. The posts were embedded 30" into the ground and set with pre-mixed concrete. The wooden planks were attached to the post using galvanized simpson brackets and lag screws. All the four test sections were constructed similarly following the same specifications. Figure 3-24 shows the construction of wooden fencing around the test sections.



Figure 3-24 Construction of Test Sections

Following the construction of the wooden fences, the sections were backfilled with native soil. The backfilling was conducted in 5 lifts – each lift being 1 ft. in thickness. Natural sand meeting the requirements as provided in TxDOT Item 423 “Retaining Walls” was used in the reinforced section of the wall. Triaxial (TX5) geogrid was used as reinforcement to wrap each layer. The sequential steps carried out during backfilling were as follows:

1. The first geogrid layer was placed at the base of the wall by cutting holes for the pins. About 5-6 ft. of geogrid was left in front to wrap the soil lift.
2. Sand layer was placed at the front 5 ft. of the wall using an excavator. This was followed by placement of in-situ clay behind the sand layer.
3. Both the sand and clay layer were levelled and compacted using Jumping Jack compactor. The area near the pressure plate was compacted using manual tamping rod so as not to damage the plate.
4. The geogrid was wrapped around the soil layer and tension was applied, while soil was simultaneously placed to hold the geogrid wrap.
5. The next layer of geogrid was placed, and the same steps as above were repeated until a full height of 5 ft. was achieved.

All the four sections were flushed to the existing slope as well. CAT D6T track-type tractor was used for flushing the backfilled materials inside the section to the existing slope. The medium-bulldozer scrapped soil from the surface of the existing slope and pushed it towards the section. Figure 3-25 shows the backfilling process and the completed sections.



A second phase of loading was conducted on September 24, 2019 where two more ft. of soil was added on top of all the sections. A similar equipment was used to scrap soil from the existing slope and add to all the four test sections.



Placement of sand layer



Placement of clay layer



Compaction using Jumping Jack compactor



Backfilling from behind the section



Completed sections

Figure 3-25 Backfilling of the Test Sections

Sand replacement method was used to determine the in-situ density of the backfill sand layer. The average dry density of the sand layer was found to be 116.9 pcf.



### 3.8 Performance Monitoring Plan

The field instrumentations were used to regularly monitor the performance of the test sections. Table 3-6 shows the monitoring schedule followed for the study. The inclinometers were monitored on a bi-weekly basis for few months just after construction. The monitoring frequency after that was changed to monthly. The pressure plates were programmed to record data at one-hour intervals. A data-logger was connected to the four pressure plates which stored the recorded pressure data.

Table 3-6 Performance Monitoring Schedule

<b>Instrumentation</b>	<b>Monitoring Frequency</b>
Horizontal Inclinometer	Monthly
Vertical Inclinometer	Monthly
Earth Pressure Plates	Continuous

## Chapter 4

### RESULTS AND DISCUSSION

#### 4.1 Background

MSE walls tend to move outwards when there is insufficient resistance at the wall base against the lateral earth pressures. Recycled plastic pins were installed at the base of three MSE wall test sections to improve the lateral resistance. One control section was also constructed without RPP reinforcement. The performance monitoring of the test sections was carried out regularly to evaluate the effectiveness of the approach. The following sections discuss the results obtained from the field monitoring data. Comparisons of the results from the different sections have been presented. Furthermore, the results from the current study have also been assessed with findings from previous studies.

#### 4.2 Lateral Displacement of Wall Base

The lateral displacement of the test sections was monitored using vertical inclinometer. An inclinometer probe was inserted into the inclinometer casings installed in front of each test section, and readings were recorded to calculate the cumulative displacement of the foundation soil till a depth of 20 ft. DigiPro2 software was used to download the recorded data which were later analyzed to obtain the cumulative displacement graphs.

##### 4.2.1 Vertical Inclinometer Results

Figure 4-1 shows the lateral displacement of soil just in front of SR\_4x3. The maximum deformation was seen at the ground level as expected. The ground surface moved a maximum of 0.521 inches laterally as of February 08, 2021 (Day 662). The lateral movement of the foundation was seen up to 14 ft. depth which might be due to high amount of rainfall in the past months which percolated to deeper depths with time. The

top 10 ft. foundation soil is composed of clayey sand, so the relatively higher permeability of sand might have drained the rainfall to deeper depths composed of clayey soils.

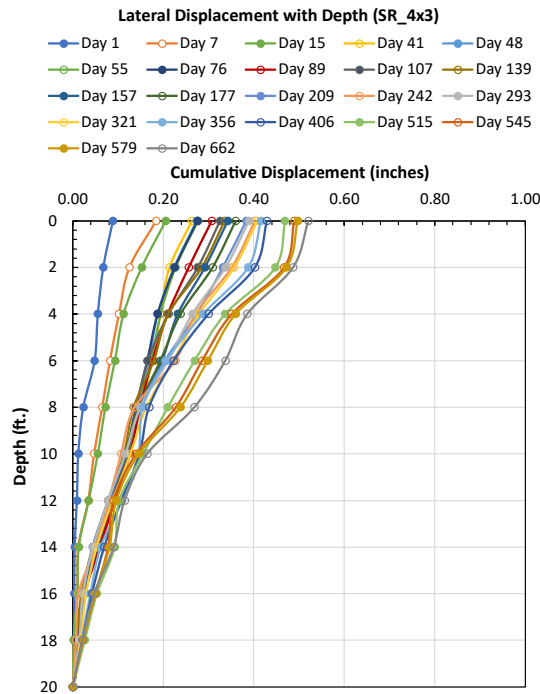


Figure 4-1 Lateral Displacement with Depth of Section SR\_4x3

Figure 4-2 shows the lateral displacement of soil in front of SR\_4x2. The ground surface moved 0.412 inches laterally as of February 08, 2021 (Day 662). SR\_4x2 performed quantitatively better than SR\_4x3 due to the closer spacing of RPPs. The greater number of pins in SR\_4x2 helped in resisting the lateral movement of wall base, thereby limiting the lateral movement of the inclinometer. Also, the major movement was seen till a depth of around 14 ft. The high number of pins might have improved the stiffness of the foundation as well due to which the soil at deeper depths showed comparatively less displacement. The better performance could be attributed to the group action of closely spaced RPPs.

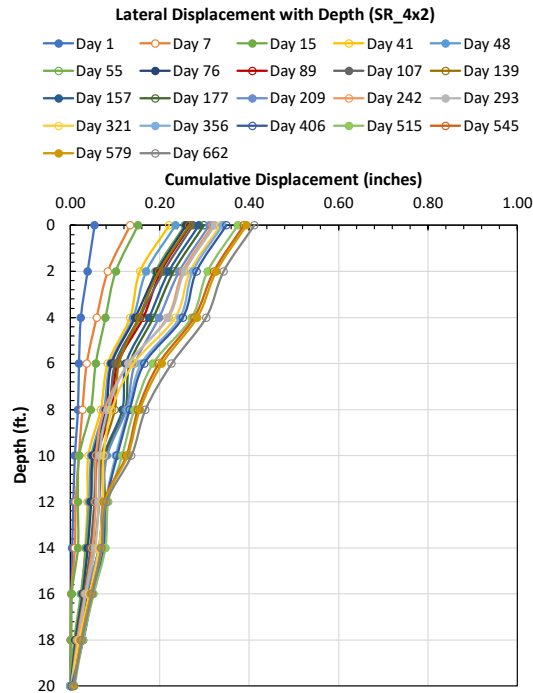


Figure 4-2 Lateral Displacement with Depth of Section SR\_4x2

SR\_6x3 and SC\_Control were backfilled on May 05, 2019 (Day 1). Figure 4-3 and Figure 4-4 show the lateral movement of vertical inclinometer casings in SR\_6x3 and SC\_Control, respectively. It can be seen from Figure 4-3 that the lateral movement at the ground surface was found to be 0.264 inches as of February 08, 2021 (Day 648). The lateral displacements gradually decreased with depth and were almost negligible after 10 ft. This section, being reinforced with 6" x 6" RPPs, performed the best among the three reinforced sections. The larger cross-section of RPPs provided better resistance against lateral displacement. This can be attributed to the higher flexural strength of the pins. The RPPs improve the lateral resistance by providing additional passive force from the soil in front of the RPPs. It has been later shown in the following chapter that a larger cross-section gives rise to a larger area of soil resistance.

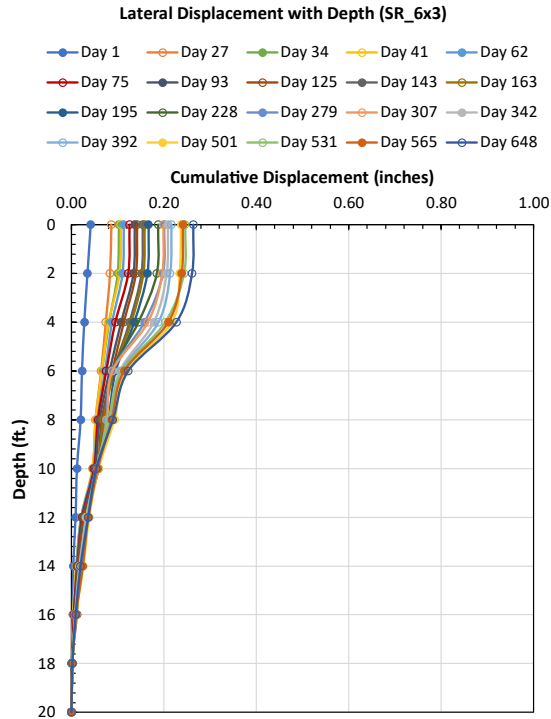


Figure 4-3 Lateral Displacement with Depth of Section SR\_6x3

Figure 4-4 shows a maximum lateral movement of 1.636 inches in the control section. It can be clearly seen that the control section displaced significantly during May 2019 (Day 27). Most of the lateral displacement was observed till around 8 ft., however, the deeper depths also showed comparatively higher movement. The top 5 ft. of the foundation displaced more than 0.5 inches in less than a month after construction. The last reading of the control section was taken on December 2019 (Day 228). Due to excessive movement of the wall facing, the inclinometer casing was inaccessible. Figure 4-5 shows the failure progression of the wall. It can be seen that the front face of the wall has tilted with a maximum shift of more than 24 inches at the top. The tilting of the face along with the high lateral displacement signifies that the control section is imminent to displace further with increasing precipitation events.

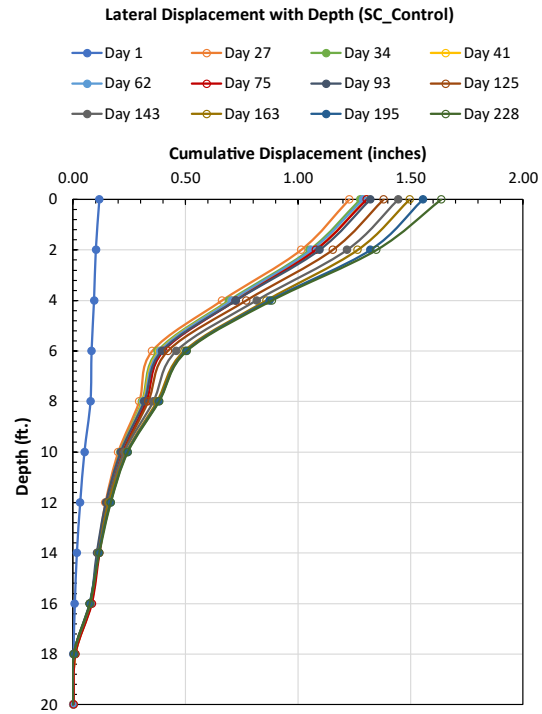


Figure 4-4 Lateral Displacement with Depth of Section SC\_Control



Sept 2019

March 2020

Feb 2021

Figure 4-5 Failure of the Control Section (SC\_Control)

Pressure plate readings, which have been presented in the following sections, indicate that the control section moved suddenly after May 19, 2019. There was 2.6 inches of heavy rainfall on the same day, which might have increased the pore water pressure behind the wall face. In addition to this, there was movement of soil mass from the retained slope was well. The combined action initiated the failure of the control section. Since there are no RPPs in the control section, the lateral movement was not controlled as in the other sections with RPP acting as a shear key. Also, there was not much improvement in the stiffness of the foundation soil which made the foundation susceptible to higher displacement.

Geogrid reinforcement has been used while filling all the sections which is anticipated to work as a composite structure with the extended portion of the RPPs. However, it generally takes some time for the load to mobilize and the composite structure to perform better. We can see from the results that the change in lateral displacements became relatively smaller compared to the days just after loading. This shows that the composite structure started to perform as expected after the load mobilization.

#### Comparison Between Control and Reinforced Test Sections

Figure 4-6 compares the lateral movement as of February 08, 2021 of all the wall sections. The section stabilized with 6"x6" RPPs performed the best with the least movement. With the same soil and loading conditions, the control section seems to fail with significant movement. The other two sections stabilized with 4"x4" RPPs performed satisfactorily as well with results in an acceptable range. It is to be noted that the last data of SC\_Control was from December 2019. The actual displacement till date is anticipated to have been much larger than that presented on the chart.

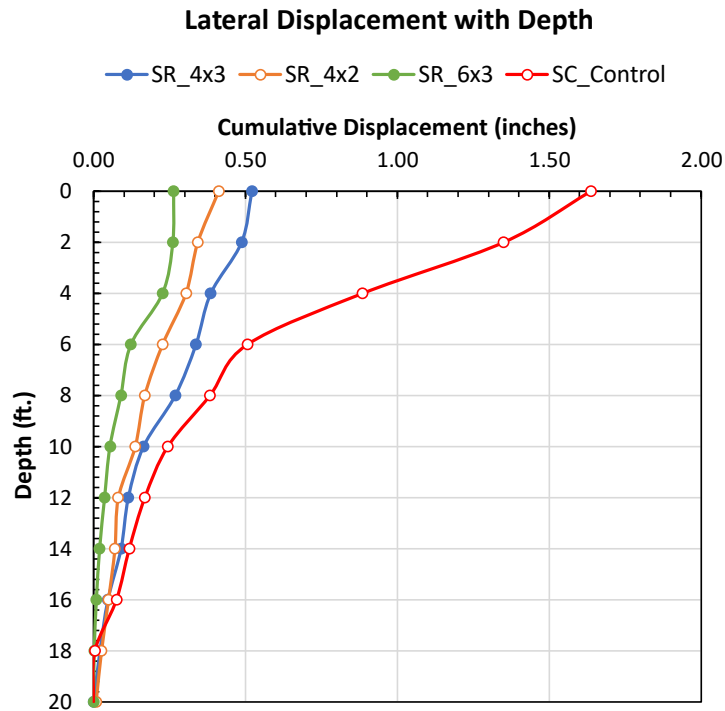


Figure 4-6 Comparison of Lateral Displacement of Wall Base

#### Effect of Rainfall

A comparison of the lateral movement of the ground surface at all the sections was carried out with rainfall. It can be seen from Figure 4-7 that the movement of the reinforced sections increased in a similar ratio after the rainfall events. However, the displacement of SR\_4x3 was comparatively more due to presence of a smaller number of RPPs. High rainfall events recorded might have increased the pore water pressure in the retained soil which is mainly composed of clay. Furthermore, the clay might have undergone swelling due to water intrusion, thereby applying more pressure on the wall face. Also, the ground itself is composed of soft fill soil which might be susceptible to lateral movement. However, there are additional two layers of RPPs in front of the wall sections. These RPPs also help in stabilizing the lateral deformation of wall base.



The second phase of loading (additional 2 ft.) was carried out on September 24, 2019. It can be seen that the reinforced sections did not move considerably after the loading. However, the control section showed continuous movement even after the second phase of loading.

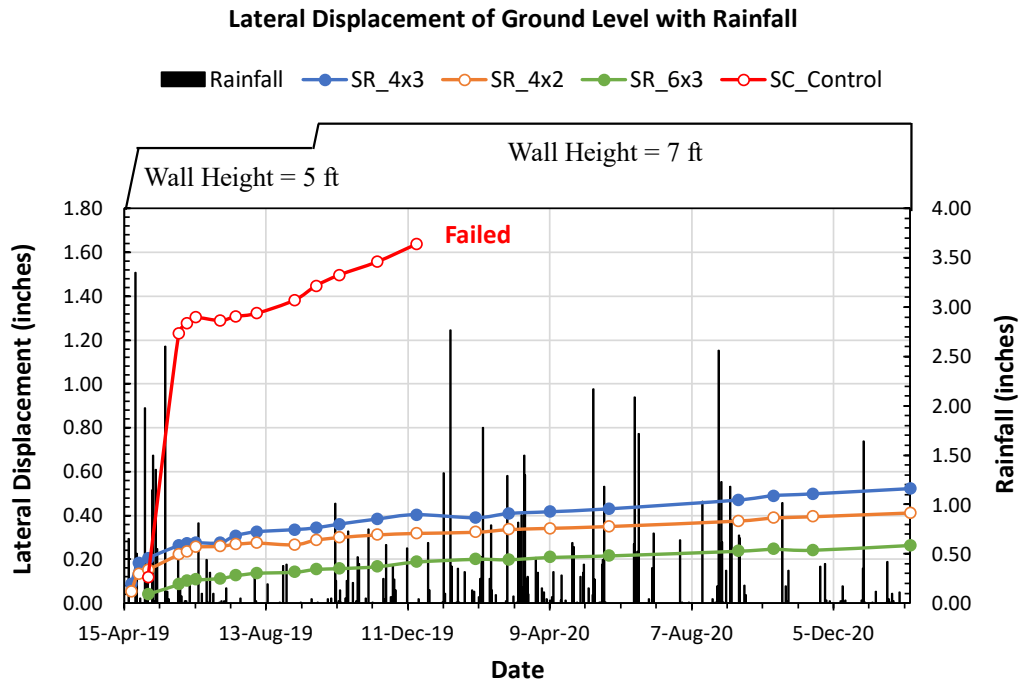


Figure 4-7 Comparison of Lateral Displacement of Ground Level with Rainfall

#### 4.2.2 Comparison with Previous Studies

Stark et al. (2019) published a case study about a 32 ft. (9.75 m) high MSE wall for supporting a highway bridge abutment. Rammed Aggregate Piers were installed in the foundation soil prior to the construction of MSE wall to improve the bearing capacity of the soil. However, due to excessive movements, the wall failed. The authors concluded that deep seated shear failure was responsible for the wall failure based on vertical inclinometer readings. Cumulative displacement profiles (Figure 4-8) from two inclinometers just in front of the wall facing (SI-1 and SI-2) and one inside the backfill (SI-

3) show spikes in the displacements at deeper depths, 6 m (20 ft.) and 17 m (55 ft.), respectively. These specific locations with a higher lateral movement signify the failure shear surface. It is to be noted that the sensors were installed after most of the settlement and lateral movement had already taken place. This explains the small displacements recorded and presented in Figure 4-8 even though the final lateral movement was about 18 inches. Incremental lateral displacement profiles with depth were plotted for the current study which are shown in Figure 4-9. All the sections show increased movements around the top 8-10 ft. depth. These results were compared to the findings from Stark et al. (2019). Since, none of the four inclinometer readings showed higher incremental displacements at deeper depths, it can be stated that the lateral sections have not experienced deep seated movements. These charts also support the fact that the incremental lateral displacements in the control section are much higher than in the reinforced sections and even comparatively deeper.

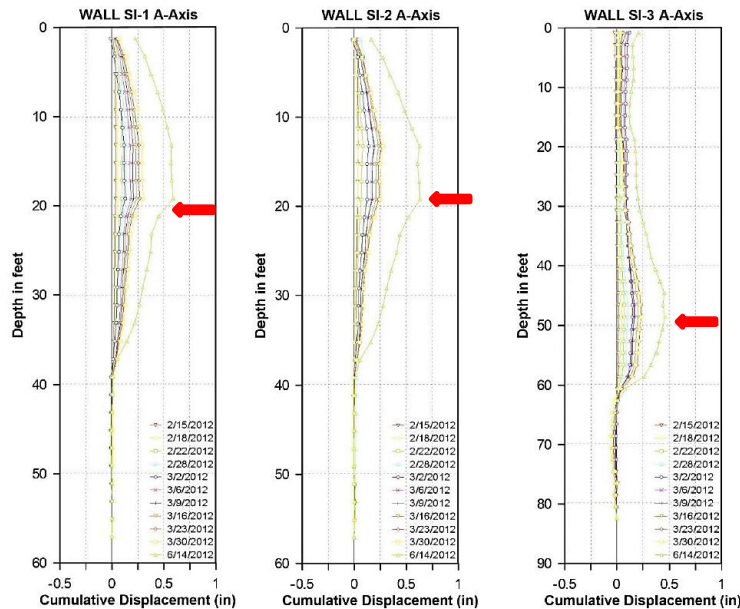


Figure 4-8 Cumulative Lateral Displacement Profiles with Depth

(Reprinted from Stark et al., 2019, © ASCE)

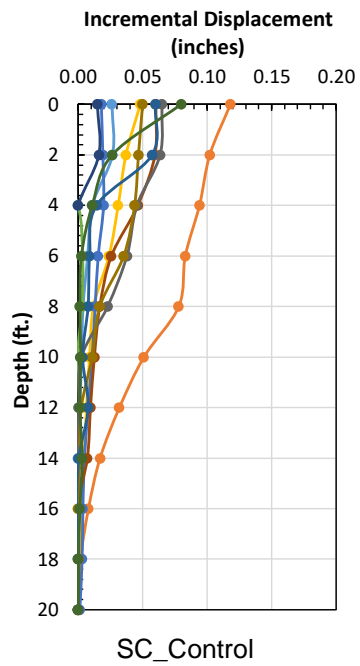
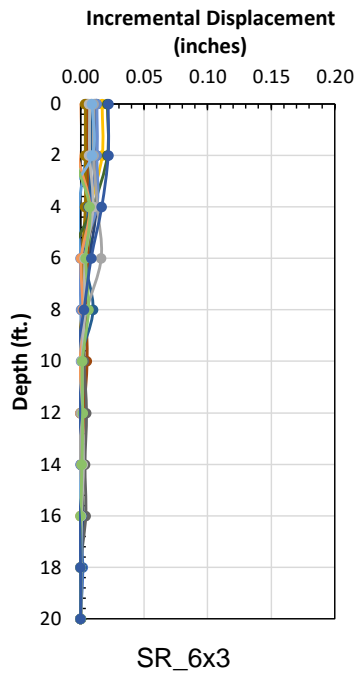
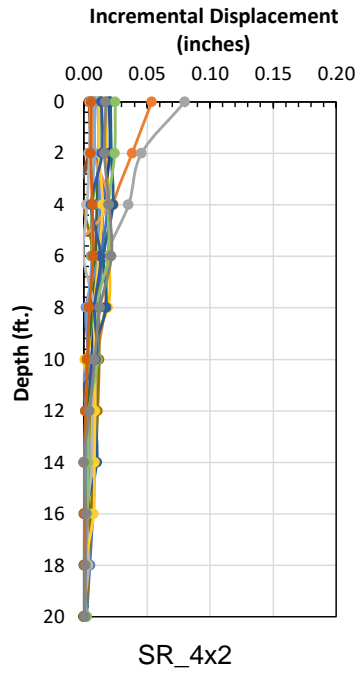
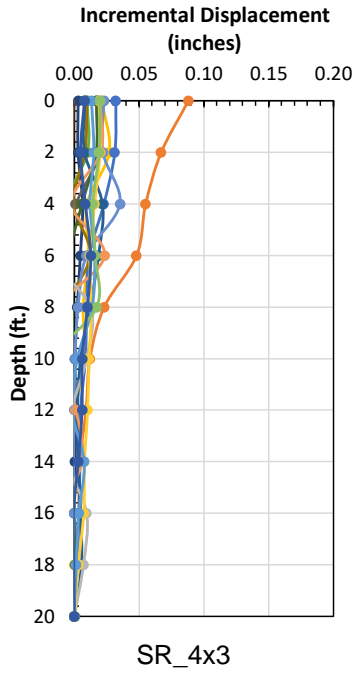


Figure 4-9 Incremental Lateral Displacement Profiles with Depth of the Test Sections

The displacement trends are in good agreement with previous findings (Briancon and Simon, 2012; Zhao et al., 2019) where comparable trends in lateral displacements of the foundation were observed in pile-supported embankments. These earlier studies have demonstrated that the use of piles confine the lateral displacement to a shallow depth from the base of an embankment or retaining wall.

Ahmadi and Bezuijen (2018) studied the performance of a full-scale MSE wall with plywood as a flexible facing using earth pressure cells to measure the horizontal stresses. The study measured the maximum lateral pressure to be approximately 8 kN/m<sup>2</sup> which showed non-linear distribution with depth. Rouili et al. (2005) performed combinations of numerical and experimental tests on an L-shaped concrete retaining wall. The authors showed that due to the non-linear distribution of lateral pressure behind the wall face, the retaining wall failed with a combination of rotation and translation. A similar observation was made for the control section in the present study. As seen from the inclinometer results and actual section photos, it can be stated that the wall is failing with a combination of both rotation and lateral displacement of the base.

A major portion of the base movement in all the sections was observed just after the construction. The control section displaced by a large factor on May 19, 2019, after a series of high rainfall events. Benjamin et al. (2007) discussed a similar observation of increased wall movement following rainfall. The paper illustrated that the rate of MSE wall movement increased from 0.028 inches/month (0.7 mm/month) to 0.04 inches/month (1.0 mm/month) when the rainfall increased from 0.04 inches/day (1 mm/day) to 0.4 inches/day (10 mm/day). In the current study, the lateral displacement of the control section increased from 0.033 inches/month (0.83 mm/month) to 0.07 inches/month (1.78 mm/month) when the rainfall increased from less than 0.2 inches/day (5 mm/day) to

about 0.98 inches/day (25 mm/day). Interestingly, no significant increase in lateral displacements was observed after rainfall events in the reinforced sections.

### 4.3 Settlement of Wall Base

The wall base settlements were measured using a horizontal inclinometer probe. The probe was inserted into the inclinometer casings installed at the base of each test section and two sets of readings were recorded for each survey. The casings were placed in the middle of the reinforced soil section since previous studies (Benjamin et al., 2007) reported the largest vertical displacements to occur in the middle of the reinforced zone. DigiPro2 software was used to download the recorded data which were later analyzed to obtain the cumulative displacement graphs. The fixed end of the inclinometer casings was taken as the zero reading (start point). The baseline reading was taken just after the backfilling.

#### 4.3.1 *Horizontal Inclinometer Results*

Figure 4-10 to Figure 4-13 show the vertical displacement of wall base at sections SR\_4x3, SR\_4x2, SR\_6x3, and SC\_Control, respectively. A maximum deformation of 0.977 inches, 0.648 inches, 0.597 inches, and 1.888 inches were measured at SR\_4x3, SR\_4x2, SR\_6x3, and SC\_Control, respectively. The settlement in the most reinforced section (SR\_6x3) is comparatively smaller than the other sections owing to the larger cross-section area of the pins, which might have helped in carrying the backfill load and distributing less load to the wall base. Also, the foundation soil was better stiffened in the 6"x6" section, thereby, limiting the settlement of the soil. A larger cross-section provides more end bearing which lead to the reduction in soil settlement. The settlements in SR\_4x2 and SR\_6x3 were fairly similar. This can be credited to the similar spacing by equivalent diameter (s/d) ratio. Since the RPP has its influence around a limited area

which is dependent on the s/d ratio, a similar ratio might have resulted in similar reinforcing actions.

The settlement was close to 2 inches in the control section (SC\_Control). As there are no pins, the soft foundation soil settled considerably with the load. As the existing retained slope has not been compacted, runoff from the slope due to rainfall carries some amount of soil with it. This gradually increased the load on the section. Thus, more settlement was observed in SC\_Control where RPPs were not present to carry the load. However, with the same load and climatic conditions, the RPP reinforced sections showed considerable reduction of settlement.

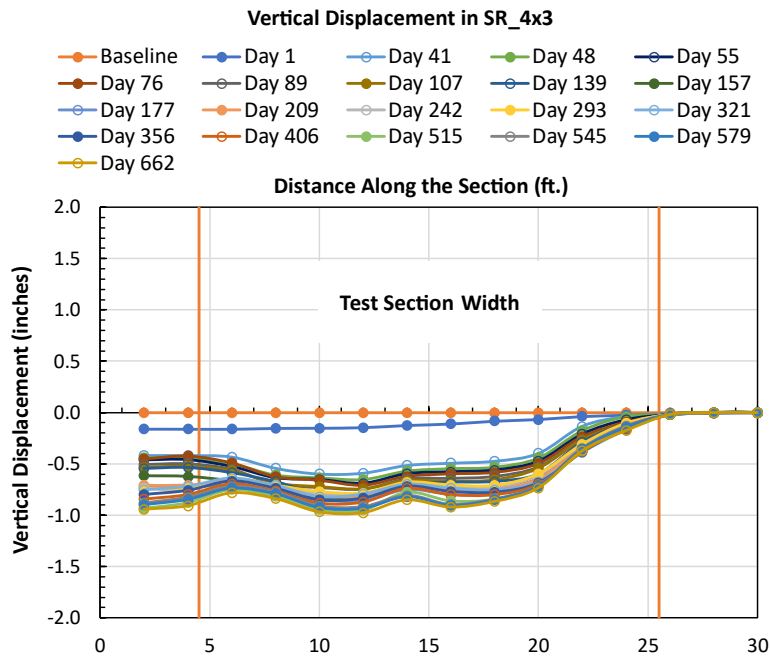


Figure 4-10 Vertical Displacement of Wall Base in SR\_4x3

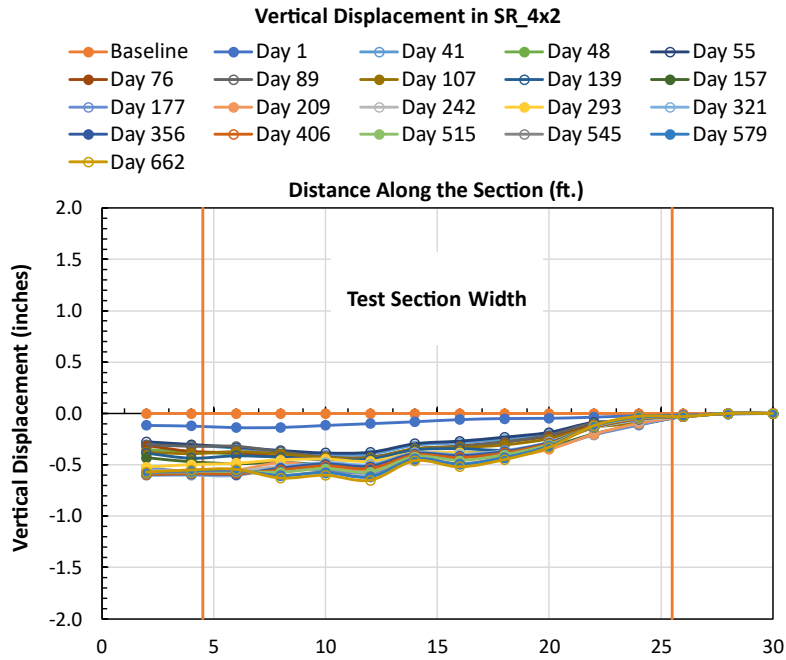


Figure 4-11 Vertical Displacement of Wall Base in SR\_4x2

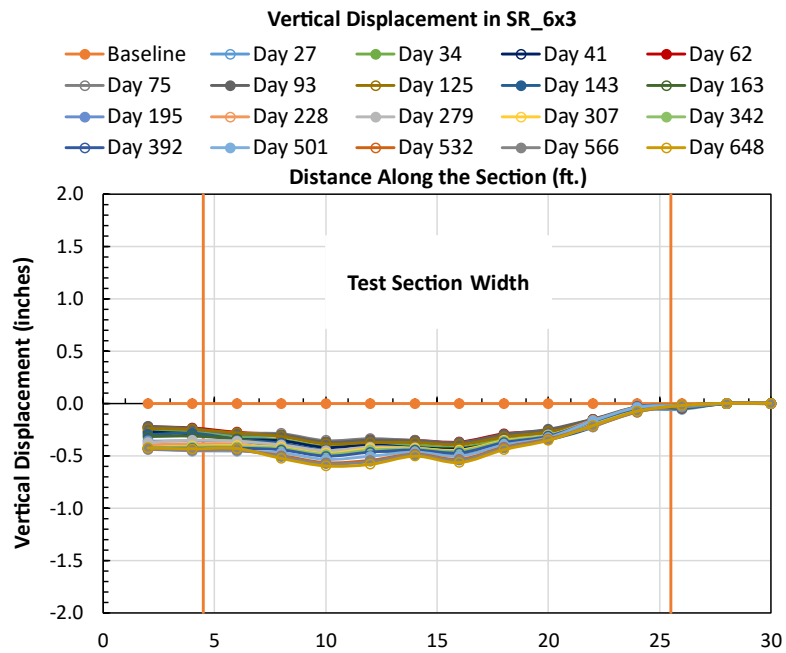


Figure 4-12 Vertical Displacement of Wall Base in SR\_6x3

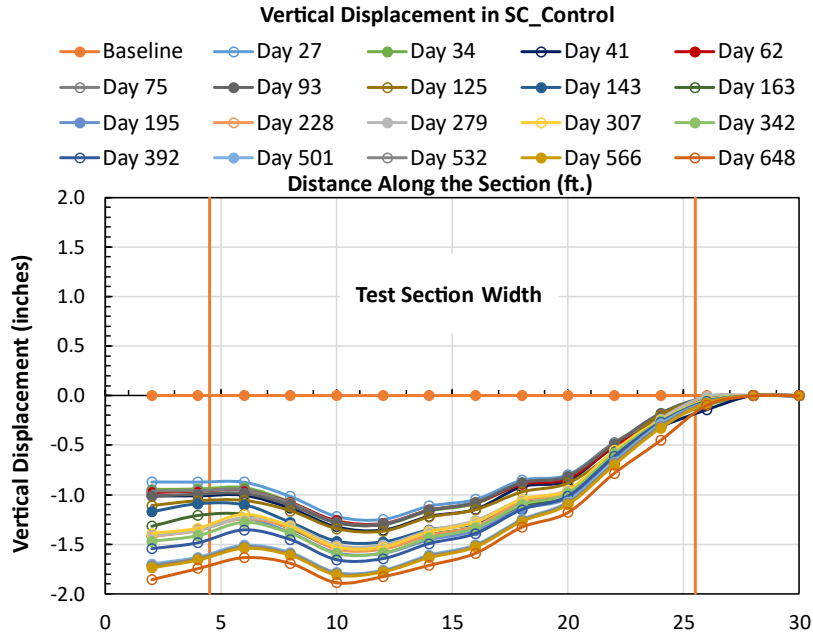


Figure 4-13 Vertical Displacement of Wall Base in SC\_Control

The individual settlement charts can be used to assess the incremental settlement pattern. The RPP reinforced sections underwent negligible settlements after a certain period, preferably the load mobilization period. Conversely, the control section is still experiencing measurable settlements even after two years from construction. This demonstrates that RPPs can be effective for long term stabilizations.

Comparison Between Control and Reinforced Test Sections

Figure 4-14 presents a comparison of the vertical settlement of foundation soil at all the four sections. It can be clearly seen that the control section settled far more than the other RPP reinforced sections. Performance-wise, all the RPP sections deformed similarly, with SR\_4x3 exhibiting slightly more settlement than SR\_4x2 and SR\_6x3. Again, more number and larger cross-section area of the RPP improved the performance of the lateral loaded sections.



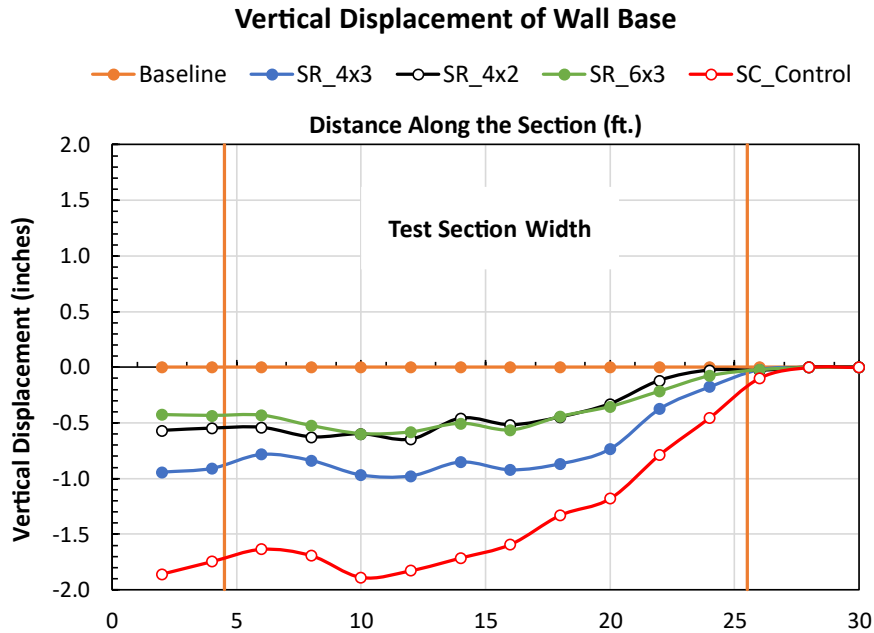


Figure 4-14 Comparison of Vertical Displacement of Wall Base

#### 4.3.2 Comparison with Previous Studies

Comparable settlement profiles were outlined by previous investigations as well (Bell et al., 1983; Briancon and Simon, 2012; Zhao et al., 2019). Bell et al. (1983) investigated the effect of various geotextile fabrics in stabilizing MSE wall sections in Colorado. Foundation settlements ranging from 9 inches (230 mm) to 18 inches (460 mm) were measured in MSE walls about 15 ft. (4.6 m) high. By normalizing the height of the wall and comparing the ground settlements, the improvements in the current study are extensive by a factor as high as 10. Zhao et al. (2019) presented a case study in which prestressed tubular concrete (PTC) piles and geogrids were utilized to stabilize an embankment section in China. PTC piles, 1.3 ft. (0.4 m) in diameter and 52.5 ft. (16 m) deep, were used to decrease the soft soil foundation settlement of a 15.8 ft. (4.8 m) high embankment sloping at 1 Vertical: 1.5 Horizontal. The largest settlement measured at the center of the embankment was 1.36 inches (34.6 mm). However, for comparison with the

current study, the corresponding settlement at an embankment height of 7.4 ft. (2.25 m) was about 1.18 inches (30 mm). Considering the extensive reinforcement, albeit the soft nature of foundation soil, in the referenced case study, the settlement reductions produced in the present study exhibit promising application of RPPs in reducing the foundation settlement of MSE walls.

Settlement improvement factor ( $n$ ) is the ratio between the maximum settlement of the unreinforced soil and the reinforced soil (Elsawy and El-Garhy, 2017). It can be defined as follows:

$$n = \frac{S_{\max(\text{control})}}{S_{\max(\text{reinforced})}}$$

The settlement improvement factor for the field test sections were calculated and compared with the spacing to equivalent diameter ratio ( $s/d$ ). The percentage area coverage of the RPP reinforcement was also calculated. The results are tabulated in Table 4-1. The improvement factor increased proportionally with the reinforcement area coverage. The higher area of reinforcement replaced a higher area of foundation soil and consequently increased the stiffness of the soil. This led to an increase in the bearing capacity of the foundation soil due to which the settlement was less.

A numerical study of granular pile improved soft ground was conducted by Elsayy and El-Garhy (2017). The authors reported a maximum 'n' value of about 2.85. Similarly, Oh and Sin (2007) reported a maximum 'n' value of 1.7 for a geogrid reinforced pile supported embankment. The present approach showed better settlement improvement factors compared to previous studies in the literature. This suggests that RPP reinforcement is a promising approach for controlling the base settlement of MSE walls.

Table 4-1 Settlement Improvement Factor of the Test Sections

<b>Section</b>	<b>Settlement Improvement Factor (n)</b>	<b>s/d</b>	<b>Reinforcement Area Coverage (%)</b>
SR_4x3	1.93	7.98	1.38
SR_4x2	2.91	5.32	2.65
SR_6x3	3.16	5.32	3.10

Suzuki (1988) conducted a study on 11 embankment sites by measuring the underground horizontal displacement, horizontal displacement on the ground surface, and embankment settlement. The author estimated the lateral displacement of ground to be 5-20% of the vertical settlement. A similar calculation was carried out for this study where average incremental displacements were determined for both the horizontal and vertical movements. The average lateral displacements were found to be 14%, 11%, 10%, and 34% of the respective vertical settlements in test sections SR\_4x3, SR\_4x2, SR\_6x3, and SC\_Control, respectively. A distinctive trend to be noted is that the control section showed the maximum lateral spreading, as a substantial percentage of the vertical settlement brought about a lateral displacement. On the other hand, the reinforced sections show a considerable decrease in the lateral spreading, with SR\_6x3 demonstrating the least lateral spread. These data show that the RPPs are serving their purpose of controlling the lateral displacement.

#### 4.4 Earth Pressure Plate Results

The pressure plates which were attached to the inside of the front face of each test section were connected to a datalogger which was kept at the site. The datalogger recorded pressure data every hour. LogView software provided by Geokon was used for downloading the data to a computer. The pressure values for a day were averaged and

plotted against rainfall (Figure 4-15) to evaluate the variation of lateral pressure on the test sections.

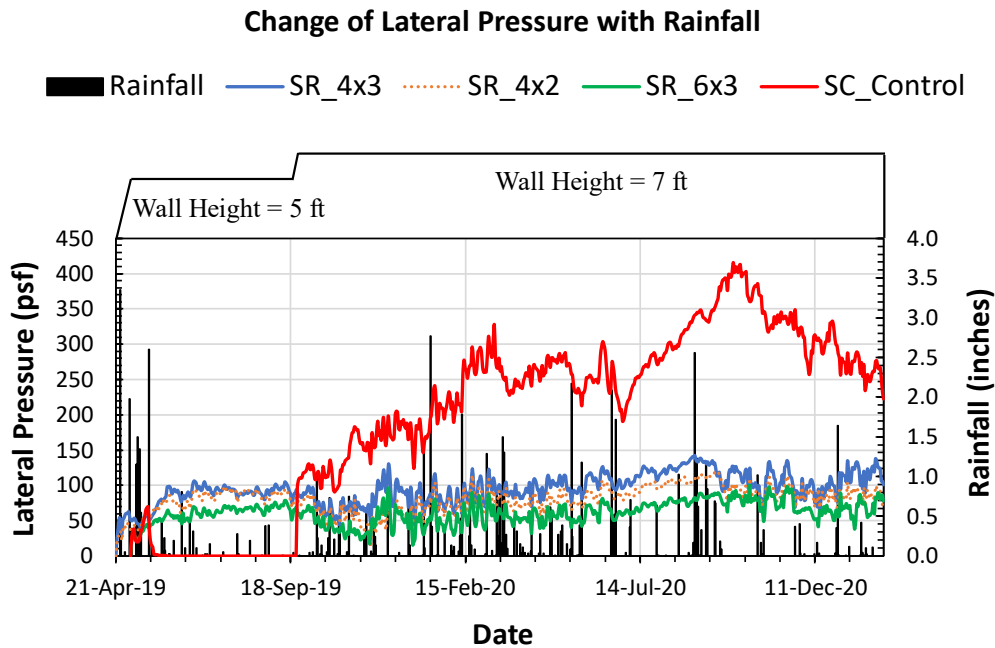


Figure 4-15 Change of Lateral Pressure with Rainfall

The chart shows that total lateral pressure increased gradually after loading for 4-5 days at all the sections due to the build-up of soil pressure at the back of the wall. However, after the rainfall events, the pressure decreased for couple of days. The same trend was observed by Zaman (2019) as well. The wall facing is flexible in nature and moves laterally with increasing pressure. Due to the rainfall, soil pressure from the backfill increased, inducing a lateral movement of the wall. This, in turn, released some pressure on the pressure plate itself, which is reflected from the decreasing trend as seen in Figure 4-15.

The similar trend of decreasing pressure after rainfall events can be observed throughout the monitoring period. The fluctuation of lateral pressure on the pressure cells can act as an indication of the lateral movement of the wall base. For instance, if we look at the rainfall events on May 08 and May 09, 2019, it can be quantitatively discussed that the control section displaced the most laterally. This is due to the higher decrease in pressure after rainfall, which indicates that the lateral movement might have been more as well in the control section. Similarly, SR\_6x3 with 6" x 6" RPPs performed the best as the decrease in lateral pressure was observed to be the least among all the sections.

The pressure data of control section abruptly decreased after May 19, 2019. This can be taken as a major indication of the potential failure of the control section. The significant movement of control section decreased the lateral pressure on the cell. This is clearly reflected from the figure. Also, there was minimal contact between the pressure cell, which has been attached to the wall face, and the soil after the movement of the wall face. Due to this, some readings showed almost negligible pressure. The soil just behind the wall face might have been washed away due to heavy rainfall after the wall movement. After the second phase of loading, the pressure cell was brought back in contact with the soil. This is seen from the chart as the lateral pressure on the control section increased significantly. After the second phase of loading, the change in lateral pressure behind the reinforced sections has been almost constant. However, the control section exhibited a substantial increase of lateral pressure after the additional load.

#### 4.5 Correlation Between Earth Pressure and Lateral Displacement

Fang and Ishibashi (1986) conducted a study on various wall movements associated to earth pressure and demonstrated that the earth pressure on the back of the wall decreased quickly with increasing wall displacement. To demonstrate this, normalized

lateral pressure was back calculated using the measured lateral earth pressure and overburden stress. The calculated normalized lateral pressure was then plotted against the translational wall displacement (Figure 4-16 a). A similar computation was carried out for the current study as well and compared to the findings of Fang and Ishibashi (1986) as shown in Figure 4-16 b. As anticipated, the normalized lateral pressures for the three reinforced sections decreased rapidly with the wall displacement. Furthermore, the plot in Figure 4-16 b highlights the fact that the normalized lateral pressure decreased with increasing reinforcement. The low normalized lateral pressure in SR\_6x3 suggests that the net lateral pressure on its wall is the least among the reinforced sections.

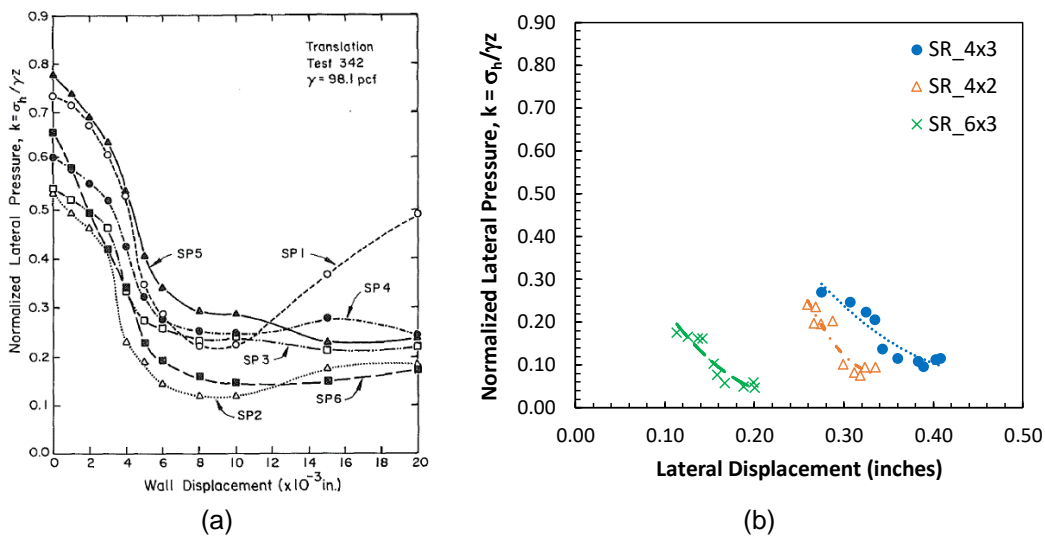


Figure 4-16 Change in Normalized Lateral Pressure with Lateral Wall Displacement (a).

Reprinted from Fang and Ishibashi (1986), © ASCE (b). Current Study

#### 4.6 Effectiveness of the RPP Reinforcement Approach

The lateral displacement and vertical settlement of the wall base in all the sections were compared with each other to evaluate the effectiveness of RPPs in improving the shearing resistance and bearing capacity of the MSE wall base, respectively. The

maximum displacement values observed in each section were plotted in a chart, and the reduction in the displacement of reinforced sections in terms of the control section were also evaluated.

Figure 4-17 shows the reduction in lateral displacement due to RPPs. The comparison was made when the last reading of the control section was taken when it displaced significantly. The 4"x4" RPP spaced at 3 ft. c/c reduced the lateral movement of the wall base by almost 75%. However, decreasing the spacing to 2 ft. c/c reduced the lateral movement by only an additional 6%. The section reinforced with 6"x6" RPP reduced the lateral movement by almost 89% than the control section. The plot clearly implies that RPPs are working very well in reducing the lateral displacement of the wall base.

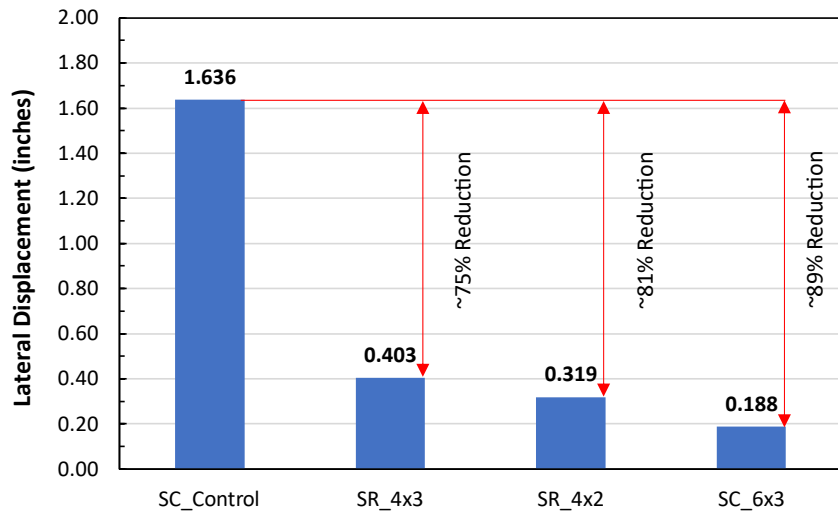


Figure 4-17 Comparison of Lateral Displacement of Ground Level

A full-scale experimental study on the performance of pile-supported embankment on soft soil was conducted by Briancon and Simon (2012). The test embankment (5 m or 16.4 ft. high) was supported by 26 ft. (8 m) to 34 ft. (10.5 m) long rigid piles embedded into foundation soil consisting of clay and sandy clay of low plasticity. Vertical inclinometers

were used to monitor the lateral soil displacement of the foundation. Compared to the control section, the study demonstrated 46-60% reductions in lateral soil displacement.

Figure 4-18 presents the reduction in maximum vertical displacement due to RPPs. The 4"x4" RPP spaced at 3 ft. c/c reduced the vertical settlement of the wall base by almost 48%. Decreasing the spacing to 2 ft. c/c controlled the vertical settlement by an additional 18%. The section stabilized with 6"x6" RPPs at 3 ft. c/c reduced the vertical settlement by about 68%. Even though the improvements seen in SR\_4x2 and SR\_6x3 are close, on an average SR\_6x3 performed better than SR\_4x2. In a nutshell, the composite action of geogrid and RPP considerably reduced the settlement of wall base when compared to the control section.

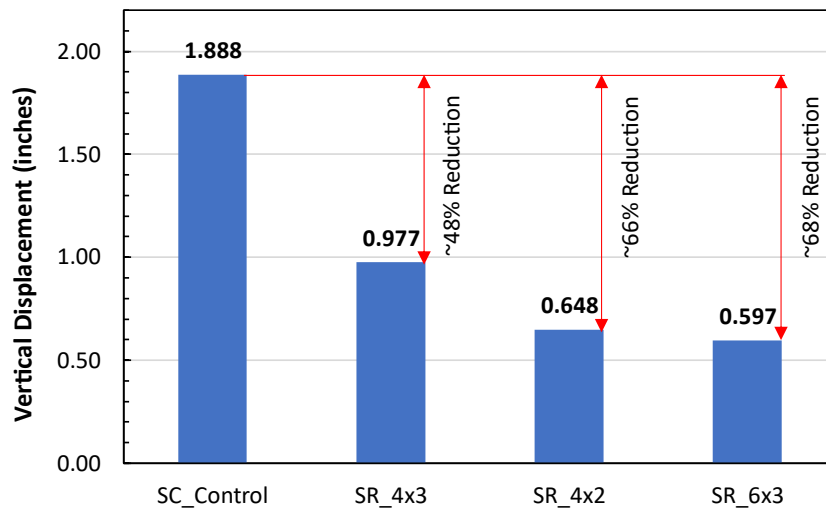


Figure 4-18 Comparison of Maximum Vertical Displacement of Wall Base

The pressure plate readings were compared with each other to evaluate the decrease in lateral pressure in the RPP reinforced sections. Figure 4-19 shows the maximum lateral pressure on the wall facing from May 2019 onwards. When compared to the control



section, there is almost a 66%, 72%, and 76% reduction in the lateral pressure in sections SR\_4x3, SR\_4x2, and SR\_6x3, respectively. This signifies that the more number and larger size of RPPs are carrying over the lateral load from the backfill, thereby decreasing the net force on the wall facing.

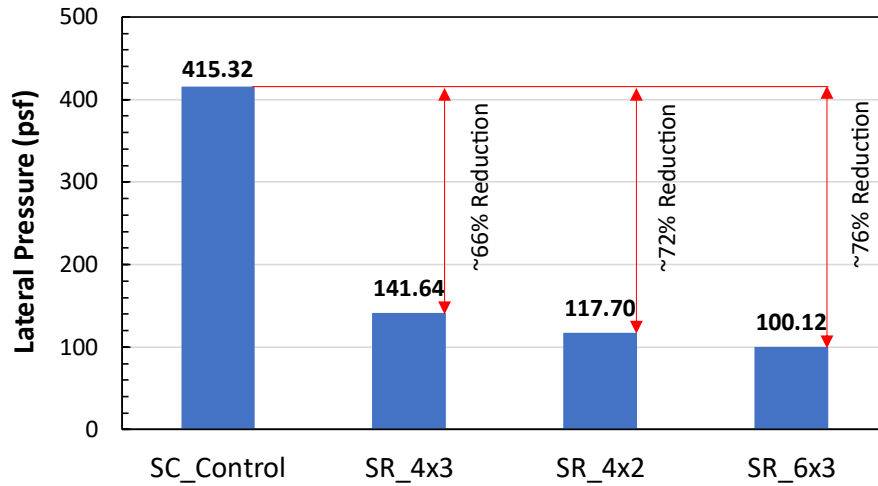


Figure 4-19 Decrease in Maximum Lateral Pressure with RPP Reinforcement

The coefficient of lateral earth pressure acting on the wall was back-calculated as discussed above and presented in Figure 4-16. This coefficient can also be normalized with respect to the Rankine's active lateral earth pressure coefficient such as  $K_r/K_a$ , where  $K_r = \sigma_h/\gamma z$  and  $K_a = \tan^2(45^\circ - \phi/2)$  (Christopher et al., 1990; Jiang et al., 2015; Jiang et al., 2016). Figure 4-20 compares the ratio  $K_r/K_a$  computed for this study with for that from Jiang et al. (2016). The straight line passing through  $K_r/K_a = 1$  is the condition when geosynthetics are used as reinforcements as calculated by AASHTO (2007). Jiang et al. (2016) estimated  $K_r$  in terms of the maximum tension measured in the reinforcement. The authors explained that a ratio of less than 1 signifies that less tension is acting on the reinforcement as opposed to when active Rankine condition is occurring.

The ratio  $K_r/K_a$  is less than unity for this study, with the control section approaching unity with a ratio of 0.98. These results suggest that the net average pressure acting on the wall face is less than that required to produce an active Rankine condition. This is visually observed as well since the wall facings show no signs of distress or displacement. However, the control section, as shown in Figure 4-5, has undergone significant wall displacement due to the development of active Rankine condition. The ratio is least for SR\_6x3, highlighting the larger resistance to active lateral pressure provided by the RPPs.

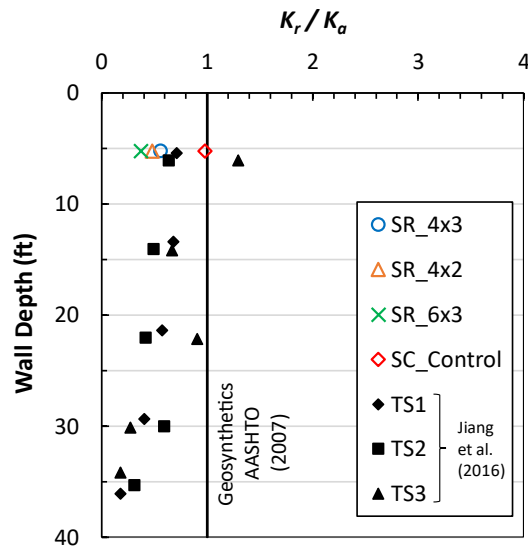


Figure 4-20 Comparison of the Coefficient of Lateral Earth Pressure in the Current Study and Jiang et al. (2016)

Mochizuki et al. (1980) stated that a major portion of lateral deformation is observed during and just after construction. Ortiz (1967) added that almost 60% of total deformation takes place during and just after construction. The displacements of the test sections in this study were analyzed to evaluate the percentage of total movements recorded in the first 30 days. On average, about 56% of the total recorded lateral ground

displacement was observed in the first month, while it was 74% for the wall base settlement. The results comport with findings from Mochizuki et al. (1980) and Ortiz (1967). Similar findings were reported by Chen et al. (2010) and Briancon and Simon (2012) as well, where the majority of the embankment vertical deformation occurred within 25-60 days of construction. In the current study, after the major displacements occurred, the recent readings have comparatively less incremental displacements. However, due to changing climatic conditions the displacements still fluctuate. To capture the effect of seasonal climatic variation in the lateral and vertical displacements of the MSE wall base, the performance monitoring should be continued regularly for a longer period of time.

## Chapter 5

### NUMERICAL STUDY

#### 5.1 Background

Computer models can be used to efficiently study the performance of geotechnical structures in different scenarios. Numerical study using Finite Element Modeling (FEM) has been utilized by researchers to evaluate the field behavior of several geotechnical structures. It provides a basis for evaluating the performance of structures based on rigorous and complicated numerical calculations. Generally, the first step during such studies is calibration of the model to match the field behavior in terms of deformation. Then, further analysis and parametric studies are carried out to evaluate the field performance in a broader aspect.

The main objective of this chapter is to numerically simulate the field behavior of the test sections using PLAXIS 2D. The calibrated model was used to study the effects of various RPP parameters and soil conditions on the performance of the MSE wall. Furthermore, the effectiveness of RPP reinforcement for greater wall heights than at the field was also evaluated. GeoStudio software was also chosen where the SLOPE/W package was used to simulate the global factor of safety of the MSE wall test sections. The details of the model calibration, parametric study, and other relevant modeling results are presented herein.

#### 5.2 Finite Element Based Numerical Model

PLAXIS 2D developed by Bentley Systems was used for the numerical study (PLAXIS 2D Reference Manual, 2020). It is a two-dimensional finite element (FE) package which can perform deformation and stability analyses for geotechnical applications. It was assumed that the strain in the perpendicular direction to the plane was zero. Therefore, a plane-

strain condition was used for the modeling. The reinforced fill, retained soil, and the foundation soil were modeled using an elastic-perfectly plastic Mohr-Coulomb (MC) yield function with a non-associated flow rule (Kibria et al., 2014). The initial properties of the fill and the foundation soil were as per the laboratory results. The backfill soil was considered to exhibit undrained behavior, while the sand was modeled to have drained behavior with no generation of excess pore water pressure. The properties of the structural elements were in accordance with the manufacturer's specification. Since the test sections did not have any surcharge load, it was not considered in the model.

The soil reinforcement was modeled as linear elastic sheet element using geogrid element, which behaves isotropically at each node and is unable to work under compression. The wall facing, footing, and RPPs were simulated using plate elements. Standard fixities were applied for the boundary conditions, where the two vertical boundaries were free to move vertically but fixed in the horizontal direction. Full fixity was applied at the base of the geometry (Kibria et al., 2014; Ahmed et al., 2020). Table 5-1 and Table 5-2 show the properties of the structural elements and geogrid, respectively. The analyses were performed using 15 node triangular elements which furnished high-quality stress results. Since the elastic domain of the MC model exhibited a linear relationship, a global stiffness matrix was used in the elastoplastic deformation analysis to estimate the horizontal displacement (PLAXIS 2D Reference Manual, 2020). The geometry of the test wall and corresponding mesh connectivity are shown in Figure 5-1 and Figure 5-2, respectively. The area near the MSE wall, where the deformations were of interest, was simulated using the fine mesh size option. This was the reinforced fill and Layer 1 of the foundation soil. A finer mesh ensures more reliable results and thus were applied at the above-mentioned areas of interest.

Table 5-1 Properties of the Structural Elements in the FE Model

Parameter	Axial Stiffness, EA (lbf/ft) x10 <sup>6</sup>	Bending Stiffness, EI (lbf.ft <sup>2</sup> /ft) x 10 <sup>6</sup>	Size, d (ft)	w (lbf/ft/ft)
Wall Footing	110.9	1.751	0.4353	1.2
Wall Facing	143	0.331	0.1667	5
RPP (4 in. x 4 in.)	3.2	0.02963	0.333	1.85
RPP (6 in. x 6 in.)	7.2	0.15	0.50	4.167

Table 5-2 Properties of the Geogrid in the FE Model

Geogrid	Axial Stiffness, EA (lbf/ft)
TX5 Geogrid	3500

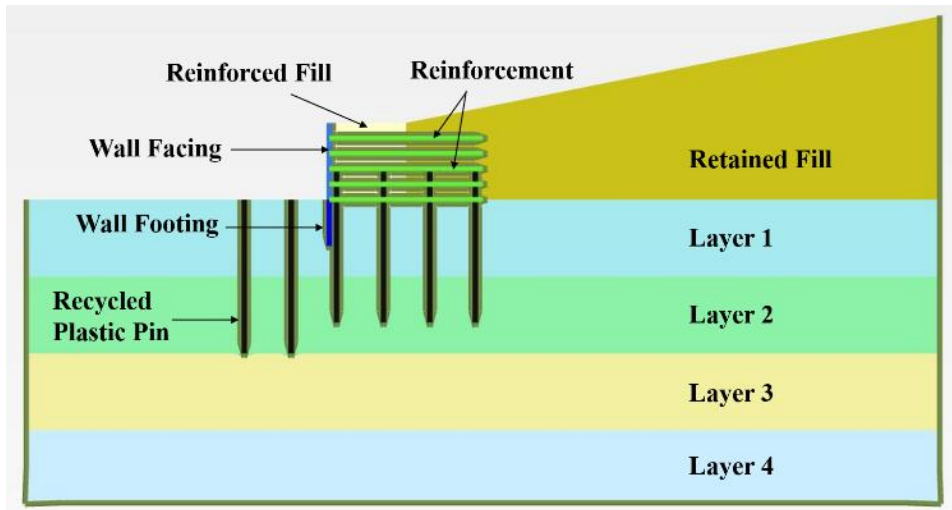


Figure 5-1 Geometry of the Wall in the FE Model

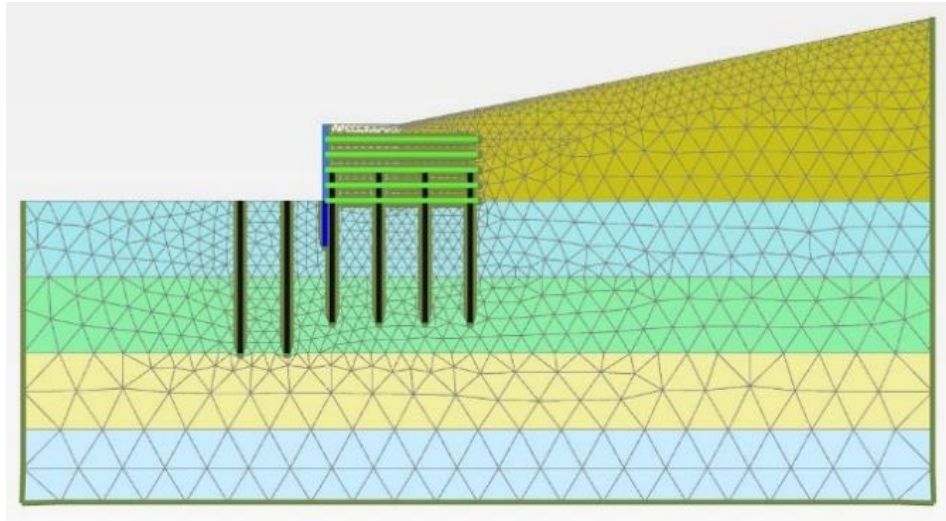


Figure 5-2 Mesh Connectivity in the FE Model

Each layer of foundation soil is 5 ft. deep. The wall height is also 5 ft. The RPPs are modeled as 10 ft. long with the ones inside the wall extended 2 ft. above the foundation. The geogrid length is 10 ft. to cover the reinforced area. The distance between the test section and the boundaries were chosen in such a way that there was no boundary effect on the deformation outputs.

#### *5.2.1 Model Calibration Using the Control Section*

The deformations as seen in the field control section (SC\_Control) were used to calibrate the FE model. Mochizuki et al. (1980) stated that a major portion of lateral deformation is observed during and just after construction. Ortiz (1967) added that almost 60% of total deformation takes place during and just after construction. The displacements of the field test sections in this study were analyzed to evaluate the percentage of total movements recorded in the first 30 days. On average, about 56% of the total recorded lateral ground displacement was observed in the first month. Moreover, 75% of the maximum lateral displacement of the control section was observed in the first 30 days after construction.

Therefore, the FE model was simulated to determine the lateral displacement after 30 days of construction. The calibration was performed by back analysis of the foundation soil (Layer 1) properties. Several iterations were performed by changing the soil parameters within a certain range as obtained from the laboratory tests. Table 5-3 shows the back-calculated soil properties along with all the soil parameters used in the calibrated FE model. Various interface friction angles were chosen for the soil blocks as shown in Table 5-3. It was previously reported that a reduction in interface angle of reinforced fill from 1.0 to 0.67 produces a negligible variation in displacement (Rowe and Ho, 1998).

The inclinometer results of SC\_Control from the field showed that the base of the control section displaced laterally by 1.23 inches after 30 days. The FE model predicted a base movement of 1.33 inches for the same time period. Furthermore, the FE model could fairly predict similar values for the whole depth of the inclinometer (20 ft.). Figure 5-3 compares the field and model horizontal displacements of the control section foundation soil at different depths. The magnitude and location of the maximum lateral displacement predicted from PLAXIS was fairly similar to the actual movement as measured in the field section. Apart from the ground surface (0 ft. depth), the field measured lateral displacements were slightly higher than the model predicted values. This variation could be due to infiltration of surface water to deeper depths, which was not accounted for in the FE model (Kibria et al., 2014). Besides, the effect due to compaction was also not modeled which could have been one factor for the slightly higher lateral displacements in the field section. It is to be noted that the FE model could successfully simulate the trend/behavior of foundation soil movements.



Table 5-3 Properties of the Soil in the FE Model

Parameter	Layer 1	Layer 2	Layer 3	Layer 4	Retained Fill	Reinforced Fill
Unsat. Unit Wt. (pcf)	103.4	108.6	121.4	129.7	102	116.9
Sat. Unit Wt. (pcf)	108	115	126	135	105	118
Stiffness x 10 <sup>3</sup> (psf)	30	150	300	500	200	100
Angle of Internal Friction (degree)	30	27	15	5	5	32
Poisson's Ratio	0.4	0.3	0.3	0.25	0.4	0.35
Cohesion (psf)	30	300	1796	3300	350	1
Interface	0.7	0.7	0.7	0.7	0.67	0.5

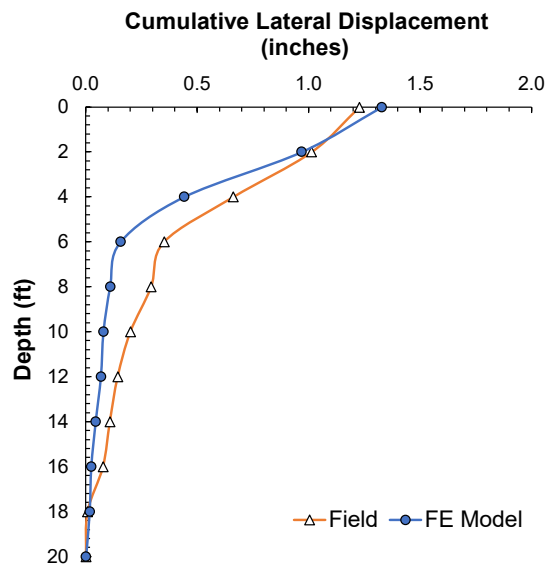


Figure 5-3 Comparison of Field and Model Horizontal Displacements of SC\_Control

Stability analyses of the numerical model showed that the control section failed through rotational movement of the wall. There was both translational movement and tilting of the face panel. This is in good agreement to the failure pattern of the field control section as

seen in Figure 5-4. The numerical model showed high lateral displacement at the wall base which was seen in the field section as well. Moreover, the lateral displacement of the top of the wall facing was also similar to the field observed displacement.

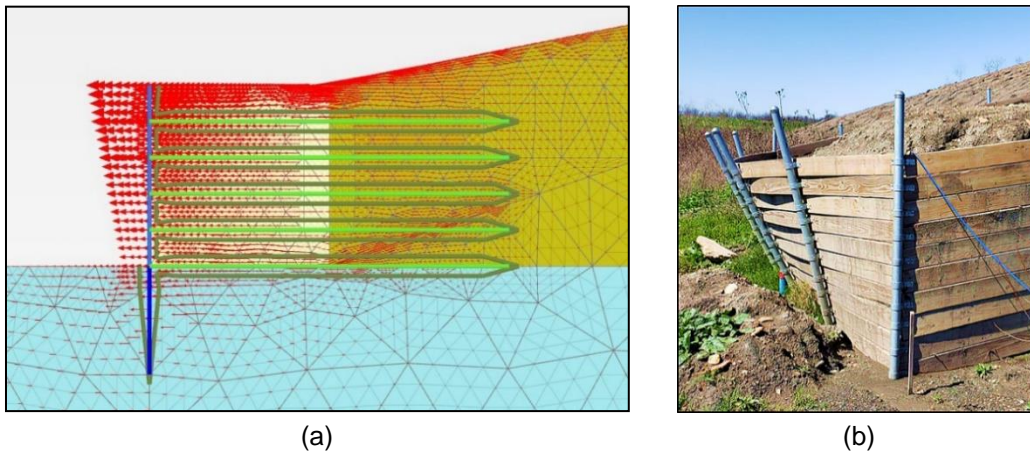


Figure 5-4 Failure Pattern of (a) FE Model and (b) Field Control Section

### 5.2.2 Numerical Modeling of the Reinforced Sections

The calibrated control section was reinforced with RPPs to match the deformations as recorded in the field test sections. All the three reinforced sections, SR\_4x3, SR\_4x2, and SR\_6x3, were modeled with the respective RPP parameters. The lateral displacement profiles comparing the field and FE model outputs for the three reinforced test sections are presented in Figure 5-5.

The maximum lateral displacements in SR\_4x3, SR\_4x2, and SR\_6x3 in the FE model were 0.26 inches, 0.22 inches, and 0.11 inches, respectively. The actual displacements in the field sections were very close to the FE model values. Moreover, the trend or pattern of the foundation soil displacement was also similar for the total depth (20 ft.) of interest. The FE model could effectively simulate the better resistance provided by the closer spacing and larger size of RPPs.

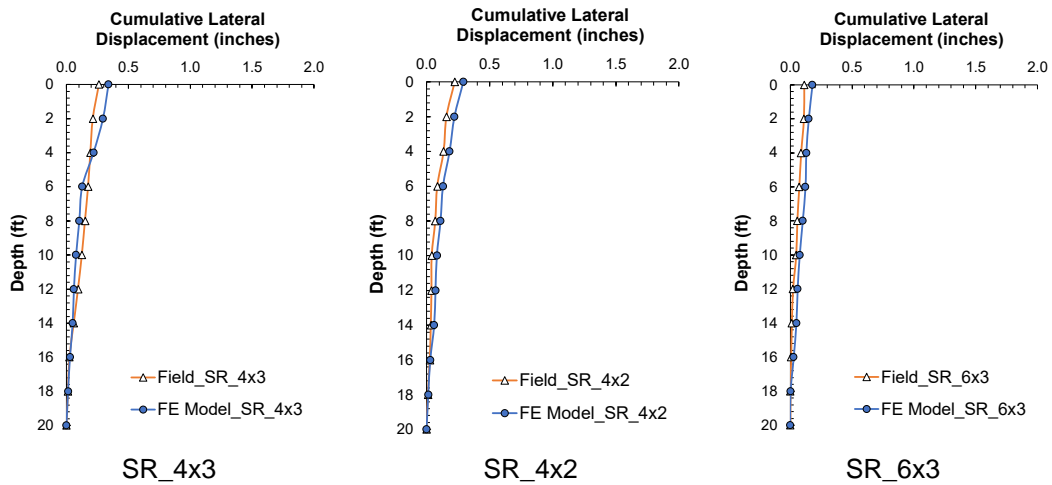


Figure 5-5 Comparison of Field and Model Horizontal Displacements of the Reinforced Test Sections

The charts presented above validate the FE model since the lateral displacements predicted by the numerical model are very close to the actual measurements recorded in the field. The slight variations encountered can be attributed to the soil heterogeneity in the real field condition.

### 5.3 Parametric Study

After the calibration of the FE model, a parametric study was conducted to investigate the effect of varying soil and RPP parameters on the lateral displacement of the MSE wall base. The primary objective of the parametric study was to develop a comprehensive dataset to understand the behavior of RPP reinforced MSE wall in terms of lateral resistance. A parametric study matrix was formulated, as shown in Figure 5-6, considering the probable associated parameters. Five different foundation soil conditions were investigated with more focus on varying friction angles. The soil properties of only Layer 1 were varied for the parametric study. Since the majority of the change in lateral displacement is dependent on the soil in Layer 1, it was decided that only the properties

of that layer would be altered. A standard practice while constructing MSE walls is to replace the top foundation soil with granular soil so as to increase the friction between the foundation and the wall base. Also, presence of granular soil provides a better drainage of water. Thus, the soil properties for the parametric study were chosen in such a way that the cohesion values were less and that the soil was mostly granular with high friction angle.

The RPP cross-sections were limited to 4 inch x 4 inch and 6 inch x 6 inch since larger sizes are difficult to install at field conditions, and require bigger equipment ultimately incurring extra costs. The 4 inch and 6 inch size RPPs can be installed with an excavator equipped with hydraulic hammer which is comparatively less cost-intensive compared to other heavy equipment. The use of an excavator also ensures reduced installation time and better mobility at site. Three RPP center-to-center spacings at 1 ft. increments were chosen. The basis for this was the group action of RPPs. The RPP spacing was limited to a maximum of 4 ft. c/c since a spacing more than this might result in a reduced group efficiency.

It was observed that the base of MSE walls taller than 10 ft. displaced by a relatively large factor with the current wall footing and facing specifications. Therefore, the wall height was limited to 10 ft. for this study to be consistent with the field results. Later in the following chapters, the effectiveness of higher size of RPPs for taller walls is studied. The effect of RPP extension above the foundation soil into the MSE wall reinforced fill was also considered. Since the extended RPP portion plays a very important role in reducing the net lateral pressure on the wall face, as seen from the field results, it was desired to investigate the effect of varying extension lengths.

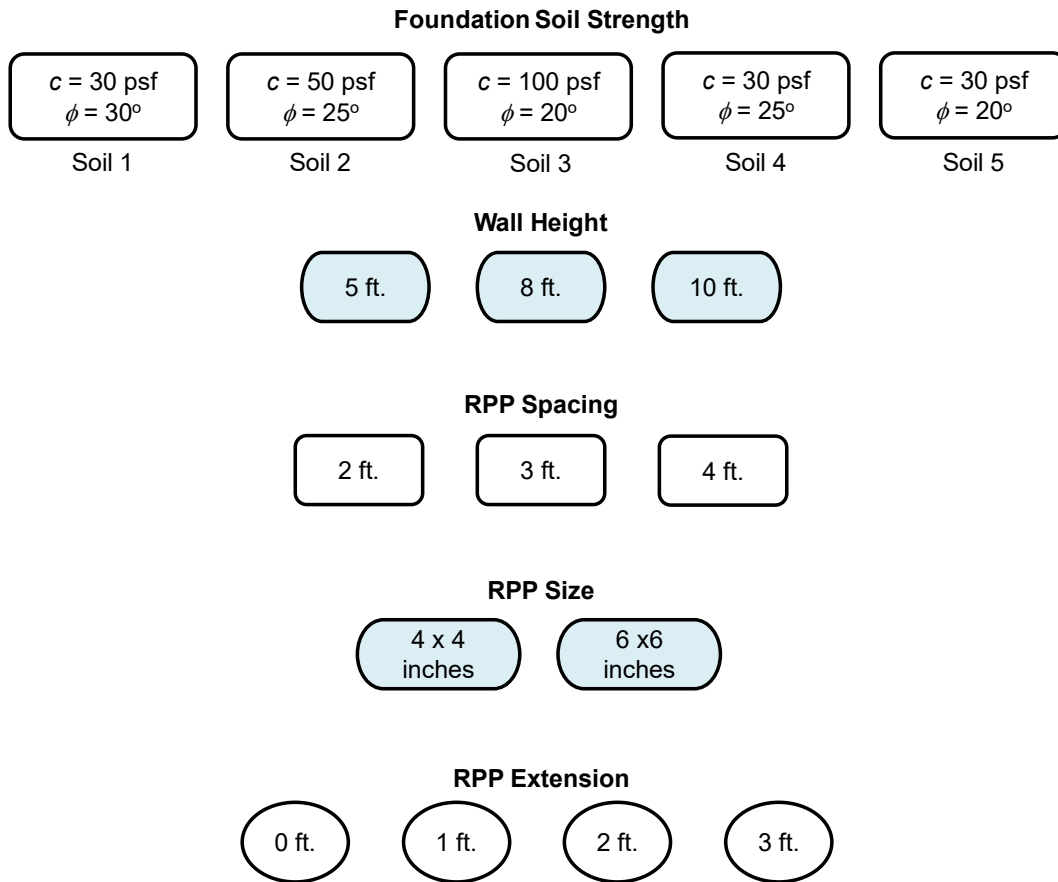


Figure 5-6 Parametric Study Matrix

### 5.3.1 Effect of Foundation Soil Strength

The effect of three different foundation soil cohesions and frictions angles were investigated using the calibrated model. The lateral displacement of an MSE wall is dependent on the shear strength of the foundation soil, as more shear strength produces better resistance against sliding (Das, 2015). Conventionally, only the friction angle of the foundation soil is considered for calculating the stability against sliding (AASHTO, 2014). However, the cohesion also plays some part if the foundation is a  $c-\phi$  soil. It is to be noted that the three soil conditions (Soil 1, Soil 2, Soil 3) have both the cohesion and

friction angles varied. These combinations were selected to investigate the effect of decreasing friction angle and increasing cohesion. Soil 4 and Soil 5 have the same cohesion as Soil 1; however, the friction angle was varied to study the effect of only the friction angle on lateral displacement.

The study was conducted for both the sizes of RPPs. However, the lateral displacement trends were similar. Figure 5-7 compares the base lateral displacement at three wall heights with different foundation soil strengths ( $c$  and  $\phi$ ). The RPP spacing and extension were kept constant at 3 ft. and 2 ft., respectively. An interesting trend was found from the numerical analysis, such that, even though the friction angle decreased, the increase in cohesion restricted the lateral displacement to some extent. The lateral displacements at all wall heights were the smallest for Soil 3 where the friction angle is the least and cohesion the most. The reason behind this might be that the soil in front of the wall does not fail due to higher cohesion, and thus prevents lateral movement of the wall base. The difference in sliding was more pronounced at greater wall heights for both the RPP sizes.

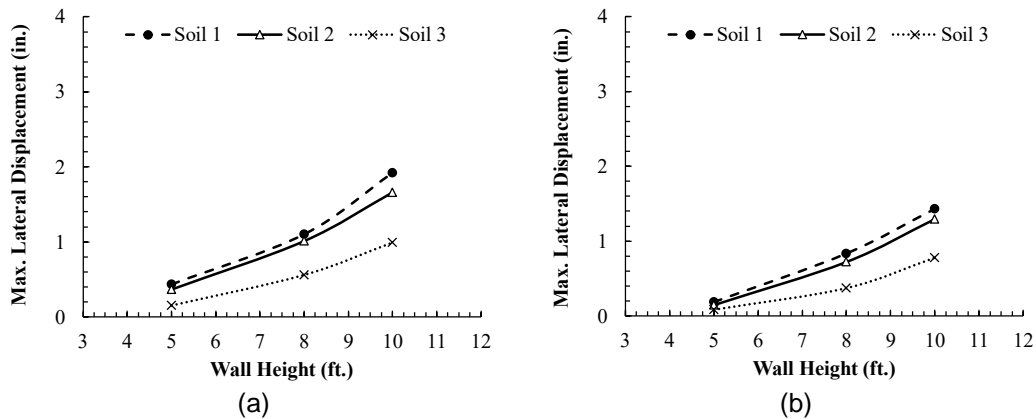


Figure 5-7 Effect of Foundation Soil Strength ( $c$ - $\phi$ ) on Lateral Displacement of MSE Wall Base (a). RPP Size 4x4 inches (b). RPP Size 6x6 inches

Figure 5-8 shows the lateral base displacement of a 5 ft. high MSE wall at different RPP spacings and foundation soil with varying friction angles. The RPP size and extension were fixed at 4x4 inches and 2 ft., respectively. As expected, the lateral displacement in the case of Soil 1 (friction angle 30°) was the least at all RPP spacings and was the highest in the case of Soil 5 (friction angle 20°). The higher friction angle provided better shear resistance against sliding of the wall base (Das, 2015). The displacements were relatively closer for Soil 1 and 4. The friction angle of Soil 5 might have been very less for resisting the lateral displacement.

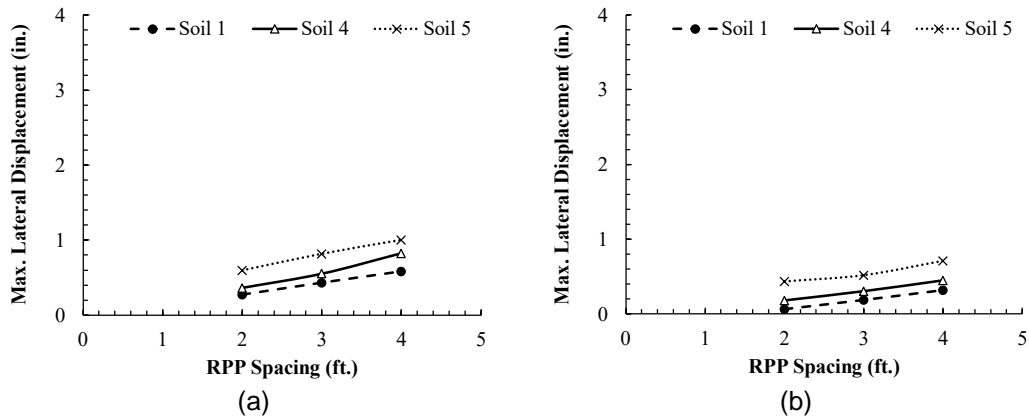


Figure 5-8 Effect of Foundation Soil Friction Angle ( $\phi$ ) on Lateral Displacement of MSE Wall Base (a). RPP Size 4x4 inches (b). RPP Size 6x6 inches

### 5.3.2 Effect of RPP Parameters

The effect of different RPP parameters on the lateral displacement response can be beneficial in evaluating an appropriate design layout for MSE wall. It is a known fact that larger cross-section and closer spacing of RPPs provide better resistance against the lateral displacement of soil (Khan, 2014; Zaman, 2019). The field results of the current study point towards the same inference. However, it is important to quantify the reduction of lateral displacement to facilitate the design process.

### RPP Size

As expected, the higher size RPP (6x6 inches) restricted the lateral displacement by a greater extent at all RPP spacings and wall heights. Figure 5-9 a compares the lateral displacement of wall base at variable RPP size and spacing. The RPP extension and wall height were kept constant at 2 ft. and 10 ft., respectively. The 6x6 inches RPP provided a better resistance as the reduction in lateral displacements were within 26-37% compared to the displacements in 4x4 inches RPP reinforced section. The difference in displacements at all RPP spacings were very close, which signifies that at a constant wall height, the degree of resistance provided by a larger size RPP is almost the same regardless of the spacing. Figure 5-9 b compares the lateral displacement of wall base at variable RPP size and wall height. The RPP spacing and extension were fixed at 3 ft. and 2 ft., respectively. Although the lateral displacement increased sharply with increasing wall height, the degree of resistance provided by a larger size RPP was almost the same at all wall heights. However, the 6x6 inches RPP provided a slightly better resistance at the 10 ft. wall height compared to the other wall heights.

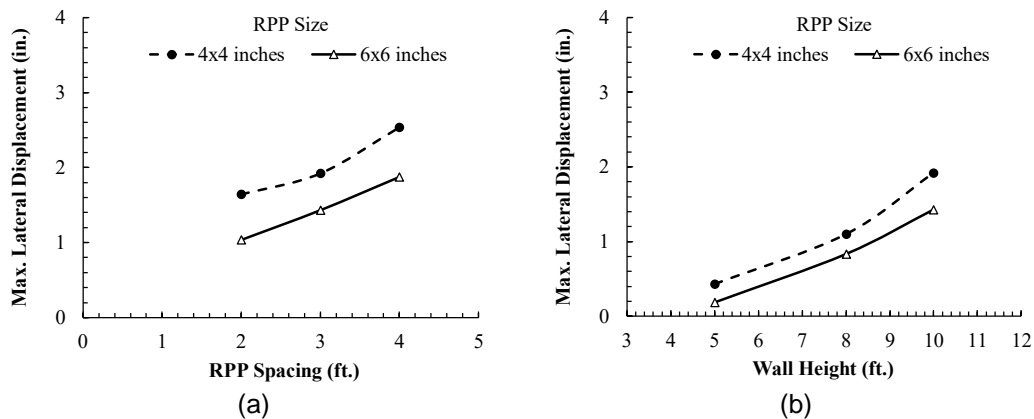


Figure 5-9 Effect of RPP Size on Lateral Displacement of MSE Wall Base (a). Variable RPP Spacing (b). Variable Wall Height



### RPP Spacing

The effect of RPP spacing on the base movement of MSE wall was analyzed at different wall heights. Figure 5-10 shows the variation of maximum lateral displacement of wall base at different RPP spacings. The RPP extension above the foundation was fixed at 2 ft. as in the field test sections. It can be observed that the closer spacings of RPP restrict the lateral displacement of the wall base. The decrease in lateral movement is more visual at a wall height of 10 ft. Both the RPP sizes show similar patterns of movement with the 6x6 inches RPP producing comparatively smaller lateral displacements. The reduction percentage in lateral displacement with a closer spacing of RPPs was more significant for the 5 ft. high wall. The base movement reduced by 53% and 81% when the RPP spacing was lowered from 4 ft. to 2 ft. for the 5 ft. high wall at RPP size 4x4 inches and 6x6 inches, respectively. A similar reduction of RPP spacing for the other wall heights reduced the lateral displacement by 33-53%. Zaman (2019) presented similar findings where the closer spacing of RPPs provided better results with lower lateral base movements.

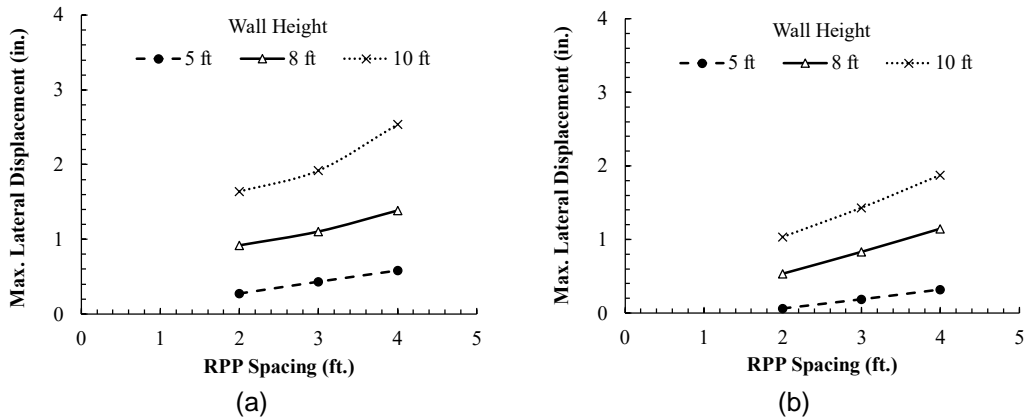


Figure 5-10 Effect of RPP Spacing on Lateral Displacement of MSE Wall Base (a). RPP Size 4x4 inches (b). RPP Size 6x6 inches

### RPP Extension

The variations in base lateral displacement with RPP extension were identified for three different wall heights as shown in Figure 5-11 a. The RPP size and spacing were kept fixed at 4x4 inches and 3 ft., respectively. The effect of the extended portion can be clearly seen in the chart as the lateral displacement decreased significantly after the RPP was extended above the foundation. The rate of decrease in lateral movement gradually reduced with increasing RPP extension. This shows that even a small portion of RPP above the foundation can help to resist the lateral pressure from the backfill thereby reducing the outward movement of the wall. However, the rate of decrease is more for taller walls. The change of RPP extension from 0 ft. to 3 ft. reduced the lateral displacement by 53% for the 10 ft. wall, while it was about 41% for the shorter walls. The reason behind this could be the point of application of active pressure at the back of the wall. The distance between the resultant active pressure on the wall face and the foundation will increase with an increase in the wall height (Das, 2015). Furthermore, the active earth pressure at the base of the wall also increases with the wall height (Bang, 1985; Chang, 1997). Thus, increasing the RPP extension upto the resultant point of application can help in controlling the lateral displacement of the wall base. Nevertheless, the depth of RPP inside the foundation which helps in stiffening the foundation and providing passive resistance should also be considered. Hence, an extension upto 3 ft. can be considered satisfactory for a 10 ft. wall, while smaller extensions will provide similar results for shorter walls.

Figure 5-11 b shows the variations in base movement with RPP extension for different RPP spacings. The wall height and RPP size were kept constant at 5 ft. and 4x4 inches, respectively. Following the initial decrease in lateral movement after the RPP was

extended 1 ft., there was insignificant change in the displacement. These results show that the effect of RPP extension is more substantial with changing wall height.

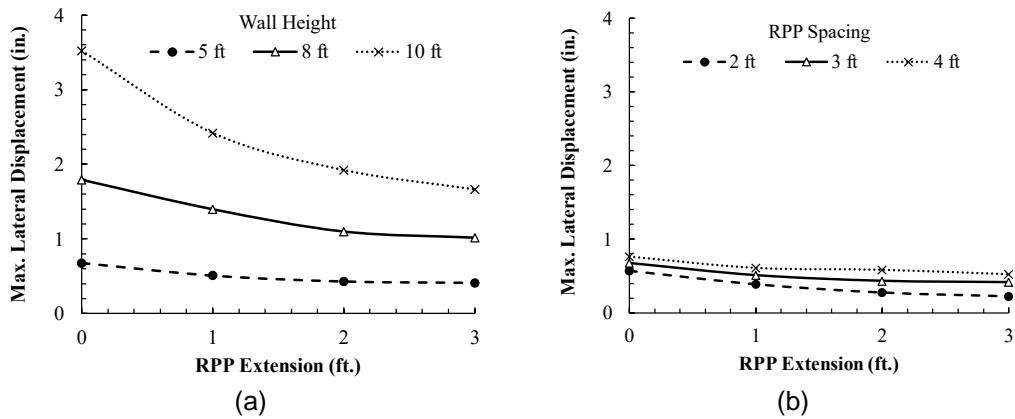


Figure 5-11 Effect of RPP Extension on Lateral Displacement of MSE Wall Base (a). Variable Wall Height (b). Variable RPP Spacing

### 5.3.3 Effect of MSE Wall Height

The numerical study showed that the most important variable influencing the lateral displacement of wall base is the MSE wall height. Among all the parameters studied, the wall height brought about the highest change in lateral displacement. Similar effects of wall height were seen at all the soil strengths investigated. Figure 5-12 compares the change in base displacement with varying wall height and RPP spacing. The RPP extension above the foundation was kept fixed at 2 ft. The increase in lateral displacement is significant with increasing wall height. The lateral displacement increased by an average of about 1.6 inches when the wall height changed from 5 ft. to 10 ft. for the 4x4 inches RPP reinforced sections. The same increase in wall height for the 6x6 inches RPP reinforced sections increased the lateral displacement by about 1.2 inches. Even though the larger size RPP provided better resistance, the effect of wall height was the same for both the sizes of RPPs.

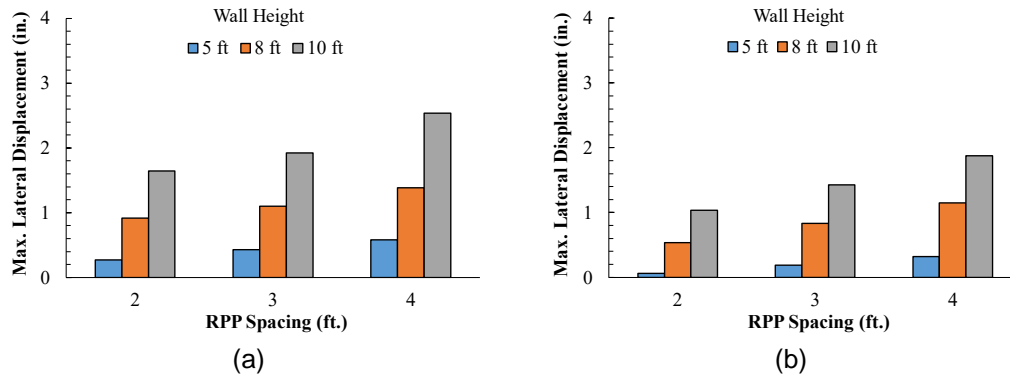


Figure 5-12 Effect of Wall Height on Lateral Displacement of MSE Wall Base (a). RPP Size 4x4 inches (b). RPP Size 6x6 inches

#### 5.4 Passive Pressure Due to RPPs

The RPPs improve the lateral resistance by providing additional passive pressure from the soil in front of the RPPs. The RPPs move in the direction of the acting lateral pressure. A passive wedge develops in front of the RPPs due to this movement. Previous studies (Ashour et al., 1998; Mei et al., 2009; Ni et al., 2018) have shown the relations involved in the calculation of this passive wedge. A general strain wedge model in uniform soil was devised by Ashour et al. (1998). The model (Figure 5-13) shows the formation of a mobilized passive wedge in front of a pile subjected to lateral force. It was reported that the width of the wedge fans out relative to the mobilized friction angle ( $\phi_m$ ). This suggests that friction angle is directly proportional to the passive pressure providing greater resistance. The height ( $h$ ) indicates that portion of the pile that is deflected, while 'D' represents the pile width. The angle of the passive wedge is shown by  $\beta_m$ . The horizontal stress change at the passive wedge is symbolized by  $\Delta\sigma_h$ . The passive wedge characteristics can be calculated at any depth 'x' using the relations provided by Ashour et al. (1998).



to the reduction of lateral pressure on the wall face. This, in turn, reduced the lateral displacement.

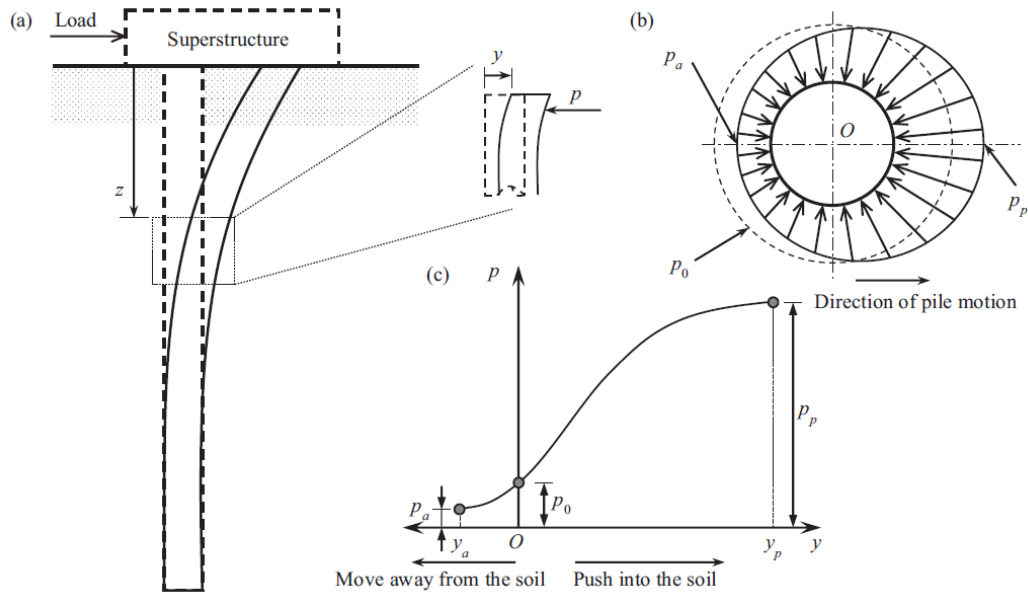


Figure 5-14 Schematics of (a). Laterally Loaded Pile (b). Soil Pressure Around Circumference of Pile (c). Variation of Earth Pressure with Displacement (Adapted from Mei et al., 2009 and Ni et al., 2018)

Mei et al. (2009) proposed a displacement-dependent model to calculate soil reactions due to lateral pile movement, which was rearranged by Ni et al. (2018) as follows:

$$p = \left[ \frac{m}{1 + \exp(by)} - n \right] * \gamma z$$

$$m = 2 * (k_p - k_o)$$

$$n = k_p - 2 * k_o$$

$$b = \frac{\ln \left[ \frac{k_p - k_a}{k_p - 2 \cdot k_o + k_a} \right]}{\gamma_a} < 0$$

where,  $k_p$  = Rankine's passive earth pressure coefficient  $[\tan^2 (45^\circ + \phi'/2)]$

$k_a$  = Rankine's active earth pressure coefficient  $[\tan^2 (45^\circ - \phi'/2)]$

$k_o$  = Jaky's at-rest earth pressure coefficient  $[1 - \sin\phi']$

$y_a$  = Displacement to mobilize the full active pressure

$y$  = Pile deflection

$\gamma$  = Unit weight of soil

$z$  = Depth of pile location of interest

Previous studies have correlated the displacement required to mobilize the full active pressure ( $y_a$ ) to pile width/diameter ( $d$ ). Some correlations and their respective studies are presented below:

- $y_a/d = 0.5-3\%$  for medium dense to dense sand (Fang et al., 2002; Rollins and Sparks, 2002; Fan and Long, 2005)
- $y_a/d = 11-15\%$  for loose sand (Fang et al., 2002; Rollins and Sparks, 2002; Cubrinovski et al., 2006)
- $y_a/d = 3-5\%$  for stiff to soft clay (Hansen, 1961)
- $y_a/d = 2-3\%$  for dense sand (Hansen, 1961)
- $y_a/d = 3-5\%$  for medium sand (Hansen, 1961)
- $y_a/d = 7-10\%$  for loose sand (Hansen, 1961)

Considering medium sand,  $y_a/d = 5\%$  was taken for this study. A similar approach as given by Mei et al. (2009) was used to demonstrate the increase of passive pressure in SR\_4x3. The first RPP inside the test section (closest to the wall facing) was chosen.

Relevant calculations using the above-mentioned equations were performed to get a displacement-dependent soil reaction curve. Figure 5-15 shows the final curve obtained for the RPP. It can be seen that the at-rest pressure when there is no RPP deflection is 110.94 psf. However, with increasing deflection, the active pressure decreases and successively the passive pressure increases. It can be seen that the active pressure becomes stable after a small movement; however, the passive pressure keeps on increasing until a larger deflection. This shows that the capacity of the RPP to provide lateral resistance is very high. A larger deflection is required to mobilize the full passive pressure. At the same deflection, the passive pressure is higher than the active pressure. Thus, the net pressure is acting against the active force, thereby, providing lateral resistance.

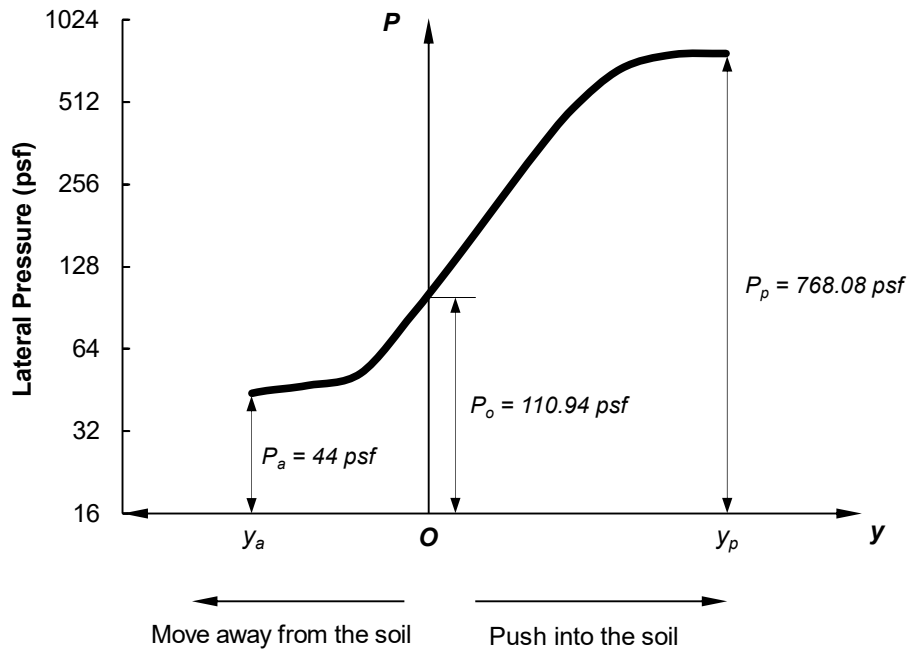


Figure 5-15 Variation of Earth Pressure with Displacement for the First Row of RPP in

SR\_4x3



This was also demonstrated using the FE model results. Lateral stresses acting on the same RPP in the calibrated FE model were estimated. The estimated pressures were smoothed out to get a better understanding. Figure 5-16 shows that at all the depths, the passive pressure was more than the active pressure. For instance, at the 2 ft. depth, the active pressure was 100 psf, while the passive pressure was 150 psf. The net pressure of 50 psf is the  $\Delta\sigma_h$  in the passive strain wedge. This strengthens the outcomes of the analytical study using the approach given by Mei et al. (2009).

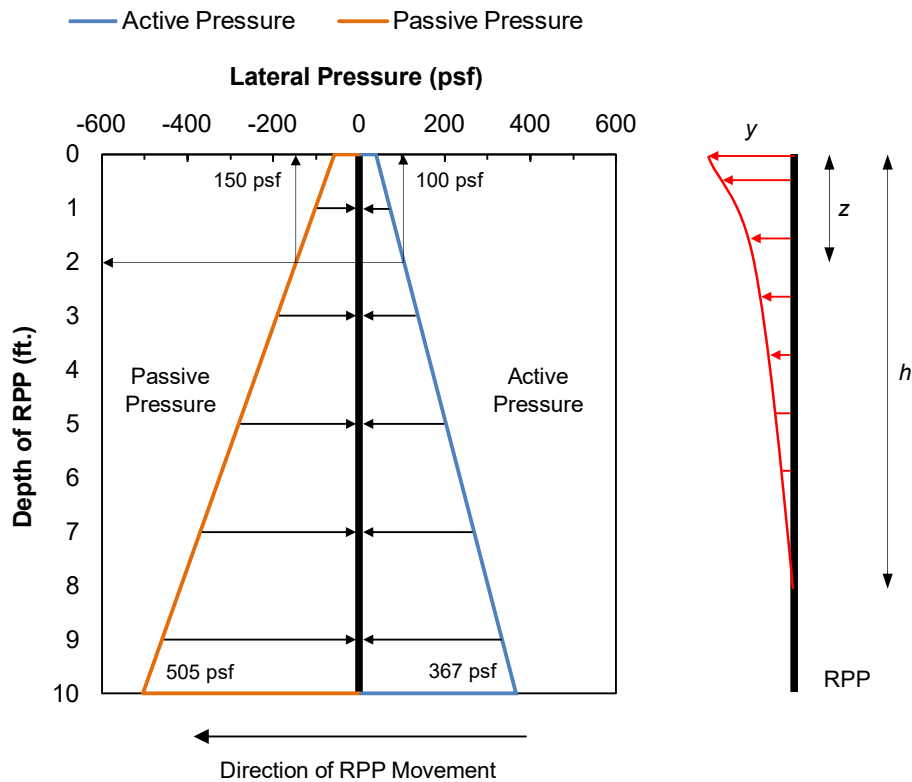


Figure 5-16 Distribution of Lateral Pressure on the First Row of RPP in SR\_4x3

Further evaluations could be done similarly for the other RPPs as well. Ashour et al. (1998) also demonstrated the calculation of passive strain wedge for layered soil, which

better resembles the actual site conditions. The main aim of this section was to demonstrate the mechanism of lateral resistance provided by the RPP, which eventually helps in reducing the outward lateral movement of the MSE wall.

#### 5.5 Reduction in Active Lateral Pressure Due to RPPs

The reduction in the lateral displacement of the wall base was due to a decrease in the active lateral pressure on the wall facing. The RPPs acted as shear keys and resisted the lateral pressure, thereby decreasing the net pressure reaching the wall face. The development of a passive resistance in front of the RPPs help in resisting the lateral pressure from the backfill. It was necessary to quantify this reduction in lateral pressure to evaluate the effectiveness of using RPPs. These reduction factors are later used to develop design charts for MSE walls reinforced with RPPs. The calibrated FE model was used to quantify the reduction factor. However, the calibrated model needed to be checked first for consistency in lateral pressure data according to the field obtained values. Thus, Figure 5-17 was plotted where the lateral pressure at the wall base in the field and from the FE model were compared. Figure 5-17 a compares the lateral pressure at 5 ft. wall height. Since the control section failed without reaching its peak pressure due to excessive wall displacement, only the RPP reinforced sections were compared. It can be visualized that the field and FE model pressures are close to each other. The FE model pressures are slightly higher than the corresponding field values, however, they are within reasonable limits. Figure 5-17 b compares the lateral pressure of the field test sections at 7 ft. height (after second phase of backfilling) and the FE model sections at 8 ft. height. The FE model values are higher than the ones seen at the field because the model wall was 1 ft. higher than the field sections. However, the numerical model could effectively capture the trend of lateral pressure at the wall base. Therefore, the calibrated model can be used to conduct a parametric study of the lateral pressure reductions.

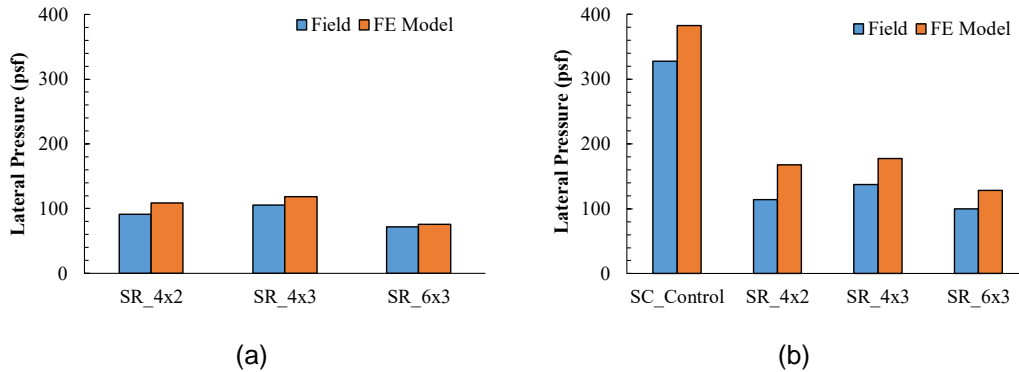


Figure 5-17 Comparison of Field and Model Lateral Pressure at the Base of the Test Sections (a). First Phase Loading (b). Second Phase Loading

Lateral pressure/stress acting on the wall face at the base level was calculated for the control and RPP reinforced sections. Then, the difference of the stresses in the control and reinforced section was calculated. Finally, the reduction factor was estimated by dividing the stress difference by the stress in the control section, such as:

$$SR = (P_C - P_R) / P_C$$

where,

SR = Lateral stress/pressure reduction factor

$P_C$  = Lateral pressure acting on the wall face at the base level of the control section

$P_R$  = Lateral pressure acting on the wall face at the base level of the RPP reinforced section.

The same parametric matrix as shown in Figure 5-6 was used for calculating the SR as well. However, based on the satisfactory performance of the field test sections, and results obtained from the lateral displacement parametric study, only 2 ft. RPP extension above the foundation soil was used for this part of the study. Some of the results

obtained from the study are presented here. All the data from the study were used to develop a prediction model which is shown in the following chapter.

Figure 5-18 a shows the change in lateral pressure reduction due to changing RPP spacing and wall height. The RPP size and extension were constant at 4x4 inches and 2 ft., respectively. As anticipated, an increase in wall height and RPP spacing decreased the reduction factor. Since lateral pressure is directly proportional to wall height, the same RPP configuration could not reduce the increasing pressure from higher walls at the same ratio. However, the average pressure reduction was within 25-62% of that of the control section for the RPP configuration shown in the chart. It can also be seen that the reduction for the 10 ft. high wall is far more less than that for the 5 ft. and 8 ft. walls. Also, at 4 ft. RPP spacing, the reductions for the 5 ft. and 8 ft. walls were almost the same.

Figure 5-18 b shows the change in lateral pressure reduction due to changing RPP spacing and size. The wall height and RPP extension were fixed at 5 ft. and 2 ft., respectively. The larger cross-section of RPP provided better resistance and reduced the backfill pressure by a greater extent. However, at 4 ft. RPP spacing, the reduction factors were very close for the two sizes of RPP.

Figure 5-18 c indicates the change in lateral pressure reduction due to changing RPP spacing and foundation soil properties ( $c$  and  $\phi$ ). The wall height, RPP size and extension were kept constant at 5 ft., 4x4 inches, and 2 ft., respectively. The soil with the higher cohesion (Soil 3) provided comparatively better resistance. However, the difference in pressure reductions were not significant. Interestingly, at 4 ft. RPP spacing, the pressure reductions were almost the same. This along with the results from Figure 5-18 a-b indicate that 4 ft. can be regarded as a maximum limit for the RPP spacing, specifically

for the 5 ft. wall height. Since the effect of other parameters are almost nulled at this spacing, going further beyond this spacing is not recommended.

Bhuiyan (2014) showed that the group effect of RPPs decreases with increasing RPP spacing. This might be the reason why the RPPs at 4 ft. spacing are not following the reduction trend as shown by 2 ft. and 3ft. spacings. Bhuiyan (2014) also reported that the cohesion of the foundation soil plays a very important role in increasing the lateral resistance of RPPs. The same trend was observed in the current study as well where Soil 3 performed the best.

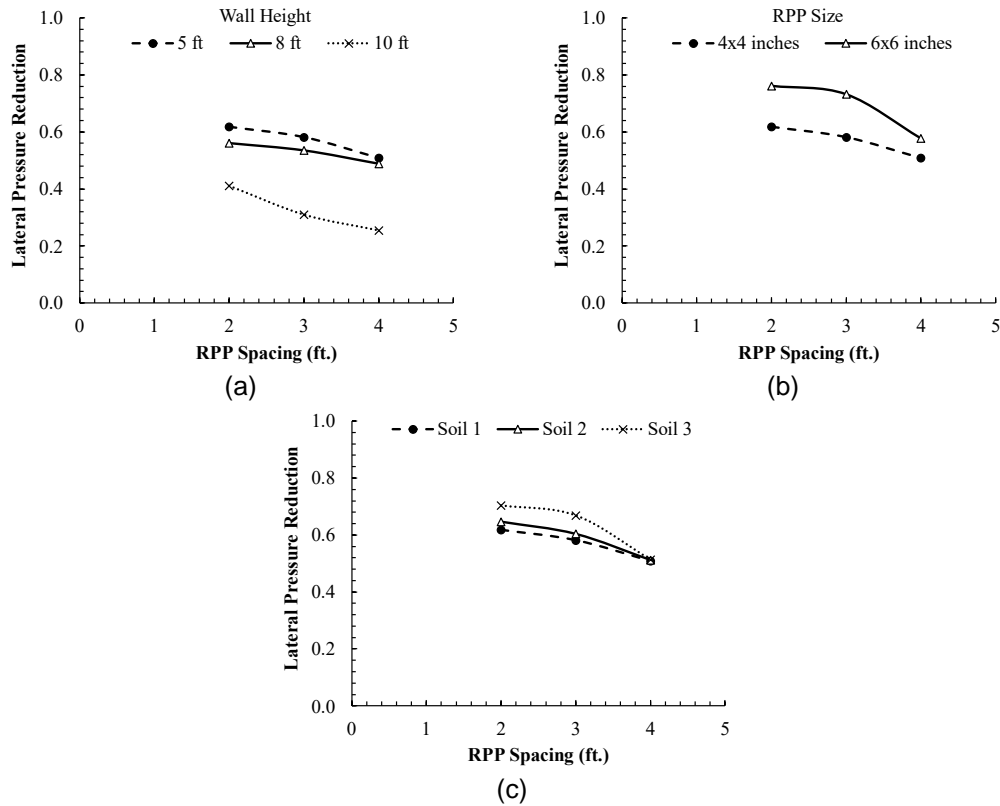


Figure 5-18 Effect of RPP Spacing on Lateral Pressure Reduction at MSE Wall Base (a). Variable Wall Height (b). Variable RPP Size (c). Variable Foundation Soil Strength ( $c-\phi$ )

## 5.6 Global Stability

MSE walls not only fail simply by lateral sliding or overturning, but complex failure mechanisms are equally probable. For walls built on weak foundation soils, slopes, or for tiered wall sections, global stability needs to be checked. Department of Transportations (DOTs) in the US mandate a check of global stability factor for MSE walls. Several conventional methods such as Bishop or Janbu have been used to compute the global factor of safety. However, since these methods are conservative in nature, a more realistic Morgenstern-Price or Spencer method are also preferred. The Bishop or Janbu method focus on either the force or moment equilibrium only. The Bishop's method considers only the normal interslice force but ignores the interslice shear force (Geo Studio, 2020). It satisfies the overall moment equilibrium; however, it does not satisfy the overall horizontal force equilibrium. The Janbu method, on the other hand, satisfies over all horizontal force equilibrium, but not over all moment equilibrium (Geo Studio, 2020). This leads to over-conservative factors of safety which may not be realistic. The Morgenstern-Price and Spencer methods consider both shear and normal interslice forces. Thus, they satisfy both moment and force equilibrium. This results in realistic factors of safety. Figure 5-19 shows that Janbu method generally gives the least factor of safety, while Bishop method also gives less safety factors making the methods conservative. The parameter lambda ( $\lambda$ ) relates the interslice normal and shear forces.

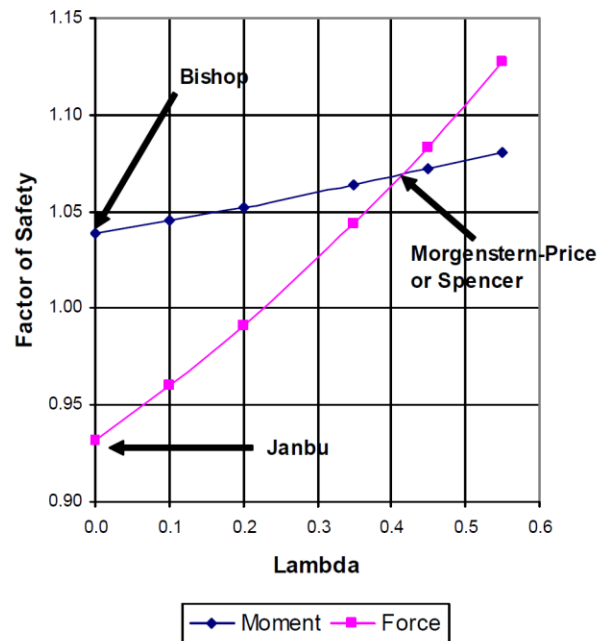


Figure 5-19 Factor of Safety Versus Lambda ( $\lambda$ ) Plot (Geo Studio, 2020)

SLOPE/W package of the Geo Studio software was used for the stability analysis. It is a Limit Equilibrium (LE) approach. Mohr-Coulomb model was chosen for the soil. The same soil parameters as used in the finite element numerical model presented before were used for the global stability analysis as well. For the sake of understanding the variation in factor of safety from different methods, the following analysis methods were chosen:

- Ordinary Method
- Bishop Method
- Janbu Method
- Morgenstern-Price Method
- Spencer Method

The control section along with the RPP reinforced sections constructed at field were modeled in SLOPE/W. Furthermore, the effect of the two rows of front pins were also investigated. The factors of safety from the analyzed methods are tabulated in Table 5-4.

Table 5-4 Global Factor of Safety of the Test Sections

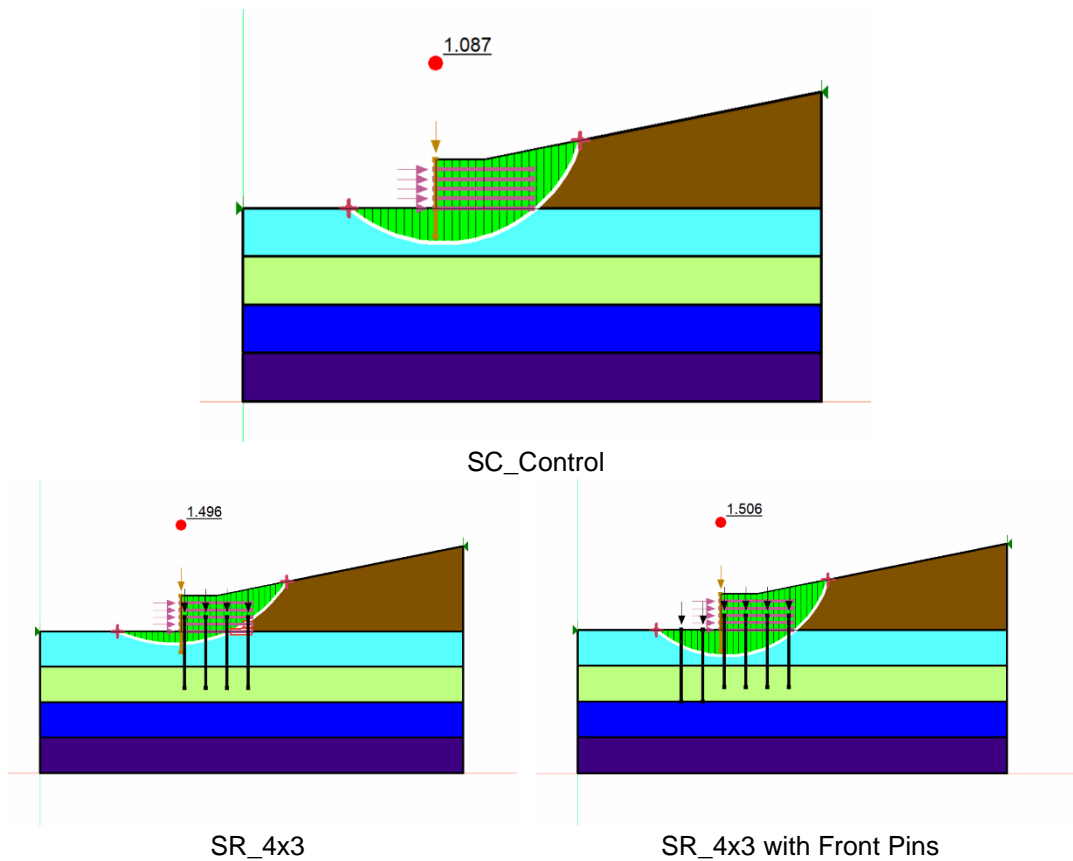
Section	Analysis Method				
	Ordinary	Bishop	Janbu	Morgenstern-Price	Spencer
SC_Control	0.920	1.031	0.888	1.087	1.095
SR_4x3	1.214	1.349	1.113	1.496	1.497
SR_4x3 with Front Pins	1.274	1.432	1.162	1.506	1.647
SR_4x2	1.367	1.501	1.201	1.585	1.711
SR_4x2 with Front Pins	1.502	1.668	1.288	1.750	2.014
SR_6x3	1.295	1.431	1.162	1.506	1.647
SR_6x3 with Front Pins	1.402	1.575	1.243	1.654	1.928

The outputs from the SLOPE/W analysis are presented in Figure 5-20. The figures show the outputs from the Morgenstern-Price method of analysis. Some key points to be noted from the analysis results are listed below:

- AASHTO (2014) recommends a minimum of 1.3 global factor of safety for MSE walls in normal conditions, while a minimum of 1.5 global factor of safety is recommended for MSE walls with weak foundation soils, or walls on slopes. The results from the stability analysis showed that all the RPP reinforcement configurations increased the factor of safety to 1.5 or more (Morgenstern-Price method). This satisfies the criteria set by AASHTO (2014).



- The inclusion of the two front rows of RPPs increased the factor of safety by a satisfactory degree in SR\_4x2 and SR\_6x3. The increase was about 10% (based on Morgenstern-Price method). The front two rows of RPPs are more beneficial in the case of deeper slip surfaces. Since the two rows are deeper than the RPPs inside the MSE wall, they will restrict the deeper slip surfaces if they are not restricted by the inside RPPs.
- An interesting trend shown is that the spacing of RPPs played a better role in resisting the failure plane. SR\_4x2 provided better resistance than the other two reinforced sections. SR\_4x2 performed better than SR\_6x3 even though by a small factor.



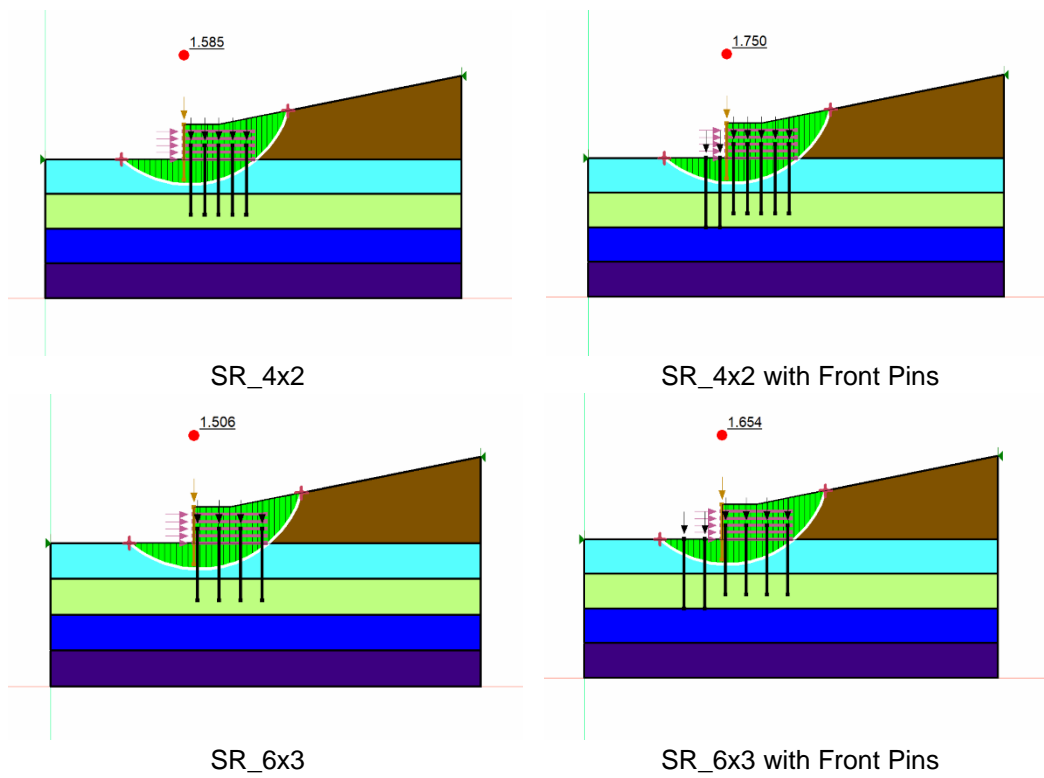


Figure 5-20 SLOPE/W Outputs of the Global Factor of Safety

The RPPs restrict the failure planes and push them below show that the critical failure planes pass through stronger foundation soil. This eventually increases the global factor of safety. A few analyses were performed for a wall height of 10 ft. The factor of safety for the section without RPP was 0.857. Reinforcing the section with 4x4 inches RPP at 2 ft. c/c spacing increased the factor of safety to 1.219. Furthermore, the factor of safety increased to 1.392 with 6x6 inches RPP at 2 ft. c/c spacing.

## Chapter 6

### DEVELOPMENT OF DESIGN METHODOLOGY

#### 6.1 Background

The objective of this study was to develop an innovative approach for increasing the lateral resistance of MSE wall base. Four field test sections were constructed where the base of three sections was reinforced with RPPs. One section was left unreinforced as a control section. Vertical inclinometers, horizontal inclinometers, and earth pressure plates were installed in each section to monitor the lateral base displacement, base settlement, and lateral pressure at the wall base, respectively. Regular performance monitoring results showed that the RPP reinforced sections performed better than the control section as both the lateral displacement and base settlement of the reinforced sections reduced significantly. Furthermore, the lateral pressure acting on the wall base were very less in the RPP reinforced section compared to that of the control section. Numerical study was conducted using finite element modeling to evaluate the variation of lateral displacement of wall base with changing RPP and soil parameters. Limit equilibrium analysis was also undertaken to estimate the factor of safety against global failure. The field results along with the numerical study outputs confirmed that the RPPs are working effectively to improve the lateral resistance of MSE wall base.

The next phase of the study was to develop a design methodology to incorporate RPPs in the design specifications of MSE walls. This would help DOTs and developers to follow a guideline on designing MSE walls reinforced with RPPs at the base. The numerical study performed in the previous chapter were used for developing the design charts. The comprehensive data from the modeling were analyzed statistically to generate Multiple

Linear Regression (MLR) prediction models. The generated prediction models were then used to develop design charts. The tasks performed for this are discussed in this chapter.

## 6.2 Statistical Analysis

Construction of field test sections or laboratory experimental analysis are not always feasible due to budget and time constraints. Even though FE modeling can produce reliable results for a wide array of scenarios, it can be time and labor consuming (Ahmed et al., 2020). On the other hand, statistical modeling can extensively reduce the time and effort needed to achieve similar results as from the numerical modeling. Previous studies have adopted different statistical analysis approaches to assess the performance of MSE walls (Kibria et al., 2014; Lin et al., 2016; Bathrust and Yu, 2018; Allen et al., 2019). Yu and Bathrust (2017) have shown how a comprehensive data set obtained from a calibrated numerical model could be used to evaluate the behavior of MSE walls.

Therefore, the objective of the following sections is to develop simple statistical models using the data obtained from the parametric studies described in the previous chapter. Multiple linear regression (MLR) models were developed from the data, which were then validated against the required MLR assumptions. Statistical models to predict lateral base displacement and lateral pressure reduction of RPP reinforced sections were developed. Commercially available software RStudio ver 1.4.1103 was used for performing the statistical analyses (RStudio, 2021). The flow of the analysis is presented in Figure 6-1.

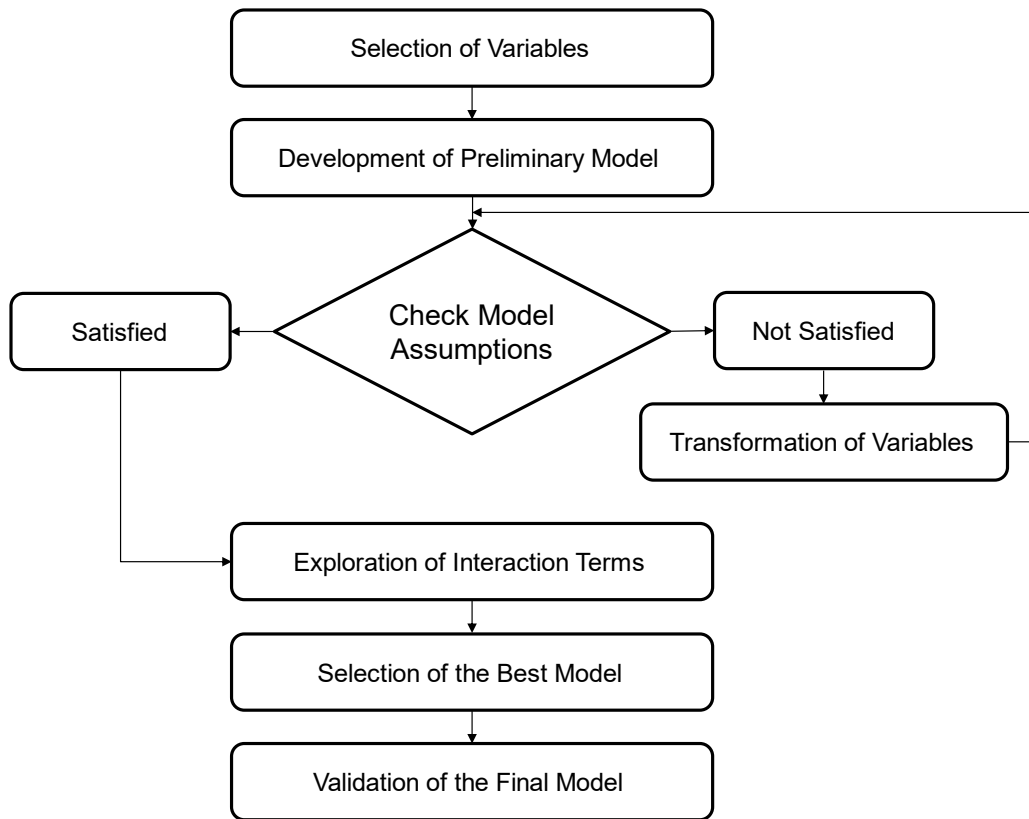


Figure 6-1 Statistical Analysis Flow for the Model Development

### 6.3 Statistical Analysis of Lateral Displacement

#### 6.3.1 Selection of Parameters

The predictors for the model were selected in such a way that they were not highly correlated to each other. If the predictors have a high degree of collinearity among each other, the developed model might not be very reliable. This could lead to smaller coefficient of regression, higher variance, and difficulty in explaining the effect of unit change of predictor on the response (Stevens, 1996). The lateral base displacement was modeled to be the response, while the foundation soil strength, RPP size, spacing, extension, and wall height were the predictors. The foundation soil strength included

cohesion and friction angle. Since all the independent predictors affect the response to some extent, it was decided to include all the parameters in the preliminary statistical model. The parameters were denoted as follows:

LD = Lateral displacement of MSE wall base (inches)

C = Cohesion of foundation soil (psf)

F = Friction angle of foundation soil (degrees)

S = RPP size (ft.)

Sp = RPP center-to-center spacing (ft.)

E = RPP extension above the foundation soil into the reinforced soil (ft.)

H = MSE wall height (ft.)

### 6.3.2 *Correlation Analysis*

Correlation analysis was performed between the response variable and each of the predictor variables to evaluate the relationship between them. It was also performed among to predictor variables to assess any multicollinearity, if present. There should be no multicollinearity among the predictor variables (Kutner et al., 2005). The existence of multicollinearity means that two or more predictors can explain the same variation of the response. If a strong correlation exists among the predictor variables, it will pose setbacks to the MLR model. The Pearson Correlation Coefficients between the predictors are shown in Table 6-1. The highest correlation was found to be between the foundation soil cohesion and friction angle, i.e., -0.5109. However, Kutner et al. (2005) states that any correlation less than 0.7 can be regarded as weak. Thus, no significant collinearity was observed among the predictor variables.

Table 6-1 Correlation Between the Predictor Variables

<b>Variables</b>	<b>Cohesion</b>	<b>Friction Angle</b>	<b>RPP Size</b>	<b>RPP Spacing</b>	<b>RPP Extension</b>	<b>Wall Height</b>
<b>Cohesion</b>	1	-0.5109	0	0	0.14	0.04
<b>Friction Angle</b>	-0.5109	1	0	0	-0.25	-0.02
<b>RPP Size</b>	0	0	1	0	0	0
<b>RPP Spacing</b>	0	0	0	1	0	0
<b>RPP Extension</b>	0.14	-0.25	0	0	1	0.0422
<b>Wall Height</b>	0.04	-0.02	0	0	0.0422	1

The linear strength between the response and the predictor variables were also measured using the correlation coefficient. Based on the statistical analysis (Table 6-2), foundation soil cohesion, friction angle, RPP size, and extension have negative correlation with the lateral displacement. This means that an increase in any of the above-mentioned factors will reduce the lateral displacement. Likewise, RPP spacing, and wall height have positive correlation coefficients, such that an increase of these factors will increase the lateral displacement as well. The relations were in agreement with the numerical modeling results from PLAXIS. Wall height was found to have the highest correlation (0.8437) with lateral displacement suggesting that the height of the wall could explain most of the variability in lateral displacement prediction. Similarly, the foundation soil friction angle also showed strong correlation (-0.6231). This suggests that when the shear strength of the foundation soil increases, the lateral displacement decreases proportionally. Among the RPP parameters, spacing and extension showed similar correlation with lateral displacement. The RPP size showed slightly less correlation with the lateral displacement.

Table 6-2 Correlation Between the Lateral Displacement and Predictor Variables

<b>Cohesion</b>	<b>Friction Angle</b>	<b>RPP Size</b>	<b>RPP Spacing</b>	<b>RPP Extension</b>	<b>Wall Height</b>
-0.3146	-0.6231	-0.2443	0.2992	-0.3081	0.8437

### 6.3.3 Development of Preliminary Model

After it was confirmed that no multicollinearity existed between the predictor variables, a preliminary MLR model was formulated as follows:

$$LD = \beta_0 + \beta_1C + \beta_2F + \beta_3S + \beta_4Sp + \beta_5E + \beta_6H + \varepsilon_i$$

Where,  $\beta_0$ ,  $\beta_1$ ,  $\beta_2$ ,  $\beta_3$ ,  $\beta_4$ ,  $\beta_5$ , and  $\beta_6$  are correlation coefficients which are determined through regression analysis by minimizing the sum of squared errors for the model data.  $\varepsilon_i$  is the random error. The physical meaning of the correlation coefficients is that they explain the variation in mean response per unit change of a predictor variable when all other predictor variables are kept constant. Multiple linear regression was performed on the model data. The parameter estimates and summary of the analysis of variance (ANOVA) are presented in Table 6-3 and Table 6-4, respectively. The sign conventions of the correlation coefficients are as expected and follow the results obtained from field performance and numerical study data. Apart from RPP spacing and wall height, all other parameters had negative coefficients, i.e., an increase in those coefficients reduced the lateral displacement. The ANOVA summary showed that the adjusted  $R^2$  was satisfactory and is acceptable. The p-value of the residuals was also very less. The preliminary fitted MLR equation can thus be presented as follows:

$$LD = 0.910206 - 0.013287C - 0.035878F - 2.298704S + 0.284293Sp - 0.268685E + 0.294097H$$



Table 6-3 Parameter Estimates of the Preliminary Model

	<b>Coefficient</b>	<b>Std. Error</b>	<b>t value</b>	<b>Pr(&gt; t )</b>	<b>VIF</b>
(Intercept)	0.910206	0.315362	2.886	0.00453	-
C	-0.013287	0.001350	-9.842	< 2e-16	1.57
F	-0.035878	0.007751	-4.629	8.44e-06	1.66
S	-2.298704	0.299277	-7.681	2.71e-12	1
Sp	0.284293	0.030545	9.307	2.86e-16	1
E	-0.268685	0.031272	-8.592	1.71e-14	1.08
H	0.294097	0.012137	24.231	< 2e-16	1

Table 6-4 ANOVA Summary of the Preliminary Model

<b>Residual Standard Error</b>	<b>R<sup>2</sup></b>	<b>Adjusted R<sup>2</sup></b>	<b>F-statistic</b>	<b>p-value</b>
0.2993	0.8698	0.864	152.5	< 2.2e-16

The next step is to check if the MLR model assumptions are verified. The model should satisfy the constant error variance, normality of residuals, outliers, and multicollinearity among the predictor variables checks (Stevens, 1996; Kutner et al., 2005, Faysal, 2017). Graphical plots and different statistical tests will be used to verify the following model assumptions:

- There should be a linear relationship between the response and predictor variables.
- The residuals should have constant variance.
- The residuals should be normally distributed.
- The residuals should not be auto correlated.

#### 6.3.4 Verification of Preliminary Model

##### Constant Error Variance

Plots showing residuals vs. predictor variables and residuals vs. fitted values help to determine constant error variance or homoscedasticity. The residuals should be randomly scattered without any trend when plotted against predictor variables. Similarly, there should be no specific trend of residuals when plotted against fitted values. This ensures that the constant error variance of an MLR model has been fulfilled. The presence of funnel shape or any curvilinear trend indicates presence of non-constant variance. The regression in such a case might not be valid. This condition can be mitigated by transformation of variables. Figure 6-2 shows the residuals vs. fitted values plot for the preliminary MLR model.

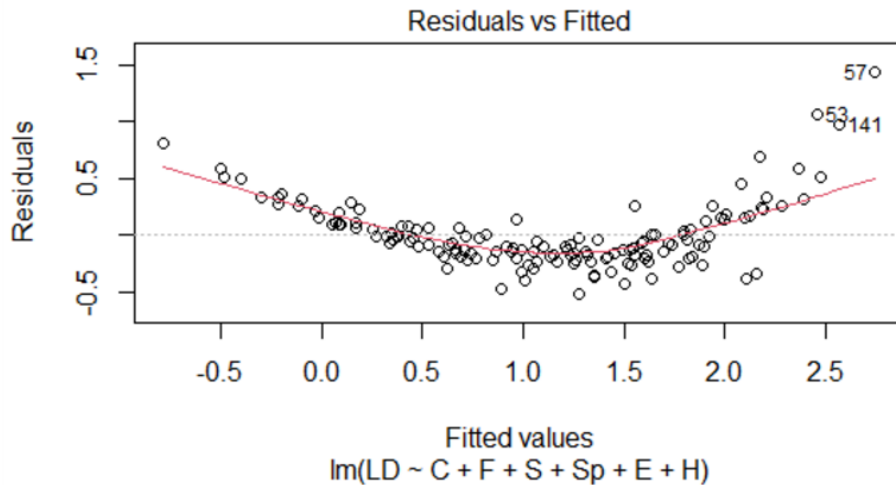


Figure 6-2 Residuals vs. Fitted Values Plot for the Preliminary Model

A clear curvilinear trend (marked by red) can be seen in the plot. This indicates absence of constant error variance and thus, points towards a need for transformation of the response variable. Further analysis was done by conducting the studentized Breusch-

Pagan test in RStudio. The p-value from the test was 0.006233, which is smaller than  $\alpha = 0.01$ . So, the null hypothesis was rejected indicating that the residuals are not homoscedastic at  $\alpha = 0.01$ .

### Normality

The error or the residuals of an MLR should be normally distributed. The normality of the residuals can be determined from a normal probability plot. A moderately linear plot signifies that the residuals are normally distributed. Figure 6-3 shows the normal probability plot for the preliminary MLR model.

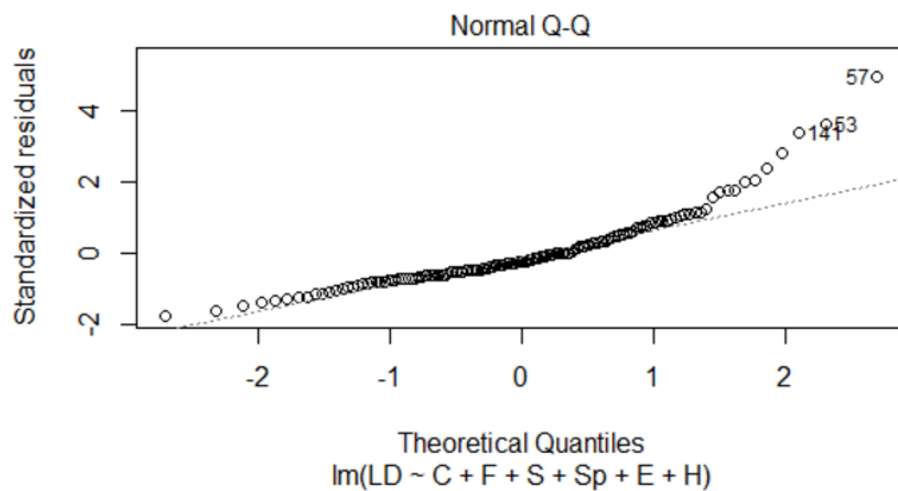


Figure 6-3 Normal Probability Plot for the Preliminary Model

A long tail at the right side and a short tail at the left side can be seen from the plot. This indicates that the distribution of the residuals might not be normal. To further verify the normality assumption, Shapiro-Wilk normality test was carried out in RStudio. The test estimated a p-value of  $1.342\text{e-}09$  which is smaller than  $\alpha = 0.01$ . So, the null hypothesis was rejected indicating that residuals were not normally distributed at  $\alpha = 0.01$ .

### Outlier Test

Outliers are some extreme observations in a data set. They can mislead the regression by pulling the fitted line disproportionately towards the extreme observation (Kutner et al., 2005). The outliers, if any, were checked using several standard tests in RStudio. Bonferroni outlier test was used to detect outliers. DFFITS, DFBETAS, and Cook's Distance were used to determine the influence of the outliers in the preliminary model. DFFITS (Difference in fits) estimates the influence of an observation in the predicted value. It is suggested that an absolute DFFITS value greater than 1 (for small to medium data set) for an observation is to be flagged for further check. An absolute DFBETAS value greater than 1 (for medium to large data sets) also suggests flagging the corresponding observation. Similarly, the observation with Cook's Distance ( $D_i$ )  $>$   $F(p, n-p)$  should also be flagged. The F-statistic to compare the Cook's Distance for this set was 2.0096 for  $\alpha = 0.05$ . It is also suggested that  $D_i$  greater than 0.5 should be investigated, as it may be influential (Faysal, 2017).

Based on the Bonferroni outlier test, one of the observations resulted in a p-value of 0.0294, which is greater than  $\alpha = 0.01$ , thus the corresponding observation was identified as an outlier. The observation was flagged as per DFFITS, DFBETAS, and Cook's Distance tests as well.

### Multicollinearity

An important assumption of an MLR model is that the predictors should not be highly correlated among each other. Variation Inflation Factor (VIF), which quantifies how much the variation is inflated, can be used to detect multicollinearity in a model. If  $VIF > 1$ , multicollinearity occurs among the predictors. However, only predictors with a  $VIF > 5$  maybe problematic. A  $VIF > 10$  suggests high multicollinearity and indicates a poor

estimate of the response. Thus, the VIF is preferable to be less than 5. Based on the VIF in Table 6-3, all the VIFs are within the suggested range. Thus, no serious multicollinearity exists among the predictor variables.

### 6.3.5 Transformation of Variables

Since the preliminary model did not satisfy the constant error variance and normality assumptions, transformation of the response variable was performed. Box-Cox plot method was used in RStudio to determine the optimum transformation variable for the response. Figure 6-4 shows that the optimum value for the transformation, i.e., the power of the variable, was 0.384. The transformed model took the form as follows:

$$LD' = \beta_0 + \beta_1C + \beta_2F + \beta_3S + \beta_4Sp + \beta_5E + \beta_6H + \epsilon_i$$

Where,  $LD' = LD^{0.384}$

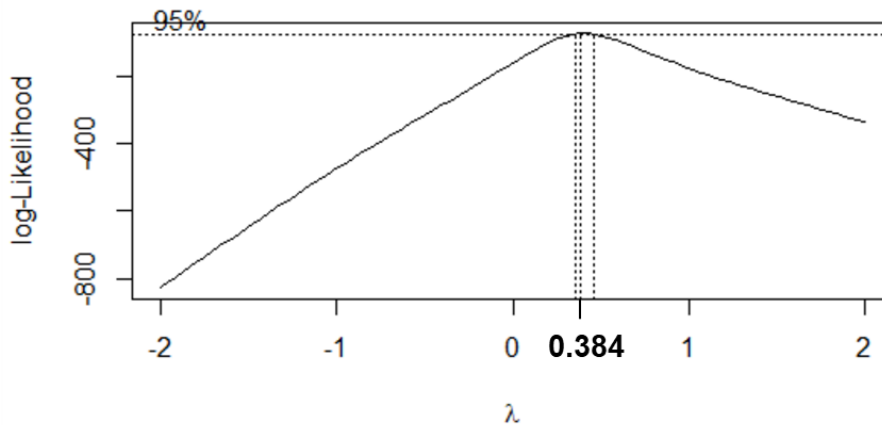


Figure 6-4 Box-Cox Plot for Transformation of Response Variable ( $\lambda = 0.384$ )

Multiple linear regression was performed with the transformed model. The parameter estimates and summary of the analysis of variance (ANOVA) for the final model are presented in Table 6-5 and Table 6-6, respectively. The sign conventions of the

correlation coefficients are as expected and follow the results obtained from field performance and numerical study data. Apart from RPP spacing and wall height, all other parameters had negative coefficients, i.e., an increase in those coefficients reduced the lateral displacement. The ANOVA summary showed that the adjusted R<sup>2</sup> was satisfactory and is acceptable. The p-value of the residuals was also very less. The final fitted MLR equation can thus be presented as follows:

$$LD^{0.384} = 0.870035 - 0.005755C - 0.014714F - 0.887577S + 0.107705Sp - 0.083719E + 0.118413H$$

Table 6-5 Parameter Estimates of the Final Model

	<b>Coefficient</b>	<b>Std. Error</b>	<b>t value</b>	<b>Pr(&gt; t )</b>	<b>VIF</b>
(Intercept)	0.870035	0.052536	16.561	< 2e-16	-
C	-0.005755	0.000229	-25.134	< 2e-16	1.58
F	-0.014714	0.001303	-11.289	< 2e-16	1.65
S	-0.887577	0.050197	-17.682	< 2e-16	1
Sp	0.107705	0.005131	20.991	< 2e-16	1
E	-0.083719	0.005312	-15.761	< 2e-16	1.07
H	0.118413	0.002048	57.812	< 2e-16	1

Table 6-6 ANOVA Summary of the Final Model

<b>Residual Standard Error</b>	<b>R<sup>2</sup></b>	<b>Adjusted R<sup>2</sup></b>	<b>F-statistic</b>	<b>p-value</b>
0.04939	0.972	0.971	770.8	< 2.2e-16

The next step is to check if the MLR model assumptions are verified.

### 6.3.6 Verification of Final Model

#### Constant Error Variance

Figure 6-5 shows the residuals vs. fitted values plot for the final MLR model.

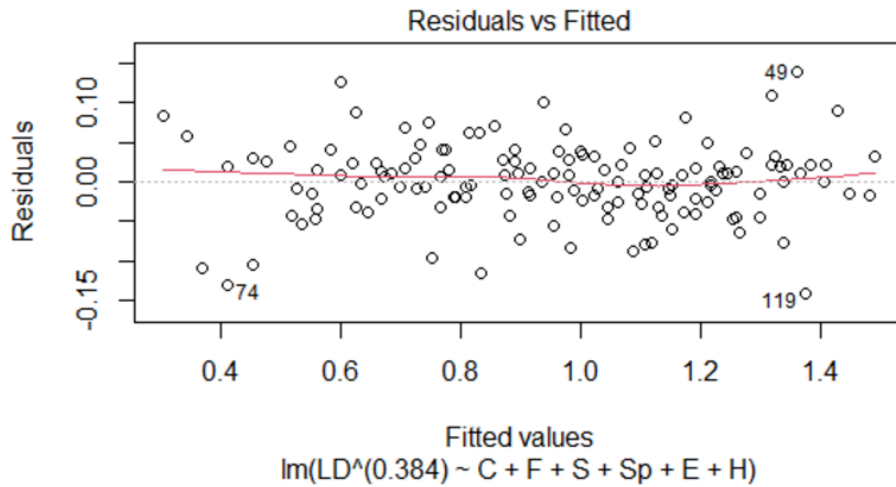


Figure 6-5 Residuals vs. Fitted Values Plot for the Final Model

No curvilinear trend or funnel shape was detected from the plot. The residuals seem to be randomly scattered. Further analysis was done by conducting the studentized Breusch-Pagan test in RStudio. The p-value from the test was 0.25, which is greater than  $\alpha = 0.01$ . So, the null hypothesis was failed to be rejected indicating that the residuals are homoscedastic at  $\alpha = 0.01$ . The constant error variance assumption was fulfilled for the final model.

#### Normality

Figure 6-6 shows the normal probability plot for the final MLR model.

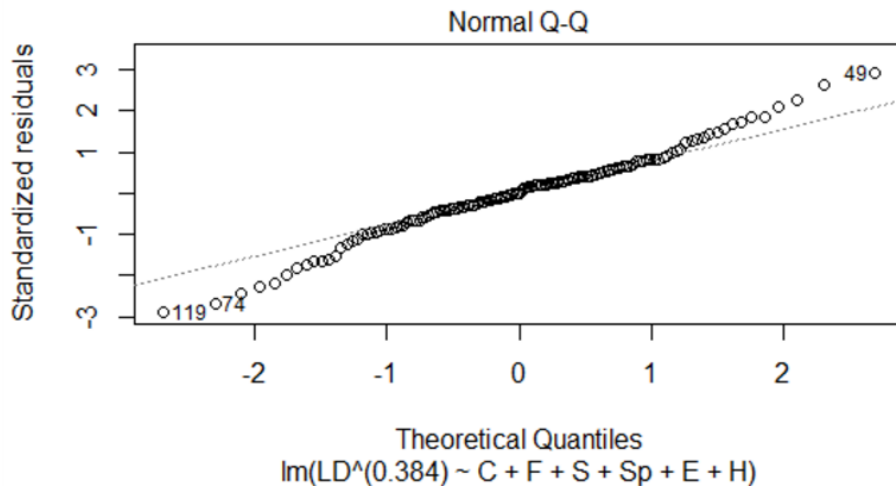


Figure 6-6 Normal Probability Plot for the Final Model

Short tails on both sides can be seen from the plot. To further verify the normality assumption, Shapiro-Wilk normality test was carried out in RStudio. The test estimated a p-value of 0.099, which is greater than  $\alpha = 0.01$ . So, the null hypothesis was failed to be rejected indicating that the residuals are normally distributed at  $\alpha = 0.01$ .

#### Outlier Test

The outliers, if any, were checked using several standard tests in RStudio. Bonferroni outlier test was used to detect outliers. DFFITS, DFBETAS, and Cook's Distance were used to determine the influence of the outliers in the final model. The F-statistic to compare the Cook's Distance for this set was 2.0096 for  $\alpha = 0.05$ . It is also suggested that  $D_i$  greater than 0.5 should be investigated, as it may be influential (Faysal, 2017).

Based on the Bonferroni outlier test, none of the observations were flagged as potential outliers. All the observations satisfied the assumptions as per DFFITS, DFBETAS, and Cook's Distance tests as well.



### Multicollinearity

Based on the VIF in Table 6-5, all the VIFs are within the suggested range. Thus, no serious multicollinearity exists among the predictor variables.

### 6.3.7 Selection of Final Model

Best subset method, stepwise regression, and backward elimination were performed in RStudio to finalize the best prediction model.

### Best Subset Selection

The best subset selection method uses certain parameters to determine the best model. It performs the analyses for different combinations of predictor variables. The parameters under consideration are  $R^2$ , adj.  $R^2$ , Mallow's  $C_p$ , and Bayesian Information Criteria (BIC). The method selects the best model with the highest  $R^2$  and adj.  $R^2$ , and the lowest Mallow's  $C_p$  and BIC. Based on this method, the combination with all the six predictor variables was selected as the best model. Table 6-7 summarizes the parameter values for the criteria under consideration.

Table 6-7 Summary of Best Subset Selection Method

Predictor Variables						$R^2$	Adj. $R^2$	$C_p$	BIC
C	F	S	Sp	E	H				
-	-	-	-	-	✓	0.641	0.638	1573	-133
✓	-	-	-	-	✓	0.760	0.756	1010	-185
✓	-	-	✓	-	✓	0.844	0.841	608	-241
✓	-	✓	✓	-	✓	0.906	0.903	316	-307
✓	-	✓	✓	✓	✓	0.945	0.943	132	-377
✓	✓	✓	✓	✓	✓	<b>0.972</b>	<b>0.971</b>	<b>7</b>	<b>-466</b>

### Backward Elimination

The backward elimination method starts with all the predictor variables in the model. Then, it incrementally removes statistically insignificant variables. The analysis is completed when there is no insignificant variable remaining in the model. Based on this method, all the predictor variables were significant at  $\alpha = 0.01$  significance level and no variables were removed.

### Stepwise Regression

Stepwise regression method utilizes both the backward selection and forward selection algorithms. The model starts with the most significant predictor variable. The regression is carried out and the parameters under consideration are calculated. Then, other variables are incrementally added as per their significance. The procedure is repeated until the model with the best criteria parameters is obtained. The F-statistic test is used to conduct the statistical significance tests (Kutner et al., 2005). Based on this method, the inclusion of all the six predictor variables formed the best model.

#### *6.3.8 Validation of the Final Prediction Model*

The final prediction model was validated using a different set of data. Numerical analysis was again conducted on the calibrated numerical model with randomly selected variables. Both the foundation soil and RPP parameters were varied to get a set of independent responses. The same parameters were used in the final prediction model to estimate lateral displacement. Figure 6-7 visualizes the comparison of lateral displacement values from the prediction model and the numerical model. Three lateral displacements from the field test sections (SR\_4x3, SR\_4x2, SR\_6x3) were also plotted to compare with the predicted estimates. The developed model could explain 98.57% of the variation in lateral displacement at different combinations. The bias values were

calculated by taking a ratio of numerical model values to predicted values. The mean of the bias values was 1.35. This suggests that the statistical model slightly underpredicts the lateral displacement values. This demonstrates a good agreement between the numerical and statistical methods.

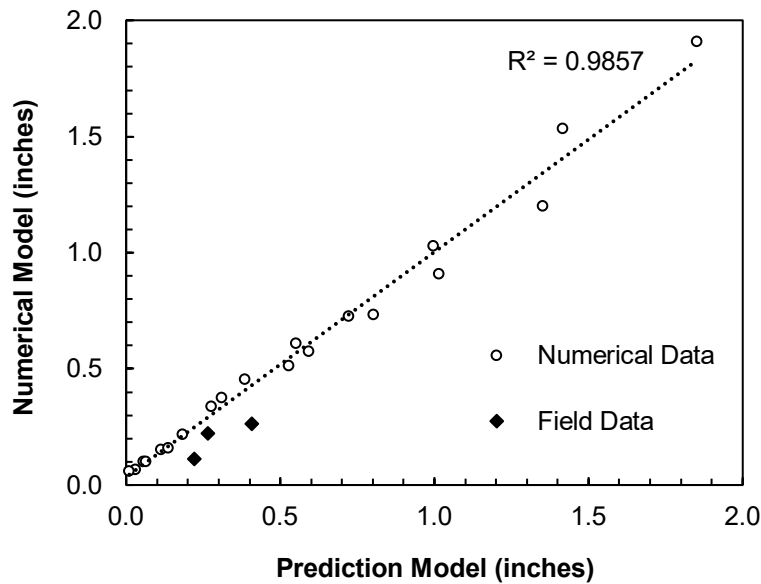


Figure 6-7 Validation of Final Prediction Model

#### 6.4 Statistical Analysis of Lateral Pressure Reduction

##### 6.4.1 Selection of Parameters

Lateral pressure/stress acting on the wall face at the base level was calculated for the control and RPP reinforced sections from the numerical study. Then, the difference of the stresses in the control and reinforced section was calculated. Finally, the reduction factor was estimated by dividing the stress difference by the stress in the control section, such as:

$$SR = (P_C - P_R) / P_C$$

where,

$SR$  = Lateral stress/pressure reduction factor

$P_C$  = Lateral pressure acting on the wall face at the base level of the control section

$P_R$  = Lateral pressure acting on the wall face at the base level of the RPP reinforced section.

The predictors for the statistical model were selected in such a way that they were not highly correlated to each other. The lateral pressure reduction factor was modeled to be the response, while the foundation soil strength, RPP size, spacing, and wall height were the predictors. The foundation soil strength included cohesion and friction angle. Since all the independent predictors affect the response to some extent, it was decided to include all the parameters in the preliminary statistical model. Based on the satisfactory performance of the field test sections, and results obtained from the lateral displacement numerical study, only 2 ft. RPP extension above the foundation soil was used for this part of the study. Thus, all the stress reductions are at 2 ft. extension of RPP above the foundation soil. The parameters were denoted as follows:

$SR$  = Lateral pressure/stress reduction factor at the base of MSE wall

$C$  = Cohesion of foundation soil (psf)

$F$  = Friction angle of foundation soil (degrees)

$S$  = RPP size (ft.)

$Sp$  = RPP center-to-center spacing (ft.)

$H$  = MSE wall height (ft.)

#### 6.4.2 Correlation Analysis

Correlation analysis was performed between the response variable and each of the predictor variables to evaluate the relationship between them. It was also performed

among to predictor variables to assess any multicollinearity, if present. The Pearson Correlation Coefficients between the predictors are shown in Table 6-8. The highest correlation was found to be between the foundation soil cohesion and friction angle, i.e., -0.51. However, Kutner et al. (2005) states that any correlation less than 0.7 can be regarded as weak. Thus, no significant collinearity was observed among the predictor variables.

Table 6-8 Correlation Between the Predictor Variables

<b>Variables</b>	<b>Cohesion</b>	<b>Friction Angle</b>	<b>RPP Size</b>	<b>RPP Spacing</b>	<b>Wall Height</b>
<b>Cohesion</b>	1	-0.51	0	0	0
<b>Friction Angle</b>	-0.51	1	0	0	0
<b>RPP Size</b>	0	0	1	0	0
<b>RPP Spacing</b>	0	0	0	1	0
<b>Wall Height</b>	0	0	0	0	1

The linear strength between the response and the predictor variables were also measured using the correlation coefficient. Based on the statistical analysis (Table 6-9), foundation soil cohesion, friction angle, and RPP size have positive correlation with the lateral pressure reduction. This means that an increase in any of the above-mentioned factors will increase the lateral pressure reduction factor as well. Likewise, RPP spacing, and wall height have negative correlation coefficients, such that an increase of these factors will decrease the lateral pressure reduction factor. The relations were in agreement with the numerical modeling results from PLAXIS. Wall height was found to have the highest correlation (-0.67) with stress reduction suggesting that the height of the wall could explain most of the variability in the prediction of stress reduction. Among the RPP parameters, spacing showed a slightly higher correlation than the size.

Table 6-9 Correlation Between the Lateral Pressure Reduction and Predictor Variables

<b>Cohesion</b>	<b>Friction Angle</b>	<b>RPP Size</b>	<b>RPP Spacing</b>	<b>Wall Height</b>
0.32	0.03	0.29	-0.40	-0.67

#### 6.4.3 Development of Preliminary Model

After it was confirmed that no multicollinearity existed between the predictor variables, a preliminary MLR model was formulated as follows:

$$SR = \beta_0 + \beta_1C + \beta_2F + \beta_3S + \beta_4Sp + \beta_5H + \varepsilon_i$$

Where,  $\beta_0$ ,  $\beta_1$ ,  $\beta_2$ ,  $\beta_3$ ,  $\beta_4$ , and  $\beta_5$  are correlation coefficients which are determined through regression analysis by minimizing the sum of squared errors for the model data.  $\varepsilon_i$  is the random error. The physical meaning of the correlation coefficients is that they explain the variation in mean response per unit change of a predictor variable when all other predictor variables are kept constant. Multiple linear regression was performed on the model data. The parameter estimates and summary of the analysis of variance (ANOVA) are presented in Table 6-10 and Table 6-11, respectively. The sign conventions of the correlation coefficients are as expected and follow the results obtained from field performance and numerical study data. Apart from RPP spacing and wall height, all other parameters had positive coefficients, i.e., an increase in those coefficients increased the lateral pressure/stress reduction factor. The ANOVA summary showed that the adjusted  $R^2$  was 0.8119 and could explain about 81.2% of the variability in the predicted values. The p-value of the residuals was also very less. The preliminary fitted MLR equation can thus be presented as follows:

$$SR = 0.616129 + 0.002105C + 0.006792F + 0.484851S - 0.068335Sp - 0.045328H$$

Table 6-10 Parameter Estimates of the Preliminary Model

	<b>Coefficient</b>	<b>Std. Error</b>	<b>t value</b>	<b>Pr(&gt; t )</b>	<b>VIF</b>
(Intercept)	0.616129	0.072528	8.495	6.16e-13	-
C	0.002105	0.000274	7.687	2.55e-11	1.36
F	0.006792	0.001986	3.421	9.66e-04	1.36
S	0.484851	0.076566	6.332	1.14e-08	1
Sp	-0.068335	0.007814	-8.745	1.94e-13	1
H	-0.045328	0.003105	-14.597	< 2e-16	1

Table 6-11 ANOVA Summary of the Preliminary Model

<b>Residual Standard Error</b>	<b>R<sup>2</sup></b>	<b>Adjusted R<sup>2</sup></b>	<b>F-statistic</b>	<b>p-value</b>
0.06053	0.8225	0.8119	77.82	< 2.2e-16

The next step is to check if the MLR model assumptions are verified. The model should satisfy the constant error variance, normality of residuals, outliers, and multicollinearity among the predictor variables checks (Stevens, 1996; Kutner et al., 2005, Faysal, 2017). Similar statistical tests as conducted for the previous statistical model predicting lateral displacement was undertaken for this part as well.

#### 6.4.4 Verification of Preliminary Model

##### Constant Error Variance

Plots showing residuals vs. predictor variables and residuals vs. fitted values help to determine constant error variance or homoscedasticity. The residuals should be randomly scattered without any trend when plotted against predictor variables. Similarly, there should be no specific trend of residuals when plotted against fitted values. Figure 6-8 shows the residuals vs. fitted values plot for the preliminary MLR model.

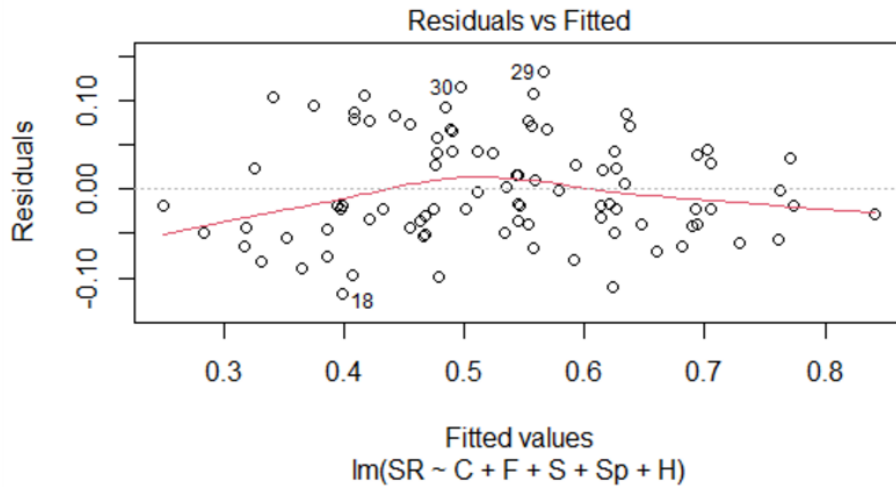


Figure 6-8 Residuals vs. Fitted Values Plot for the Preliminary Model

A slightly curvilinear trend (marked by red) can be seen in the plot. This might indicate absence of constant error variance. Further analysis was done by conducting the studentized Breusch-Pagan test in RStudio. The p-value from the test was 0.003775, which is smaller than  $\alpha = 0.01$ . So, the null hypothesis was rejected indicating that the residuals are not homoscedastic at  $\alpha = 0.01$ .

#### Normality

The error or the residuals of an MLR should be normally distributed. The normality of the residuals can be determined from a normal probability plot. A moderately linear plot signifies that the residuals are normally distributed. Figure 6-9 shows the normal probability plot for the preliminary MLR model.



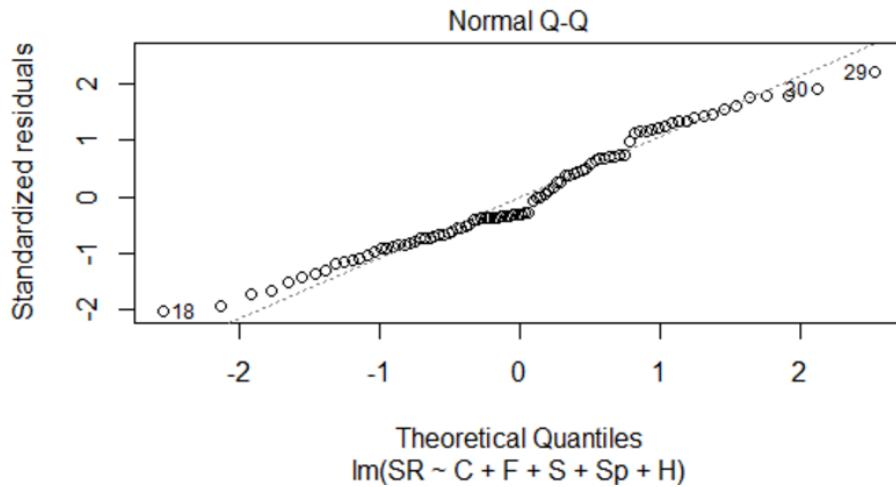


Figure 6-9 Normal Probability Plot for the Preliminary Model

Short tails on both right and left sides can be seen from the plot. To further verify the normality assumption, Shapiro-Wilk normality test was carried out in RStudio. The test estimated a p-value of 0.0365 which is greater than  $\alpha = 0.01$ . So, the null hypothesis was failed to be rejected indicating that the residuals were normally distributed at  $\alpha = 0.01$ .

#### Outlier Test

The outliers, if any, were checked using several standard tests in RStudio. Bonferroni outlier test was used to detect outliers. DFFITS, DFBETAS, and Cook's Distance were used to determine the influence of the outliers in the preliminary model. The F-statistic to compare the Cook's Distance for this set was 2.2225 for  $\alpha = 0.05$ . It is also suggested that  $D_i$  greater than 0.5 should be investigated, as it may be influential (Faysal, 2017).

Based on the Bonferroni outlier test, none of the observations were flagged as potential outliers. All the observations satisfied the assumptions as per DFFITS, DFBETAS, and Cook's Distance tests as well.

### Multicollinearity

An important assumption of an MLR model is that the predictors should not be highly correlated among each other. Variation Inflation Factor (VIF), which quantifies how much the variation is inflated, can be used to detect multicollinearity in a model. If  $VIF > 1$ , multicollinearity occurs among the predictors. However, only predictors with a  $VIF > 5$  maybe problematic. A  $VIF > 10$  suggests high multicollinearity and indicates a poor estimate of the response. Thus, the VIF is preferable to be less than 5. Based on the VIF in Table 6-10, all the VIFs are within the suggested range. Thus, no serious multicollinearity exists among the predictor variables.

#### 6.4.5 Transformation of Variables

Since the preliminary model did not satisfy the constant error variance assumption, transformation of the variable was tried. Box-Cox plot method was used in RStudio to determine the optimum transformation variable for the response. However, a clear peak of the  $\lambda$  value was not found from the method. Another approach to transform the variables is to add a quadratic term in the equation. Residuals vs. predictor plots were drawn to assess which predictor did not show a random scatter with the residuals. It was found that the wall height reflected a curvilinear relationship with the residuals (Figure 6-10). Other predictor variables showed fairly random scatter around the horizontal axis. Thus, it was decided that a square/quadratic term of the wall height should also be added to the preliminary model. The transformed model took the form as follows:

$$SR = \beta_0 + \beta_1C + \beta_2F + \beta_3S + \beta_4Sp + \beta_5H + \beta_6H^2 + \varepsilon_i$$

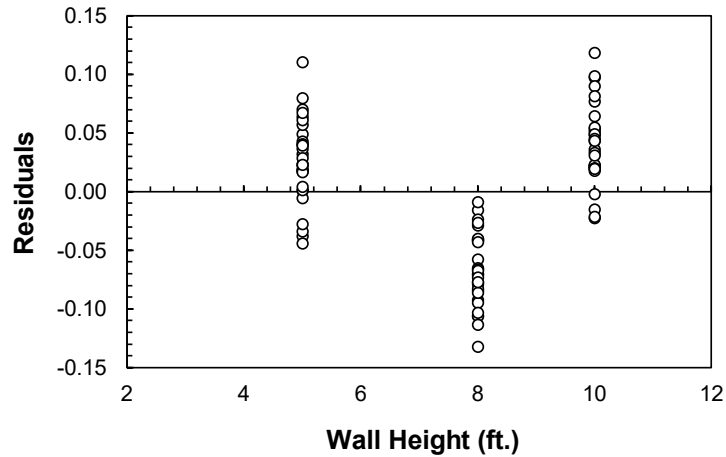


Figure 6-10 Residuals vs. Wall Height Plot for the Preliminary Model

Multiple linear regression was performed with the transformed model. The parameter estimates and summary of the analysis of variance (ANOVA) for the final model are presented in Table 6-12 and Table 6-13, respectively. The sign conventions of the correlation coefficients are as expected and follow the results obtained from field performance and numerical study data. Apart from RPP spacing and square of wall height, all other parameters had positive coefficients, i.e., an increase in those coefficients increased the lateral pressure/stress reduction factor as well. The ANOVA summary showed that the adjusted  $R^2$  was 0.938 and could explain about 93.8% of the variability in the predicted values. The p-value of the residuals was also very less. The final fitted MLR equation can thus be presented as follows:

$$SR = -0.251707 + 0.002105C + 0.006792F + 0.484851S - 0.068335Sp + 0.208278H - 0.017087H^2$$

Table 6-12 Parameter Estimates of the Final Model

	<b>Coefficient</b>	<b>Std. Error</b>	<b>t value</b>	<b>Pr(&gt; t )</b>	<b>VIF</b>
(Intercept)	-0.251707	0.078255	-3.216	0.00185	-
C	0.002105	0.000157	13.384	< 2e-16	1.36
F	0.006792	0.001140	5.956	6e-08	1.36
S	0.484851	0.043978	11.025	< 2e-16	1
Sp	-0.068335	0.004488	-15.225	< 2e-16	1
H	0.208278	0.019441	10.713	< 2e-16	118.81
H <sup>2</sup>	-0.017087	0.001304	-13.100	< 2e-16	118.81

Table 6-13 ANOVA Summary of the Final Model

<b>Residual Standard Error</b>	<b>R<sup>2</sup></b>	<b>Adjusted R<sup>2</sup></b>	<b>F-statistic</b>	<b>p-value</b>
0.03477	0.942	0.938	225.2	< 2.2e-16

The next step is to check if the MLR model assumptions are verified.

#### 6.4.6 Verification of Final Model

##### Constant Error Variance

Figure 6-11 shows the residuals vs. fitted values plot for the final MLR model.

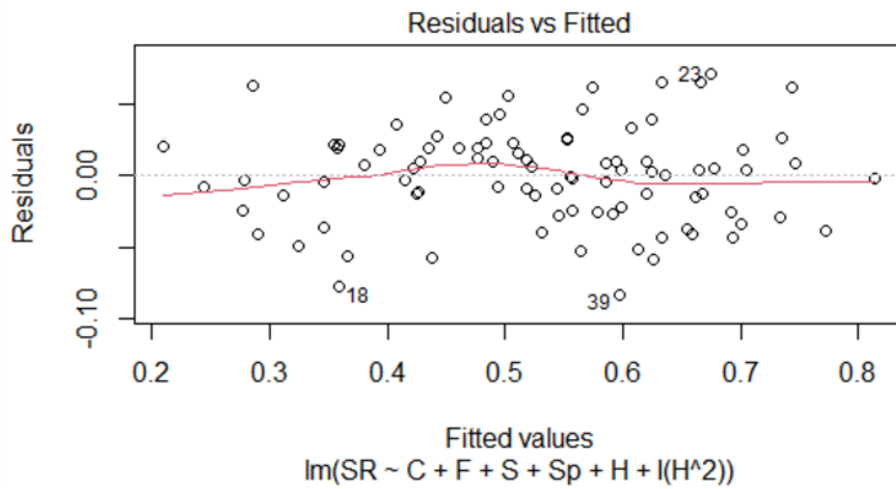


Figure 6-11 Residuals vs. Fitted Values Plot for the Final Model

No curvilinear trend or funnel shape was detected from the plot. The residuals seem to be randomly scattered. Further analysis was done by conducting the studentized Breusch-Pagan test in RStudio. The p-value from the test was 0.09433, which is greater than  $\alpha = 0.01$ . So, the null hypothesis was failed to be rejected indicating that the residuals are homoscedastic at  $\alpha = 0.01$ . The residuals vs. wall height plot (Figure 6-12) also showed random distribution around the horizontal axis without any distinct trend or curve. The constant error variance assumption was fulfilled for the final model.

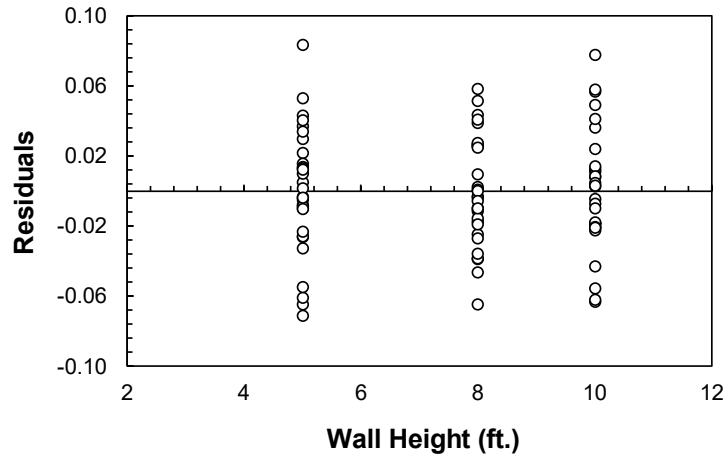


Figure 6-12 Residuals vs. Wall Height Plot for the Final Model

Normality

Figure 6-13 shows the normal probability plot for the final MLR model.

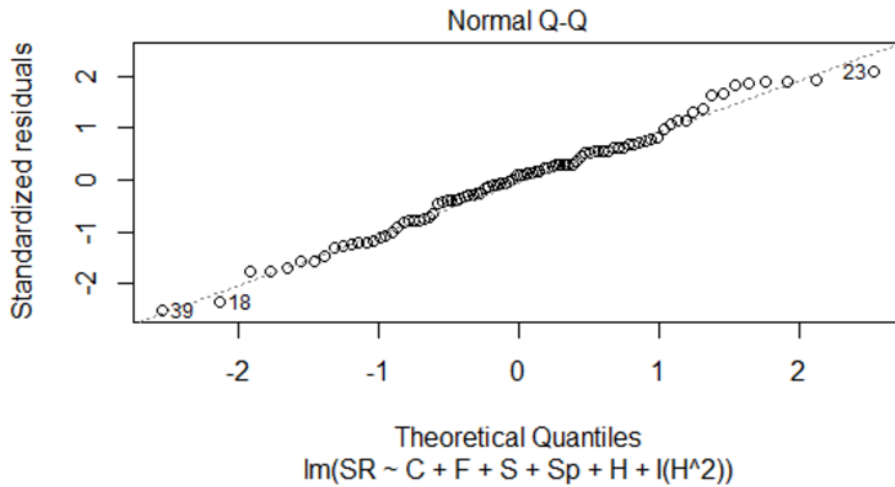


Figure 6-13 Normal Probability Plot for the Final Model

Short tails on both sides can be seen from the plot. To further verify the normality assumption, Shapiro-Wilk normality test was carried out in RStudio. The test estimated a

p-value of 0.5296, which is greater than  $\alpha = 0.01$ . So, the null hypothesis was failed to be rejected indicating that the residuals are normally distributed at  $\alpha = 0.01$ .

#### Outlier Test

The outliers, if any, were checked using several standard tests in RStudio. Bonferroni outlier test was used to detect outliers. DFFITS, DFBETAS, and Cook's Distance were used to determine the influence of the outliers in the final model. The F-statistic to compare the Cook's Distance for this set was 2.1346 for  $\alpha = 0.05$ . It is also suggested that  $D_i$  greater than 0.5 should be investigated, as it may be influential (Faysal, 2017).

Based on the Bonferroni outlier test, none of the observations were flagged as potential outliers. All the observations satisfied the assumptions as per DFFITS, DFBETAS, and Cook's Distance tests as well.

#### Multicollinearity

Based on the VIF in Table 6-12, all the VIFs, except wall height and square of wall height, are within the suggested range. The high VIF of wall height and square of wall height are expected since they are the same variables, so a relation is inevitable. Thus, no serious multicollinearity exists among the predictor variables.

#### *6.4.7 Selection of Final Model*

Best subset method, stepwise regression, and backward elimination were performed in RStudio to finalize the best prediction model.

#### Best Subset Selection

The parameters under consideration for the best subset selection method are  $R^2$ , adj.  $R^2$ , Mallow's  $C_p$ , and Bayesian Information Criteria (BIC). The method selects the best model with the highest  $R^2$  and adj.  $R^2$ , and the lowest Mallow's  $C_p$  and BIC. Based on this

method, the combination with all the six predictor variables was selected as the best model. Table 6-14 summarizes the parameter values for the criteria under consideration.

Table 6-14 Summary of Best Subset Selection Method

Predictor Variables						R <sup>2</sup>	Adj. R <sup>2</sup>	C <sub>p</sub>	BIC
C	F	S	Sp	H	H <sup>2</sup>				
-	-	-	-	-	✓	0.490	0.484	645.3	-51.6
-	-	-	✓	-	✓	0.652	0.644	415.6	-81.4
✓	-	-	✓	-	✓	0.753	0.744	272.8	-107.7
✓	-	✓	✓	-	✓	0.837	0.830	153.2	-141.0
✓	-	✓	✓	✓	✓	0.917	0.912	40.5	-197.4
✓	✓	✓	✓	✓	✓	<b>0.942</b>	<b>0.938</b>	<b>7.0</b>	<b>-225.0</b>

#### Backward Elimination

The backward elimination method starts with all the predictor variables in the model. Then, it incrementally removes statistically insignificant variables. The analysis is completed when there is no insignificant variable remaining in the model. Based on this method, all the predictor variables were significant at  $\alpha = 0.01$  significance level and no variables were removed.

#### Stepwise Regression

Stepwise regression method utilizes both the backward selection and forward selection algorithms. The model starts with the most significant predictor variable. The regression is carried out and the parameters under consideration are calculated. Then, other variables are incrementally added as per their significance. The procedure is repeated until the model with the best criteria parameters is obtained. The F-statistic test is used to



conduct the statistical significance tests (Kutner et al., 2005). Based on this method, the inclusion of all the six predictor variables formed the best model.

#### *6.4.8 Validation of the Final Prediction Model*

The final prediction model was validated using a different set of data. Numerical analysis was again conducted on the calibrated numerical model with randomly selected variables. Both the foundation soil and RPP parameters were varied to get a set of independent responses. The same parameters were used in the final prediction model to estimate lateral pressure reduction factor. Figure 6-14 visualizes the comparison of lateral pressure reduction from the prediction model and the numerical model. Three pressure reduction factors from the field test sections (SR\_4x3, SR\_4x2, SR\_6x3) were also plotted to compare with the predicted estimates. The developed model could explain 93.72% of the variation in lateral pressure reduction at different combinations. The bias values were calculated by taking a ratio of numerical model values to predicted values. The mean of the bias values was exactly 1. The coefficient of variation (COV) of the bias values was 7.7%. This demonstrates an excellent agreement between the numerical and statistical methods.

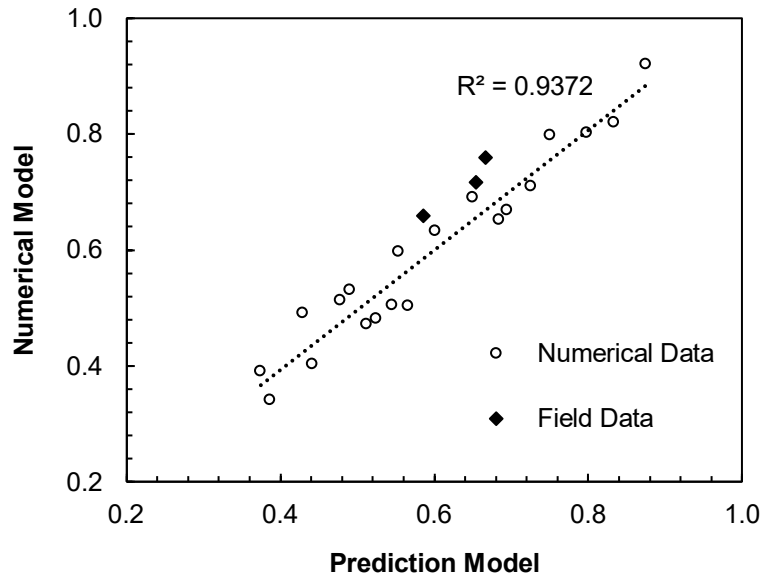


Figure 6-14 Validation of Final Prediction Model

### 6.5 Probabilistic Analysis

Performance evaluation of MSE walls can be conducted through field scale study by constructing actual test sections. The results of the field study can be used for numerical study with finite element approach. Furthermore, the data from field and numerical study can be applied in statistics to develop prediction models. All these methods depend on the assumption that the design parameters, most importantly the soil properties, are uniform or accurate as per the lab/field tests. Nevertheless, in reality, soil is highly heterogenous, with its properties varying both spatially and temporally. Other sources of uncertainty can be errors due to measurements or calculations. The soil properties determined at the field or laboratory always yield values in a range. The actual soil properties can change within that range. The method of using a fixed soil or material property can be regarded as deterministic approach. This approach uses the best estimates of the input parameter values, for instance the mean values (Lin et al., 2016).

However, this does not quantitatively explain the uncertainty associated with the prediction. The materials, and more importantly the soil, properties can vary within a specified range. There will be a high probability that the output obtained from the deterministic approach might not be certain at all times.

Probabilistic estimates, on the other hand, provide the probabilities of expected output and how often the designer can rely on a specific output. It can quantify the uncertainties involved with varying soil and material properties (Sayed et al., 2010). It has been reported that uncertainties and associated risks in geotechnical engineering analysis and design are inevitable, the quantification of which can be advantageous (Duncan, 2000; Sayed et al., 2010). A geotechnical reliability-based approach can design structures with very low probability of failure ( $P_f$ ). Probability of failure can be defined as the ratio of the number of times the FS is less than 1 to the total number of calculations performed (Chalermyanont and Benson, 2005). The target  $P_f$  for MSE wall failures related to foundations are within 0.01 to 0.001 (Chalermyanont, 2002). Typical accepted target  $P_f$  for geotechnical structures are 0.01, 0.001, and 0.0001 (Baecher, 1987; Chalermyanont and Benson, 2004). The quantitative inclusion of uncertainty can produce a rational design process. Monte Carlo Simulation can be used to estimate the probabilities associated with a geotechnical engineering analysis (Yang et al., 2010; Sayed et al., 2010; Lin et al., 2016; Allen et al., 2019). The input parameters that have inherent uncertainty associated with them can be sampled from probability distributions. Previous literatures have reported the COV of common soil properties used in design and analysis (Phoon, 1995; Baecher and Christian, 2003; Sayed et al., 2010; Lin et al., 2016). The steps involved in a probabilistic analysis are outlined in Figure 6-15.

Probabilistic analyses were carried out for lateral base displacement and lateral stress reduction factor for the current study. The foundation soil properties (cohesion and friction angle) were regarded as the uncertain parameters. Since the RPP parameters and wall height are fixed (neglecting the low probability of errors during construction), they were taken as deterministic (certain) parameters. The standard deviation and COV values for cohesion and friction angle were used based upon previous studies.

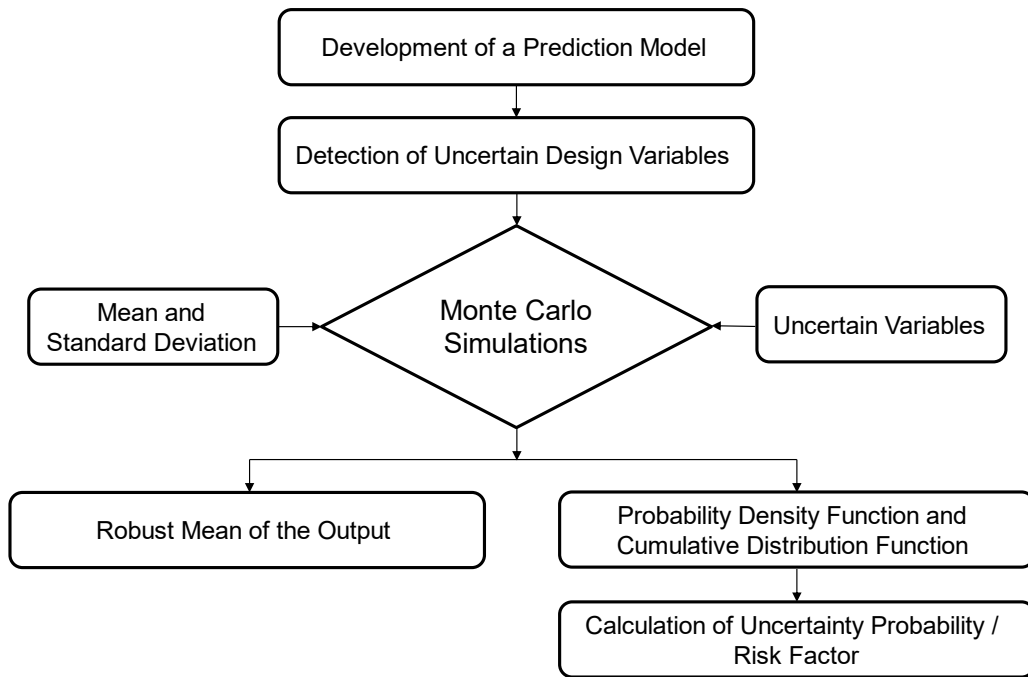


Figure 6-15 Flow for the Probabilistic Analysis

#### 6.5.1 Probabilistic Analysis for Lateral Displacement

The prediction model developed for the lateral base displacement was used for initiating the probabilistic analysis. The COV of both cohesion and friction angle was taken as 10% based on previously published studies (Phoon, 1995; Baecher and Christian, 2003; Sayed et al., 2010; Lin et al., 2016). The standard deviation was calculated accordingly

using the mean and COV values. The RPP size, spacing, extension, and wall height were fixed for each calculation. Cohesion and friction angle were chosen randomly from their respective normal probability distributions for the first calculation. The prediction model developed before was used for the first calculation. 1500 Monte Carlo simulations were then run using randomly selected cohesion and friction angle values for each calculation. Finally, the mean of the 1500 lateral displacement values was estimated which can be regarded more reliable than the value obtained through the deterministic approach. Standard deviation, minimum, and maximum of the lateral displacement values were also calculated to understand the spread of possible outcomes. Finally, the statistics from the 1500 Monte Carlo simulations were used to generate the probability density function (PDF) and cumulative distribution function (CDF). The CDF was used to evaluate the probability of exceedance values which can be used for performance-based design.

A sample PDF and CDF are presented in Figure 6-16 and Figure 6-17, respectively, for a set of parameters shown in Table 6-15. The probabilistic approach with normally distributed random variables gave a mean lateral displacement of 0.639 inches. The deterministic approach with fixed single values yielded a lateral displacement of 0.636 inches. The difference in the predictions is not significant, most probably due to the low value and spread of foundation cohesion. However, an interesting outcome from the CDF (Figure 6-17) is that the probability of getting lateral displacement less than 0.636 inches is only 47%. This proves the uncertainty risk associated with the deterministic approach. It is almost equally probable to get lateral displacement more or less than the deterministically estimated value, i.e., 0.636 inches. If the foundation soil strength values were underpredicted during design, then smaller lateral displacements than anticipated can be expected at site. For example, there is 10% probability that the lateral displacement will be less than 0.5 inches. Nevertheless, there is an equal possibility that

the soil strength might have been overpredicted, so larger lateral displacements at site should be expected as well. For instance, there is 90% probability that the lateral displacement will be less than 0.77 inches. Even though the mean was 0.639 inches, the maximum and minimum lateral displacements were 1.013 and 0.378 inches, respectively, albeit with very less probability of occurrence. It is recommended that this uncertainty risk factor be incorporated during the analysis for a reliable design.

Table 6-15 Parameters for Sample Probabilistic Analysis of Lateral Displacement

RPP	Size (ft)	0.33	Cohesion (psf)	Mean	50
	Spacing (ft)	2		COV (%)	10
	Extension (ft)	2		Standard Deviation	5
Wall Height (ft)		8	Friction Angle (°)	Mean	30
				COV (%)	10
				Standard Deviation	3

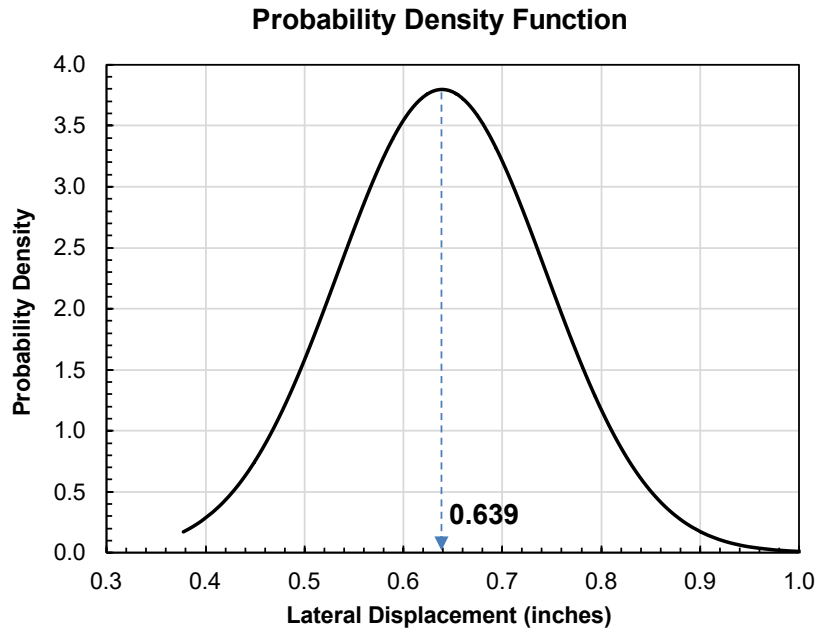


Figure 6-16 Probability Density Function for Lateral Displacement

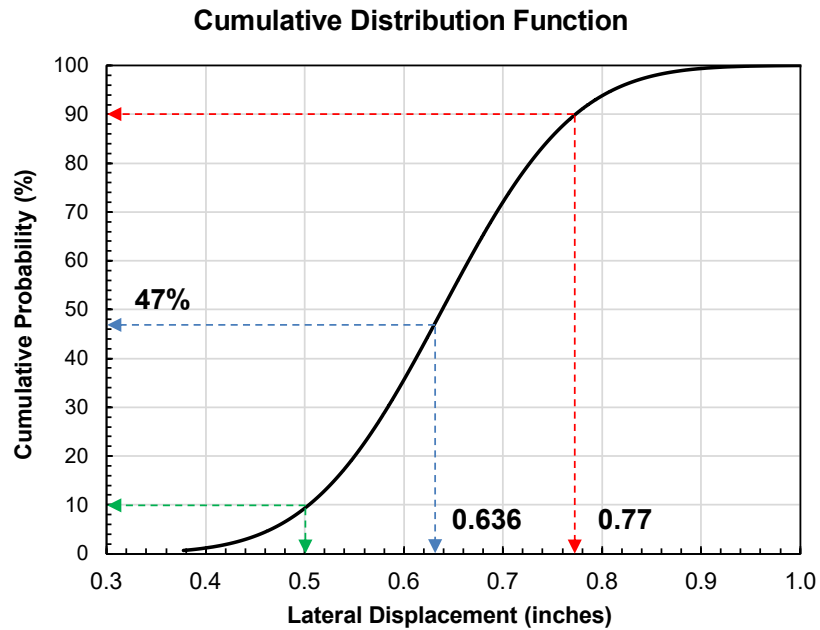


Figure 6-17 Cumulative Distribution Function for Lateral Displacement

### 6.5.2 Probabilistic Analysis for Lateral Pressure Reduction

The prediction model developed for the lateral pressure reduction was used for initiating the probabilistic analysis. The COV of both cohesion and friction angle was taken as 10% based on previously published studies (Baecher and Christian, 2003; Sayed et al., 2010; Lin et al., 2016). The standard deviation was calculated accordingly using the mean and COV values. The RPP size, spacing, and wall height were fixed for each calculation. The RPP extension was kept constant at 2 ft. Cohesion and friction angle were chosen randomly from their respective normal probability distributions for the first calculation. The prediction model developed before was used for the first calculation. 1500 Monte Carlo simulations were then run using randomly selected cohesion and friction angle values for each calculation. Finally, the mean of the 1500 lateral displacement values was estimated which can be regarded more reliable than the value obtained through the deterministic approach. Standard deviation, minimum, and maximum of the lateral pressure reduction factors were also calculated to understand the spread of possible outcomes. Finally, the statistics from the 1500 Monte Carlo simulations were used to generate the probability density function (PDF) and cumulative distribution function (CDF). The CDF was used to evaluate the probability of exceedance values which can be used for performance-based design.

A sample PDF and CDF are presented in Figure 6-18 and Figure 6-19, respectively, for a set of parameters shown in Table 6-16. The probabilistic approach with normally distributed random variables gave a mean lateral pressure reduction factor of 0.656. The deterministic approach with fixed single values yielded a lateral pressure reduction factor of 0.655. The difference in the predictions is not significant, most probably due to the low value and spread of foundation cohesion. However, an interesting outcome from the CDF (Figure 6-19) is that the probability of getting pressure reduction factor less than 0.655 is



only 49%. This proves the uncertainty risk associated with the deterministic approach. This result is similar to that obtained for the lateral displacement estimates. It is almost equally probable to get lateral pressure reduction more or less than the deterministically estimated value, i.e., 0.655. If the foundation soil strength values were underpredicted during design, then greater lateral pressure reduction than anticipated can be expected at site. For example, there is 97% probability that the pressure reduction factor will be less than 0.70. Nevertheless, there is an equal possibility that the soil strength might have been overpredicted, so smaller lateral pressure reduction at site should be expected as well. For instance, there is 10% probability that the pressure reduction will be less than 0.626. Even though the mean was 0.656, the maximum and minimum lateral pressure reduction factors were 0.733 and 0.585, respectively, albeit with very less probability of occurrence. It is recommended that this uncertainty risk factor be incorporated during the analysis for a reliable design.

Table 6-16 Parameters for Sample Probabilistic Analysis of Lateral Pressure Reduction

RPP	Size (ft)	0.33	Cohesion (psf)	Mean	50
	Spacing (ft)	2		COV (%)	10
	Extension (ft)	2		Standard Deviation	5
Wall Height (ft)		8	Friction Angle (°)	Mean	30
				COV (%)	10
				Standard Deviation	3

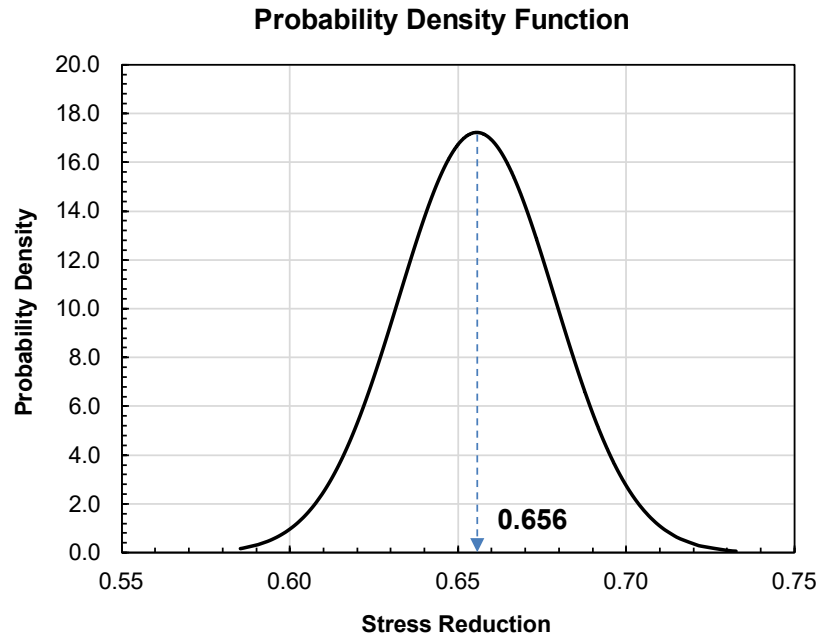


Figure 6-18 Probability Density Function for Lateral Pressure Reduction

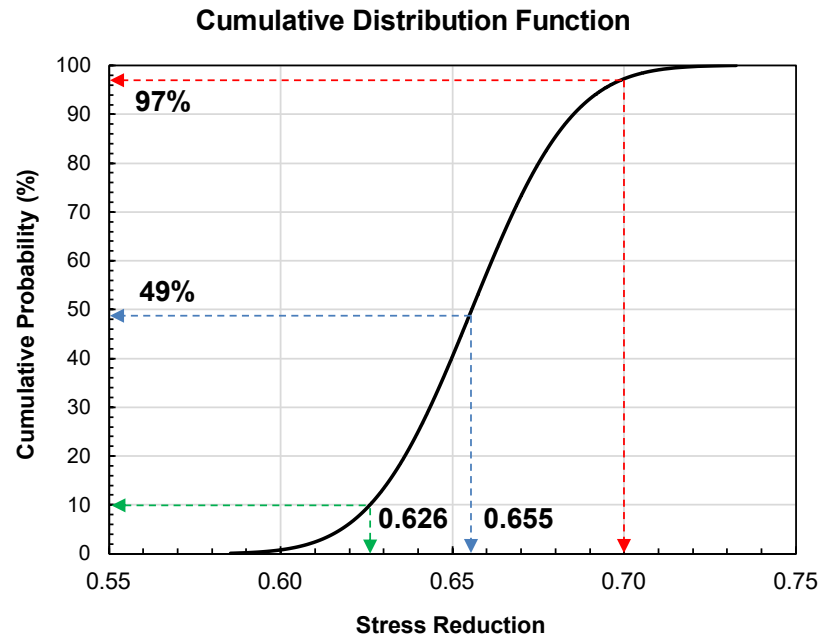


Figure 6-19 Cumulative Distribution Function for Lateral Pressure Reduction

## 6.6 Modified Factor of Safety Against Sliding

The factor of safety against sliding of an MSE wall is calculated by dividing the lateral resisting force by the lateral driving force. The lateral resisting force is provided by the frictional resistance at the interface of reinforced and foundation soil. The lateral driving force is due to the lateral pressure from the backfill, surcharge, hydrostatic force (if present). For a more realistic analysis, dynamic load from the traffic can also be included for MSE walls supporting traffic movement. The frictional resistance at the wall base depends on the weight and friction angle of the reinforced soil. The cohesion of foundation soil also plays a role in providing lateral resistance; however, it is generally neglected. The equation below shows how the factor of safety against sliding is calculated based on a typical MSE wall configuration shown in Figure 6-20 (Das, 2015).

$$FS_{(sliding)} = \frac{(W_1 + W_2 \dots + qa')[\tan(k\phi'_1)] + Bc'_a}{P_a}$$

$$P_a = \frac{1}{2} \gamma_1 K_a H^2$$

where,

$W$  = weight of reinforced soil

$q$  = surcharge per unit area

$a'$  = area of surcharge application

$k$  = coefficient for the interface friction angle at the wall base (typically 2/3)

$\phi'_1$  = friction angle of the reinforced soil

$B$  = width of wall ( $BD$  in Figure 6-20)

$c'_a$  = adhesion between the foundation and reinforced soil

$P_a$  = lateral active pressure

$\gamma_1$  = unit weight of backfill

$K_a$  = coefficient of active lateral earth pressure [ $\tan^2 (45^\circ - \phi'/2)$ ]

$H$  = height of the wall

The factor of safety against sliding increases with an increase in the unit weight or friction angle of reinforced soil, or an increase of surcharge. On the other hand, it will decrease if the active lateral pressure is more. The active lateral pressure directly depends on the height of the wall. The foundation of an MSE wall (only the topsoil) is generally replaced by granular soil so that there is an increased frictional resistance at the wall base. Also, it might help in providing better drainage of water.

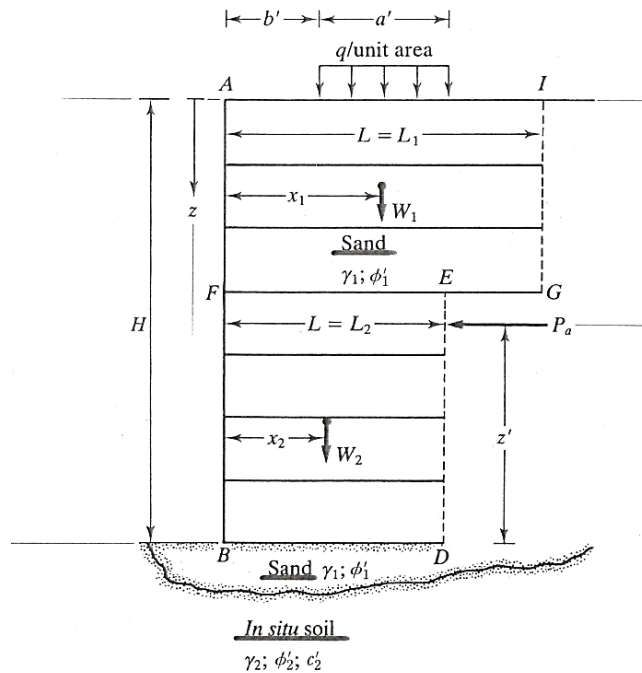


Figure 6-20 Typical Cross-Section of an MSE Wall (Das, 2015)

It would be cost-extensive to increase the unit weight of reinforced soil by means of greater compaction effort. It is also to be noted that an increase in the unit weight of reinforced or backfill soil will also provide additional active lateral pressure. Improving the factor of safety by using granular soil with high friction angle might also be unfeasible at times. Increasing the width of wall is not always possible due to space and budget constraint. Thus, the use of RPPs to increase the lateral resistance by using them as shear keys is a viable option since they are economical and do not alter the wall design or construction by a high degree.

This study quantified the effect of using RPPs as shear keys at the base of an MSE wall. It was shown that RPPs effectively reduced the lateral earth pressure at the wall base, and thus improve the lateral resistance against sliding. The final step is to incorporate the lateral reduction during design and analysis. The main function of RPPs is to reduce the lateral pressure from the backfill by providing lateral resistance. This can be incorporated at the denominator of the sliding factor of safety equation as follows.

$$\text{Modified } FS_{(sliding)} = \frac{(W_1 + W_2 \dots + qa')[\tan(k\phi'_1)] + Bc'_a}{P_a (1 - SR)}$$

where,

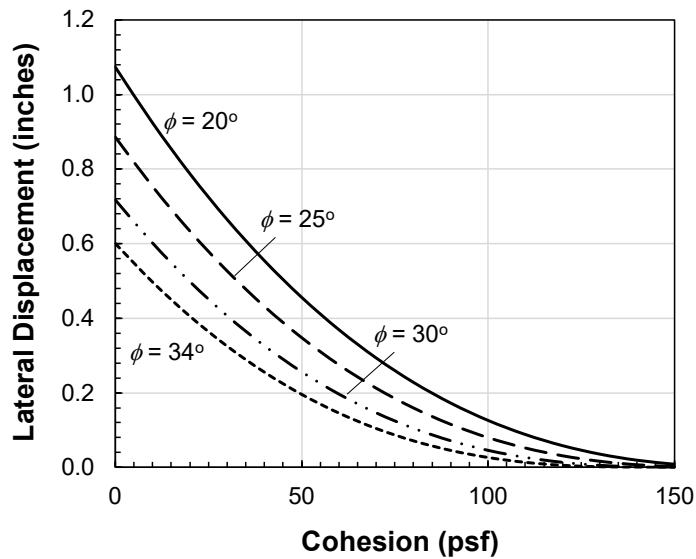
$SR$  = lateral pressure reduction factor (always less than 1)

The lateral pressure reduction factor ( $SR$ ) is the ratio of difference of lateral pressure on an unreinforced and RPP reinforced wall to the lateral pressure on the unreinforced wall. The lateral pressure here is the pressure acting on the wall face. For simplification of external stability calculation, MSE wall is regarded as a rigid mass, such that the lateral pressure acting at the front of the wall is the same as that at the back.

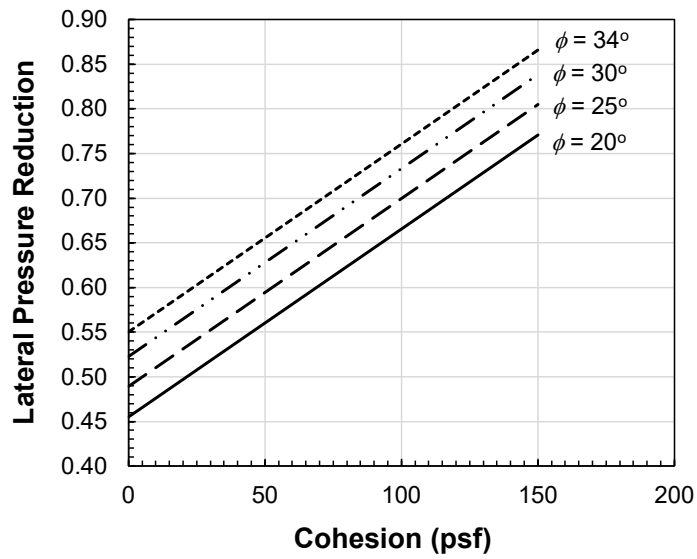
The lateral pressure reduction factor ( $SR$ ) can be calculated using the statistical model developed earlier. For ease of use, stress reduction charts were developed for different combinations of foundation soil strength. The steps to calculate the modified factor of safety against sliding are presented in the following section.

### 6.7 Design Steps for Calculation of Modified Factor of Safety Against Sliding

The statistical models developed earlier were used to develop lateral displacement and lateral pressure reduction charts for combinations of different foundation soil cohesion and friction angle. Charts were developed for 4x4, 6x6, and 10x10 inches RPP size at 2 ft., 3 ft., and 4 ft. c/c spacings. The wall heights used for the charts were 5 ft., 10 ft., and 12 ft. The RPP extension for all the charts were kept constant at 2 ft. Lateral displacement and pressure reduction values needed for RPP and soil parameters not provided in the charts can be calculated by linear interpolation. Sample charts for a 5 ft. high wall reinforced with 4x4 inches RPP spaced at 3 ft. c/c are shown in Figure 6-21.



(a)



(b)

Figure 6-21 (a). Lateral Displacement and (b). Lateral Pressure Reduction Charts

All the developed charts are provided in Appendix B. The following steps are recommended to be taken to calculate the required modified factor of safety against sliding (Figure 6-22).

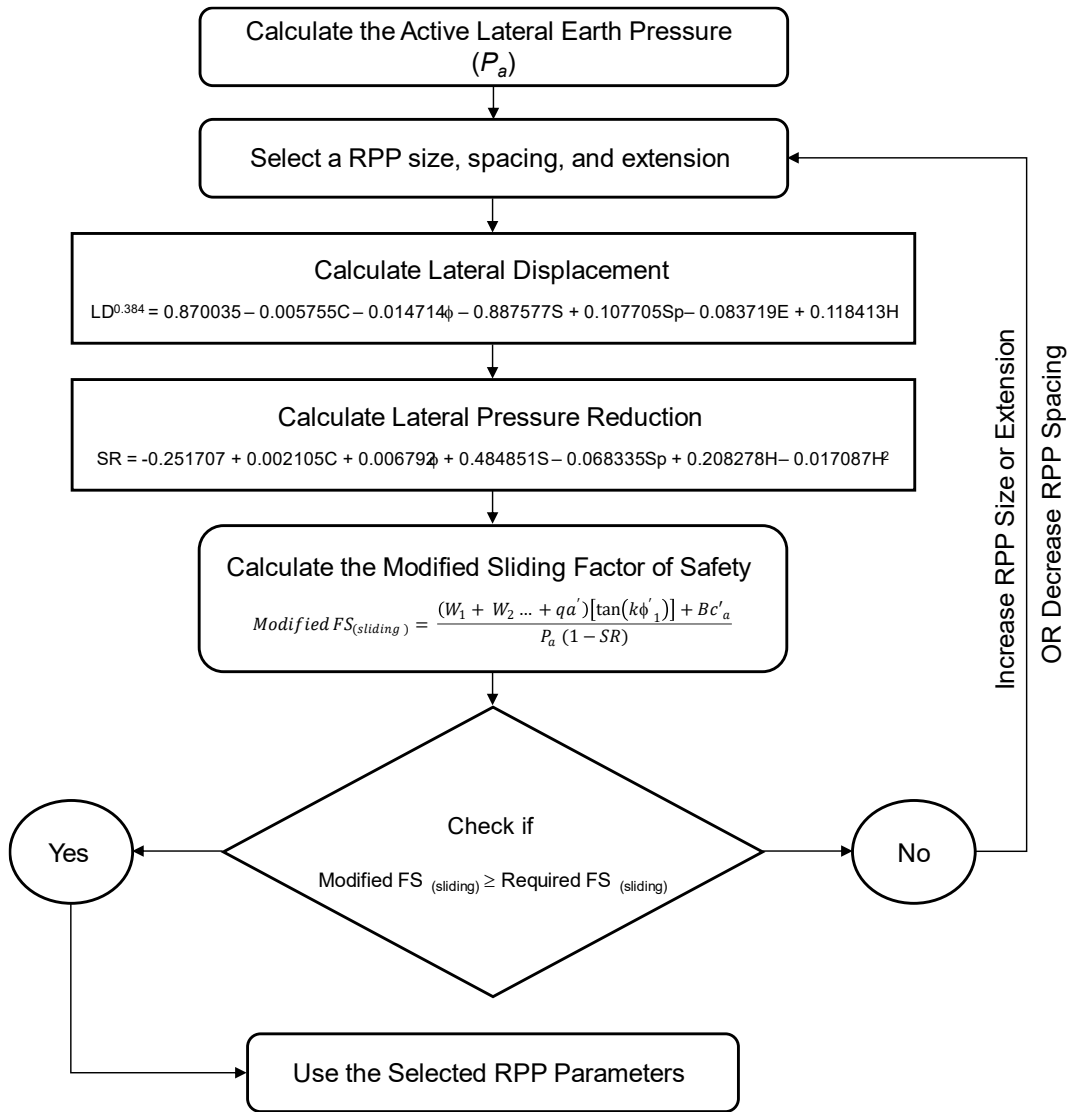


Figure 6-22 Flowchart for Calculation of Modified Factor of Safety Against Sliding

### 6.7.1 Calculation Example

A calculation example is presented in this section to show the steps involved in selecting the appropriate RPP parameters for design. Figure 6-23 shows an MSE wall configuration along with the soil properties. The height of the wall is 10 ft. with a width of 7 ft. ( $L/H = 0.7$ ). The backfill has an average unit weight of 110 pcf and mean friction



angle of  $24^\circ$ . The foundation soil has an average unit weight of 125 pcf, and mean friction angle and cohesion of  $30^\circ$  and 75 psf, respectively.

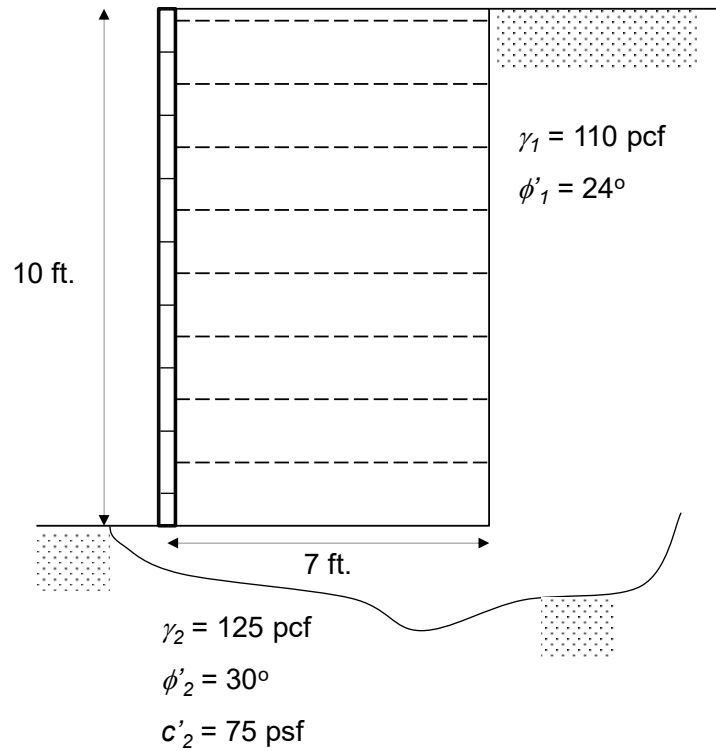


Figure 6-23 MSE Wall Configuration for Calculation Example

The first step is to calculate the active lateral earth pressure acting on the MSE wall.

$$P_a = \frac{1}{2} \gamma_1 K_a H^2 = \frac{1}{2} * 110 * \tan^2 \left( 45^\circ - \frac{24^\circ}{2} \right) * 10^2 = 2319.52 \text{ lb/ft.}$$

$$W = \gamma_1 * H * L = 110 * 10 * 7 = 7700 \text{ lb/ft.}$$

$$FS_{(sliding)} = \frac{W [\tan(k\phi'_1)]}{P_a} = \frac{7700 * [\tan(\frac{2}{3} * 24^\circ)]}{2319.52} = \mathbf{0.95} < 1.5$$

The factor of safety is 0.95 which is less than the required FS of 1.5 as per TxDOT guidelines. The cohesion factor is neglected here since standard practice recommends replacement of the topsoil with granular soil (no cohesion). Also, hydrostatic pressure is neglected because the reinforced soil is granular in nature which helps in drainage of water due to its high permeability.

Let us select a RPP configuration with 4x4 inches RPP spaced at 3 ft. c/c. The RPPs will be extended 2 ft. above the foundation soil into the reinforced soil.

The lateral displacement can be calculated as follows:

$$LD^{0.384} = 0.870035 - 0.005755C - 0.014714F - 0.887577S + 0.107705Sp - 0.083719E + 0.118413H$$

$$LD^{0.384} = 0.870035 - 0.005755 \times 75 - 0.014714 \times 30 - 0.887577 \times 0.33 + 0.107705 \times 3 - 0.083719 \times 2 + 0.118413 \times 10$$

Lateral Displacement (LD) = **1.11 inches**

Alternatively, the lateral displacement chart (Figure 6-24) developed for the corresponding RPP configuration can also be used. A similar value of 1.11 inches was determined from the chart as well.

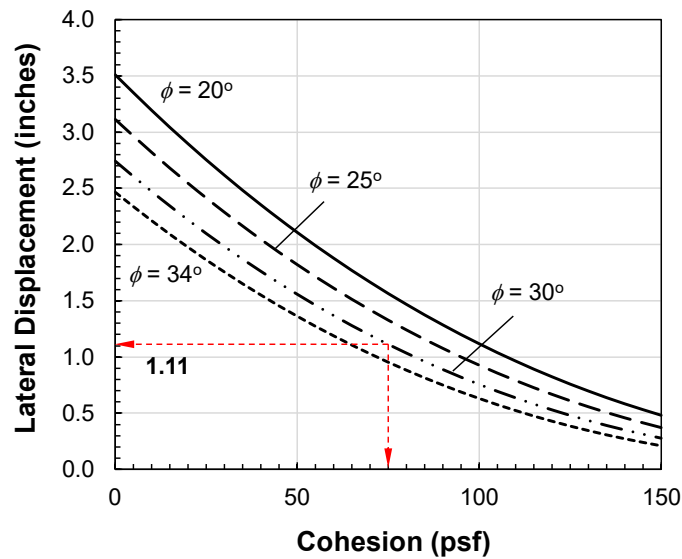


Figure 6-24 Lateral Displacement for the Calculation Example

The lateral pressure reduction factor can be calculated as follows:

$$SR = -0.251707 + 0.002105C + 0.006792F + 0.484851S - 0.068335Sp + 0.208278H - 0.017087H^2$$

$$SR = -0.251707 + 0.002105 \times 75 + 0.006792 \times 30 + 0.484851 \times 0.33 - 0.068335 \times 3 + 0.208278 \times 10 - 0.017087 \times 10^2$$

Lateral Pressure Reduction Factor (SR) = **0.44**

Alternatively, the lateral pressure reduction chart (Figure 6-25) developed for the corresponding RPP configuration can also be used. A similar value of 0.44 was determined from the chart as well.

The next step would be to calculate the modified factor of safety against sliding.

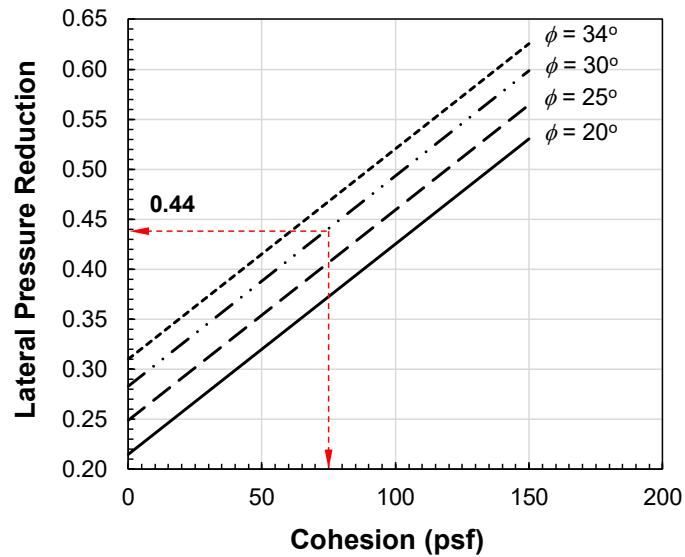


Figure 6-25 Lateral Pressure Reduction for the Calculation Example

$$\text{Modified } FS_{(\text{sliding})} = \frac{W[\tan(k\phi'_1)]}{P_a(1 - SR)} = \frac{7700 * [\tan(\frac{2}{3} * 24^\circ)]}{2319.52 * (1 - 0.44)} = 1.7 > 1.5$$

The modified factor of safety against sliding is now 1.7 which is greater than the required FS of 1.5 as per TxDOT guidelines. Thus, the selected RPP parameters can be used for the design. Figure 6-26 shows the RPP layout for the MSE wall configuration. The RPPs inside the MSE wall should be extended 2 ft. above the foundation soil into the reinforced soil. The RPPs in front of the wall must be driven fully flushed to the ground. The front rows of RPPs help in providing additional resistance against the lateral movement. Furthermore, they intercept potential sliding planes and improve the global factor of safety.

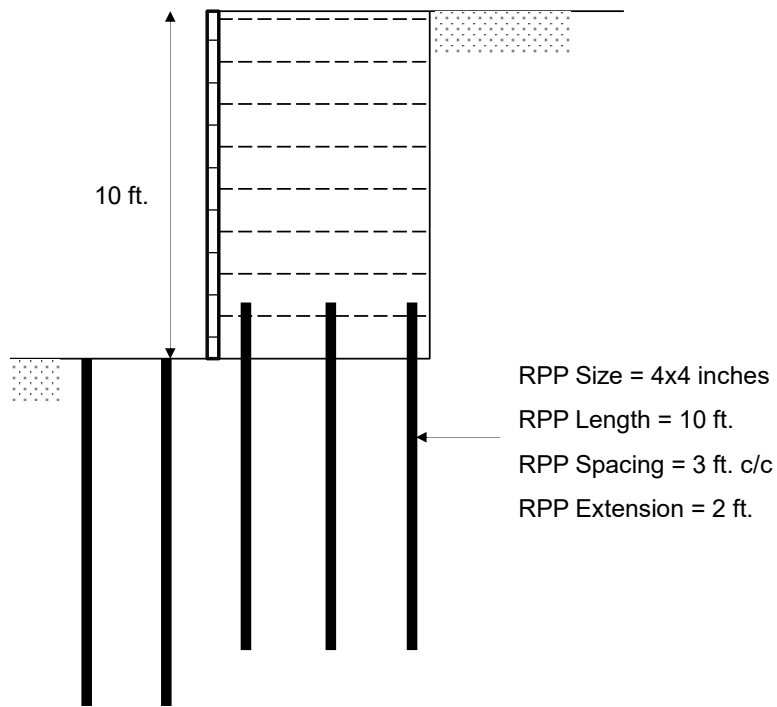


Figure 6-26 RPP Reinforcement for Calculation Example

### Probabilistic Analysis

The calculations shown above are deterministic in nature, such that, they only provide the output for a fixed set of foundation soil strength. However, due to numerous reasons outlined earlier, the foundation soil strength might not be just one single value. It can vary both spatially and temporally. Thus, it is recommended to carry out a probabilistic analysis to evaluate the risks or uncertainties associated with the variability in soil strength. A similar approach explained earlier could be used to determine the probability density function and cumulative distribution function of the lateral displacement and lateral pressure reduction factor. Monte Carlo simulations were run for this calculation example as well. Figure 6-27 shows the probabilistic analysis charts for the lateral

displacement and lateral stress reduction. It can be seen that the values obtained from the deterministic approach have around 46-48% probability of occurrence.

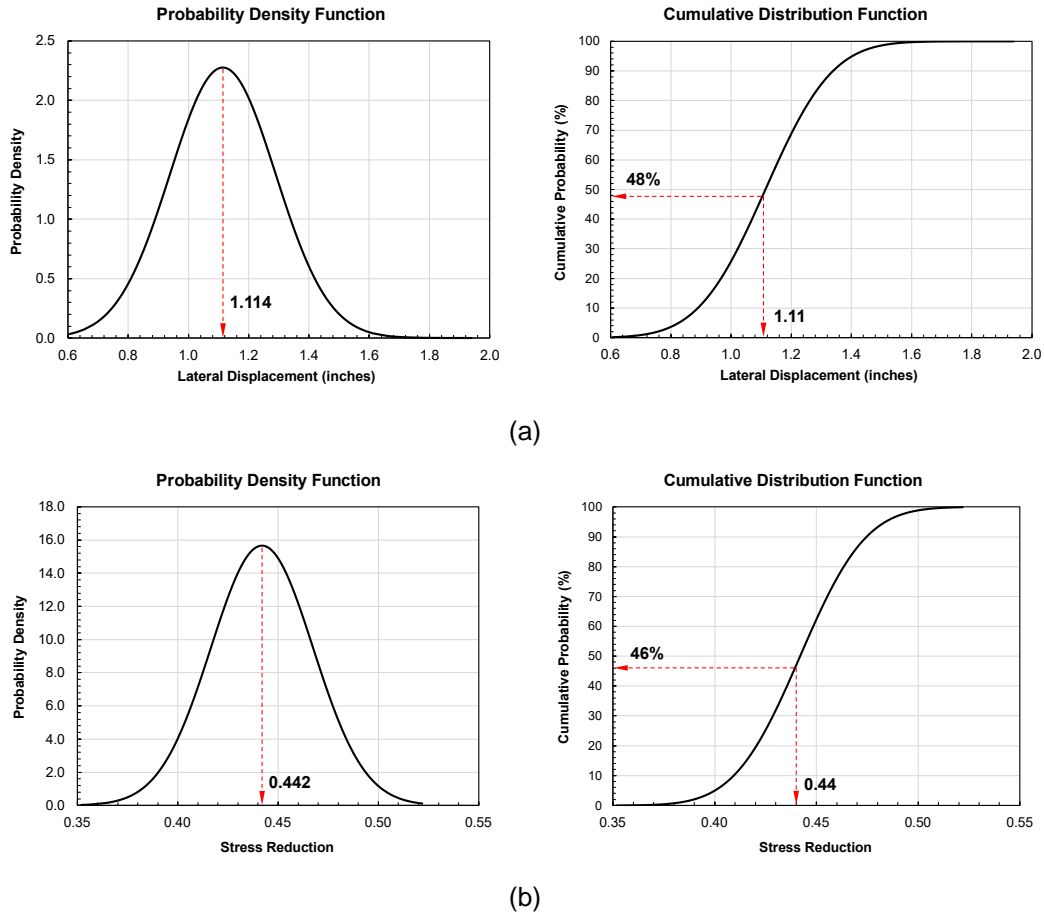


Figure 6-27 Probabilistic Analysis Charts for Calculation Example (a) Lateral Displacement (b) Lateral Pressure Reduction

These results can be used to develop probability of failure charts which will serve as a basis for reliability-based design. A range of factor of safety for all the probable stress reductions can be calculated using Monte Carlo simulations. The probability of failure ( $P_f$ ) would then be the ratio of factor of safety less than 1.5 to the total number of simulations.

The conventional definition of probability of failure is the probabilities where the FS is less than 1; however, since our target FS is 1.5, the calculations will use that value as the cut-off FS. Figure 6-28 shows that the  $P_f$  for the calculation example is 0.003. This is the area under the probability density curve for FS less than 1.5. As mentioned earlier, the calculated  $P_f$  is more than 0.001 and 0.0001 (some of the widely accepted probabilities of failure). Thus, it can be argued that the selection of the RPP parameters might not yield a 100% chance that the modified FS against sliding will be more than 1.5.

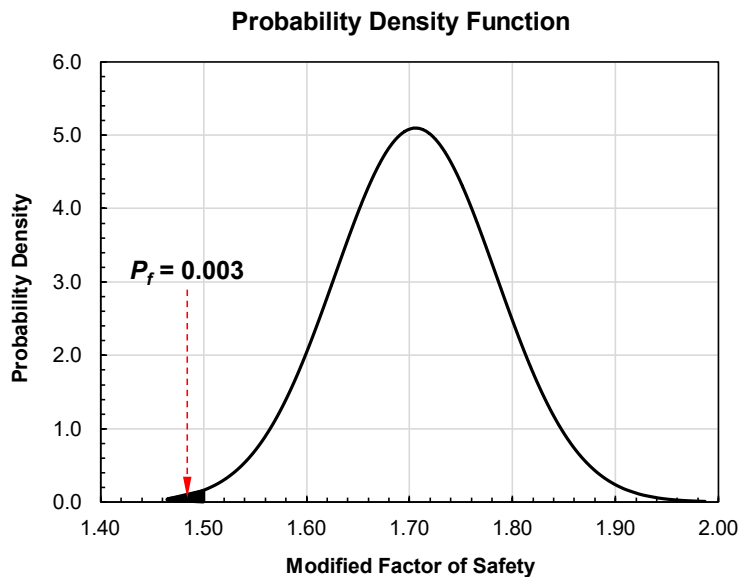


Figure 6-28 Probability Density of Modified Factor of Safety for Calculation Example

So, the designer should assess the uncertainties involved with the deterministic approach. Based on budget allowance, consequences of failure, engineer experience, and reliability of soil tests, a higher stress reduction can be targeted. This would ensure a higher probability of occurrence of the target factor of safety, and the probability of failure within the specified limit. Similar lateral pressure reductions can be obtained from

different combinations of RPPs. A simple cost analysis, including just the material and labor cost, can be carried out to finalize the most effective and economical RPP layout.

### 6.8 Limitations of the Prediction Models

The statistical prediction models were developed with few assumptions. Thus, some limitations are inevitable. They are outlined as follows:

1. The foundation soil properties (cohesion and friction angle), RPP parameters (size, spacing, extension), and the wall height were limited to a certain range in the study. The finite element models were calibrated with the field test sections where these properties varied within a certain range. Subsequently, the predictability of the statistical models developed using the finite element results are strong within that range only. Any input values outside of that range might not produce a very reliable output. The suggested range of the input parameters are shown in Table 6-17.

Table 6-17 Range of Input Parameters for the Models

Parameter		Range
Foundation Soil	Cohesion	0 – 150 psf
	Friction Angle	20 – 34°
RPP	Size	4x4 – 10x10 inches
	Spacing	2 – 5 ft.
	Extension	0 – 3 ft.
MSE Wall Height		0 – 12 ft.

The foundation soil properties included in the study are within a reasonable limit encountered at field. Since the cohesion is neglected for lateral resistance for long-



term analysis, and also the top foundation soil is replaced with granular soil, the range was chosen to include only small cohesion values.

The RPP sizes in the study are the ones which can be efficiently installed at site. Larger size RPPs are also available, however, they impede the efficient and economical aspects of using RPPs in the first place. However, it is to be noted that even though the larger size RPPs are difficult to install incurring more labor, cost, and time, they are still very efficient compared to conventional piling methods. The range of MSE wall height can be concerning since walls higher than 10 ft. are frequently built. The facing and footing used for the field test sections, which were eventually modeled to calibrate the numerical models, could reasonably be used for walls only within 10 ft. Nevertheless, slight modifications to the numerical model can be done to study higher walls as well. This can be included in future studies.

2. The study was conducted assuming hydrostatic pressure from any water table is relieved by drainage of water from the granular backfill. Current design guidelines (Elias et al., 2001; AASHTO, 2007) recommend using cohesionless granular material for the wall backfill. The high permeability of these materials helps in effectively draining any water. Furthermore, drainage pipes, blankets, and weep holes are generally required to expedite drainage as per the design guidelines.
3. The prediction models did not incorporate the effects of foundation soil unit weight. A similar study as was done for cohesion and friction angle can also be done for quantifying the effects of changing soil unit weight.

## Chapter 7

### SUMMARY AND CONCLUSIONS

#### 7.1 Background

MSE retaining walls are prone to lateral sliding when the shear resistance at the base of the wall is not enough to hold the wall in place. Sliding failure of the wall can affect structures near the base and top of the wall. This will in turn impose additional repair and maintenance costs to Department of Transportations. Furthermore, MSE walls also undergo global failure due to weak soil conditions along with high lateral pressures. Incorporation of shear keys at the wall base can provide additional resistance against the lateral force, thereby, increasing the lateral resistance of the wall. Recycled Plastic Pins (RPP) can be an effective and sustainable solution to the lateral sliding of MSE walls. RPPs when driven through the wall foundation with a certain portion extended into the reinforced zone can provided resistance against the active lateral force. Thus, they can be integrated in the wall design to act as shear keys. The main objective of this study was to evaluate the performance of RPPs in increasing the lateral resistance of MSE wall base. Furthermore, they were also evaluated on their resistance against global failure.

An area inside Hunter Ferrell Landfill in Irving, Texas was chosen for the field study. Four test sections were constructed, out of which three were reinforced with 10 ft. long RPPs at the wall base. One test section was left unreinforced as a control section (SC\_Control). The three test sections were reinforced with 4x4 inches RPP at 3 ft. c/c, 4x4 inches RPP at 2 ft. c/c, and 6x6 inches RPP at 3 ft. c/c. They were designated as SR\_4x3, SR\_4x2, and SR\_6x3 accordingly. The RPPs inside the wall were extended 2 ft. above the foundation into the reinforced zone. Two rows of RPPs were installed fully flushed to the ground surface in front of the test wall. The height of each test section was 5 ft. The wall

was backfilled with in-situ sand at the front reinforced zone. Triaxial geogrid was used as reinforcement. The wall was constructed in 5 lifts, each lift being 1 ft. in thickness. About 5 months after construction, an additional 2 ft. of soil (second phase of loading) was added to each section making the wall height 7 ft. Vertical and horizontal inclinometer casings were used to monitor the lateral displacement and vertical settlement of the wall base, respectively. Earth pressure plate installed on the inside of the facing was used to monitor the lateral pressure acting on each test section. This chapter summarizes the findings from the field results and analysis of the field data. Lastly, recommendations for further study have also been provided.

#### *7.1.1 Site Investigation*

- The average TCP blow count of the foundation soil was found to be 11 (equivalent SPT=8) and 15 (equivalent SPT=10) at a depth of 5 ft. and 10 ft., respectively. The laboratory results indicated that the soil till a depth of 10 ft. from the ground surface was soft to medium clayey sand. The soil from 10-19 ft. was lean clay. Stiff shale formation was encountered after 19 ft.
- The top 10 ft. foundation soil had cohesion between 313 – 418 psf, while the friction angle for the same depth was between 25° – 27°.

#### *7.1.2 Lateral Displacement of Wall Base*

- The test sections were monitored for almost two years. The lateral displacement of the wall base was recorded to be 0.521 inches, 0.412 inches, 0.264 inches, and 1.636 inches for SR\_4x3, SR\_4x2, SR\_6x3, and SC\_Control, respectively.
- The three RPP reinforced sections were stable, while the control section failed during December 2019. The control test section exhibited significant lateral base movement along with tilting of the wall face.

- The displacements in the reinforced sections gradually decreased after a certain time once the load had mobilized. Furthermore, the second phase of loading did not produce as much displacement in the reinforced sections compared to the control section which displaced further after the addition of extra load.
- Based on the incremental inclinometer readings and comparison with previous literature, it was verified that there was no presence of deep-seated failure.
- The lateral resistance of the RPP reinforced sections increased by 75% to 89% in comparison to the control section without any RPP.

#### 7.1.3 *Settlement of Wall Base*

- A maximum vertical deformation of 0.977 inches, 0.648 inches, 0.597 inches, and 1.888 inches were measured at SR\_4x3, SR\_4x2, SR\_6x3, and SC\_Control, respectively.
- Settlement improvement factor, which is the ratio of the maximum settlement in the control section to the maximum settlement in the reinforced section, was calculated. The settlement improvement factors for SR\_4x3, SR\_4x2, and SR\_6x3 were estimated to be 1.93, 2.91, and 3.16, respectively.
- The vertical deformation/settlement of the RPP reinforced sections decreased by 48% to 68% in comparison to the control section without any RPP.

#### 7.1.4 *Earth Pressure Plates*

- The pressure plate readings showed relative fluctuation to the wall displacement. The pressure behind the wall facing decreased with lateral movement. The variation in pressure was also linked with rainfall, as increasing precipitation events brought about an increase in the lateral pressure. However, as the wall displaced laterally, the pressure on the wall facing decreased gradually along with it.

- The maximum lateral pressure in the RPP reinforced sections decreased by 66% to 76% in comparison to the control section without any RPP.
- The  $K_r/K_a$  ratio of the RPP reinforced sections were less than 1, while it was 0.98 for the control section. These results suggest that the net average pressure acting on the wall face of the RPP reinforced sections is less than that required to produce an active Rankine condition.

#### 7.1.5 Numerical Study

- A finite element study was conducted on the test sections. A FE model was calibrated according to the field results. After a satisfactory calibration was achieved, parametric studies to evaluate the effect of foundation soil strength, RPP parameters, and wall height on the base displacement were conducted.
- It was found that both cohesion and friction angle of foundation soil play an important role in increasing the lateral resistance of wall base. Higher foundation soil strength reduced the lateral displacement by a higher factor. This might be due to the fact that the passive resistance provided by the RPPs were higher when the foundation soil was stronger.
- RPPs with a larger cross-sectional area provided better lateral resistance. Although the lateral displacement increased sharply with increasing wall height, the degree of resistance provided by a larger size RPP was almost the same at all wall heights.
- Closer spacing of RPPs resulted in better lateral resistance and ultimately smaller lateral displacements of the wall base. This might be due to the group effect of RPPs at closer spacings.
- An extension of RPP above the foundation into the reinforced zone increased the lateral resistance considerably. The decrease in lateral displacement with increasing

RPP extension was more pronounced in taller walls. However, the rate of decrease in lateral movement gradually reduced with increasing RPP extension. It was found that an extension upto 3 ft. can be considered satisfactory for a 10 ft. wall, while smaller extensions will provide similar results for shorter walls.

- The numerical study showed that the most important variable influencing the lateral displacement of wall base is the MSE wall height. Among all the parameters studied, the wall height brought about the highest change in lateral displacement.
- The reduction in the lateral displacement of the wall base was due to a decrease in the active lateral pressure on the wall facing. The RPPs acted as shear keys and resisted the lateral pressure, thereby decreasing the net pressure reaching the wall face. The calibrated FE model was used to quantify the reduction factor. Similar results as seen in the lateral displacement study were seen for the stress reduction factor as well.
- The results from the global stability analysis showed that all the RPP reinforcement configurations increased the factor of safety to 1.5 or more (Morgenstern-Price method). This satisfies the criteria set by AASHTO (2014).
- The inclusion of the two front rows of RPPs increased the factor of safety by a satisfactory degree in SR\_4x2 and SR\_6x3. The increase was about 10% (based on Morgenstern-Price method). The front two rows of RPPs are more beneficial in the case of deeper slip surfaces. Since the two rows are deeper than the RPPs inside the MSE wall, they will restrict the deeper slip surfaces if they are not restricted by the inside RPPs.
- An interesting trend shown is that the spacing of RPPs played a better role in resisting the failure plane. SR\_4x2 provided better resistance than the other two

reinforced sections. SR\_4x2 performed better than SR\_6x3 even though it was by a small factor.

#### 7.1.6 Design Methodology

- The comprehensive data from the numerical modeling was analyzed statistically to generate Multiple Linear Regression (MLR) prediction models. The generated prediction models were then used to develop design charts.
- Statistical analyses were conducted in RStudio to develop prediction models to estimate lateral base displacement and stress reduction factor. The predictors used were foundation soil strength, RPP parameters, and wall height.
- The final lateral displacement prediction model is as follows:

$$LD^{0.384} = 0.870035 - 0.005755C - 0.014714F - 0.887577S + 0.107705Sp - 0.083719E + 0.118413H$$

Where, LD = Lateral displacement of MSE wall base (inches), C = Cohesion of foundation soil (psf), F = Friction angle of foundation soil (degrees), S = RPP size (ft.), Sp = RPP center-to-center spacing (ft.), E = RPP extension above the foundation soil into the reinforced soil (ft.), and H = MSE wall height (ft.).

- The final lateral stress/pressure reduction model is as follows:

$$SR = -0.251707 + 0.002105C + 0.006792F + 0.484851S - 0.068335Sp + 0.208278H - 0.017087H^2$$

Where, SR = Lateral stress/pressure reduction factor. This model was developed for a constant RPP extension of 2 ft.

- Both the developed models were validated with independent sets of data. R<sup>2</sup> values of the validation for the lateral displacement and lateral stress reduction models were 98.57% and 93.72%, respectively.
- Probabilistic analysis using Monte Carlo simulations were conducted to quantify the uncertainties in lateral displacement and stress reductions due to variability in foundation soil strengths.
- A modified factor of safety against sliding was formulated as follows:

$$\text{Modified } FS_{(sliding)} = \frac{(W_1 + W_2 \dots + qa')[\tan(k\phi'_1)] + Bc'_a}{P_a (1 - SR)}$$

Where, SR = Lateral pressure reduction factor (always less than 1)

- Design steps for calculating the modified factor of safety against sliding when RPPs are used as shear keys were outlined with a demonstration of a calculation example.

Based on the performance monitoring results and further analyses, it can be concluded that the RPPs can be effectively used as shear keys in MSE walls. They can be incorporated at the wall base during design for improving the lateral resistance of MSE walls.

## 7.2 Recommendations for Future Studies

Based on the field study and analyses, the following recommendations are proposed for future studies:

- The study was conducted on field test sections which were prototypes of MSE walls. Further studies on actual MSE walls could corroborate the results of the current study and provide further insight into the performance of RPP reinforced MSE walls.



- Future field studies could consider taller wall heights which better reflect actual real-life scenarios.
- Even though the current study presented performance monitoring of almost two years, a longer study could indicate the long-term effectiveness of the RPP reinforcement mechanism.
- The finite element study was conducted on a two-dimensional platform. Better and more reliable results can be obtained if a three-dimensional study is undertaken.
- Finite element studies on the effects of climatic or environmental loading, such as rainfall and water pressure, can be performed.
- The group effect of RPPs in improving the lateral resistance needs to be quantified.
- Since the range of the predictor variables in the design models are limited, further analyses with a broad range of foundation soil properties could strengthen the current models.

## REFERENCES

1. AASHTO (2007). *AASHTO LRFD Bridge Design Specifications: SI Units (4th Edition)*. American Association of State Highway and Transportation Officials.
2. AASHTO (2014). *AASHTO LRFD Bridge Design Specifications (7th Edition)*. American Association of State Highway and Transportation Officials.
3. Abu-Hejleh, N., Wang, T., & Zornberg, J.G. (2000). Performance of geosynthetic-reinforced walls supporting bridge and approaching roadway structures. In *Advances in transportation and geoenvironmental systems using geosynthetics* (pp. 218-243).
4. Ahmadabadi, M., & Ghanbari, A. (2009). New procedure for active earth pressure calculation in retaining walls with reinforced cohesive-frictional backfill. *Geotextiles and Geomembranes*, 27(6), 456-463.
5. Ahmadi, H., & Bezuijen, A. (2018). Full-scale mechanically stabilized earth (MSE) walls under strip footing load. *Geotextiles and Geomembranes*, 46(3), 297-311.
6. Ahmed, A., Khan, S., Hossain, S., Sadigov, T., & Bhandari, P. (2020). Safety prediction model for reinforced highway slope using a machine learning method. *Transportation research record*, 2674(8), 761-773.
7. Ahmed, F.S. (2012). *Engineering Characteristics of Recycled Plastic Pin, Lumber and Bamboo for Soil Slope Stabilization*. Master's Thesis, The University of Texas at Arlington.
8. Allan Block (2016). Best Practices for Segmental Retaining Wall Design. <https://www.allanblock.com/engineers/global-stability.aspx#9.4>
9. Allen, T.M., Bathurst, R.J., & Bozorgzadeh, N. (2019). Probabilistic tensile strength analysis of steel strips in MSE walls considering corrosion. *Journal of Geotechnical and Geoenvironmental Engineering*, 145(5), 04019016.

10. Alzamora, D.E., & Anderson, S.A. (2009, January). Review of mechanically stabilized earth wall performance issues. In *Transportation Research Board (TRB), 2009 Annual Meeting CD-ROM*.
11. Ariema, F., & Butler, B.E. (1990). Embankment Foundations - Guide to Earthwork Construction. *Transportation Research Board, National Research Council, Washington, D.C.* pp. 59-73.
12. ASCE (2021). America's Infrastructure Scores a C-. 2021 Infrastructure Report Card, <<https://www.infrastructurereportcard.org/>> (April 02, 2021).
13. Ashour, M., Norris, G., & Pilling, P. (1998). Lateral loading of a pile in layered soil using the strain wedge model. *Journal of geotechnical and geoenvironmental engineering*, 124(4), 303-315.
14. ASTM D2166 / D2166M-16 (2016). *Standard Test Method for Unconfined Compressive Strength of Cohesive Soil*. ASTM International, West Conshohocken, PA.
15. ASTM D3080 / D3080M-11 (2011). *Standard Test Method for Direct Shear Test of Soils Under Consolidated Drained Conditions* (Withdrawn 2020). ASTM International, West Conshohocken, PA.
16. ASTM D4318-17e1 (2017). *Standard Test Methods for Liquid Limit, Plastic Limit, and Plasticity Index of Soils*. ASTM International, West Conshohocken, PA.
17. ASTM D4643-08 (2008). *Standard Test Method for Determination of Water (Moisture) Content of Soil by Microwave Oven Heating*. ASTM International, West Conshohocken, PA.
18. ASTM D6528-17 (2017). *Standard Test Method for Consolidated Undrained Direct Simple Shear Testing of Fine Grain Soils*. ASTM International, West Conshohocken, PA.

19. ASTM D6913 / D6913M-17 (2017). *Standard Test Methods for Particle-Size Distribution (Gradation) of Soils Using Sieve Analysis*. ASTM International, West Conshohocken, PA.
20. Atkinson, J. (2007). *The Mechanics of Soils and Foundations*. CRC Press.
21. Aubeny, C., Biscontin, G., Huang, J., Bin-Shafique, S., Dantal, V.S., & Sadat, R. (2014). *Design Parameters and Methodology for Mechanically Stabilized Earth (MSE) Walls* (No. FHWA/TX-14/0-6716-1). Texas A & M Transportation Institute.
22. Babu, G.S., Raja, J., Basha, B.M., & Srivastava, A. (2016). Forensic analysis of failure of retaining wall. In *Forensic Geotechnical Engineering* (pp. 451-465). Springer, New Delhi.
23. Badhon, F.F., & Islam, M.A. (2017). Effect of gradation on shear strength of sand. In the *International Conference on Engineering Research, Innovation and Education, Shahjalal University of Science and Technology, Sylhet, Bangladesh, Jan* (pp. 13-15).
24. Badhon, F.F., Zaman, M.N.B., Bhandari, P., Islam, M.A., & Hossain, M.S. (2021). Performance of Recycled Plastic Pins (RPP) for improving the bearing capacity of MSE wall foundation. *International Foundations Congress & Equipment Expo*, Dallas, Texas.
25. Baecher, G. (1987). *Geotechnical risk analysis user's guide*. FHWA/RD-87-011, Federal Highway Administration, McLean, Va.
26. Baecher, G.B., & Christian, J.T. (2003). *Reliability and Statistics in Geotechnical Engineering*. John Wiley & Sons.
27. Bang, S. (1985). Active earth pressure behind retaining walls. *Journal of Geotechnical Engineering*, 111(3), 407-412.

28. Bathurst, R.J., & Yu, Y. (2018). Probabilistic prediction of reinforcement loads for steel MSE walls using a response surface method. *International Journal of Geomechanics*, 18(5), 04018027.
29. Bathurst, R.J., Vlachopoulos, N., Walters, D.L., Burgess, P.G., & Allen, T.M. (2006). The influence of facing stiffness on the performance of two geosynthetic reinforced soil retaining walls. *Canadian Geotechnical Journal*, 43(12), 1225-1237.
30. Bathurst, R.J., Walters, D., Vlachopoulos, N., Burgess, P., & Allen, T.M. (2000). Full scale testing of geosynthetic reinforced walls. In *Advances in transportation and geoenvironmental systems using geosynthetics* (pp. 201-217).
31. Bell, J.R., Barrett, R.K., & Ruckman, A.C. (1983). Geotextile earth-reinforced retaining wall tests: Glenwood Canyon, Colorado. *Transportation Research Record* 916, 59-69.
32. Benjamim, C.V.S., Bueno, B.S., & Zornberg, J.G. (2007). Field monitoring evaluation of geotextile-reinforced soil-retaining walls. *Geosynthetics International*, 14(2), 100-118.
33. Berg, R.R., Christopher, B.R., & Samtani, N.C. (2009). *Design of Mechanically Stabilized Earth Walls and Reinforced Soil Slopes—Volume I* (No. FHWA-NHI-10-024).
34. Bhandari, P., Rauss, C., Sapkota, A., & Hossain, M.S. (2020). Long term performance of shallow slopes stabilized with recycled plastic pins. In *Geo-Congress 2020: Engineering, Monitoring, and Management of Geotechnical Infrastructure* (pp. 163-172). Reston, VA: American Society of Civil Engineers.
35. Bhandari, P., Timsina, S., Ahmed, A., Hossain, M.S., & Thian, B. (2019). Development of a strength prediction model for recycled base materials with soil

- intrusion. In *Geo-Congress 2019: Geotechnical Materials, Modeling, and Testing* (pp. 204-213). Reston, VA: American Society of Civil Engineers.
36. Bhandari, P., Zaman, M.N.B., Islam, M.A., Badhon, F.F., & Hossain, M.S. (2021). Increasing shearing resistance of MSE wall base using recycled plastic pins. *International Foundations Congress & Equipment Expo*, Dallas, Texas.
37. Bhuiyan, M.R.H. (2014). *Group Resistance of Recycled Plastic Pin in Sustainable Slope Stabilization*. Master's Thesis, The University of Texas at Arlington.
38. Bhuiyan, M.Z.I., Ali, F.H., Salman, F.A., & Siau, L.S. (2012, June). Influence of plastic pins on interface shear capacity of segmental retaining wall units. In *Proceedings of the 11th International Conference on Concrete Engineering and Technology (CONCET2012)* (pp. 12-13).
39. Bilgin, Ö., & Mansour, E. (2014). Effect of reinforcement type on the design reinforcement length of mechanically stabilized earth walls. *Engineering Structures*, 59, 663-673.
40. Bowders, J., Loehr, J., Salim, H., & Chen, C.W. (2003). Engineering properties of recycled plastic pins for slope stabilization. *Transportation Research Record: Journal of the Transportation Research Board*, (1849), 39-46.
41. Breslin, V.T., Senturk, U., & Berndt, C.C. (1998). Long-term engineering properties of recycled plastic lumber used in pier construction. *Resources, Conservation and Recycling*, 23(4), 243-258.
42. Briançon, L., & Simon, B. (2012). Performance of pile-supported embankment over soft soil: full-scale experiment. *Journal of Geotechnical and Geoenvironmental Engineering*, 138(4), 551-561.

43. Brown, A.C., Dellinger, G., Helwa, A., El-Mohtar, C., Zornberg, J., & Gilbert, R.B. (2015). Monitoring a drilled shaft retaining wall in expansive clay: long-term performance in response to moisture fluctuations. In *IFCEE 2015* (pp. 1348-1357).
44. Budge, A.S., Bay, J.A., & Anderson, L.R. (2006). Calibrating vertical deformations in a finite element model of an MSE wall. In *GeoCongress 2006: Geotechnical Engineering in the Information Technology Age* (pp. 1-5).
45. Chalermyanont, T. (2002). *Reliability Analysis of Mechanically Stabilized Earth (MSE) Walls*. Doctoral Dissertation, University of Wisconsin-Madison.
46. Chalermyanont, T., & Benson, C.H. (2004). Reliability-based design for internal stability of mechanically stabilized earth walls. *Journal of Geotechnical and Geoenvironmental Engineering*, 130(2), 163-173.
47. Chalermyanont, T., & Benson, C.H. (2005). Reliability-based design for external stability of mechanically stabilized earth walls. *International Journal of Geomechanics*, 5(3), 196-205.
48. Chang, M.F. (1997). Lateral earth pressures behind rotating walls. *Canadian Geotechnical Journal*, 34(4), 498-509.
49. Chen, C.W., Salim, H., Bowders, J.J., Loehr, J.E., & Owen, J. (2007). Creep behavior of recycled plastic lumber in slope stabilization applications. *Journal of materials in civil engineering*, 19(2), 130-138.
50. Chen, R.P., Xu, Z.Z., Chen, Y.M., Ling, D.S., & Zhu, B. (2010). Field tests on pile-supported embankments over soft ground. *Journal of Geotechnical and Geoenvironmental Engineering*, 136(6), 777-785.
51. Chowdhury, M.E., Islam, M.A., Islam, T., & Khan, N. (2018). Evaluation of shear strength of cohesionless soil from maximum, minimum dry density and fines content

- using polynomial surface fitting method. *Electronic Journal of Geotechnical Engineering*, 23(1), 31-56.
52. Christopher, B.R., Gill, S., Giroud, J.P., Juran, I., Mitchell, J.K., Schlosser, F., & Dunicliff, J. (1990). *Reinforced Soil Structures. Volume I, Design and Construction Guidelines* (No. FHWA-RD-89-043). United States. Federal Highway Administration.
53. Clough, G.W., & Duncan, J.M. (1991). Earth Pressures. In *Foundation engineering handbook* (pp. 223-235). Springer, New York.
54. Cubrinovski, M., Kokusho, T., & Ishihara, K. (2006). Interpretation from large-scale shake table tests on piles undergoing lateral spreading in liquefied soils. *Soil Dynamics and Earthquake Engineering*, 26(2-4), 275-286.
55. Damians, I.P., Bathurst, R.J., Josa, A., & Lloret, A. (2014). Numerical analysis of an instrumented steel-reinforced soil wall. *International Journal of Geomechanics*, 15(1), 04014037.
56. Dantal, V.S. (2013). *Material Characterization and Design Recommendations for Mechanically Stabilized Earth Retaining Walls*. Doctoral Dissertation, Texas A&M University.
57. Das, B.M. (2015). *Principles of Foundation Engineering*. Cengage learning.
58. Delphia, J.G. (2011). Presentation titled "MSE Wall Case Studies." <<https://static.tti.tamu.edu/conferences/tsc12/presentations/structhydraulics/delphia.pdf>>.
59. Duncan, J.M. (2000). Factors of safety and reliability in geotechnical engineering. *Journal of geotechnical and geoenvironmental engineering*, 126(4), 307-316.
60. Duncan, J.M., Williams, G.W., Sehn, A.L., & Seed, R.B. (1991). Estimation earth pressures due to compaction. *Journal of geotechnical engineering*, 117(12), 1833-1847.



61. Ehrlich, M., Mirmoradi, S.H., & Saramago, R.P. (2012). Evaluation of the effect of compaction on the behavior of geosynthetic-reinforced soil walls. *Geotextiles and Geomembranes*, 34, 108-115.
62. Elias, V., Christopher, B.R., & Berg, R.R. (2001). *Mechanically Stabilized Earth Walls and Reinforced Soil Slopes Design and Construction Guidelines*. (No. FHWA-NHI-00-043).
63. Elsayy, M.B., & El-Garhy, B. (2017). Performance of granular piles-improved soft ground under raft foundation: a numerical study. *International Journal of Geosynthetics and Ground Engineering*, 3(4), 36.
64. Fan, C.C., & Long, J.H. (2005). Assessment of existing methods for predicting soil response of laterally loaded piles in sand. *Computers and Geotechnics*, 32(4), 274-289.
65. Fang, Y.S., & Ishibashi, I. (1986). Static earth pressures with various wall movements. *Journal of Geotechnical Engineering*, 112(3), 317-333.
66. Fang, Y.S., Chen, J.M., & Chen, C.Y. (1997). Earth pressures with sloping backfill. *Journal of Geotechnical and Geoenvironmental Engineering*, 123(3), 250-259.
67. Fang, Y.S., Chen, T.J., & Wu, B. F. (1994). Passive earth pressures with various wall movements. *Journal of Geotechnical Engineering*, 120(8), 1307-1323.
68. Fang, Y.S., Ho, Y.C., & Chen, T.J. (2002). Passive earth pressure with critical state concept. *Journal of Geotechnical and Geoenvironmental Engineering*, 128(8), 651-659.
69. Faysal, M. (2017). *Structural Competency and Environmental Soundness of the Recycled Base Materials in North Texas*. Doctoral Dissertation, The University of Texas at Arlington.

70. Gautam, S., Hoyos, L.R., He, S., Prabakar, S., & Yu, X. (2020). Chemical treatment of a highly expansive clay using a liquid ionic soil stabilizer. *Geotechnical and Geological Engineering*, 38, 4981-4993.
71. Geo Studio (2020). *Stability Modeling with GeoStudio*. Geoslope, Calgary, AB, Canada.
72. Han, J., & Gabr, M.A. (2002). Numerical analysis of geosynthetic-reinforced and pile-supported earth platforms over soft soil. *Journal of geotechnical and geoenvironmental engineering*, 128(1), 44-53.
73. Han, J., Bhandari, A., & Wang, F. (2011). DEM analysis of stresses and deformations of geogrid-reinforced embankments over piles. *International Journal of Geomechanics*, 12(4), 340-350.
74. Hansen, J.B. (1961). The ultimate resistance of rigid piles against transversal forces. *Danish Geotechnical Institute, Bulletin*, 12, Copenhagen, Denmark.
75. Hewlett, W.J., & Randolph, M.F. (1988). Analysis of piled embankment. *Ground Engineering*, Vol. 21, n 3.
76. Horpibulsuk, S., Suksiripattanapong, C., Niramitkornburee, A., Chinkulkijniwat, A., & Tangsutthinon, T. (2011). Performance of an earth wall stabilized with bearing reinforcements. *Geotextiles and Geomembranes*, 29(5), 514-524.
77. Horvath, J.S. (1991). Effect of footing shape on behavior of cantilever retaining wall. *Journal of geotechnical engineering*, 117(6), 973-978.
78. Hossain, M.S., Kibria, G., Khan, M.S., Hossain, J., & Taufiq, T. (2012). Effects of backfill soil on excessive movement of MSE wall. *Journal of Performance of Constructed Facilities*, 26(6), 793-802.
79. Hossain, S., Khan, S., & Kibria, G. (2017). *Sustainable Slope Stabilization Using Recycled Plastic Pins*. The Netherlands: CRC Press/Balkema.

80. <https://keystonewalls.com/application/files/7815/0957/6342/GlobalStability.pdf>
81. Huang, J., Han, J., Parsons, R.L., & Pierson, M.C. (2013). Refined numerical modeling of a laterally-loaded drilled shaft in an MSE wall. *Geotextiles and Geomembranes*, 37, 61-73.
82. Imtiaz, T., Ahmed, A., Hossain, M.S., & Faysal, M. (2020). Microstructure analysis and strength characterization of recycled base and sub-base materials using scanning electron microscope. *Infrastructures*, 5(9), 70.
83. Islam, M.A., Hossain, M.S., Badhon, F.F., & Bhandari, P. (2021a). Performance evaluation of recycled plastic pin supported embankment over soft soil. *Journal of Geotechnical and Geoenvironmental Engineering*, 147(6).
84. Islam, M.A., Islam, M.S., Chowdhury, M.E., & Badhon, F.F. (2021b). Influence of vetiver grass (*Chrysopogon zizanioides*) on infiltration and erosion control of hill slopes under simulated extreme rainfall condition in Bangladesh. *Arabian Journal of Geosciences*, 14(2), 1-14.
85. Islam, M.A., Zaman, M.N.B., Badhon, F.F., Bhandari, P., & Hossain, M.S. (2021c). Numerical modeling of recycled plastic pin reinforced embankment over soft soils. *International Foundations Congress & Equipment Expo*, Dallas, Texas.
86. Islam, M.S., & Badhon, F.F. (2020). A mathematical model for shear strength prediction of vetiver rooted soil. In *Geo-Congress 2020: Engineering, Monitoring, and Management of Geotechnical Infrastructure* (pp. 96-105). Reston, VA: American Society of Civil Engineers.
87. Jamal, H. (2017). Earth Pressure Coefficients – Types, Concept and Theory. <https://www.aboutcivil.org/earth-pressure.html>

88. Jiang, Y., Han, J., Parsons, R.L., & Brennan, J.J. (2016). Field instrumentation and evaluation of modular-block MSE walls with secondary geogrid layers. *Journal of Geotechnical and Geoenvironmental Engineering*, 142(12), 05016002.
89. Jiang, Y., Han, J., Parsons, R.L., & Cai, H. (2015). Field monitoring of mechanically stabilized earth walls to investigate secondary reinforcement effects (No. KS-15-09). *Kansas Department of Transportation, Bureau of Research, USA*.
90. Khan, M.S. (2014). *Sustainable Slope Stabilization Using Recycled Plastic Pin in Texas*. Doctoral Dissertation, The University of Texas at Arlington.
91. Khan, M.S., Hossain, S., & Kibria, G. (2016). Slope stabilization using recycled plastic pins. *Journal of Performance of Constructed Facilities*, 30(3), 04015054.
92. Kibria, G. (2014). *Evaluation of Physico-Mechanical Properties of Clayey Soils Using Electrical Resistivity Imaging Technique*. Doctoral Dissertation, The University of Texas at Arlington.
93. Kibria, G., Hossain, M.S., & Khan, M.S. (2014). Influence of soil reinforcement on horizontal displacement of MSE wall. *International Journal of Geomechanics*, 14(1), 130-141.
94. Kim, H.S., & Bilgin, Ö. (2007). Studying the effect of concrete key size on mechanically stabilized earth wall deformations using finite element method. In *Computer Applications in Geotechnical Engineering* (pp. 1-8).
95. Koerner, R.M., & Koerner, G.R. (2013). A data base, statistics and recommendations regarding 171 failed geosynthetic reinforced mechanically stabilized earth (MSE) walls. *Geotextiles and Geomembranes*, 40, 20-27.
96. Koerner, R.M., & Soong, T.Y. (2001). Geosynthetic reinforced segmental retaining walls. *Geotextiles and geomembranes*, 19(6), 359-386.

97. Krishnaswamy, P., & Francini, R., (2000). Long Term Durability of Recycled Plastic Lumber in Structural Application. <http://www.environmental-expert.com/Files/0/articles/2183/2183.pdf> July 12, 2019.
98. Kutner, M.H., Nachtsheim, C.J., Neter, J., & Li, W. (2005). *Applied Linear Statistical Model*. 5th Ed., McGraw-Hill, New York.
99. Lampo, R., & Nosker, T.J. (1997). Development and testing of plastic lumber materials for construction applications. US Army Corps of Engineers, Construction Engineering Research Laboratories, USACERL Technical Report 97/95.
100. Leshchinsky, D., & Han, J. (2004). Geosynthetic reinforced multitiered walls. *Journal of Geotechnical and Geoenvironmental Engineering*, 130(12), 1225-1235.
101. Lin, B.H., Yu, Y., Bathurst, R.J., & Liu, C.N. (2016). Deterministic and probabilistic prediction of facing deformations of geosynthetic-reinforced MSE walls using a response surface approach. *Geotextiles and Geomembranes*, 44(6), 813-823.
102. Liu, H. (2012). Long-term lateral displacement of geosynthetic-reinforced soil segmental retaining walls. *Geotextiles and Geomembranes*, 32, 18-27.
103. Loehr, J.E., & Bowders, J.J. (2007). Slope Stabilization using Recycled Plastic Pins – Phase III, Final Report: RI98-007D, Missouri Department of Transportation, Jefferson City, Missouri.
104. Loehr, J.E., Bowders, J.J., Owen, J., Sommers, L., & Liew, W. (2000). Stabilization of slopes using recycled plastic pins. In *Journal of the Transportation Research Board* (Vol. 1714, pp. 1-8). National Academy Press.
105. Mahmood, T. (2009). *Failure Analysis of a Mechanically Stabilized Earth (MSE) Wall Using Finite Element Program PLAXIS*. Master's Thesis, The University of Texas at Arlington.

106. Malcolm, G.M. (1995). Recycled plastic lumber and shapes design and specifications. *Proc. Structures congress 13, Boston, Massachusetts*, April 2-5, 1995.
107. Mei, G., Chen, Q., & Song, L. (2009). Model for predicting displacement-dependent lateral earth pressure. *Canadian Geotechnical Journal*, 46(8), 969-975.
108. Meyerhof, G.G., Sastry, V.V.R.N., & Yalcin, A.S. (1988). Lateral resistance and deflection of flexible piles. *Canadian Geotechnical Journal*, 25(3), 511-522.
109. Michhimer, T., Parra, J.R., & Williamson, T. (2009). Instrumentation and monitoring of MSE walls supported on the rammed aggregate pier system. In *Contemporary Topics in Ground Modification, Problem Soils, and Geo-Support* (pp. 337-344).
110. Mirmoradi, S.H., & Ehrlich, M. (2017). Effects of facing, reinforcement stiffness, toe resistance, and height on reinforced walls. *Geotextiles and Geomembranes*, 45(1), 67-76.
111. Mochizuki, K., Hiroyama, T., Morita, Y., & Sakamaki, A. (1980). Lateral deformation of soft ground – case of Kurasiki. *Proc. 15th Japan National Conference on Soil Mechanics and Foundation Engineering, E-2*. 216, pp. 861-864.
112. Ni, P., Song, L., Mei, G., & Zhao, Y. (2018). On predicting displacement-dependent earth pressure for laterally loaded piles. *Soils and foundations*, 58(1), 85-96.
113. Oh, Y.I., & Shin, E.C. (2007). Reinforcement and arching effect of geogrid-reinforced and pile-supported embankment on marine soft ground. *Marine Georesources and Geotechnology*, 25(2), 97-118.
114. Onodera, S., Fukuda, N., & Nakane, A. (2004). Long-term behavior of geogrid reinforced soil walls. *Proceedings of GeoAsia*, 225-264.

115. Ortiz, I.S. (1967). Zumpango test embankment. *Journal of the Soil Mechanics and Foundations Division*, 93(4), 199-209.
116. Passe, P.D. (2000). *Mechanically Stabilized Earth Wall Inspector's Handbook*. State of Florida, Department of Transportation.
117. Phoon, K. (1995). *Reliability-Based Design of Foundations for Transmission Line Structures*. Doctoral Dissertation, Cornell University.
118. Pierson, M.C., Parsons, R.L., Han, J., Brennan, J.J., & Huang, J. (2011). Influence of geogrid stiffness on shaft lateral capacities and deflections behind an MSE wall. In *Geo-Frontiers 2011: Advances in Geotechnical Engineering* (pp. 3756-3765).
119. Plaxis (2020). *PLAXIS 2D Reference Manual*. Delft University of Technology and Plaxis, Delft, Netherlands.
120. Prasad, Y.V., & Chari, T.R. (1999). Lateral capacity of model rigid piles in cohesionless soils. *Soils and Foundations*, 39(2), 21-29.
121. Pudasaini, B., & Shahandashti, M. (2020). Topological surrogates for computationally efficient seismic robustness optimization of water pipe networks. *Computer-Aided Civil and Infrastructure Engineering*, 35(10), 1101-1114.
122. Pudasaini, B., & Shahandashti, S.M. (2018). Identification of critical pipes for proactive resource-constrained seismic rehabilitation of water pipe networks. *Journal of Infrastructure Systems*, 24(4), 04018024.
123. Pudasaini, B., Shahandashti, S.M., & Razavi, M. (2017). Identifying critical links in water supply systems subject to various earthquakes to support inspection and renewal decision making. *Computing in Civil Engineering 2017, American Society of Civil Engineers, Reston, VA*, 231–238.

124. Rollins, K.M., & Sparks, A. (2002). Lateral resistance of full-scale pile cap with gravel backfill. *Journal of Geotechnical and Geoenvironmental Engineering*, 128(9), 711-723.
125. Rollins, K.M., Price, J.S., & Bischoff, J. (2011). Lateral resistance of piles near vertical MSE abutment walls. In *Geo-Frontiers 2011: Advances in Geotechnical Engineering* (pp. 3526-3535).
126. Rollins, K.M., Snyder, J.L., & Walsh, J.M. (2010). Increased lateral resistance of pile group in clay using compacted fill. In *GeoFlorida 2010: Advances in Analysis, Modeling & Design* (pp. 1602-1611).
127. Rouili, A., Djerbib, Y., & Touahmia, M. (2005). Numerical modeling of an L-shaped very stiff concrete retaining wall. *Sciences & Technologie. B, Sciences de l'ingénieur*, (24), 69-74.
128. Rowe, R.K., & Ho, S.K. (1998). Horizontal deformation in reinforced soil walls. *Canadian Geotechnical Journal*, 35(2), 312–327.
129. RStudio Team (2021). RStudio: Integrated Development Environment for R. RStudio (Version 1.4.1103) [Computer software], PBC, Boston, MA.
130. Sadat, M.R., Huang, J., Bin-Shafique, S., & Rezaeimalek, S. (2018). Study of the behavior of mechanically stabilized earth (MSE) walls subjected to differential settlements. *Geotextiles and Geomembranes*, 46(1), 77-90.
131. Salman, H., Jenkins, J., & Vedantham, R. (2017). Column-supported embankments and MSE walls in Grapevine, Texas. In *Geotechnical Frontiers 2017* (pp. 74-83).
132. Sankey, J.E., & Soliman, A. (2004). Tall wall mechanically stabilized earth applications. In *Geotechnical Engineering for Transportation Projects* (pp. 2149-2158).



133. Sapkota, A. (2019). *Effect of Modified Moisture Barriers on Slopes Stabilized with Recycled Plastic Pins*. Doctoral Dissertation, The University of Texas at Arlington.
134. Sarath, N., Shivashankar, R., & Shankar, A.R. (2011). Role of shear keys in cantilever retaining wall. *Proceedings of Indian Geotechnical Conference December 15-17, 2011, Kochi (Paper No. K-056)*.
135. Sastry, V.V.R.N., & Meyerhof, G.G. (1990). Behaviour of flexible piles under inclined loads. *Canadian Geotechnical Journal*, 27(1), 19-28.
136. Sastry, V.V.R.N., & Meyerhof, G.G. (1994). Behaviour of flexible piles in layered sands under eccentric and inclined loads. *Canadian Geotechnical Journal*, 31(4), 513-520.
137. Sawwaf, M.E. (2006). Lateral resistance of single pile located near geosynthetic reinforced slope. *Journal of geotechnical and geoenvironmental engineering*, 132(10), 1336-1345.
138. Sayed, S., Dodagoudar, G.R., & Rajagopal, K. (2010). Finite element reliability analysis of reinforced retaining walls. *Geomechanics and Geoengineering: An International Journal*, 5(3), 187-197.
139. Schmidt, J.M., & Harpstead, D.L. (2011). *MSE Wall Engineering—A New Look at Contracting, Design, and Construction*.
140. Shahandashti, S.M., & Pudasaini, B. (2019). Proactive seismic rehabilitation decision-making for water pipe networks using simulated annealing. *Natural Hazards Review*, 20(2), 04019003.
141. Shahidehpour, M., Liu, X., Li, Z., & Cao, Y. (2016). Microgrids for enhancing the power grid resilience in extreme conditions. *IEEE Transactions on Smart Grid*, 8(2), 1–1.

142. Singh, V.P., & Babu, G.S. (2010). 2D numerical simulations of soil nail walls. *Geotechnical and Geological Engineering*, 28(4), 299-309.
143. Stark, T.D., Handy, R., & Lustig, M. (2019). MSE wall global stability and lesson learned. In *Eighth International Conference on Case Histories in Geotechnical Engineering (Geo-Congress 2019) American Society of Civil Engineers*, 277-289.
144. Sterbenz, J.P.G., Hutchison, D., Çetinkaya, E.K., Jabbar, A., Rohrer, J.P., Schöller, M., & Smith, P. (2010). Resilience and survivability in communication networks: Strategies, principles, and survey of disciplines. *Computer Networks, Elsevier B.V.*, 54(8), 1245–1265.
145. Stevens, J. (1996). *Applied Multivariate Statistics for the Social Sciences*. Lawrence Erlbaum Associates, Inc., New Jersey.
146. Stuedlein, A.W., Bailey, M., Lindquist, D., Sankey, J., & Neely, W.J. (2010). Design and performance of a 46-m-high MSE wall. *Journal of Geotechnical and Geoenvironmental Engineering*, 136(6), 786-796.
147. Stuedlein, A.W., Mikkelsen, P.E., & Bailey, M.J. (2007). Instrumentation and performance of the third runway north MSE wall at Seattle-Tacoma International Airport. In *7<sup>th</sup> FMGM 2007: Field Measurements in Geomechanics* (pp. 1-14).
148. Suzuki, O. (1988). The lateral flow of soil caused by banking on soft clay ground. *Soils and foundations*, 28(4), 1-18.
149. Tamrakar, S. (2015). *Slope Stabilization and Performance Monitoring of I-35 and SH-183 Slopes Using Recycled Plastic Pins*. Master's Thesis, The University of Texas at Arlington.
150. Tex-132-E (1999). Test Procedure for Texas Cone Penetration. Texas Department of Transportation, Austin, Texas.

151. Timsina, S., Bhandari, P., Zaman, M.N.B., Ahmed, A., Hossain, M.S., & Thian, B. (2019). Effect of fine clay particles on the strength characterization of cement treated flex-base materials. In *Geo-Congress 2019: Geotechnical Materials, Modeling, and Testing* (pp. 382-390). Reston, VA: American Society of Civil Engineers.
152. TxDOT (2014). Item 423: Retaining walls. In *Standard Specifications for Construction and Maintenance of Highways, Streets, and Bridges*, Texas Department of Transportation, Austin, Texas.
153. TxDOT (2018). *Geotechnical manual*. Texas Department of Transportation, Austin, Texas.
154. Van Ness, K.E., Nosker, T.L., Renfree, R.W., & Killion, J.R., (1998) Long term creep of commercially produced plastic lumber. *SPEANTEC'98: Conference Proceedings, Brookfield, CN, 26 April 1998*. p. 2916–20.
155. Vidal, H. (1966). “La terre armée.” *Annales de l'Institut Technique du Batiment et des Travaux Publics*. In: Série Matériaux 30, Supplement Nos. 223-239, July-August 1966, pp. 888-938.
156. Vidal, H. (1969b). The principal of reinforced Earth. *Highway Engineering Record* (282), 1-16.
157. Vidal, H. (1970). Reinforced Earth steel retaining wall. *Civil Engineering, ASCE* 40(2), 72-73.
158. Yang, K.H., Ching, J., & Zornberg, J.G. (2010). Reliability-based design for external stability of narrow mechanically stabilized earth walls: calibration from centrifuge tests. *Journal of geotechnical and geoenvironmental engineering*, 137(3), 239-253.

159. Yu, Y., & Bathurst, R. J. (2017). Probabilistic assessment of reinforced soil wall performance using response surface method. *Geosynthetics International*, 24(5), 524-542.
160. Zaman, M.N.B. (2019). *Sustainable Ground Improvement Method Using Recycled Plastic Pins*. Doctoral Dissertation, The University of Texas at Arlington.
161. Zhao, M., Liu, C., El-Korchi, T., Song, H., & Tao, M. (2019). Performance of geogrid-reinforced and PTC pile-supported embankment in a highway widening project over soft soils. *Journal of Geotechnical and Geoenvironmental Engineering*, 145(11), 06019014.

## APPENDIX A

### Soil Borelogs

<b>Logo</b> uta	<b>SR_4x3</b>	<b>BORING NUMBER BH1-SR_01</b> PAGE 1 OF 1
CLIENT <u>TxDOT</u>	PROJECT NAME <u>Lateral</u>	
PROJECT NUMBER _____	PROJECT LOCATION <u>Hunter Ferrell Landfill, Irving, TX</u>	
DATE STARTED <u>3/20/19</u> COMPLETED <u>3/20/19</u>	GROUND ELEVATION _____	HOLE SIZE <u>6</u>
DRILLING CONTRACTOR _____	GROUND WATER LEVELS:	
DRILLING METHOD <u>Hollow Stem Auger</u>	AT TIME OF DRILLING <u>---</u>	
LOGGED BY <u>Prabesh Bhandari</u> CHECKED BY _____	▼ AT END OF DRILLING <u>10.20 ft</u>	
NOTES _____	AFTER DRILLING <u>---</u>	

GEOTECH.BH.COLUMNS - GINT STD US GDT - 3/31/19 20:44 - C:\USERS\PKB3319\ONE\DRIVE - UNIVERSITY OF TEXAS AT ARLINGTON\INSTALLATION\DRILLING\PRABESH LATERAL GINT.GPJ

DEPTH (ft)	GRAPHIC LOG	MATERIAL DESCRIPTION	SAMPLE TYPE NUMBER	BLOW COUNTS (N VALUE)	MOISTURE CONTENT (%)
0					
5		Dark Brown	ST SPT	7-4 (11)	10.58%
10		Dark Grey	ST SPT	8-7 (15)	12.72%
15		Brown	ST SPT	29-22 (51)	10.06%
20		Grey; Shale	ST SPT	35-35 (70)	21.93%
Bottom of borehole at 20.0 feet.					

Logo uta

# SR\_4x2

**BORING NUMBER BH2-SR\_02**

PAGE 1 OF 1

CLIENT TxDOT PROJECT NAME Lateral  
 PROJECT NUMBER \_\_\_\_\_ PROJECT LOCATION Hunter Ferrell Landfill, Irving, TX  
 DATE STARTED 3/20/19 COMPLETED 3/20/19 GROUND ELEVATION \_\_\_\_\_ HOLE SIZE 6  
 DRILLING CONTRACTOR \_\_\_\_\_ GROUND WATER LEVELS: \_\_\_\_\_  
 DRILLING METHOD Hollow Stem Auger AT TIME OF DRILLING ---  
 LOGGED BY Prabesh Bhandari CHECKED BY \_\_\_\_\_ AT END OF DRILLING 12.00 ft  
 NOTES \_\_\_\_\_ AFTER DRILLING ---

GEO TECH BH COLUMNS - GINT STD US GDT - 3/31/19 20:44 - C:\USERS\PIXB331\PIBONE\DRIVE - UNIVERSITY OF TEXAS AT ARLINGTON\INSTALLATION\DRILLING\PRABESH\LATERAL-GINT.GPJ

DEPTH (ft)	GRAPHIC LOG	MATERIAL DESCRIPTION	SAMPLE TYPE NUMBER	BLOW COUNTS (N VALUE)	MOISTURE CONTENT (%)
0					
5		Dark Grey	ST SPT	4-4 (8)	19.76%
10		Dark Grey	ST SPT	7-6 (13)	20.74%
15		Brown; Clay with sand and gravel			13.14%
		Grey; Shale	SS	8-10-6/0"	16.75%
20			ST	35-35 (70)	
Bottom of borehole at 20.0 feet.					

Logo uta



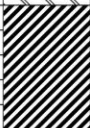

# SR\_6x3

**BORING NUMBER BH3-SR\_03**

PAGE 1 OF 1

CLIENT TxDOT PROJECT NAME Lateral  
 PROJECT NUMBER \_\_\_\_\_ PROJECT LOCATION Hunter Ferrell Landfill, Irving, TX  
 DATE STARTED 3/20/19 COMPLETED 3/20/19 GROUND ELEVATION \_\_\_\_\_ HOLE SIZE 6  
 DRILLING CONTRACTOR \_\_\_\_\_ GROUND WATER LEVELS: \_\_\_\_\_  
 DRILLING METHOD Hollow Stem Auger AT TIME OF DRILLING ---  
 LOGGED BY Prabesh Bhandari CHECKED BY \_\_\_\_\_ AT END OF DRILLING 9.30 ft  
 NOTES \_\_\_\_\_ AFTER DRILLING ---

G:\GEO\BH\COLUMNS - GINT STD US GDT - 3/20/19 2:44 - C:\USERS\PRABESH\BANDARI\GINT\PRABESH\LATERAL - GINT.GPJ

DEPTH (ft)	GRAPHIC LOG	MATERIAL DESCRIPTION	SAMPLE TYPE NUMBER	BLOW COUNTS (N VALUE)	MOISTURE CONTENT (%)
0					
5		Dark Brown	ST SPT	4-4 (8)	11.04%
10		Dark Brown	ST SPT	3-4 (7)	19.19%
15		Dark Brown	ST SPT	35-35 (70)	13.53%
20		Dark Grey; Shale			17.87%

Bottom of borehole at 20.0 feet.



Logo uta


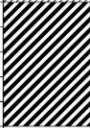


# SC\_Control

**BORING NUMBER BH4-SC\_01**

PAGE 1 OF 1

CLIENT TxDOT PROJECT NAME Lateral  
 PROJECT NUMBER \_\_\_\_\_ PROJECT LOCATION Hunter Ferrell Landfill, Irving, TX  
 DATE STARTED 3/20/19 COMPLETED 3/20/19 GROUND ELEVATION \_\_\_\_\_ HOLE SIZE 6  
 DRILLING CONTRACTOR \_\_\_\_\_ GROUND WATER LEVELS:  
 DRILLING METHOD Hollow Stem Auger AT TIME OF DRILLING ---  
 LOGGED BY Prabesh Bhandari CHECKED BY \_\_\_\_\_ AT END OF DRILLING 8.50 ft  
 NOTES \_\_\_\_\_ AFTER DRILLING ---

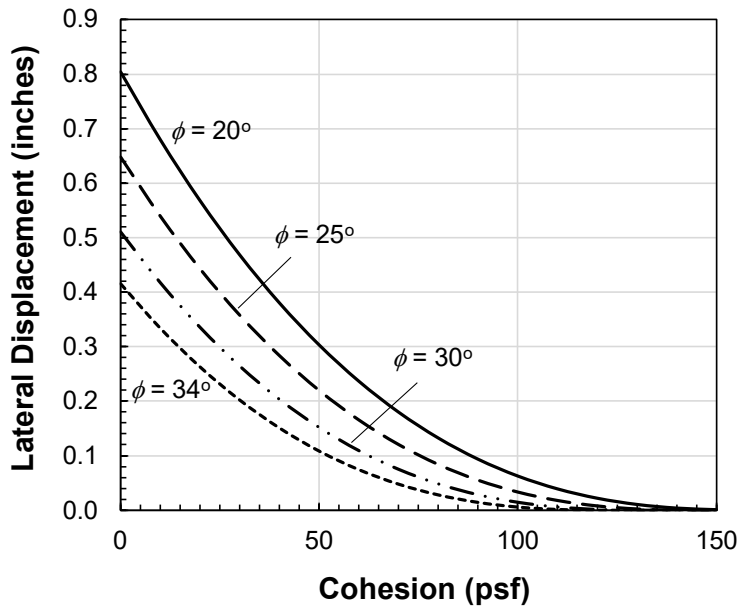
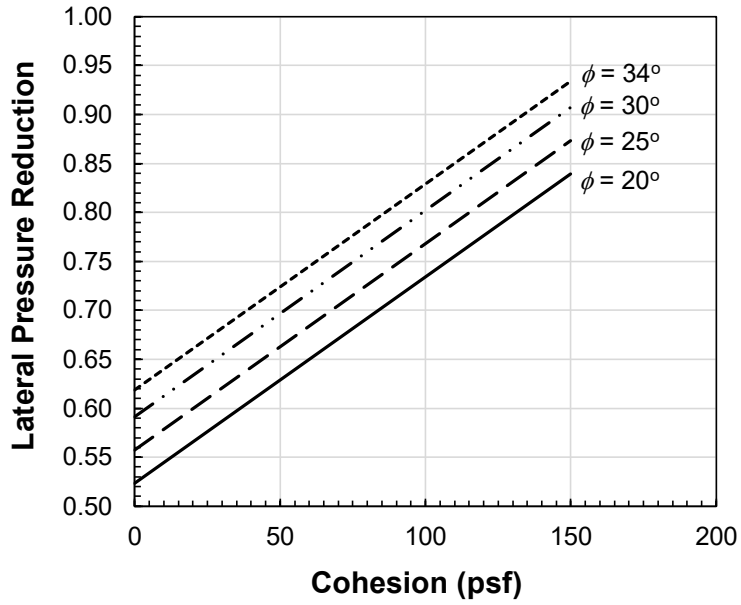
GEO TECH BH COLUMNS - GINT STD US GDT - 3/31/19 20:44 - C:\USERS\PIXB331\90\ONE\DRIVE - UNIVERSITY OF TEXAS AT ARLINGTON\INSTALLATION\DRILLING\PRABESH\LATERAL-GINT.GPJ

DEPTH (ft)	GRAPHIC LOG	MATERIAL DESCRIPTION	SAMPLE TYPE NUMBER	BLOW COUNTS (N VALUE)	MOISTURE CONTENT (%)
0					
5		Dark Grey	ST SPT	2-2 (4)	14.88%
10		Dark Grey			14.05%
15		Grey; Shale	SS	3-3-8/0"	
20		Grey; Shale	SS ST SPT	3-10-20/0"	22.02%
				35-35 (70)	24.29%

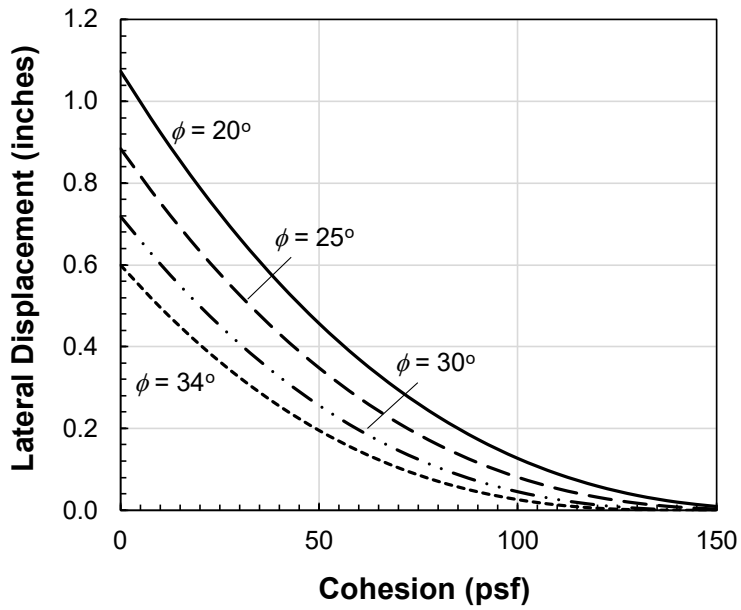
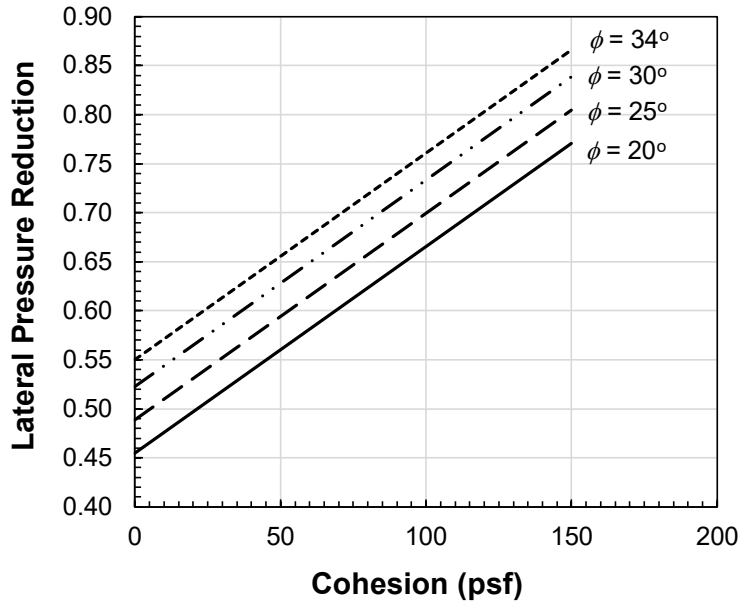
Bottom of borehole at 20.0 feet.

## APPENDIX B

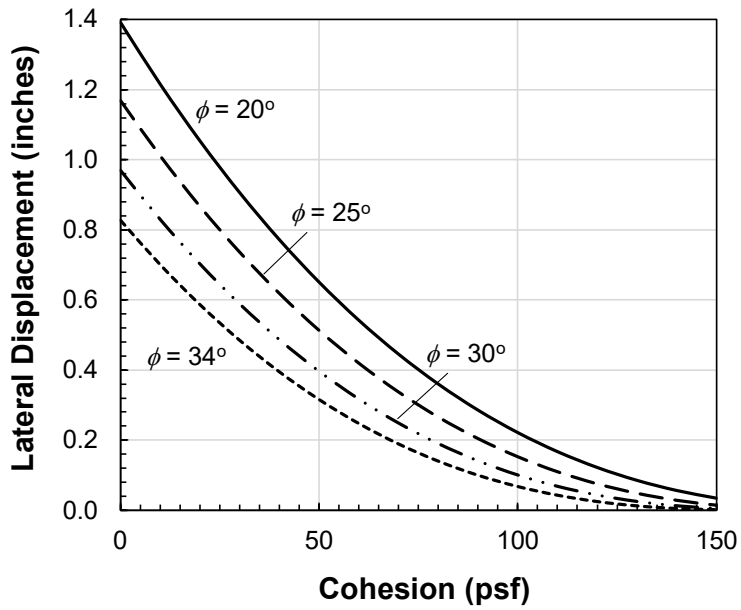
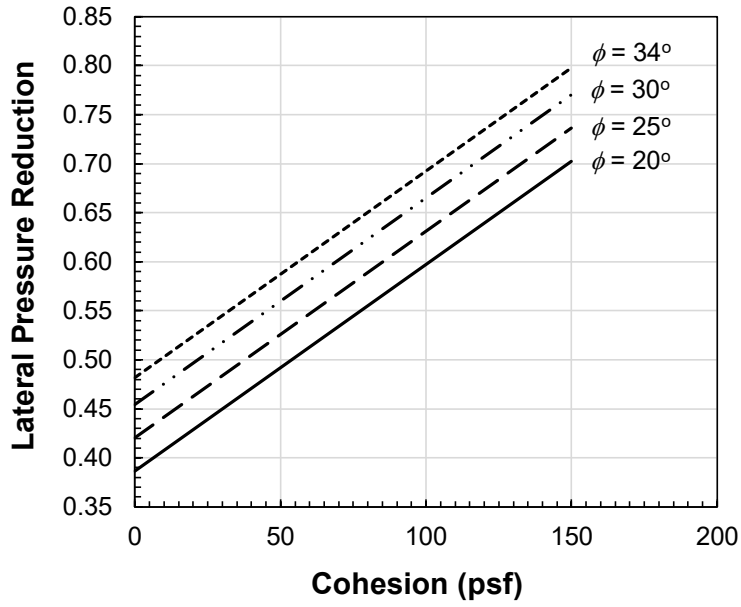
### Design Charts



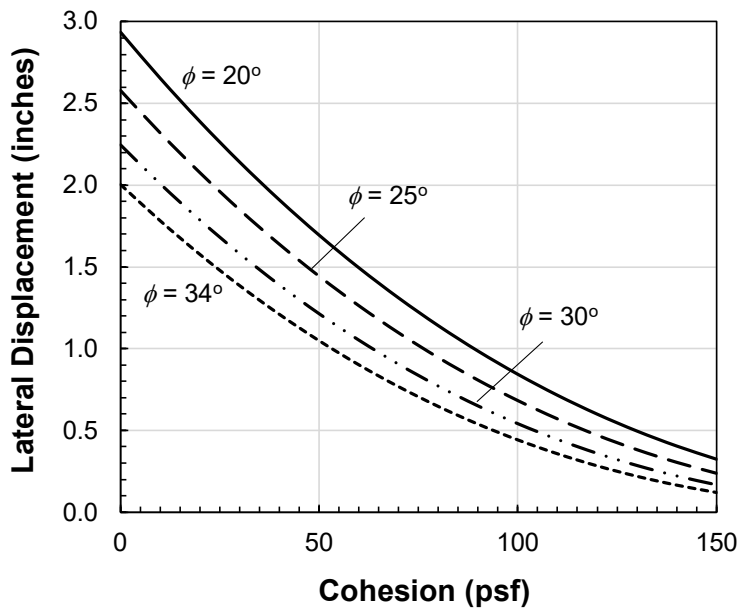
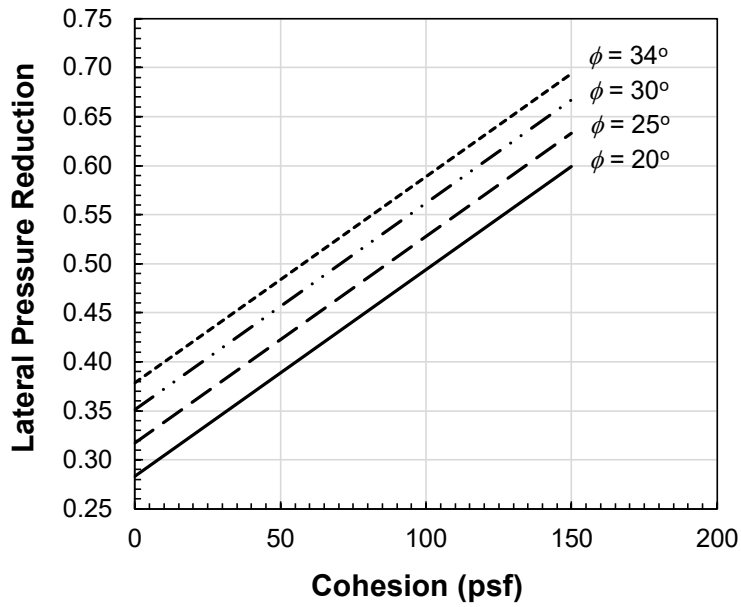
Lateral Pressure Reduction and Lateral Displacement Charts for  
 Wall Height = 5 ft.; RPP Size = 4x4 inches; RPP Spacing = 2 ft. c/c



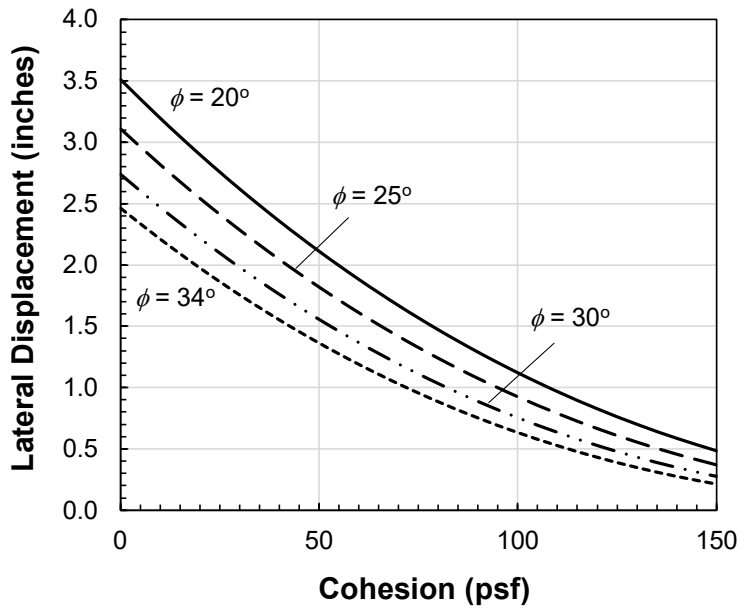
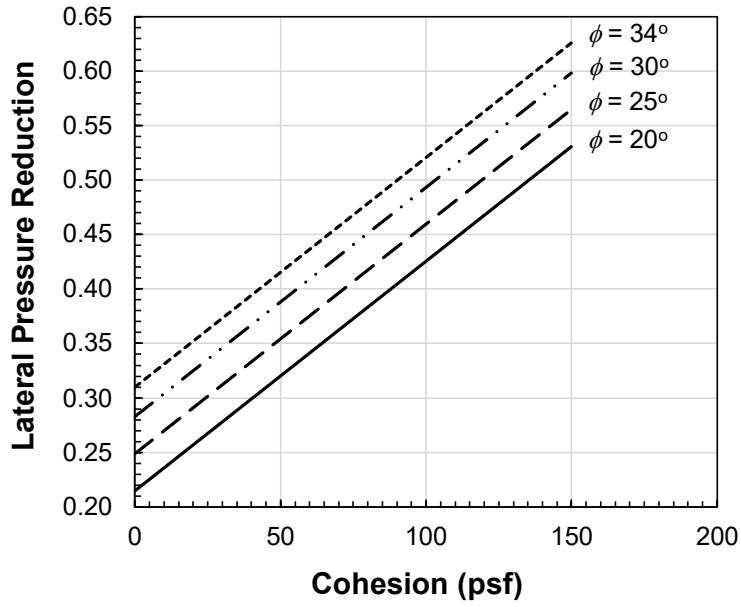
Lateral Pressure Reduction and Lateral Displacement Charts for  
 Wall Height = 5 ft.; RPP Size = 4x4 inches; RPP Spacing = 3 ft. c/c



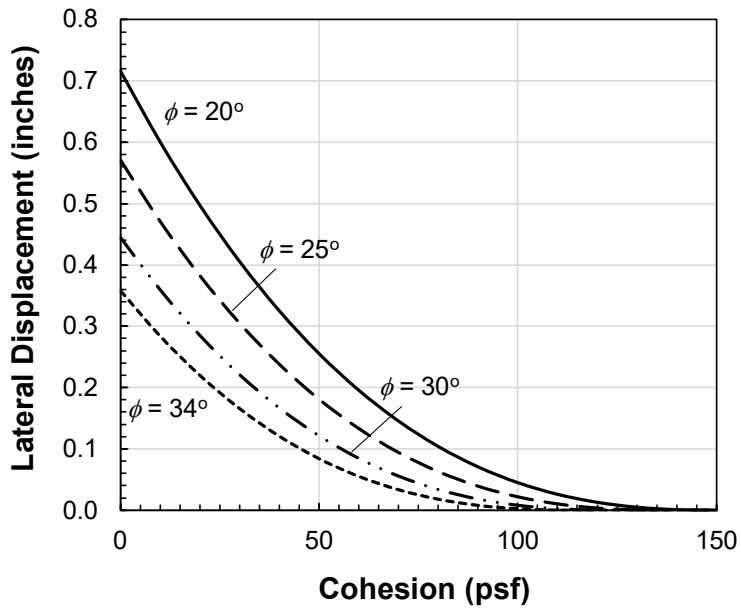
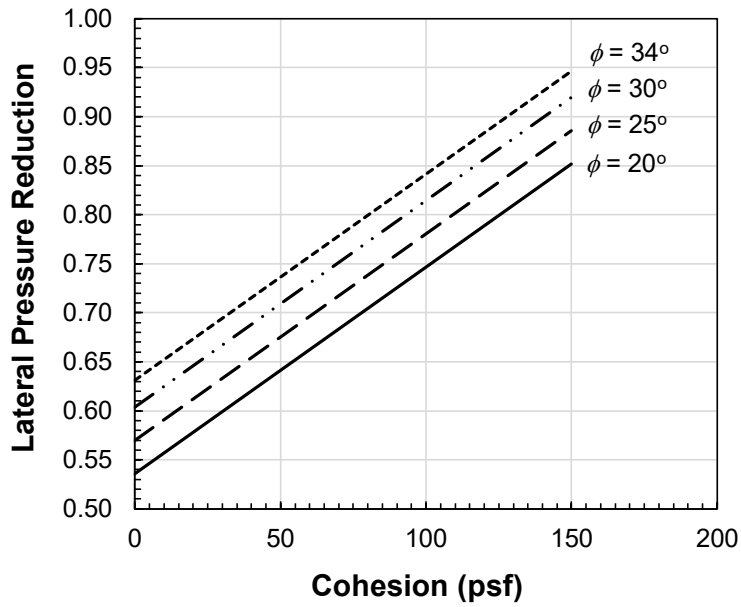
Lateral Pressure Reduction and Lateral Displacement Charts for  
 Wall Height = 5 ft.; RPP Size = 4x4 inches; RPP Spacing = 4 ft. c/c



Lateral Pressure Reduction and Lateral Displacement Charts for  
 Wall Height = 10 ft.; RPP Size = 4x4 inches; RPP Spacing = 2 ft. c/c

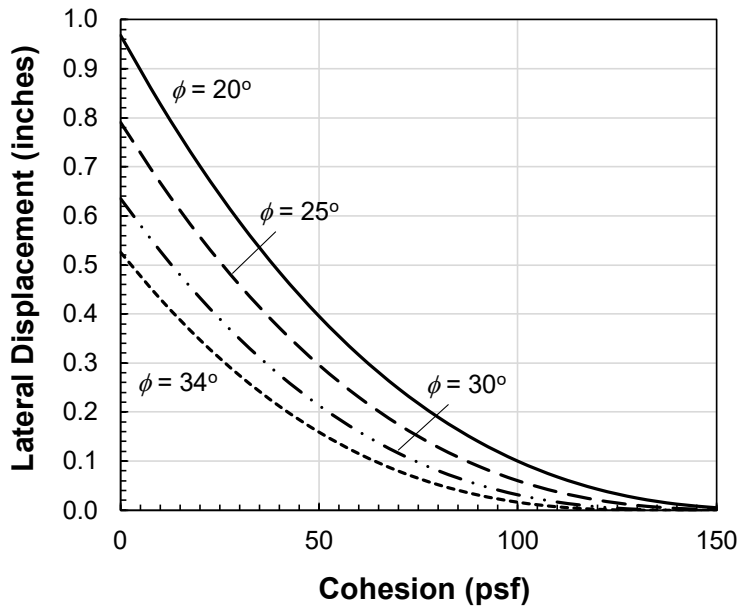
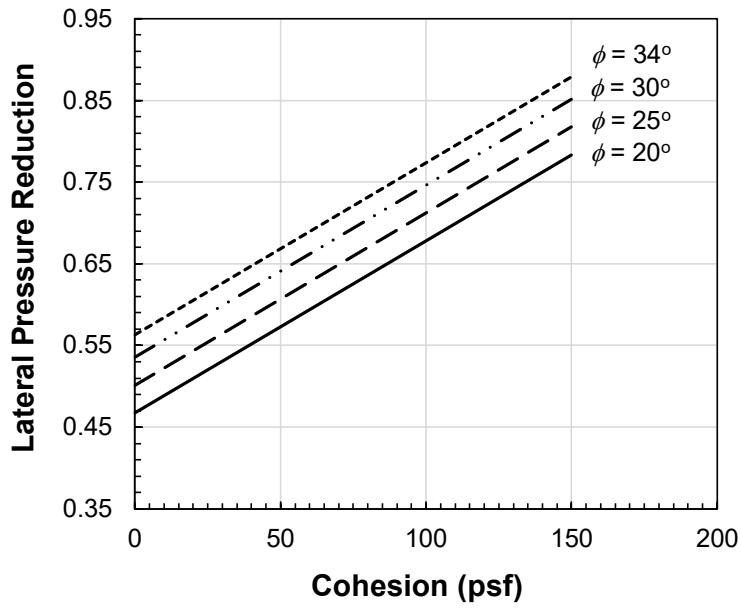


Lateral Pressure Reduction and Lateral Displacement Charts for  
 Wall Height = 10 ft.; RPP Size = 4x4 inches; RPP Spacing = 3 ft. c/c

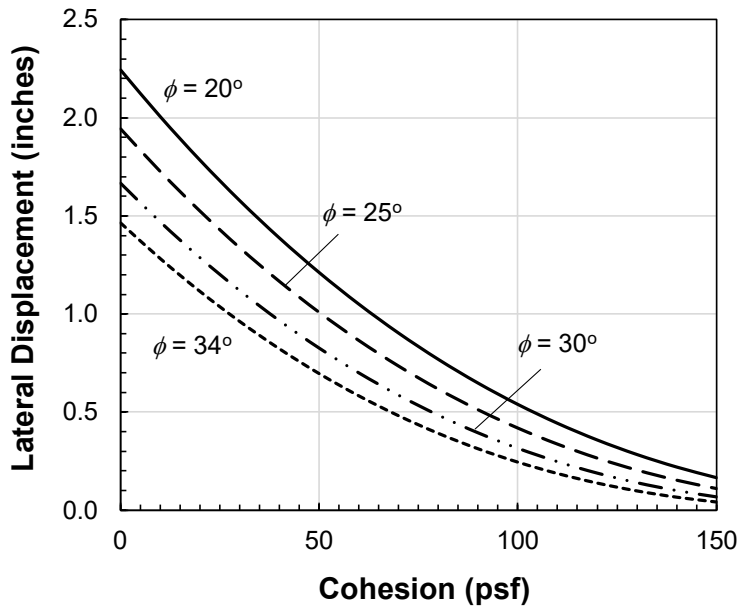
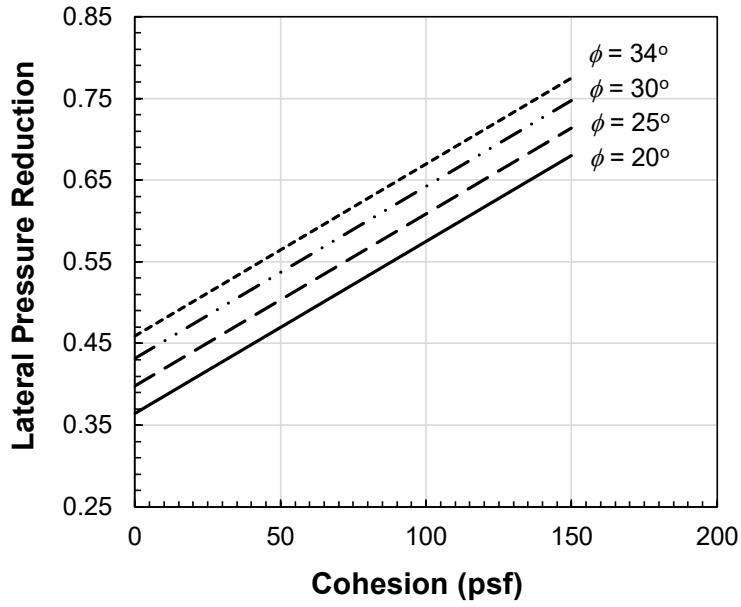


Lateral Pressure Reduction and Lateral Displacement Charts for  
 Wall Height = 5 ft.; RPP Size = 6x6 inches; RPP Spacing = 3 ft. c/c

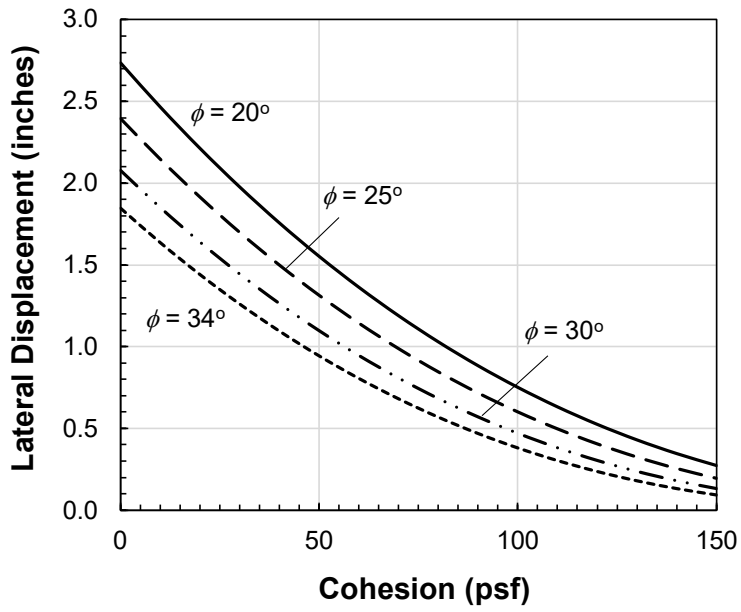
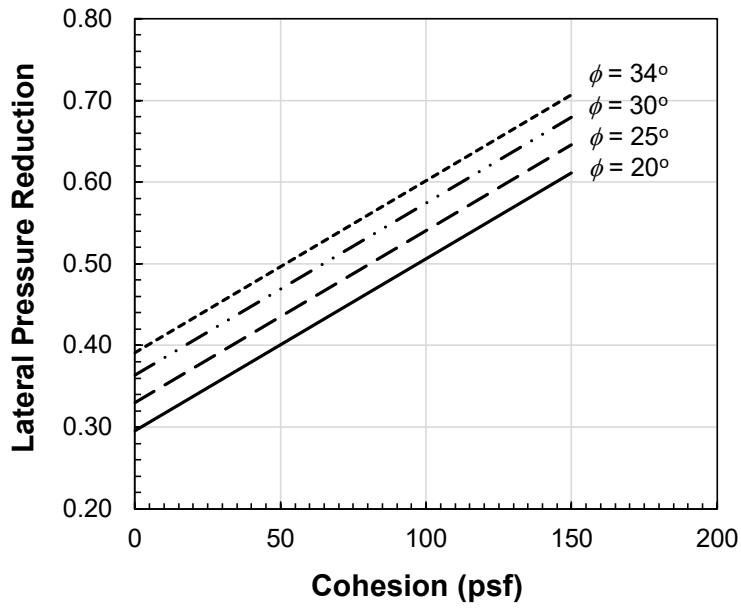




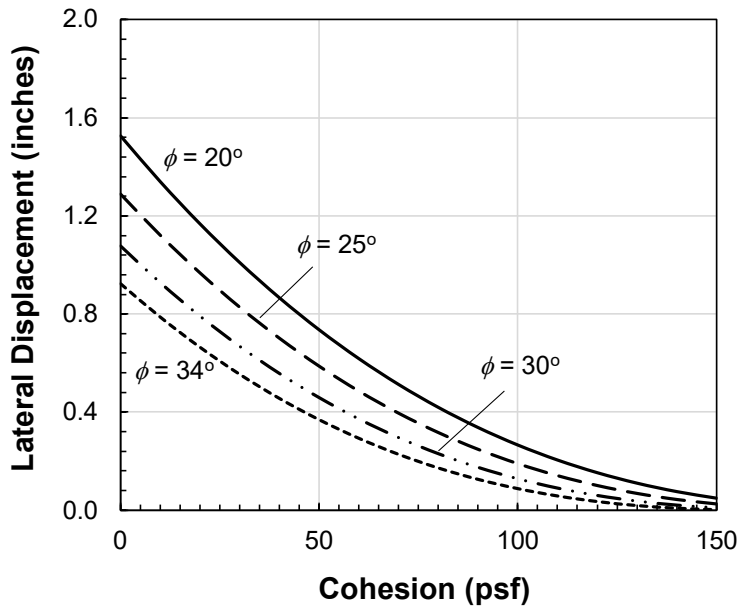
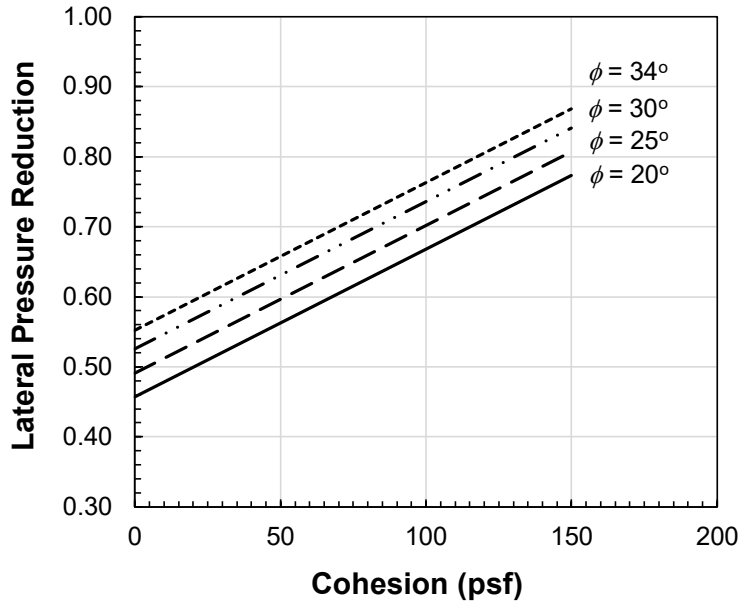
Lateral Pressure Reduction and Lateral Displacement Charts for  
 Wall Height = 5 ft.; RPP Size = 6x6 inches; RPP Spacing = 4 ft. c/c



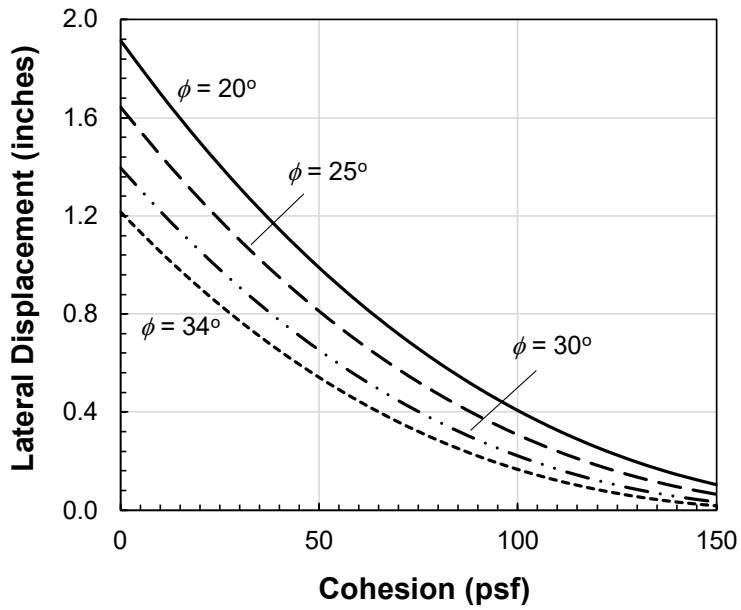
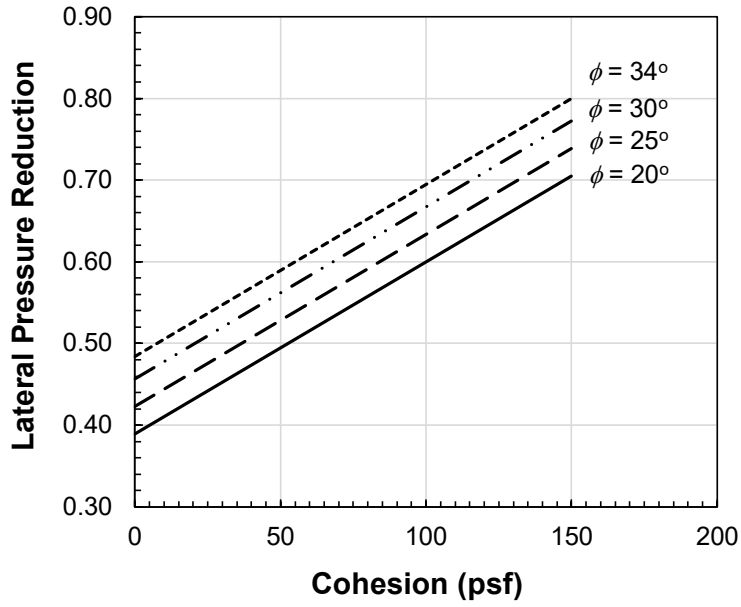
Lateral Pressure Reduction and Lateral Displacement Charts for  
 Wall Height = 10 ft.; RPP Size = 6x6 inches; RPP Spacing = 2 ft. c/c



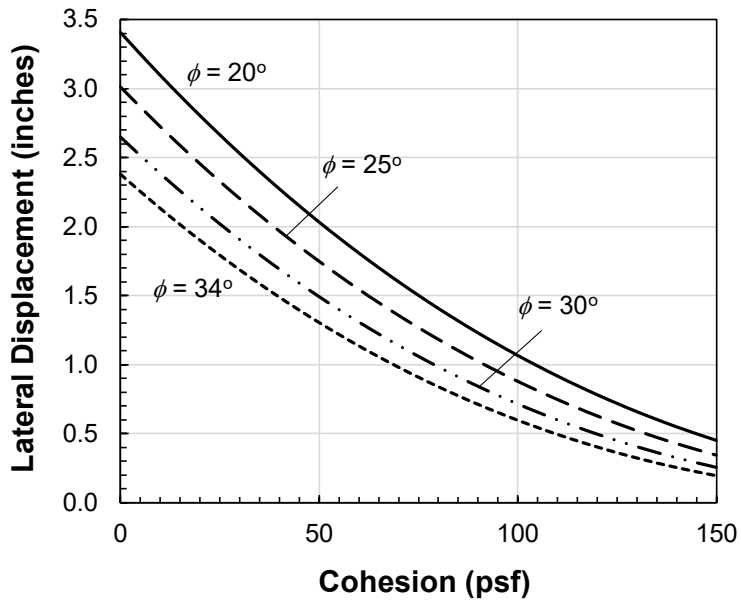
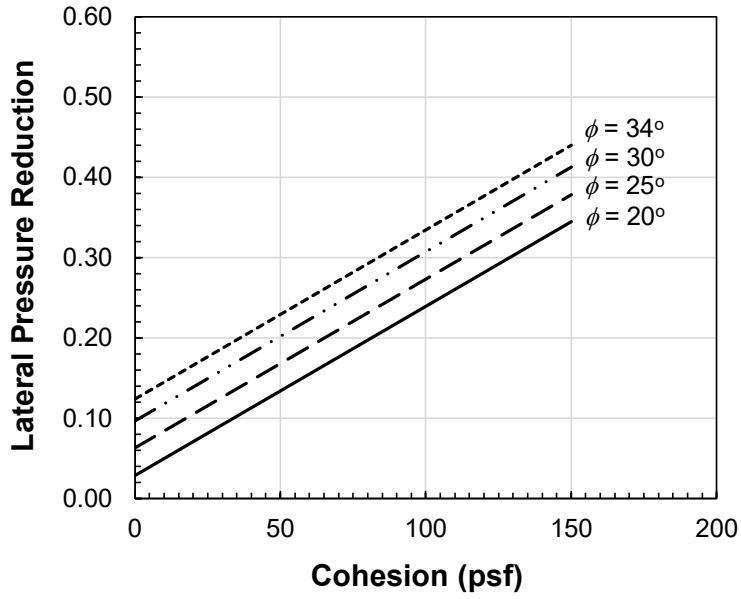
Lateral Pressure Reduction and Lateral Displacement Charts for  
 Wall Height = 10 ft.; RPP Size = 6x6 inches; RPP Spacing = 3 ft. c/c



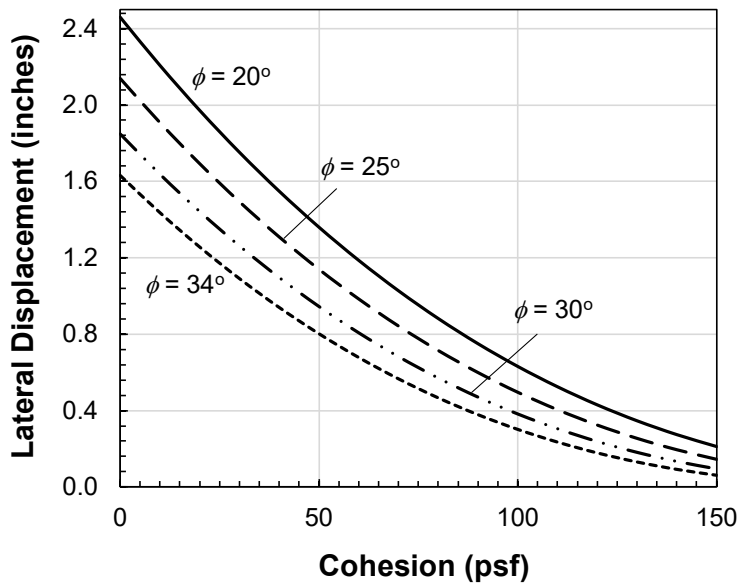
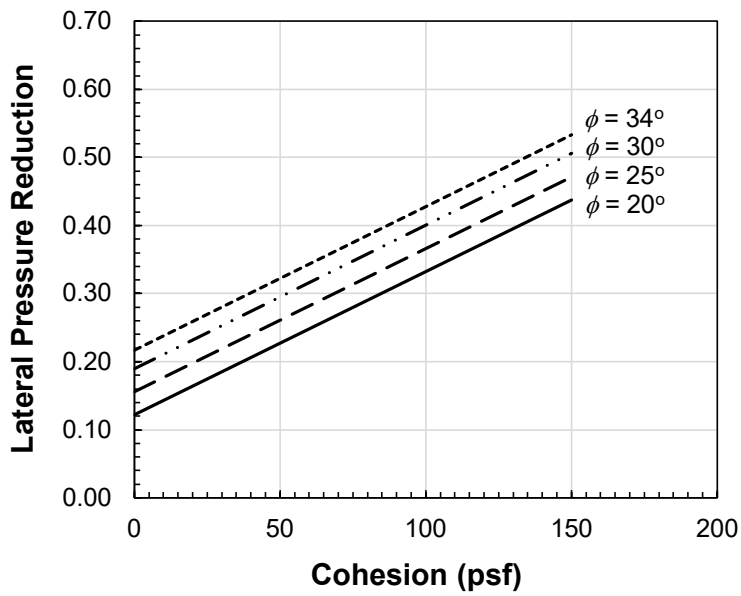
Lateral Pressure Reduction and Lateral Displacement Charts for  
 Wall Height = 10 ft.; RPP Size = 10x10 inches; RPP Spacing = 3 ft. c/c



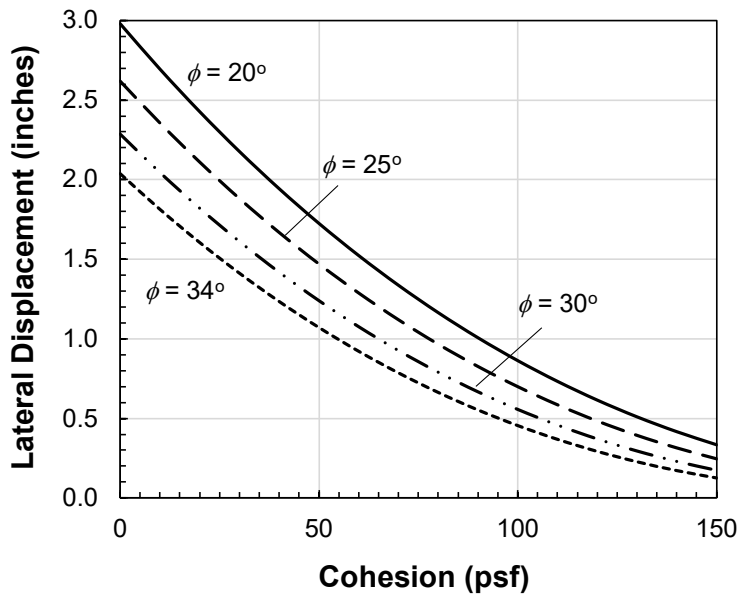
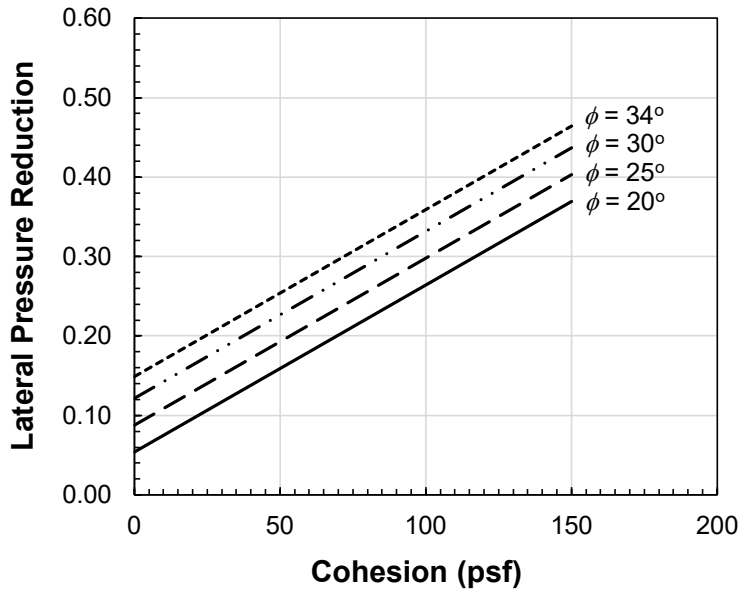
Lateral Pressure Reduction and Lateral Displacement Charts for  
 Wall Height = 10 ft.; RPP Size = 10x10 inches; RPP Spacing = 4 ft. c/c



Lateral Pressure Reduction and Lateral Displacement Charts for  
 Wall Height = 12 ft.; RPP Size = 6x6 inches; RPP Spacing = 2 ft. c/c



Lateral Pressure Reduction and Lateral Displacement Charts for  
 Wall Height = 12 ft.; RPP Size = 10x10 inches; RPP Spacing = 3 ft. c/c



Lateral Pressure Reduction and Lateral Displacement Charts for  
 Wall Height = 12 ft.; RPP Size = 10x10 inches; RPP Spacing = 4 ft. c/c



## BIOGRAPHY

Prabesh Bhandari was born in Kathmandu, Nepal. He earned his bachelor's degree in Civil Engineering from Advanced College of Engineering and Management, Tribhuvan University in Kathmandu, Nepal in 2014. He then worked as a Senior Inspector of Works at a Joint Venture Consultant in Nepal for a road construction project from November 2014 to September 2016. After that he worked as a Civil Engineer in a Tunnel Design Project for Eptisa Servicios De Ingenieria, S.L. from November 2016 to July 2017. Prabesh joined the University of Texas at Arlington in Fall 2017 for the Geotechnical program and worked as a graduate research assistant under Dr. MD. Sahadat Hossain. The author's research experience and interests include the areas of retaining walls, slope stability, foundation systems, numerical modeling, statistical analysis, forensic study, geophysical investigation, expansive subgrade soil, recycled base materials, geotechnical laboratory testing, landfills, and sustainable waste management, among others.